

Mapping PAMP Responses and Disease Resistance in Brassicas

Simon Rhys Lloyd

A thesis submitted to the University of East Anglia for the degree of Doctor of Philosophy

John Innes Centre

March 2014

© This copy of the thesis has been supplied on condition that anyone who consults it is understood to recognise that its copyright rests with the author and that use of any information derived there from must be in accordance with current UK Copyright Law. In addition, any quotation or extract must include full attribution.

Abstract

The first layer of active defence in plants is based on the perception of pathogen-associated molecular patterns (PAMPs) leading to PAMP-triggered immunity (PTI). PTI is increasingly being investigated in crop plants, where it may have potential to provide durable disease resistance in the field. Limiting this work, however, is an absence of reliable bioassays to investigate PAMP responses in some species. Presented here is a series of methods to investigate PTI in *Brassica napus*. The assays allow measuring early cell signalling responses, gene expression changes, cell wall reinforcement, metabolome changes and scoring PAMP-Induced resistance. Illumina-based RNA sequencing analysis produced a genome-wide survey of transcriptional changes upon PAMP treatment seen in both the A and C genomes of the allotetraploid *B. napus*.

Using these assays substantial variation in PAMP-responsiveness was observed amongst elite varieties of *B. napus*. Taking this further, a genome wide association study (GWAS) of the flg22 and elf18 triggered oxidative bursts, resistance to *Pseudomonas syringae* and *Botrytis cinerea* was carried out in a population of *B. napus*. A substantial number of molecular markers, covering both sequence and expression variation, have been identified as having significant association with these four traits.

QTL mapping of the flg22 triggered oxidative burst in the ADxGD double haploid cross identified a major quantitative trait loci (QTL) on C9 of *B. oleracea*. mRNA-seq of the parents led to a non-synonymous single nucleotide polymorphism (SNP) list and enabled fine mapping through the addition of KASPar markers to the original map. This produced a relatively small list of candidate genes including CYLIC NUCLEOTIDE GATED ION CHANNEL 4 (*CNGC4*) also known as DEFENCE NO DEATH 2 (*DND2*). An insertion in *Arabidopsis thaliana* *DND2* showed phenotypic difference in the oxidative burst between the insertion line and Col-0, potentially indicating a role for the gene in regulating early PTI.

Acknowledgements

I would like to thank my supervisory committee, Dr Chris Ridout, Dr Cyril Zipfel, Professor Bruce Fitt and Dr Yong-ju Huang for their advice and guidance, and my original supervisor, the late Chris Lamb, for offering me the studentship.

All experimental work presented here was done by me, with lignification experiments done alongside Jodie Daniels, and phenotyping of the association mapping panel done with Katherine Orman and sometimes Henk-jan Schoonbeek, which I am very grateful for.

The project encompasses a lot of different techniques, and I'm very thankful for technical help and training from Dr Colin Morgan, Dr Judith Irwin, Dr Andrea Harper and Dr Rachel Wells for mapping; Dr Gary Criesson, Professor Jun Fan, Dr Cecile Segonzac, Dr Freddy Boutrot, Dr Grant Calder for help with pathology, molecular genetics and cell biology assays; and Dr Martin Trick for bioinformatics support and training.

On a personnel note, I thank my family and friends for support and encouragement and I would like to thank all members of the Lamb, Ridout and Zipfel labs particularly Ruth Bryant, Stuart King, Alex Coleman, Bethan Edmunds, Ellen Colebrook and Katherine Orman for making the past few years so enjoyable. I offer special thanks to Dr Henk-jan Schoonbeek, whose endless expertise, patience, approachability and support has been highly valued over the past four years.

Table of Contents

Chapter 1 : General Introduction.....	16
1.1. The Plant Immune System.....	17
1.2. PAMPs and PRR's.....	20
1.3. PAMP Signalling.....	22
1.4. The Brassicas	29
1.5. Research Aims	36
1.6. Research Questions:.....	37
1.7. Research Objectives:	38
Chapter 2 : Materials and Methods.....	40
2.1. Materials.....	41
2.1.1 Plant materials and growth conditions.....	41
2.1.2 Pathogens used and culture conditions.....	42
2.1.3 Culture Media used.....	42
2.1.4 Antibiotics	43
2.1.5 Plant Growth Mixes.....	43
2.1.6 Chemicals	44
2.1.7 Primer design and synthesis	45
2.2. General Molecular Methods	49
2.2.1 Plant genomic DNA isolation.....	49
2.2.2 Plant RNA isolation and quantitative RT-PCR	49
2.2.3 First strand cDNA synthesis.....	49
2.2.4 Quantification of nucleic acids.....	50
2.2.5 qRT-PCR.....	50
2.2.6 PCR	50

2.2.7	Genotyping.....	50
2.3.	PAMP-Response Assays.....	51
2.3.1	Oxidative burst	51
2.3.2	MAP kinase phosphorylation	51
2.3.3	Callose staining.....	52
2.3.4	PAMP Induced Lignification	52
2.3.5	Seedling Growth Inhibition	53
2.4.	Pathology Methods	54
2.4.1	PAMP-induced resistance	54
2.4.2	<i>Botrytis cinerea</i>	54
2.4.3	<i>Sclerotinia sclerotiorum</i>	55
2.4.4	<i>Pseudomonas syringae</i>	56
2.5.	Metabolomic Methods.....	57
2.5.1	Metabolite Extractions.....	57
2.5.2	HPLC	58
2.5.3	Metabolite Effect on Pathogen Growth.....	59
2.6.	Analytical Methods.....	60
2.6.1	Illumina-based RNAseq	60
2.6.2	Aligning Illumina reads to <i>B. napus</i> pseudomolecules	60
2.6.3	PAMP-induced transcriptome analysis	60
2.6.4	Mapman Analysis	61
2.6.1	Association Genetics	61
2.6.2	QTL Mapping	61
2.6.3	Prediction of codon use changes of A12xGD SNPs	62
2.6.4	Genotyping with KASPar markers	62
2.6.5	Sequence alignments	65

2.6.6	Statistical Tests Used.....	65
2.6.7	Bioinformatics Tools Used	65
Chapter 3 : Methods to Study PAMP-Triggered Immunity in <i>Brassica napus</i>		67
3.1.	Aim.....	68
3.2.	Introduction.....	68
3.3.	Results	71
3.3.1	The Oxidative Burst in <i>Brassica napus</i>	71
3.3.2	Map kinases are rapidly phosphorylated after flg22 treatment in <i>B. napus</i> 77	77
3.3.3	PAMP-Induced Callose Deposition in <i>B. napus</i>	77
3.3.4	PAMP-Induced Seedling Growth Inhibition	80
3.3.5	PAMP-Induced Lignification	80
3.3.6	Identifying PAMP-responsive marker genes in <i>Brassica napus</i>	85
3.3.7	Genome wide changes upon PAMP treatment in <i>B. napus</i>	85
3.3.8	Co-ordination of PAMP-Responsive Transcription Between the A and C Genomes.....	88
3.3.9	Functional Characterisation of up-regulated unigenes in <i>B. napus</i>	88
3.3.10	PAMP Induced Resistance in <i>B. napus</i>	96
3.3.11	PAMP Induced Metabolome Changes in <i>B. napus</i>	99
3.3.12	Natural Variation in PAMP Responsiveness in <i>B. napus</i>	106
3.4.	Discussion	108
Chapter 4 : Association Transcriptomics of PAMP Responses and Pathogen Resistance in <i>Brassica napus</i>		116
4.1.	Aim.....	117
4.2.	Introduction.....	117
4.3.	Results	120

4.3.1	Overview of Associative Transcriptomics Method	120
4.3.2	Associative Transcriptomics of the flg22 Triggered Oxidative Burst In <i>B. napus</i>	120
4.3.3	Associative transcriptomics of the elf18 triggered oxidative burst In <i>B. napus</i>	128
4.3.4	Associative Transcriptomics of <i>B. cinerea</i> resistance in <i>B. napus</i>	135
4.3.5	Associative Transcriptomics of <i>Pseudomonas syringae</i> resistance in <i>B. napus</i>	141
4.3.6	Correlation of phenotypes	148
4.3.7	Correlation of GEMS.....	148
4.3.8	Functional Annotation of Significantly Associated GEMs	151
4.4.	Discussion	153
Chapter 5 : QTL Mapping of PAMP Responses in the A12 x GD <i>B. oleracea</i> Cross		159
5.1.	Aim.....	160
5.2.	Introduction.....	160
5.3.	Results	162
5.3.1	There is segregating variation in oxidative burst in the A12xGD cross.	162
5.3.2	The parental lines A12 and GD have contrasting resistance phenotypes to <i>P. syringae</i> and <i>B. cinerea</i>	164
5.3.3	Offspring of the A12xGD cross are highly polymorphic in ROS responses and resistance to <i>B. cinerea</i> and <i>P. syringae</i>	166
5.3.4	A significant QTL on C9 was found for the flg22 triggered ROS burst	169
5.3.5	No significant QTLs for elf18 ROS, <i>B. cinerea</i> resistance or <i>P. syringae</i> resistance were found in A12 x GD.....	173

5.3.6	The Locus resulting in low flg22 triggered ROS is likely to sit between the markers pN105E4NM and pO160E1	174
5.3.7	Confirmation of the flg22 ROS C9 QTL through Substitution lines....	176
	Multiple QTL Mapping of flg22 triggered ROS in A12 x GD	178
5.3.8	Illumina Sequencing of A12 and GD.....	180
5.3.9	Identificantion of Non-synonymous SNPs in coding genes from A12 and GD	180
5.3.1	Transferring Markers from the Genetic Map to the Physical Map Based on the <i>B. napus</i> C genome Unigene Assembly	181
5.3.1	The Initial Candidate Gene list	183
5.3.2	PAMP-responsiveness of genes within the QTL in <i>A. thaliana</i> and <i>B. napus</i>	186
5.3.3	Comparing Expression of all Genes between A12 and GD	188
5.3.1	Obvious candidate genes for the flg22 triggered ROS burst did not have sequence or expression polymorphism in C9	189
5.3.1	Adding KASPar Markers to A12 x GD	189
5.3.2	The New Map of C9.....	191
5.3.1	QTL Mapping using the New Integrated Map.....	194
5.3.2	Single Marker Analysis of flg22 ROS in the New Map of C9	194
5.3.3	Establishing a new gene list	196
5.3.4	DND2 is highly conserved between <i>A. thaliana</i> and <i>B. napus</i> , and GD has a number of potentially deleterious NS SNPS in the coding sequence	198
5.4.	Discussion	200
Chapter 6 :	General Discussion	205
6.1.	Key questions addressed in this thesis.....	207
6.2.	Summary of key findings	217
Chapter 7 :	Appendices.....	237

7.1.	Appendix 1: flg22-Induced Transcriptomic Changes in <i>Brassica napus</i>	237
7.2.	Appendix 2: Association Mapping of SNP Markers in <i>Brassica napus</i>	238
7.3.	Appendix 3: Association Mapping of GEM Markers in <i>Brassica napus</i>	238
7.4.	Appendix 4 : QTL Maps Of elf18 Triggered Oxidative Burst, <i>Botrytis cinerea</i> Resistance and <i>Pseudomonas syringae</i> Resistance in A12 x GD.....	238
	241
7.5.	Appendix 5: SNP List Between A12 and GD	242
7.6.	Appendix 6: Codon Use and Amino Acid Changes for SNPs between A12 and GD.....	242
7.7.	Appendix 7: Predicted Synonymous, Non-synonymous and Unknown SNPs on C9	242
7.8.	Appendix 8: Basal Unigene Expression Level in A12 and GD	242
7.9.	Appendix 9: PAMP Induced Expression Changes of Unigenes Within the C9 QTL in <i>B. napus</i> and <i>A. thaliana</i>	243
7.10.	Appendix 10: Genotyping Matrix of AFLP, RFLP and KASPar Markers For the A12 x GD Mapping Population.....	243
7.11.	Appendix 11: New Integrated C9 Map	243
7.12.	Appendix 12: Full Length DND2 from C9 consensus extraction for A12 and GD	245
7.13.	Appendix 13: Alignment of JCVI_20335 and JCVI_20553 against full length AtDND2 cDNA.....	245
7.14.	First author publications of candidate.....	248
7.14.1	“Methods to Study PTI in <i>Brassica napus</i> ”	248

List of Illustrations

Figure 1.1 PTI, ETS and ETI.	18
Figure 1.2 Overview of cellular PAMP-responses.	23
Figure 1.3 Early regulation of the oxidative burst	27
Figure 1.4 Evolution of the brassicacea.	31
Figure 1.5 Genotypes used in OREGIN diversity set.	33
Figure 2.1 AFLP/RFLP Map of <i>B. Oleracea</i> chromosomes 1-4	63
Figure 2.2 AFLP/RFLP map of <i>B. oleracea</i> chromosomes 5-9.	64
Figure 3.1 Dose response curves of the PAMP-triggered oxidative burst in <i>Brassica napus</i>	72
Figure 3.2 Relative ROS levels after PAMP treatment in <i>B. napus</i>	73
Figure 3.3 Optimising the oxidative burst in <i>Brassica napus</i>	75
Figure 3.4 Comparison of the oxidative burst in <i>Brassica napus</i> and <i>Arabidopsis thaliana</i>	76
Figure 3.5 flg22-triggered MAPK phosphoprylation.	78
Figure 3.6 Callose deposition in <i>B. napus</i>	79
Figure 3.7 Seedling growth inhibiton in <i>B. napus</i>	81
Figure 3.8 PAMP treatment enhances wound-induced lignification and vascular lignification staining in <i>B. napus</i>	82
Figure 3.9 Lignin quantification in PAMP treated <i>Brassica napus</i> tissue.	84
Figure 3.10 PAMP-responsive marker genes in <i>B. napus</i>	86
Figure 3.11 Co-expression of homologous genes after flg22 treatment in <i>Brassica napus</i>	89
Figure 3.12 Functional characterisation of flg22 responsive genes in <i>Brassica napus</i>	90
Figure 3.13 Subcellular location of products of PAMP responsive genes in <i>Brassica napus</i>	92
Figure 3.14 Metabolomic pathways up and down regulated by flg22 in <i>Brassica napus</i>	93
Figure 3.15 RLKs and transcription factor families up and down regulated by flg22 in <i>Brassica napus</i>	94

Figure 3.16 RLK Expression in <i>Brassica napus</i> after PAMP treatment.....	95
Figure 3.17 Luminoimetric quantification of <i>Pseudomonas syringae</i> growth in <i>Brassica napus</i>	97
Figure 3.18 PAMP-Induced resistance in <i>Brassica napus</i>	98
Figure 3.19 Salicylic acid is induced by flg22 treatment in <i>Brassica napus</i>	102
Figure 3.20 Quantification of camalexin and scopoletin after flg22 Treatment.	103
Figure 3.21 Growth of <i>B. cinerea</i> in metabolite extractions after flg22 treatment.	105
Figure 3.22 Variation in PAMP responses between <i>B. napus</i> cultivars.	107
Figure 4.1 The flg22 triggered oxidative burst in the association genetics mapping panel of <i>Brassica napus</i>	121
Figure 4.2 SNP markers associated with the flg22-triggered oxidative burst in <i>Brassica napus</i>	123
Figure 4.3 GEM markers associated with the flg22-triggered oxidative burst in <i>Brassica napus</i>	124
Figure 4.4 FLS2 expression correlates with the flg22 triggered ROS burst in different <i>Brassica napus</i> varieties.....	127
Figure 4.5 The elf18 triggered Oxidative Burst in the Association Genetics Mapping Panel.....	129
Figure 4.6 SNP markers associated with the elf18-triggered oxidative burst.	130
Figure 4.7 GEM markers associated with the elf18-triggered oxidative burst.....	132
Figure 4.8 <i>Botrytis cinerea</i> resistance in the association genetics mapping panel.	136
Figure 4.9 SNP markers associated with <i>Botrytis cinerea</i> resistance.	137
Figure 4.10 GEM markers associated with <i>Botrytis cinerea</i> resistance.....	138
Figure 4.11 <i>Pseudomonas syringae</i> resistance in the association genetics mapping panel.....	142
Figure 4.12 SNP markers associated with <i>Pseudomonas syringae</i> resistance.	143
Figure 4.13 GEM markers associated with <i>Pseudomonas syringae</i> resistance.....	144
Figure 4.14 Correlations between pathogen resistance related phenotypes in the association mapping panel.....	149
Figure 4.15 Correlation of GEM association significance between the flg22 and elf18 triggered oxidative burst phenotypes for the A and C <i>B. napus</i> genomes.....	150

Figure 4.16 <i>Arabidopsis</i> GO-term annotation of GEM markers significantly linked to defence phenotypes.....	152
Figure 5.1 Oxidative burst phenotypes in <i>Brassica oleracea</i> lines A12, GD and AG1012.....	163
Figure 5.2 Resistance of A12 and GD to <i>Pseudomonas syringae</i> and <i>Botrytis cinerea</i>	165
Figure 5.3 Phenotyping the A12xGD cross of <i>B. oleracea</i> for response to flg22, elf18 and disease resistance to <i>P. syringae</i> and <i>B. cinerea</i>	167
Figure 5.4 Distribution frequencies of variation in defence phenotypes in the <i>B. oleracea</i> A12 x GD cross.....	168
Figure 5.5 QTL profiles of the flg22 triggered ROS burst in A12 x GD.	170
Figure 5.6 The C9 QTL controlling the flg22 triggered ROS burst in A12 x GD <i>B. oleracea</i> cross.....	171
Figure 5.7 The flg22 and <i>Agrobacterium</i> QTL peaks in A12xGD do not overlap.	172
Figure 5.8 Genotype matrix of C9 the A12xGD population phenotyped in this study	175
Figure 5.9 ROS phenotypes of the C9 substitution lines.....	177
Figure 5.10 MQM mapping of the flg22 triggered ROS burst in A12xGD taking the C9 QTL as a Co-factor	179
Figure 5.11 PAMP induced expression changes of candidate genes in the C9 QTL.	187
Figure 5.12 KASPar marker locations on the pseudomolecule assembly of C9	190
Figure 5.13 QTL on C9 of the flg22 triggered ROS burst using the new integrated map.	195
Figure 5.14 Position of the integrated genetic map markers in <i>Brassica oleracea</i> on the C9 pseudomolecule assembly of <i>B. napus</i>	197
Figure 5.15 Allignment of JCVI_20335 and JCVI_20553 from the <i>B. napus</i> C genome consensus sequence, A12 and GD mRNA seq and <i>A.thaliana</i> DND2 cDNA.....	199

List of Tables

Table 1 Primers used to investigate expression of <i>Brassica napus</i> PAMP responsive marker genes at 1 and 3 hours post PAMP treatment.	46
Table 2 KASPar primers for use in genotyping the A12 x GD mapping population...	47
Table 3 Primers used in genotyping SALK insertion lines.	48
Table 4 Databases and bioinformatics tools used in this study.....	66
Table 5 Genome wide changes in gene regulation after flg22 treatment in <i>B. napus</i>	87
Table 6 PAMP-Induced Metabolites in <i>B. napus</i>	100
Table 7 The 50 SNP markers most significantly associated with the flg22-triggered oxidative burst.	125
Table 8 The 50 most significantly associated GEM markers for the flg22-triggered oxidative burst.	126
Table 9 The 50 SNP markers most significantly associated with the elf18-triggered oxidative burst.	133
Table 10 Top 50 most significantly associated GEM markers for the elf18-triggered oxidative burst.	134
Table 11 The 50 SNP markers most significantly associated with the <i>Botrytis cinerea</i> resistance	139
Table 12 Top 50 most significantly associated GEM markers for <i>Botrytis cinerea</i> resistance.	140
Table 13 The 50 SNP markers most significantly associated with <i>Pseudomonas syringae</i> resistance.....	145
Table 14 Top 50 most significantly associated GEM markers for <i>Pseudomonas syringae</i> resistance.....	146
Table 15 Summary of significant associations found in the GWAS of four defence related traits.....	147
Table 16 BLAST summary of C9 markers against the Pseudomolecules.	182
Table 17 Candidate genes in the C9 QTL.	185
Table 18 New intergated map of C9 and single markler analysis for the flg22 - triggered oxidative burst.....	193

Abbreviations

AA	Amino Acid
BAK1	BRI1 ASSOCIATED KINASE 1
BIK1	BOTRYTIS-INDUCED KINASE 1
BP	Base Pair
BR	Brassinosteroid
CEBIP	CHITIN ELICITOR BINDING PROTEIN
CER	Controlled Environment Room
CERK1	CHITIN ELICITOR RECEPTOR KINASE 1
CNGC	CYCLIC NUCLEOTIDE GATED ION CHANNEL
CSC	Crab Shell Chitin
CWD	Cell Wall Damage
DH	Double Haploid
DNA	Deoxyribose Nucleic Acid
DND1/2	DEFENCE NO DEATH 1/2
EFR	ELONGATION FACTOR TU RECEPTOR
ET	Ethylene
ETI	Effector Triggered Immunity
ETS	Effector Triggered Susceptibility
FLS2	FLAGELLIN SENSITIVE 2
GEM	Gene Expression Marker
GFP	GREEN FLUORESCENT PROTEIN
GWAS	Genome Wide Association study
HR	Hypersensitive Response
JA	Jasmonic Acid
KASPAR	Kbioscience Competitive Allele Specific PCR
LRR	Leucine Rich Repeat
LYS-M	Lysin Motif
MAPK	MITOGEN ACTIVATED PROTEIN KINASE
NS	Non-Synonymous
PAMP	Pathogen Associated Molecular Pattern
PCR	Polymerase Chain Reaction
PRR	Pattern Recognition Receptor
PTI	PAMP Triggered Immunity
PTO	<i>Pseudomonas syringae</i> p.v Tomato
QRTPCR	Quantitative Real-time PCR
QTL	Quantitative Trait Loci
RBOHD	RESPIRATORY BURST OXIDASE HOMOLOG D
RLK	Receptor Like Kinase
RLP	Receptor Like Protein
RNA	Ribose Nucleic Acid
ROS	Reactive Oxygen Species
SA	Salicylic Acid
SNP	Single Nucleotide Polymorphism
TGA	Thioglycolic Acid
TILLING	Targetted Induced Local lesions in Genomes
TTSS	Type Three Secretion System

Chapter 1 : General Introduction

1.1. The Plant Immune System

Any organism that is alive, and intends to stay so, must have an immune system. This is no different for plants. Despite being surrounded by bacteria capable of consuming the nutrients within them, plants are thriving all around us. Plants are so effective at defending themselves from would be pathogens that disease is the exception rather than the norm. As organisms without mobile immune cells, every plant cell must be capable of detecting pathogens and mounting a defence response. The mechanisms of pathogen detection employed by the host cell are what define the current paradigm of plant immunity.

Active plant defence comprises two levels of threat detection employed by the host. The first level involves recognition of pathogen- (or microbe-) associated molecular patterns (PAMPs/MAMPs) at the cell membrane by pattern recognition receptors (PRRs) (Boller & Felix 2009; Dodds & Rathjen 2010). PAMPs are conserved molecules present in entire groups of microbes that are important for the normal life cycle of the organism (Medzhitov 1997). The resulting PAMP-triggered immunity (PTI) downstream of the PRR comprises a series of defence reactions often sufficient to halt further pathogen growth. In response, pathogens have evolved effector proteins which suppress signalling and resistance processes within in the plant to facilitate growth, a process called effector-triggered susceptibility (ETS). The second level of pathogen detection by the host is defined as effector-triggered immunity (ETI). This is the recognition of specific effectors intended to subvert or evade PTI that are delivered by a host-adapted pathogen (reviewed in Jones & Dangl 2006; Chisholm et al. 2006; Dodds & Rathjen 2010). The PTI – ETS - ETI model is summarised in figure 1.1.

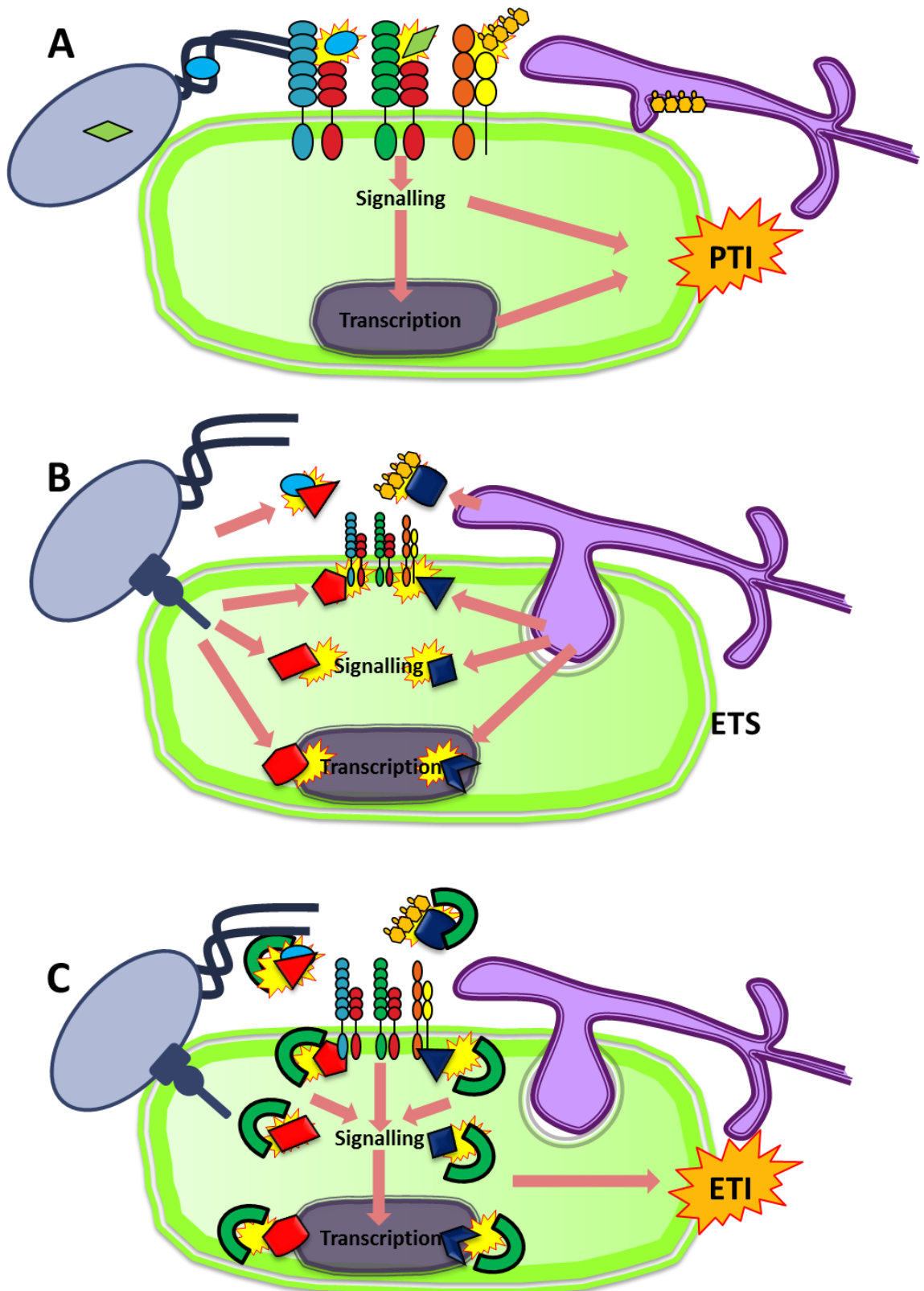


Figure 1.1 PTI, ETS and ETI.

A) PAMPs from pathogens are perceived by PRRs to initiate defence signalling. The resultant responses constitute PTI and pathogen development is arrested or slowed. B) Secreted effectors from pathogens inhibit PTI. Virulence functions of effectors include scavenging PAMPs to prevent recognition, destabilising PRR complexes, preventing or subverting defence signalling and changing gene expression. C) Effectors trigger ETI when recognised by a corresponding R gene. R genes act to identify the presence of a specific effector or to sense perturbations to defence signalling pathways. The resulting ETI triggered by the R genes is often associated with localised cell death in a hypersensitive response (HR), and pathogen growth is arrested.

The separation of PTI and ETI was incorporated into the “zig-zag model” of plant defence, in which the level of resistance was summarised as PTI - ETS +ETI in a back-and-forth model of immune signalling (Jones & Dangl, 2006). Although a rapidly adopted paradigm when first introduced, the model has since fallen out of use. The overlap in timing and magnitude of defence responses that is shared between PTI and ETI is huge. The effect of weak R genes that do not result in a hypersensitive response (HR) for example is almost indistinguishable from PTI (Boller, 2009), and in many pathogen interactions the signalling from PAMP perception and effector perception are so intertwined as to make functional separation of the two branches of immunity difficult (reviewed in Thomma, 2011). Furthermore the distinction between “PAMP” and “effector” is blurred in some cases. For example the effector ECP6, a chitin scavenging Lys-M domain containing protein, is widely found across the fungal kingdom (Bolton, 2008).

A further issue with the model is that during ETS, the magnitude of PTI is depicted as being much less than ETI. However, PTI is involved in resistance to adapted as well as non-adapted or non-host pathogens (Boller, 2009), suggesting that even in situations where PTI signalling is reduced, it is not redundant. For example, FLAGELLIN SENSITIVE 2 (*FLS2*) knockouts in *Arabidopsis thaliana* are more susceptible to *Pseudomonas syringae* DC3000 p.v tomato (PTO) (Zipfel, 2004), a host adapted pathogen with an active complement of effectors. PTI should not be seen as a qualitative switch then, but rather signalling that continually acts to quantitatively restrict pathogen growth.

In recent years some attempt has been made to modify the PTI/ETI model, including descriptions of ‘surface immunity’ and ‘intracellular immunity’, or even reducing multi-layered plant perception systems further to just the perception of overlapping “danger signals” as suggested by Boller & Felix (2009). Although our model of the plant immune system is rapidly changing, the purpose of this thesis is primarily studying responses to the classically defined bacterial PAMPs flagellin, elongation factor-Tu (EF-TU) and the fungal PAMP chitin. These three PAMPs fit

neatly into the stereotypically-described model as widely distributed conserved microbial molecules detected by cell surface localised receptor-like kinases (RLKs).

1.2. PAMPs and PRR's

PAMP-PRR pairs have been identified in a growing number of different plant species (Monaghan & Zipfel 2012). Most currently known plant PRRs are either RLKs or receptor-like proteins (RLPs). The leucine-rich repeat (LRR)-RLK family XII includes the PRRs *FLS2* and *EFR* (EF-Tu RECEPTOR) in *A. thaliana* and *Xa21* in rice. These PRRs recognise the proteinaceous bacterial PAMPs flagellin (Felix et al. 1999; Gomez-Gomez and Boller 2000), EF-Tu (Kunze et al. 2004; Zipfel et al. 2006) respectively. *Xa21* was previously reported as recognising the type-I secreted sulphated peptide Ax21, (Song et al. 1995; Lee et al. 2009), but this has since been retracted and the identity of the *Xa21* ligand is currently unclear. *FLS2* was first identified in *A. thaliana* (Gomez-Gomez, 1999), but functional orthologues have been found since in other species with flagellin perception probably occurring in most higher plants (Felix et al. 1999; Boller & Felix 2009; Albert et al. 2010). Functional *FLS2* orthologues have been identified in *Nicotiana benthamiana* (Hann et al. 2007), tomato (Robatzek et al. 2007) and rice (Takai et al. 2008). In contrast to *FLS2*, the presence of *EFR* and *Xa21* appear to be restricted to Brassicaceae and to rice respectively (Kunze et al. 2004; Zipfel et al. 2006; Lee et al. 2009; Boller and Felix 2009; Schwessinger and Ronald 2012).

The first PRR identified as recognising chitin, a β -1,4-linked polymer of N-acetylglucosamine and essential constituent of the fungal cell wall and insect exoskeleton, was the LysM motif-containing the RLP CHITIN ELICITOR BINDING PROTEIN (*CEBiP*) in rice (Kaku et al. 2006). Another LysM-containing protein is CHITIN ELICITOR RECEPTOR-LIKE KINASE 1 (*CERK1*) first identified in *A. thaliana* (Miya et al. 2007; Wan et al. 2008). While both *CERK1* and *CEBiP* are widely distributed amongst plant species, AtCERK1 directly binds to chitin (Ilizasa et al.

2010; Petutschnig et al. 2010; Liu et al. 2012), whereas CEBiP is the chitin receptor in rice forming a ligand-induced complex with *OsCERK1* (Shimizu et al. 2010). CEBiP-like RLPs were reported as not contributing to chitin perception in *A. thaliana* (Shinya et al. 2012; Wan et al. 2008). However, recent evidence suggests the RLP LYM2 is essential for chitin induced plasmodesmatal closure, whereas *CERK1* is dispensable potentially indicating two distinct chitin perception systems (Faulkner, 2013).

Consistent with the potential existence of multi-protein receptor complexes, *CERK1* has also been implicated in the recognition of the bacterial PAMP peptidoglycan in *A. thaliana* (Willmann et al. 2012). In rice, two additional LysM-RLPs are important for both chitin and PGN recognition (Liu et al. 2012a). Another LysM-RLK, *LYK4* has also been recently linked to chitin perception in *A. thaliana* (Wan et al. 2012). In tomato, the LRR-RLP ETHYLENE-INDUCING XYLANASE RECEPTOR 2 (*EIX2*) is a receptor for xylanase from *Trichoderma* species (Ron & Avni 2004). Also in tomato, the LRR-RLP Ve1 recognises Ave1 from multiple strains of *Verticillium* (Fradin et al. 2009; de Jonge et al. 2012).

Other receptors for conserved microbial molecules that do not have an effector-like function have also been described. The lectin domain containing MANNOSE BINDING LECTIN 1 (*MBL1*) in pepper is an extracellular soluble receptor that binds mannose containing molecules from *Xanthomonas campestris vesicatoria* and promotes SA mediated signalling and cell death (Hwang, 2011). In wheat and barley, cytoplasmic kinases that confer durable broad-spectrum resistance have been identified. REACTION TO PUCCINIA GRAMINIS 1 (*RPG1*) is a protein kinase that is rapidly phosphorylated after binding to two ligands that act cooperatively and were enriched from spores of *P. graminis* (Nirmala, 2010; 2011). In wheat, the protein WHEAT KINASE START 1 (*WKS1*) was found within the loci for *Yr36*, and TILLING mutants in the gene reduced resistance to yellow rust to that of a highly susceptible variety (Fu, 2009). These examples might illustrate how PAMP-triggered immunity, and partial resistance, outside of model systems might be orchestrated by highly diverse receptors.

Identification of novel PRRs and understanding differences in PTI within diverse species has the potential to be applied commercially. Taking a transgenic to disease control and expressing foreign PRRs in crop plants has been highly successful. For example, the interfamily transfer of *AtEFR* into tomato, which lacks a native *EFR* homolog, conferred responsiveness to EF-Tu and increased broad-spectrum resistance to bacteria (Lacombe et al. 2010). Similarly, transgenic *Citrus sinensis* expressing *Xa21* had higher resistance against multiple strains of *Xanthomonas axonopodis* (Mendes et al. 2010). These examples also indicate that similar downstream signalling components are shared between different PRRs and highlight the potential benefit of using PRRs in a transgenic approach to disease control.

1.3. PAMP Signalling

A wide array of downstream responses from PAMP perception have been characterised (some of which are summarised in figure 3). In the earliest stages of ligand binding, receptor complexes comprising PRRs and interacting partners form at the cell membrane. For the PRRs *FLS2* and *EFR*, the LRR-RLK BRI1 ASSOCIATED KINASE 1 (*BAK1*) is an essential early signalling adapter. Upon ligand binding, *BAK1* heteromerizes with *FLS2* before transphosphorylating BOTRYTIS INDUCED KINASE 1 (*BIK1*), active *BIK1* then phosphorylates *FLS2* and *BAK1* to initiate signalling (Monaghan, 2012). Other SOMATIC EMBRYOGENESIS RECEPTOR-LIKE KINASES (*SERKs*) are also important in receptor complex formation, including *BAK1*'s closest homolog *BKK1*, and *BAK1/BKK1* double mutants have extremely low PAMP perception and high susceptibility to a wide range of pathogens (Roux, 2011). Active *FLS2-BAK1* complexes are finally attenuated through the polyubiquitination by *PUB12/13*, and subsequent degradation, of *FLS2* (Lu, 2011). Although significantly less is known about *CERK1* signalling complexes in *A. thaliana*, its phosphorylation is a requirement of signalling (Petutschnig, 2010).

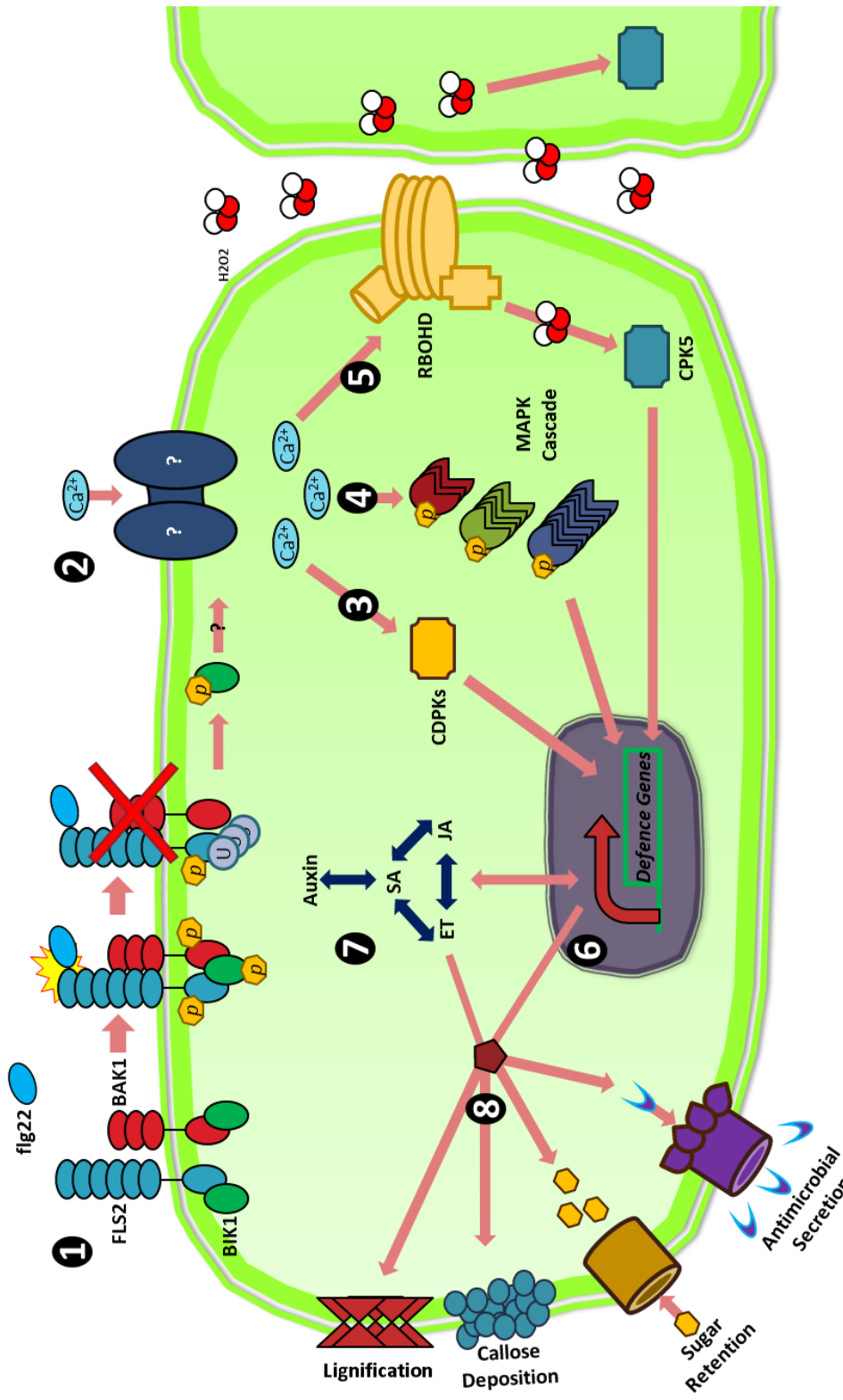


Figure 1.2 Overview of cellular PAMP-responses.

1) PRRs bind PAMPs to initiate receptor complex formation and the release of downstream signalling components such as BIK1. Signalling is attenuated through the polyubiquitination of, and subsequent endocytosis, of the PRR. 2) Ca^{2+} influx, through as yet unidentified channels, is an essential early response to PAMPs. Elevated cytosolic $[Ca^{2+}]$ results in the activation of CDPKs (3), a MAPK cascade (4) and the activation of RBOHD (5). The resulting ROS can activate CPK5 both within the initiating and local cells to perpetuate the PAMP signalling. (6) Defence gene expression and (7) hormone signalling coordinate defence responses. (8) Host responses include cell wall reinforcement through lignin and callose deposition, the restriction of apoplastic nutrients from the invading microbes and the secretion of anti-microbial compounds.

Within minutes of PAMP perception rapid MITOGEN ACTIVATED PROTEIN KINASES (MAPK) phosphorylation, Ca^{2+} influx and H_2O_2 production are observed (Boller, 2009). The identity of the Ca^{2+} channel involved in PTI signalling is currently unknown. As the primary candidates are CYCLIC NUCLEOTIDE GATED ION CHANNELS (CNGCs), which is a huge family in many plants, and as CNGCs may be capable of forming functional heterotetramers, finding direct genetic evidence for their involvement in PTI might be difficult (Ma, 2007).

Ca^{2+} influx is an absolute requirement for both the MAPK activation and ROS production that follows it (Segonzac, 2011). As such, the massive secretion of Ca^{2+} chelating compounds such as oxalic acid is a highly effective virulence strategy for many pathogens (Williams, 2011). Downstream signalling from the calcium influx appears to be threshold gated by concentration as opposed to spiking, or a unique calcium signature.

Decisive evidence for the identity of the Ca^{2+} channel or channels is currently missing. Although a growing body of research is implicating a number of CNGC's in PTI, and the functional Ca^{2+} channel in PTI may well be a hetero-tetrameric channel composed of different CNGCs, of which *DND1* and 2 are the strongest candidates. *CNGC2*, also known as DEFENCE NO DEATH 1, was previously reported as being essential for Ca^{2+} influx and nitric oxide production in response to LPS (Ali, 2007). In the study however *DND1* knockouts did not directly attenuate flg22 triggered responses. In *A. thaliana*, *DND1* and *DND2* both form a distinctive clade amongst the other CNGCs (Ma, 2011), and both *DND1* and 2 have a strange auto-immune phenotype, giving rise to the name "defence no death". Knockouts in either gene result in changes to H_2O_2 production during effector-triggered HR, with elevated ROS that does not result in cell death, spontaneous lesion formation, and other markers of constitutive defence including elevated SA levels and expression of PR1 (Clough,2000; Jurkowski, 2004). This results in a general elevation in resistance to non-adapted pathogens (Qi, 2010; Genger, 2008). Interestingly, a fusion of *CNGC11* and 12, a gain of function mutant labelled *CPR22*, also results in defence no death like symptoms (Yoshioka, 2006).

In animal systems, *CNGCs* form a function channel protein at the cell membrane by interacting to form homo and heterotetrameric units (Ali, 2007). Recently, Chin et al (2013), demonstrated that *DND1* and 2 are both capable of forming homotetramers, and hetero-tetramers with each other in-planta, when expressed in *N. benthamiana*. As part of this study, they also demonstrated a novel role for *DND1* and 2 in regulating flowering time. *DND1* and 2 are predicted to mediate Ca^{2+} and K^+ ion transport (Leng, 2002), and *DND1* knock outs show hypersensitivity to elevated Ca^{2+} (Chin, 2013). Part of the Chin et al (2013) study was the mutagenisation of the *DND1* background and identification of REPRESSOR OF DEFENCE NO DEATH 1 (*RDD1*), which removed all of the *DND1* defence related phenotypes apart from sensitivity to toxic levels of Ca^{2+} . The disparate phenotypes of *DND1* being genetically separable is further evidence for the *CNGCs* status as a guarded protein, although this hypothesis is not directly tested in Chin et al 2013.

As the possibility for heterotetrameric channels exist, and as crossing KOs in different *CNGCs* usually results in seedling mortality, identifying a clear role for the *CNGCs* in defence has been thus far been difficult. The *RDD1* background may help alleviate this in the future, providing a means to asses multiple *CNGC* KOs without the mortality currently seen in the *DND1/2* double knockouts.

One of the most characteristic PAMP responses studies is the oxidative burst, the rapid and transient accumulation of reactive oxygen species (ROS) within a few minutes of PAMP perception (Felix, 1999). In *A. thaliana* the primary source of apoplastic PAMP-triggered ROS production are *NADPH* oxidases at the cell membrane, of which RESPIRATORY BURST OXIDASE HOMOLOG D (*RBOHD*) is the most important (Torres, 2006). The activation of *RBOHD* during PTI requires both Ca^{2+} binding to the N-terminal EF hand domains and direct phosphorylation of the enzyme (Segonzac, 2011). Activated *RBOHD* produces superoxide (O_2^-), which is then converted to hydrogen peroxide (H_2O_2) by superoxide dismutase (Lamb, 1997). As opposed to the massive accumulation of H_2O_2 over a period of hours seen during a hypersensitive response, PAMP responsive ROS production is usually over within an hour and returns to a resting state afterwards (Lamb, 1997).

Despite being a characteristic response observed in many different plant species a functional role for the oxidative burst remains unclear (Dubreuil-Maurizi, 2011; Proels, 2010; Dunning, 2007; Nguyen, 2010; Valdez-Lopez, 2011). Suggested roles for the oxidative burst include direct anti-microbial activity, localised strengthening of the cell wall through cross-linking glycoproteins and direct activation of defence transcription (Levine, 2004; Lamb, 2009; Torres, 2010). *RBOHD* knockouts however only have a very mild susceptible phenotype to pathogens. Recently, Dubiella et al (2013) identified a novel role for ROS signalling in inducing resistance in tissues distal from PAMP treated ones. In the proposed model, ROS are the mobile messenger between cells that activates CALCIUM DEPENDENT PROTEIN KINASE 5 (*CPK5*) which in turn leads to defence gene activation and the phosphorylation of *RBOHD* in neighbouring cells to perpetuate a ROS burst across local tissues. ROS signalling then might be an essential component of local and systemic resistance but the subtleties of the signalling might be lost when lab studies predominantly inoculate vast quantities of bacteria throughout wide areas of leaf tissue, as opposed to natural infection with smaller more localised inoculum.

Recently, the steps between *FLS2* and the oxidative burst have been elucidated to a greater degree. In a resting state, *RBOHD* is found in complex with the PRRs *FLS2* and *EFR*, and upon ligand binding *BIK1* phosphorylates *RBOHD*, and releases it from the PRR complex (Kadota, 2014). The phosphorylation of *RBOHD* by *BIK1* is independent of its phosphorylation by other *CPKs*, but both appear to be required for a ROS burst, suggesting two levels of regulation of *RBOHD* are present (Dubiella, 2013; Kadota, 2014). The current model of *RBOHD* signalling is found in figure 1.3.

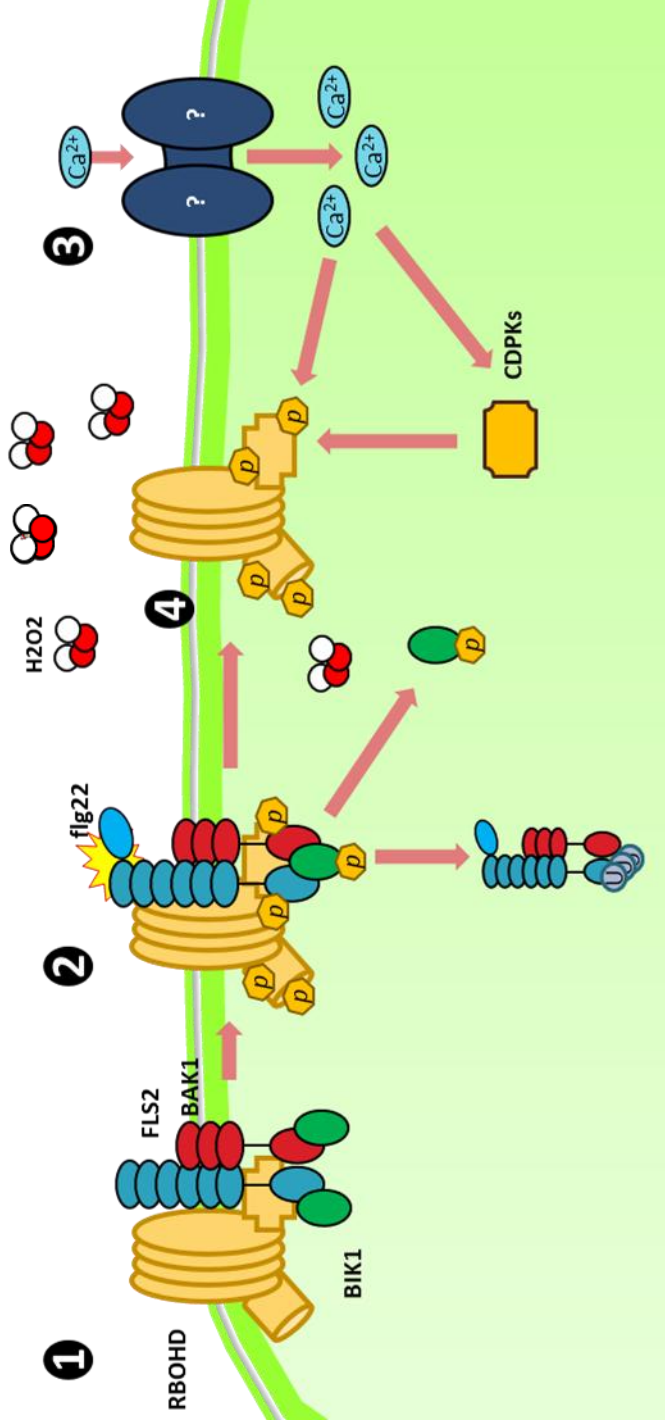


Figure 1.3 Early regulation of the oxidative burst

1) Prior to ligand binding RBOHD exists in complex with FLS2 or EFR. 2) On flg22 binding phosphorylation of RBOHD by BIK1 leads to its release from the complex. FLS2 is then endocytosed, and BIK1 is free to signal. 3) Ca^{2+} influx through as yet unidentified channels leads to the activation of CPKs, Calmodulin and both act to further phosphorylate RBOHD. 4) the phosphorylation of both BIK1 and Ca^{2+} dependent phosphatases triggers the oxidative burst. H_2O_2 then diffuses freely throughout local tissues, activating CPKs and perpetuating local defence signalling.

Within five minutes sequential phosphorylation of MAPKs is observed in response to flg22, and in *A. thaliana* there are two distinct cascades following flg22 treatment, *MEKK-MKK4/5-MPK3/6* and *MEKK1-MKK1/2-MPK4* (Nicaise, 2009). Immediate downstream targets of the phosphorylated *MPKs* include several *WRKY* transcription factors, including *WRKY33*, which act to initiate defence transcription.

Large scale transcriptional changes occur within 30 minutes of PAMP treatment. The change represents a shift into defence gene expression and is coupled with general down-regulation of many genes associated with photosynthesis and development (Navarro, 2004). Interestingly, the early transcriptional response to different PAMPs is highly similar, suggesting a stereotypical response to diverse stimuli (Libault, 2007; Boller, 2009; Zipfel, 2006; Navarro, 2004).

PAMP signalling invokes and is dependent upon multiple defence hormone signalling networks. The crosstalk between PAMP perception signalling and the classical defence hormones ethylene (ET) salicylic acid (SA) and jasmonic acid (JA) is extremely complicated, with significant spatial and temporal variation in the interactions (Spoel, 2008; Spoel, 2012). Flg22 is known to induce rapid and transient SA production (Mishina, 2007), as well as ET production within 30 minutes (Felix, 1999). *FLS2* expression is also dependent upon ET signalling (Boutrot, 2010). Neither of these hormones or JA is required for PAMP application to induce quantifiable resistance to some pathogens however (Zipfel, 2004; Tsuda, 2008). Crosstalk between PTI and auxin signalling is also observed within the first hour of PAMP perception. The antagonism between PTI and auxin is mediated by different factors including the miRNA393 which targets *TIR1*-like proteins and the effect SA has on stabilising auxin repressors (Navarro, 2006; Wang, 2007). There also exists significant unidirectional antagonism of PTI through brassinosteroid (BR) signalling, even if the underlying mechanics of the interactions are unclear (Albrecht, 2011; Lozano-Duran, 2012).

Changes in cell wall metabolism and reinforcement are common signatures of PAMP signalling. Callose deposits are matrices of polymeric β -(1-3)-glucans that form distinct papillae between the cell membrane and cell wall. The cross-linking of

beta glucans is catalysed by callose synthases, of which PMR4 is known to play a key role in responses to PAMPs (Hann et al. 2007). PMR4 mutants of *A. thaliana* show significantly more growth of *P. syringae* pv. tomato (Pto) DC3000 hrcC- than WT Col-0 highlighting the importance of callose in immunity (Hann et al. 2007). Lignification is a mechanism of cell wall reinforcement that occurs through the oxidative cross-linking of the monolignans into long chain polymers of insoluble lignin (Vanholme et al. 2010). The lignin biosynthetic genes CINNAMYL ALCOHOL DEYDROGENASE C (*CAD-C*) and CINNAMYL ALCOHOL DEYDROGENASE G (*CAD-G*) are up-regulated during interactions with certain pathogens (Tronchet et al. 2010).

1.4. The Brassicas

Brassica napus (Oilseed rape or Canola) is a good candidate for the transfer of fundamental research from *A. thaliana*. Both species are members of the *Brassicaceae*, there is a wealth of genetic and genomic resources available for brassica crop improvement and the oilseed crop is of increasing importance worldwide (Fitt, 2008). *A. thaliana* and the brassica diverged from a common ancestor over 17 MYA (fig 1.4 A; Yang et al 2006). A genome triplication event 16 MYA, and subsequent speciation produced the three diploid brassicas, *B. oleracea*, *B. rapa* and *B. nigra* (fig 1.4 B). Hybridisation of the *B. rapa* 'A' genome with the *B. oleracea* 'C' genome produced the tetraploid *B. napus* 10,000 years ago. As such, modern oilseed rape contains the complete A and C genomes of *B. rapa* and *B. oleracea* respectively. The relationships between the brassica species have been summarised over the past century by the 'Triangle of U' (fig 4B) ('U', 1935).

Although similarity to the model *A. thaliana* aids in annotation and chromosome assembly, extensive gene loss has occurred since the divergence of the *Brassicaceae* (O'Neil, 2000). For every *A. thaliana* gene we expect six copies of it within *B. napus*, but in many cases gene loss has resulted in fewer functional homologues. For

example, Yang et al (2012) identified six functional copies of FATTY ACID DESTURASE 3 (*FAD3*) in *B. napus* but only four of *FAD2*.

Genetic diversity amongst commercial varieties of *B. napus* is often considered to be very low. The species originated from hybridisation events within a limited geographical range relatively recently (Mei, 2011). Furthermore intensive breeding for oil quality and resistance traits using a limited genepool from elite lines may have reduced genetic variation considerably (Hasan, 2006).

Polyploidy within the brassicas results in genomic complexity. As such sequencing the brassicas has been difficult. There is no published and widely available *B. napus* genome as yet. The genome of *Brassica rapa*, which contributes the A genome to *B. napus*, has been published (Wang, 2011). Progress on establishing a C genome is ongoing, but is currently unavailable.

Bancroft et al (2011) developed a *B. napus* SNP-linkage map of 23,037 markers based on expressed sequence tag (EST) polymorphisms assembled into a pseudomolecule scaffolds. This unigene reference has subsequently been used for large scale mRNA seq experiments within *B. napus*, and the process has been adapted to take into account polyploidy by sorting reads between genomes by using inter-homeologous polymorphisms (Higgins, 2012).

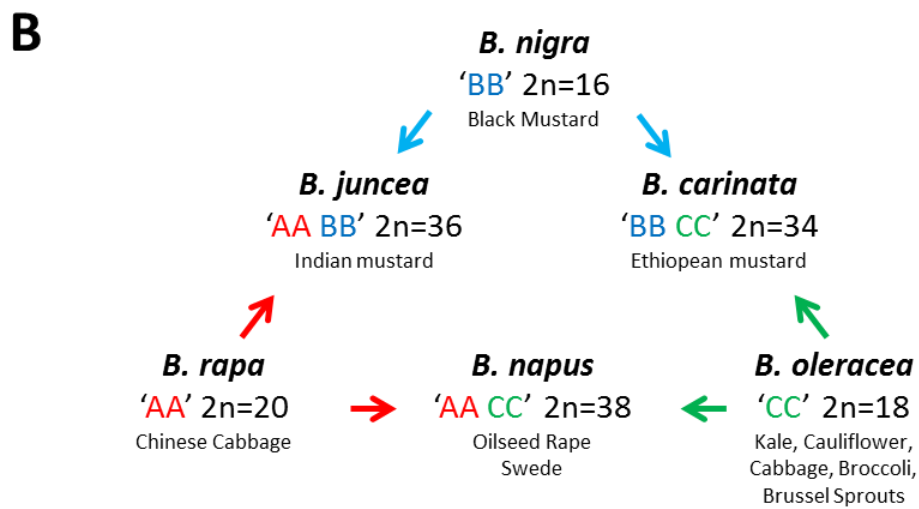
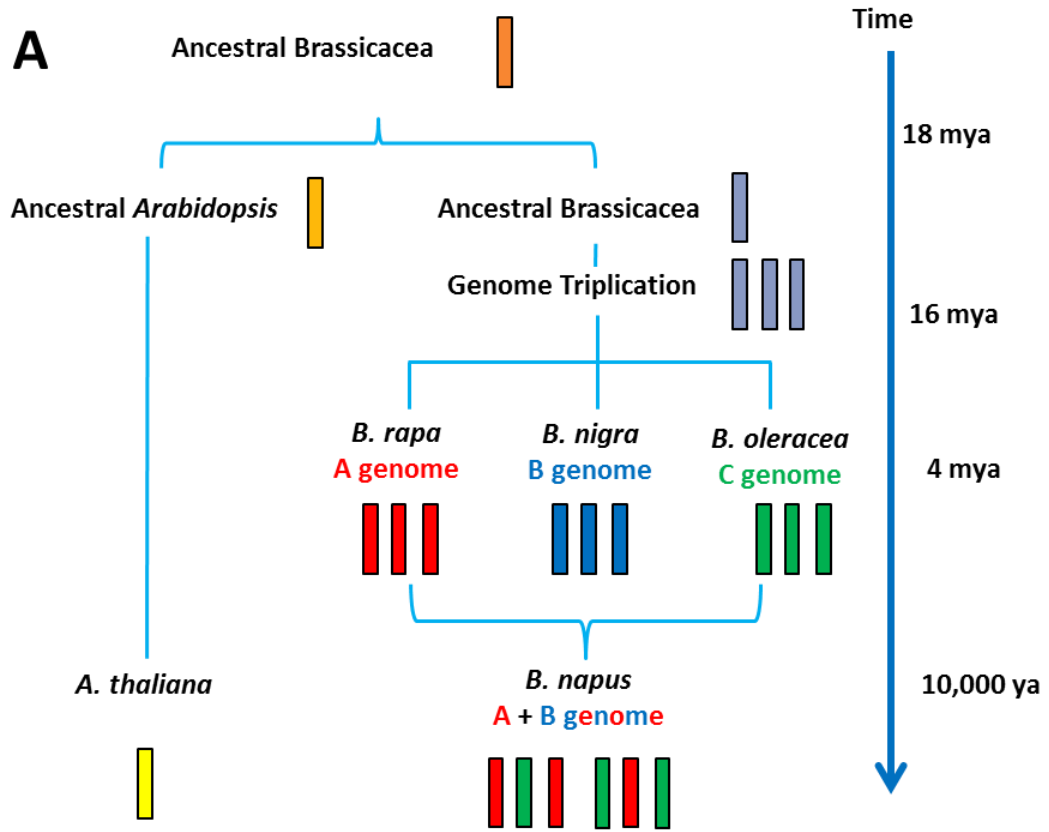


Figure 1.4 Evolution of the brassicaceae.

A) Overview of the divergence of *Arabidopsis thaliana* and the brassicas, and subsequent speciation of the diploid brassica genomes. B) The triangle of U summarising the relationships of the diploid brassicas (*rapa*, *nigra* and *oleracea*) and the allotetraploid hybridisations between them (*Juncea*, *carinata* and *napus*)

The extent of the genomic rearrangements and gene loss between *B. napus* and its progenitor species *B. rapa* and *B. oleracea* is unclear. Parkin *et al* (1995) demonstrated that synthetic *B. napus* (an interspecific hybrid of modern *rapa* and *oleracea*) when hybridizing with modern *B. napus* does display clear alignment between the progenitor and *B. napus* chromosomes, suggesting that at the chromosomal level at least there is a high homology between the species. At the molecular level however, the extent of gene-by-gene rearrangement between the species is largely unknown at present. As such, the accuracy of using the *rapa* or *oleracea* genome as a *napus* reference, or vice versa, is unknown.

A wide array of genetic resources and germplasm exist for mapping studies within the brassicas. Quantitative trait loci (QTL) mapping of defence traits is commonplace in *B. napus* and examples include QTLs for *Sclerotinia sclerotiorum* in the Huashang 5 x J7005 and the Zhonghu 821 x Bao604 crosses (Wu, 2012; Yin, 2010), *Leptosphaeria maculans* resistance QTLs in many different mapping populations (for example, Kaur, 2009; Delourme, 2004; Dion 1995) and QTLs for resistance to *Pyrenopeziza brassicae* in the Darmor x Yudal cross (Pilet, 1998). QTL mapping of resistance traits is also common in *B. oleracea*, including a QTL for *Agrobacterium tumefaciens* susceptibility in the double haploid (DH) A12 x Green Duke cross (Sparrow, 2004). The cross identified the line 'AG1012' as being highly susceptible to *Agrobacterium*, and this has since become a standard transformation line for *B. oleracea*. This cross might be particularly relevant for investigating PTI as the QTL governs resistance to a non-host pathogen.

The OREGIN diversity set is a collection of oilseed rape germplasm displaying differential quality characteristics in flowering time, oil content, pod shatter and resistance (fig 1.5, <http://www.oregin.info>). Mapping populations for these diverse traits have been built up and all of them share a common female parent, Temple. As such the variety Temple could be considered a Col-0 for *B. napus*.

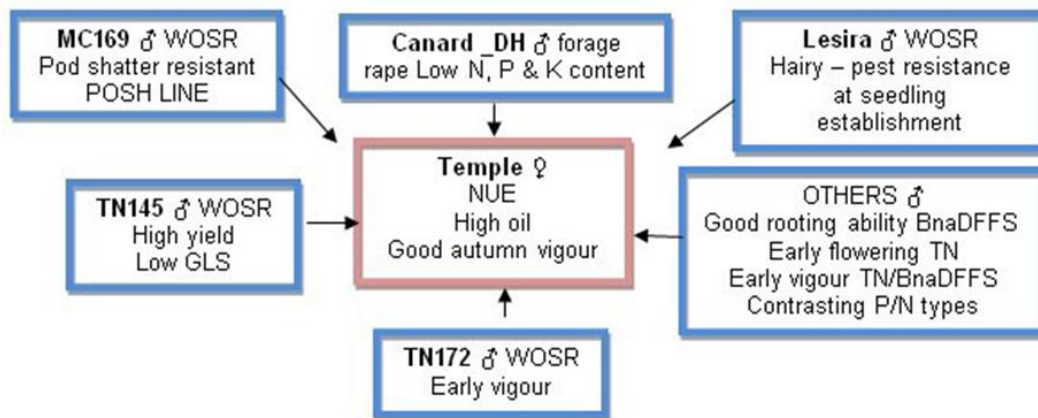


Figure 1.5 Genotypes used in OREGIN diversity set.
The mapping project has Temple as the common parent in multiple crosses.

mRNA sequencing is increasingly being used within the brassicas for large scale transcriptomics and sequencing experiments. Using the unigene reference developed by Higgins et al (2012), Illumina sequencing of 84 diverse *B. napus* accessions enabled a large scale genome wide association study (GWAS) of oil quality traits (Harper, 2012). Because the SNP reference for the GWAS was based around mRNA seq, expression level of every unigene was also collated. This transcription information could be used in a further association study with the phenotypic data to identify novel loci where expression directly correlated with the trait of interest. As the first example of its kind, Harper *et al.* termed the process “associative transcriptomics” and the process might become commonplace in crop science where there is often a lack of genomic information and mRNA seq can quickly, and increasingly affordably, identify polymorphism amongst a population. Whether the association mapping panel developed by Harper *et al.* can be used to characterise quantitative resistance and PTI linked traits remains to be seen.

There is a need to identify sources of durable and effective partial resistance to common *Brassica* pathogens such as *Leptosphaeria maculans*, *Sclerotinia sclerotiorum* and *Botrytis cinerea* (Aubertot et al., 2006). Although strain-specific resistance (*R*) genes provide extremely strong levels of disease control, this effectiveness can be rapidly lost, for example, in the breakdown of *Rlm1*-mediated resistance within five years of deployment (Sprague, 2006). Conversely, lines with strong quantitative disease resistance have often been deployed for longer periods of time, such as in the European cultivar ‘Jet Neuf’ which was widely grown for over twenty years and is still used in breeding programs today (Delourme, 2006). Developing the tools to identify potential sources of durable quantitative resistance has proven difficult however.

Although limited work has been done assaying natural variation in PAMP responses, assays such as the measurement of oxidative burst have been utilised to map key components of PTI within crop species (Valdés-López et al. 2011). Substantial variation exists in *FLS2* abundance and specific binding capacity for flg22 between a range of different *A. thaliana* ecotypes and other species of the *Brassicaceae*, and this variation has been shown to directly correlate with seedling growth inhibition

by flg22 (Vetter, 2012). Furthermore sequence analysis of *FLS2* within the *Brassicaceae* revealed higher variation in the LRR domain between *Brassicas* (56% universal amino acid identify) than in all sequenced *A. thaliana* ecotypes (98.8% identity) suggesting the brassicas might represent diversity in PTI not present in the model system (Dunning et al. 2007).

1.5. Research Aims

The research presented here is part of larger direction to understand variation in PAMP-triggered Immunity at the population level, to transfer fundamental knowledge of immunity from models into crop species and to use this understanding and modern technology to produce more pathogen resistant crops in the future. The central hypothesis underlying this wider body of work is that PTI is a major determinant of quantitative resistance in the field. Although likely to be a major factor in most plant-pathogen interactions, the contribution of 'PTI' from a scientific model to 'quantitative resistance' as it is observed in the field remains to be determined. There are numerous difficulties within this overarching hypothesis. Primarily this hypothesis cannot be tested directly: studying PTI in abstract from all other aspects of defence and development, particularly when so many unknown PAMPs and PRRs are likely to exist, is impossible. This central hypothesis is beyond the scope of a single research project, and has numerous aspects that cannot be addressed here.

There are several smaller unknowns within the current literature that this thesis is attempting to address. At the outset of this project there had been no reported studies using the PAMPs flg22, elf18 and CSC in *B. napus*. Whether or not the brassicas respond to the same PAMPs as *A. thaliana* is not clear, although chitin treatments are known to have an effect on field resistance. There have been no previous reports of measuring PAMP responses in brassica, although many pathogen response assays might be applicable to PAMP treatment as well, and whether *B. napus* responds to PAMPs in the same manner as *A. thaliana* has not been reported. There were no published PAMP responsive genes identified and relatively little work on whole-genome transcriptional responses to PAMPs or pathogens have emerged.

Surveying natural variation in PAMP responses had not been reported, even in *A. thaliana*, at the outset of the project. Whether or not natural variation in PTI can be used in a GWAS to identify meaningful genetic variation that gives rise to diverse

resistance phenotypes also needs to be addressed. The usefulness of the Harper *et al.* (2012) association mapping panel for characterising truly quantitative traits is also unknown. The involvement of PTI in previously characterised QTLs for resistance, particularly the *Agrobacterium* resistance QTL on C9 of *B. oleracea* (Sparrow, 2009), is unknown. Why the *B. oleracea* line AG1012 is notably susceptible to multiple non-host pathogens is also a challenge to be addressed (Sparrow, 2009).

The extent PAMP perception and PTI contribute to partial resistance in the field is also unclear. Whether or not assays recording PAMP response can predict pathogen resistance is also unknown.

1.6. Research Questions:

1. Can methods to study PTI in *A.thaliana* be used in *B. napus*?
2. What transcriptional changes are seen upon PAMP treatment in *B. napus*?
How is the transcriptional response of a tetraploid organised between homeologous genomes? How does the gene expression profile of *B. napus* compare to *A. thaliana*?
3. Are PAMP-responses polymorphic between genotypes of *B. napus*?
4. Can PAMP responses predict disease resistance scores in a population of *B. napus*?
5. Is the susceptibility of the *B. oleracea* line AG1012 and its parent GD a result of an impairment in PTI?
6. Can genes regulating PAMP-responses and disease resistance within *Brassica napus* populations be identified using a GWAS approach?

1.7. Research Objectives:

With these questions in mind, the research presented here had the following objectives:

1) Develop a toolkit of assays to study PTI in *Brassica* species.

The assays should cover early molecular signalling events, metabolomics changes, cell wall reinforcements and PAMP-induced resistance. The body of work should produce a reference useable by brassica researchers in the future.

2) Use mRNA-seq to capture the transcriptional changes PAMP treatment induces in *Brassica napus*.

The PAMP-induced transcriptome can act as a reference for *Brassica* research in the future, and consideration about how the PAMP induced transcriptome is regulated as a result of tetraploidy needs to be taken into account.

3) Assess the natural variation in PAMP responses between *Brassica* lines.

The extent to which PAMP responses are polymorphic amongst populations of *B. napus* are unknown. The possibility that PAMP responses could predict resistance needs to be assessed.

4) Perform a GWAS of PAMP responses in *B. napus*.

Test the feasibility of using the Harper *et al.* (2012) *B. napus* mapping panel for PTI and resistance traits. Identify the underlying genetic polymorphism that gives rise to any variation in PTI.

5) Map PAMP responses in the *B. oleracea* A12 x GD cross

Understand why the line AG1012 has high susceptibility to non-host pathogens, and assess the possibility this is due to impairment in PTI. Use QTL mapping to identify PTI relevant polymorphism in the cross, and

produce a candidate gene list by combining next generation sequencing and fine mapping.

Chapter 2 : Materials and Methods

2.1. Materials

2.1.1 Plant materials and growth conditions

Brassica napus

Seeds for all *B. napus* cultivars from the OREGIN (Oilseed Rape Genetic Improvement Network) diversity project (<http://www.oregin.info>), and seed from the association mapping panel of diverse *B. napus* lines was kindly provided by Colin Morgan (JIC, Norwich, UK).

Most *B. napus* used in this study was grown in a lit glasshouse with a 16 hour photoperiod at 18°C/12°C day/night temperatures at approximately 100 $\mu\text{mol m}^{-2} \text{s}^{-1}$. *B. napus* from the association mapping panel were grown in containment glasshouses to limit pathogen exposure. Glasshouse grown plants were maintained by George Aris and Damian Alger. Some experiments (as described where relevant) used *B. napus* grown in controlled environment rooms (CER) or growth cabinets set to a 16 hour photoperiod with 18°C/12°C day/night temperatures at 500 $\mu\text{mol m}^{-2} \text{s}^{-1}$, unless otherwise stated. All *B. napus* grown in growth cabinets were surface sterilised in 10% sodium hypochlorite for five minutes followed by repeated (at least 3 times) rinsing in 10% EtOH before being pre-germinated on 1% MS media for five days prior to transplant into soil.

B. napus used in seedling growth inhibition experiments were cultured in liquid MS media on a shaker within a growth cabinet set to a 16 hour photoperiod at 18°C/12°C day/night temperatures.

B. oleracea

Seed from the DH A12xGD *B. oleracea* mapping population were kindly provided by Penny Sparrow and Judith Irwin (JIC, Norwich, UK). Substitution lines of A12 were kindly provided by Dr Graham Teakle, (Warwick HRI, Coventry UK) *B. oleracea* growth conditions and surface sterilisation were as described above for *B. napus*.

Arabidopsis thaliana

All *A. thaliana* seed of the Col-0 ecotype were provided by Henk-jan Schoonbeek (JIC, Norwich, UK). All SALK lines used in the study were ordered from (NASC,

Nottingham, UK). All *A. thaliana* used in experiments in this study were grown in growth cabinets set to a 16 hour photoperiod at 18°C/12°C day/night temperatures unless otherwise stated.

A. thaliana seed was surfaced sterilised as described above for *B. napus*. *A. thaliana* seed were stratified in H₂O for two days at 4°C before being pre-germinated on 1% Murashige and Skoog (MS) media. After 3-5 days they were then transferred to *A. thaliana* mix soil.

2.1.2 Pathogens used and culture conditions

Pseudomonas syringae pv. tomato

PTO strains DC3000 and DC3000 hrcC- luxCDABE (Fan et al., 2008) were kindly provided by Dr Jun Fan (JIC, Norwich, UK). All *P. syringae* were streaked from glycerol stocks on plates of Kings Broth (KB) media with or without selection and placed in an incubator set to 28°C for two days prior to use in disease assays.

Botrytis cinerea

Botrytis cinerea strain BO5.10 and a GREEN FLUORESCENT PROTEIN (GFP) tagged strain in the same background was kindly provided by Henk-jan Schoonbeek (JIC, Norwich, UK). All *B. cinerea* strains were grown on Potato Dextrose agar (PDA) at 21°C with no selection. Some strains were cultured on 1/5th PDA as described in the disease assays below.

Sclerotinia sclerotiorum

Sclerotinia sclerotiorum, isolated from pea plants in 2009, was provided by Jane Thomas (NIAB, Cambridge, UK). *Sclerotinia* was cultured from dried sclerotia placed on PDA plates grown at 21°C for three days prior to use in a disease assay.

2.1.3 Culture Media used

Some of the media produced in this study was produced by the JIC media kitchen. Most plates were 1% agar unless otherwise stated.

KB media

Proteose peptone	20g/L
Glycerol	10mL
K ₂ HPO ₄	1.6g/L
pH 7.2 (with NaOH)	

LB media

Yeast extract	5g/L
NaCl	10g/L
Tryptone	10g/L
pH 7 (with NaOH)	

PDA

Potato Dectrose Agar 39g/L

MS media

Murashige and Skoog medium 4.41g/L
(including vitamins)
Sucrose 30g/L

2.1.4 Antibiotics

Where necessary media was supplemented with antibiotics at the following final concentrations:

Kanamycin	50mg/L
Gentamcin	25mg/L
Rifampicin	50mg/L
Streptomycin	50mg/L

2.1.5 Plant Growth Mixes

Peat and Sand

85% Fine Peat
15% Grit
2.7kg/m³ Osmocote 3-4 months
Wetting Agent
4kg/m³ Maglime
1kg PG Mix

Cereal mix

40% Medium Grade Peat
40% Sterilised Soil
20% Horticultural Grit

1.3kg/m³ PG Mix 14-16-18 + Te Base Fertiliser
1kg/m³ Osmocote Mini 16-8-11 2mg + Te 0.02% B
Wetting Agent
3kg/m³ Maglime
300g/m³ Exemptor

2.1.6 Chemicals

General Chemicals

General purpose chemicals were from Sigma-Aldrich (St. Louis, MO, USA) unless otherwise stated.

PAMPs

Flg22 (QRLSTGSRINSAKDDAAGLQIA) and elf18 (Ac-SKEKFERTKPHVNVGTIG) peptides were ordered from Peptron (<http://www.peptron.co.kr>, Korea) and re-suspended in sterile H₂O. Peptides were divided between 1 mM and 100 µM aliquots and stored at -20°C before use.

The chitin used in this study was Crab shell chitin (CSC) supplied as NA-COS-Y by Yaizu Suisankagaku Industry CO (Yaizu, Japan). The CSC was dissolved in sterile H₂O (10% w::v) on a shaker overnight and autoclaved before being kept in 10 or 100g/L aliquots at -20°C.

Buffers

Protein extraction (Lacus Buffer)

TRIS-HCl 50 mM pH7.5
10 mM MgCl₂
15 mM EGTA
100 mM NaCl
2 mM DTT
1 mM NaF
1 mM NaMO
0.5 mM NaVO₃
30 mM β-glycero-phosphate
0.1% NP-40 with 0.5 mM PMSF
1% protease inhibitor cocktail

DNA Extraction (Shorty buffer)

0.2M Tris/HCL pH 9
0.4M LiCl
0.025M EDTA
1% SDS

Gel Electrophoresis Loading Buffer

0.1M EDTA
0.1% bromophenol blue
0.1% xylene cyanol
30% glycerol

2.1.7 Primer design and synthesis

Primers used were either previously published as working in *Brassica* species or were designed using the software Primer3 v4.0 (Untergrasser, 2007, 2012). Genotyping primers were designed using the SALK T-DNA primer design tool (<http://signal.salk.edu/tdnaprimers.2.html>). KBioscience Competitive Allele-Specific polymerase chain reaction (KASPar) primers were designed with assistance from Judith Irwin (JIC, Norwich). All primers were ordered from SigmaGenosys (Sigma). A Full list of primers used in this study can be found in tables 1-3.

Gene	Direction	Primer Sequence	Reference
BnMPK3	Forward	GAGATGTGGTTCCTCCACCA	Jianwei, 2009
	Reverse	ACTTGAGCCCTCGAAGAAGC	
BnMPK4	Forward	GCCAATGTGTTACACCCGAGATC	Jianwei, 2009
	Reverse	CCGAAATCCCCAAGCTTTAGA	
BnWRKY33	Forward	GGACTCATCGTTTGGTTCTTCTTTT	Jianwei, 2009
	Reverse	CGTTTTGGTTACGCTATGAACAGTC	
BnEF1a	Forward	ATACCAGGCTTGAGCATAACCG	Jianwei, 2009
	Reverse	GCCAAAGAGGCCATCAGACAA	
BnFLS2	Forward	AAAAGTCGACATGAAGTTACTCTCAAAGAC	Dunning, 2007
	Reverse	AAGGATCCCTAAACTTCTCGATCCTCG	

Table 1 Primers used to investigate expression of *Brassica napus* PAMP responsive marker genes at 1 and 3 hours post PAMP treatment.

Gene	SALK Accession	Direction	Primer Sequence
AtDND1	N681039	Forward	TTCGGCACAACTAACCAAAAC
	N681039	Reverse	CTTTCCCGGAAAAATCACTC
AtDND1	N681220	Forward	ATATCCAACGTGCTTGTCGG
	N681220	Reverse	CTTTCCATTCAACTAGCTGCG
AtDND1	N684864	Forward	ACGCTGAATTTTATCCAACCC
	N684864	Reverse	AAATAGAGGAACCACCATGGG
AtDND2	N6524	Forward	TCCAAATGGGTCGAGCAT
	N6524	Reverse	GCAATCTTGAACCTGAATCC
AtDND2	N318552	Forward	TCTCTGTGTGCATGCGTTAG
	N318552	Reverse	CACACGAAACATGATTAGGTCAG
AtDND2	N66537	Forward	CTGTTGTGCTCTCCAAATCC
	N66537	Reverse	TCACATGGACCTTTCCATTG

Border Primer	T-DNA Border Primer Sequence
LBb1	TTCGGCACAACTAACCAAAAC
LBb1.3	CTTTCCCGGAAAAATCACTC

Table 3 Primers used in genotyping SALK insertion lines.

2.2. General Molecular Methods

2.2.1 Plant genomic DNA isolation

50mg of leaf tissue homogenised using a TissueLyser LT (Qiagen, West Sussex, UK). DNA was isolated either using a DNeasy Plant Mini Kit (Qiagen) according to manufacturer's instructions or via a method supplied by Dr Jun Fan. 50ml of Shorty buffer was added to the homogenised leaf tissue before a second homogenisation step. A further 450ml of Shorty buffer was then added and the samples were centrifuged at 13,000 rpm for 5 mins. 350mls of the supernatant was transferred to a fresh tube containing 350ml of isopropanol before a further centrifugation at 13,000 RPM for 5 mins. The supernatant was decanted away and the pellet was left to dry for 2 minutes. The dry pellet was re-suspended in 100ml TE and was left on a shaker for 30 mins at room temperature. The gDNA was diluted 10x in water, with 4ul of the diluted mix used in PCR reactions.

2.2.2 Plant RNA isolation and quantitative RT-PCR

Leaf discs (d=4mm) from five week old plants were vacuum-infiltrated with H₂O or PAMP solution, sampled and flash frozen in liquid nitrogen at various time points thereafter. RNA was extracted from homogenised tissue using a TissueLyser LT (Qiagen) and purified using an RNeasy plant mini-kit (Qiagen) according to manufacturer's instructions. RNA samples were treated with Turbo DNA-free DNase (Ambion) according to manufacturer's instructions.

2.2.3 First strand cDNA synthesis

cDNA was synthesised from 2 µg total RNA in a 20µl reaction volume. 200ng of oligo(dT) or 2 pmol of gene specific primers and 1µl 10mM dNTP mix were added to the extracted RNA and diluted to 13 µl with sterile water. The mixture was heated to 65°C for five minutes before being incubated on ice for at least one minute. The contents of the tube were collected by brief centrifugation and 4µl of 5X First strand buffer (Invitrogen), 1µl 0.1M DTT, 1µl of RNaseOUT Recombinant RNase Inhibitor (Invitrogen) and 1µl Superscript III RT (Invitrogen) were added to each of

the samples. The samples were incubated at 50°C for thirty minutes, before being deactivated by heating at 70°C for fifteen minutes.

2.2.4 Quantification of nucleic acids

DNA was quantified using a spectrophotometer measuring the OD₂₆₀ of the sample in water. RNA was quantified using a Picodrop (Picodrop Ltd, Cambridge, UK) or a NanoDrop ND-1000 (Thermo Scientific, Wilmington, DE, USA) by measuring the OD₂₆₀ / OD₂₈₀ of the Sample.

2.2.5 qRT-PCR

20µl reaction volume PCRs were setup in a 96-well white PCR plate (Thermo Scientific, UK) and qRT-PCR was performed using a Chromo 4 qPCR machine (Bio-Rad) with SYBR Green RT-PCR Master Mix (Sigma). Relative transcript levels were determined at each time point from cycle threshold (CT) values according to the $2^{-\Delta CT}$ method using EF1a as a reference. Fold-induction was determined by comparing transcript levels in PAMP-treated samples with water treated controls.

2.2.6 PCR

PCR was performed using Taq DNA Polymerase (Qiagen) in a final reaction volume of 20µl (25 ng DNA template, 0.5 µM primers, 0.2 x polymerase buffer, 1.25 units Taq polymerase, 9.2 mM dNTPs, and water to 20 µl). PCR had an initial denaturation step at 94°C for 2 minutes followed by 35 cycles of 94°C for 15 s, 58°C for 15s, 72°C for 1 minute. The PCR ended with a final elongation at 72°C for 10 minutes. Visualisation of nucleic acids was achieved by adding 6x loading buffer to DNA samples before loading onto an agarose gel containing ethidium bromide.

2.2.7 Genotyping

SALK T-DNA insertion lines were genotyped using gene specific primers and a T-DNA insertion specific border primer LBb1 (Table 3). When PCR products were run on an agarose gel single bands indicated homozygosity with and without the insert and double bands indicated heterozygosity.

2.3. PAMP-Response Assays

2.3.1 Oxidative burst

ROS measurement was performed with a luminol/peroxidase-based assay essentially as described in Felix et al. (1999). Leaf discs (d=4 mm) were cut with a cork borer from 5-week-old *B. napus* plants or 4 week old *A. thaliana* plants and incubated in 200 μ L sterile water in a 96-well plate for 24hr. The water was drained and replaced by a solution containing 34 mg/L (0.2 nM) luminol, 20 mg/l horseradish peroxidase (HRP) and the PAMP to be tested. The luminescence was recorded as photon count in 100 reads over a 40-minute period using a Varioskan Flash plate reader (Thermo Fisher Scientific, Waltham, MA, USA).

2.3.2 MAP kinase phosphorylation

Leaf discs from 5-week-old *B. napus* leaves were vacuum-infiltrated with sterile water and incubated at room temperature. After 16 hours, PAMPs (flg22 1 μ M, elf18 1 μ M or CSC 1g/L) or an equivalent volume of water was added. Samples were taken at various time points after treatment and flash frozen in liquid nitrogen. Frozen samples were kept on ice and ground using a TissueLyser LT (Qiagen) and thawed in Lacus buffer with 100 nM Calyculin A (LC laboratories <http://www.lclabs.com>, Woburn, MA, USA) added immediately before use. The homogenates were centrifuged for 30 minutes at 16,000 g and filtered through Miracloth. Total protein levels were quantified by Bradford assay. Samples (40 μ g) were loaded in 3xLDS loading buffer (Invitrogen), separated by SDS-PAGE on a 12% acrylamide gel (Invitrogen) and transferred to a nitrocellulose membrane with an I-blot transfer system (Invitrogen). Total protein was visualised by staining with Ponceau solution. The blot was blocked with 5% (w/v) BSA (Sigma) in TBS-Tween (0.1%) for 2 hours before three washes in TBS-Tween (0.1%). Phospho-p44/42 MAPK (Erk1/2) (Thr202/Tyr204) rabbit monoclonal antibodies (NEB) diluted 1:2000 in TBS were incubated overnight according to manufacturer's protocol, followed by

an anti-rabbit-HRP conjugated antibody (Sigma) for two hours. The blot was revealed with ECL Plus Western Blotting Detection System (GE healthcare) with a 2-minute exposure.

2.3.3 Callose staining

Leaves were infiltrated with PAMP solution or H₂O using a 1 ml needleless syringe and leaf discs (d=4mm) were taken after 24 hours from within the infiltrated zone, but distal from the wounded inoculation site. The discs were cleared with 70% EtOH for 1 hour, 95% EtOH with 1% chloroform for 16 hours, then 100% EtOH for 2 hours. The final wash in 100% EtOH was repeated until all chlorophyll was removed. The samples were rehydrated sequentially for 30 min each in 70% EtOH, 50% EtOH and 67 mM K₂HPO₄ at pH 11. Callose was stained in a 0.01% (w/v) aniline blue solution in 67 mM K₂HPO₄ at pH 9.5 for 1 hour. The leaf discs were mounted in 70% glycerol/30% stain, and viewed under a Nikon Eclipse 800 microscope. Callose foci within the frame of a single image (magnification x10) were counted.

2.3.4 PAMP Induced Lignification

Wounded Leaf Surface Lignin Stain

Leaf discs (d=10mm) or leaf strips (approximately 60x30mm) were surface sterilised with 70% EtOH and rinsed with H₂O in sterile conditions. Each leaf disc was wounded using forceps and transferred to 30 ml H₂O or PAMP solution overnight. Leaf discs were cleared as above (see callose deposition) and transferred to a 2% (w/v) phloroglucinol (Pomar et al., 2002) solution in 20% HCl. The stained leaf discs were photographed after 5 minutes.

Seedling Root Lignin Staining

Sterile seeds were pre-germinated on 0.6% MS media for 7 days before being transferred to liquid MS media. After 1 day in liquid media the respective treatment of H₂O +/- Isoxaben, or PAMP (elf18/flg22/CSC) +/- Isoxaben was added and the seedlings were incubated for 24 hours at room temperature. The seedlings were then stained with 2% phloroglucinol in 20% HCl for 3 minutes and mounted in 7:3

(v:v) glycerol : HCL. The stains were observed under the using the Nikon Eclipse 800 brightfield microscope.

Thioglycolic acid precipitation

Leaf discs (d=10mm) were surface sterilised with 70% EtOH and rinsed with H₂O in sterile conditions. Samples were vacuum-infiltrated with H₂O or various PAMP solutions and floated in water until sampling at various time points after infiltration. Pigmentation and soluble phenolics were removed through repeated incubation with absolute methanol over a course of three days. Following this the cleared tissue was dried at 55°C for one day before the dry weight of the sample was recorded. Each sample was suspended in 0.5ml 10% thioglycolic acid (TGA) in 2M HCL before being heated for 4 hours at 100°C. These were then vortexed, transferred to a fresh tube and centrifuged at 14,000 g for 15 minutes. The supernatant was decanted and the pellet re-suspended in 0.5ml H₂O before being centrifuged again at 14,000g for 10 minutes. The resulting supernatant was then decanted out and the pellet was then suspended in 0.5ml 1M NaOH and vortexed to solubilise the TGA derivatives. These were incubated overnight at 4°C. The next day the solutions were centrifuged at 14,000g for ten minutes before the supernatants were decanted into a fresh tube along with 0.2ml concentrated HCL. These were kept on ice to precipitate for 1 hour before the supernatant was decanted. The pellet was then dissolved in 1ml 0.5M NaOH, and absorbance at 486nm was recorded, with final data presented as absorbance at 486 nm per gram of sample dry weight.

2.3.5 Seedling Growth Inhibition

Seeds were pre-germinated on 1% water agar for 48 hours before transfer to 250 ml glass flasks containing 200 ml liquid MS media. PAMP solutions or water were added and the seedlings left shaking (60 RPM) at 21°C with 12 hour light and 12 hours dark conditions. Fresh weight was recorded 10 days after transfer to liquid media.

2.4. Pathology Methods

2.4.1 PAMP-induced resistance

Where the intent was to assess the effect a prior PAMP treatment had on subsequent pathogen growth compared to a water control, PAMPs (typically flg22 100nM, elf18 100nM CSC 1g/L) were either vacuum-infiltrated or syringe-infiltrated 24 hours before pathogen inoculation. In the case of stem inoculations, 5µl of PAMP solution was applied to a wounded site 24hr prior to inoculation.

2.4.2 *Botrytis cinerea*

Inoculum Preparation

Fresh PDA plates of *B. cinerea* were prepared from glycerol stocks maintained at -70°C. When a matt of aerial hyphae was clearly visible 10ml 0.05% tween 20 was added, and the spores and hyphae disturbed by abrasion with the flat side of a glass pipette. The spore solution was collected and spore density counted with a haemocytometer. Suspensions were usually diluted to approximately 1×10^8 spores/ml for storage at 4°C. The spore solutions were stored at 4°C and used 3 days of collection.

Leaf Disc Assay

A 200 µl suspension of 2.5×10^6 spores/ml was spread evenly on a fresh plate of 1/5th potato dextrose agar (PDA) and incubated at 21°C. Twenty-four hours later, agar plugs (d= 4mm) from the colony were transferred to the centre of 20mm leaf discs which were incubated in closed (but not tightly sealed) square petri dishes in a growth cabinet with high humidity at constant 21°C. At least 12 leaf discs were used per treatment/genotype/time point in each experiment. Lesion size was recorded 3dpi.

Whole Leaf Assay

Where the whole leaf was utilised for disease assay, leaves of *B. napus* were severed at the stem and immediately wrapped in damp blue tissue paper. Leaves were arranged on top of petri dishes within a large covered tray filled with wet

tissue paper. 5µL droplets of a 2.5×10^5 spore solution in ½ PDB were placed on the adaxial surface of the leaf. The sealed tray was placed in a growth cabinet with high humidity at constant 21°C. Lesion size was recorded 3dpi.

96-well Plate Based Quantification of GFP Tagged B. cinerea

Strains of *B. cinerea* expressing GFP under a constitutive promoter were quantified fluorometrically during assays looking at the effect of host derived metabolites on pathogens. In this case 5µl of a 2.5×10^5 spores/ml suspension were pipetted into a 96 well plate filled with various metabolite samples in 50% PDB. Fluorescence at 512nm after excitation at 471nm was recorded daily over 3 days using a Varioskan Flash plate reader (Thermo Fisher Scientific, Waltham, MA, USA).

2.4.3 *Sclerotinia sclerotiorum*

Inoculum Preparation

Sclerotinia sclerotiorum were stored as dried sclerot, and cultured on 1/5th PDA plates with a dried sclerot placed in the centre. Spore suspensions were prepared as described above for *B. cinerea*, from plates

Leaf Disc Assay

The assay was performed as described above for *B. cinerea* leaf disc assays but was scored on a scale of 1-5. The scale corresponds to:

- I. No lesion
- II. No spreading lesion beyond inoculated region
- III. Lesion $\varnothing \leq 10\text{mm}$,
- IV. Lesion $\varnothing > 10\text{mm}$, emergence of some aerial hyphae.
- V. 5- Leaf disc fully consumed by pathogen ($\varnothing = 20\text{mm}$) with extensive aerial hyphae

Disease was usually scored 3dpi. It was necessary to closely monitor symptom progression – in some cases measurements had to be made 2dpi after very rapid pathogen growth.

2.4.4 *Pseudomonas syringae*

Inoculum Preparation and Infiltration

All *P. syringae* strains were cultured on Kings Broth (KB) agar with 25 mg/ml kanamycin and 50 mg/ml rifampicin for two days at 28°C. A sample of the bacteria was transferred to liquid KB with the same antibiotics and incubated for 16 hours at 200 rpm and 28°C. The bacterial solution was diluted to OD600 of 0.02 in 10 mM MgCl₂ and vacuum-infiltrated into leaf discs.

CFU counting

Leaf discs (0.5mm) in diameter were placed in 1ml of KB broth and ground using a GenoGrinder 2000 (Thomas Scientific, NJ, USA). Leaf disc suspensions were diluted serially with KB and plated on KB agar plates with selection. Plates were incubated at 28°C with colony numbers counted the next day.

Luminometric Quantification of *P. syringae*

Luminometric quantification of the *Pst* DC3000 luxCDABE and *Pst* DC3000 hrcC-luxCDABE strains was recorded by measuring emitted photons over 3 seconds from a 5mm diameter leaf disc in a FB12 Luminometer (Berthold Detection Systems, Pforzheim, Germany).

96-well Luminometric Quantification of *P. syringae*

In larger assays involving infiltrating Lux tagged strains of *P. syringae* a 96 well plate assay was used. Leaf discs (5mm diameter) were floated on 100µL H₂O after vacuum infiltration (as described above). The luminescence was recorded as photon count in 2 seconds per well using a Varioskan Flash plate reader (Thermo Fisher Scientific, Waltham, MA, USA).

2.5. Metabolomic Methods

2.5.1 Metabolite Extractions

Crude Metabolite Extraction

The method of metabolite extraction was based on that described by Meuwley and Metraux (1993) which was designed to maximise the amount of free and conjugated SA and camalexin extracted. Approximately 150mg (or 4x4mm leaf discs) were placed in a 2ml round bottomed Eppendorf tube, flash frozen in liquid nitrogen and then homogenised tissue using a TissueLyser LT (Qiagen). This was suspended in 500µL EtOH and 100µL of the internal standard, ortho-anisic acid at 1ng/µL. The samples were homogenised again using the TissueLyser LT (Qiagen) before being centrifuged for 5 mins at 12,000g. The supernatant was decanted into a fresh tube and the pellet was homogenised again with 500µL of 90% MeOH. The methanol suspension was then centrifuged for 5 mins at 12,000g with the resulting supernatant pooled into the ethanol extraction. The pellets were discarded. The organic solvents were evaporated under reduced pressure using a SpeedVac (ThermoScientific) and care was taken to ensure the samples did not completely dry out.

Organic Phase Extraction

500µL ethyl acetate was added to the extracts before mixing vigorously and centrifuging at 12,000g for 2 minutes. The organic phase of the supernatant was then collected. These steps were repeated by adding a further 500µL ethyl acetate with approximately 900µL of the organic phase collected at this point. The pooled organic phases were then evaporated to dryness using the Speed Vac.

Aqueous Phase Extraction

The aqueous phase contains conjugates of phenolic compounds that had to be hydrolysed before further analysis. The procedure we used was suitable for hydrolysing esters and glycosides. 200µL 12M HCL was added to the aqueous phase (with an approximate final HCL concentration of 4M) before heating at 80°C for 60 minutes. The samples were then allowed to cool to room temperature. 100µL of

the internal standard, ortho-anisic acid was then added to the samples and the liberated phenolics were extracted as for the organic phase extraction listed above.

2.5.2 HPLC

Sample preparation

Sample preparation prior to HPLC was performed by Lionel Hill (JIC). 120 μ L MeOH was added to each sample, vortexed and another 120 μ L of water were added. This was mixed again before brief centrifugation at 12,000 rpm. 200 μ L of the supernatant was removed and inserted into glass HPLC vials. Internal standards used were 4.387 μ M Orthoanisic acid mixed with a secondary standard of 33.3 μ M camalexin. When HPLC runs were set up to specifically look for SA a 10 μ M salicylate in 50% MeOH standard was used. Where runs were set up to specifically look for scopoletin a 0.1mM scopoletin in 50% MeOH standard was used.

HPLC Analysis

HPLC analysis was performed by Lionel Hill (JIC) as described below. Samples were analysed on a Surveyor HPLC system attached to a DecaXPplus ion trap MS (both Thermo). Separation was on a 100 \times 2mm 3 μ Luna C18(2) column (Phenomenex) using a gradient of methanol versus 0.1% formic acid in water, run at 250 μ L.min⁻¹ and 30°C.

Detection was by light absorbance and electrospray MS. Absorbance spectra were collected from 200-600nm, and additionally single-wavelength chromatograms at 298nm (bandwidth 9nm) and 320nm (bandwidth 19nm). Positive and negative mode electrospray MS data were collected in separate runs as the instrument is slow when collecting both at the same time, leading to inadequate spectra measured per chromatographic peak. In positive mode runs, the instrument was set up to collect full MS from m/z 100-2000 and data-dependent MS² of the most abundant precursor ions at an isolation width of m/z 4.0 and 35% collision energy. Dynamic exclusion was used to ensure that after two spectra had been collected in 0.5min, the precursor would be neglected in favour of the next most abundant precursor for a further 0.5min; this maximises the amount of precursor ions for which MS² data are available. Additionally, in positive mode, the instrument

collected targeted MS2 data for the transitions 201→201 (camalexin), 153→135 (ortho-anisic acid) and 193→ any possible fragment above m/z 50 (scopoletin). Targeted MS2 was carried out at an isolation width of m/z 3.0 and a collision energy of 35%.

In negative mode, the instrument was set up to collect full MS and data-dependent MS2 as for positive mode, but additionally targeted MS2 of precursor ion m/z 137 at an isolation width of 3.0 and 35% collision energy.

Spray chamber conditions were 50 units sheath gas, 5 units aux gas, 350°C capillary temperature, and a spray voltage of 3.8kV (positive) or 3.5kV (negative) using a steel needle kit.

2.5.3 Metabolite Effect on Pathogen Growth

To assess the ability of PAMP-induced metabolites to inhibit pathogen growth aqueous and organic extracts from *B. napus* tissues at various time points and treatments were collected as described above and mixed with a 50% PDB growth media. Specific quantification of different pathogen strains subsequently is described elsewhere.

2.6. Analytical Methods

2.6.1 Illumina-based RNAseq

RNA samples sent for analysis were composed of RNA pooled from 8 different biological replicates per treatment and time-point. The samples were analysed by Glasgow Polynomics at the University of Glasgow, prepared according to Illumina TruSeq RNA Sample Preparation Guide using the Illumina TruSeq RNA sample preparation kit starting with 1µg of total RNA. For the library validation, the library concentration was measured with Qubit, followed by quality assessment with a Bioanalyser and library quantification with Kapa kit using Optikon 2 RT-PCR machine. The libraries were then sequenced on Illumina Genome Analyser IIx (GAIIx), and the raw fastq data files containing quality-passed 73base long reads, were generated for each sample separately with CASAVA software.

2.6.2 Aligning Illumina reads to *B. napus* pseudomolecules

Reads were aligned with Maq v0.7.1 (Li et al. 2008) against a pseudo-reference sequence specially developed for *B. napus* as described in Higgins *et al.* (2012). Reads were aligned to the pseudomolecule assembly version 4 (Bancroft, 2011). This comprises two variants of around 90,000 *Brassica* unigenes representing the A and C genome homoeologues for each. The Maq pileup files were parsed to count aligned reads and calculate a normalised RPKM value (reads per kilobase per million mapped reads) for each unigene variant. *Brassica* unigenes were functionally annotated by programmatic reference to a pre-computed BLASTN analysis versus the TAIR10 *A. thaliana* gene models.

2.6.3 PAMP-induced transcriptome analysis

Any unigene with less than 0.02 RPKM at any time point or treatments was removed before further analysis. Fold expression data was calculated between 1 and 0 hours, and 3 and 0 hours, and converted to log₂ expression. Raw data was deposited in the EMBL short read archive under accession number ERA248806.

2.6.4 Mapman Analysis

The unigene expression dataset annotated with TAIR9 AGI numbers was adapted for use in the Mapman program in the following ways. Only a single AGI number could be inputted into the program, so redundancy (as a result of homeologous copies of the gene in *B. napus* or false positive BLASTN hits) was removed by including only the unigene with the highest basal expression at the 0 h time point. Expression was converted to log₂ reads per million and inputted into Mapman using the *A. thaliana* accession number references as described by Thimm et al. 2004. Specific MAPMAN modules used in the analysis were the Metabolism Overview, RLKs (Shiu, 2001), Transcription Factors and the Cellular Response Overview module.

2.6.1 Association Genetics

Association mapping was performed as described by Harper et al (2012). A mixed linear model Genome Wide Association Study (GWAS) was run using TASSEL (Trait Analysis by aSSociation, Evolution and Linkage, www.maizegenetics.net). Trait data used was the predicted mean of each trait. SNP data was produced as described in Harper et al 2012, with alleles below a frequency of 0.05 omitted leaving 62,980 SNPs assigned to the A and C genome pseudomolecule assembly (Bancroft, 2011, Higgins 2012). The Traits, kinship matrix (Harper, 2012) and SNP map were entered into Tassel V.3.0 (Bradbury, 2007) to run a mixed linear model to give the statistical significance of the association and the trait being investigated.

2.6.2 QTL Mapping

For QTL mapping the lines of the double haploid *B.oleracea ssp alboglabra* ("A12" A12Dhd) and *B.oleracea ssp italic* ("Green Duke" GDDH33) were used. Bouhan et al (1996) produced an original restriction fragment length polymorphism (RFLP) map of this cross, and this population was subsequently used to develop an integrated map with additional amplified fragment length polymorphisms (AFLP) and simple

repeat sequence (SSP) markers also included (Sebastian, 2000). The integrated AFLP-RFLP map (available from <http://www.brassica.info/CropStore/maps.php>) used in this study can be seen in figure 2.1 and 2.2. Quantitative trait loci were identified using MapQTL version 5 (Van Ooijen, 2004) taking a LOD threshold of 3.0.

2.6.3 Prediction of codon use changes of A12xGD SNPs

Codon use of the SNPs within A12 and GD, used to produce a non-synonymous (NS) SNP list, were created by a custom script courtesy of Martin Trick (JIC, Norwich, UK). The script aligned unigene sequence from the *B. napus* consensus with *A. thaliana* cDNA sequence to identify the most likely ORF for the unigene. A12 and GD consensus unigene sequences were then aligned in the predicted ORF to produce a NS SNP list.

2.6.4 Genotyping with KASPar markers

Genotyping the A12 x GD cross using KASPar markers was performed by Richard Goram. DNA was amplified using a Kbioscience (now LGC Genomics) HC16 hydrocycler, with PCR conditions set according to manufacturer's instructions. DNA was stamped on to 96 well PCR plates using a FluidX DNA stamper then dried. Each sample then had PCR mastermix dispensed on to it using a Kbioscience Meridian liquid dispenser. A BMG Pherastar plate reader was used to measure final fluorescence, with KlusterCaller software used for genotyping.

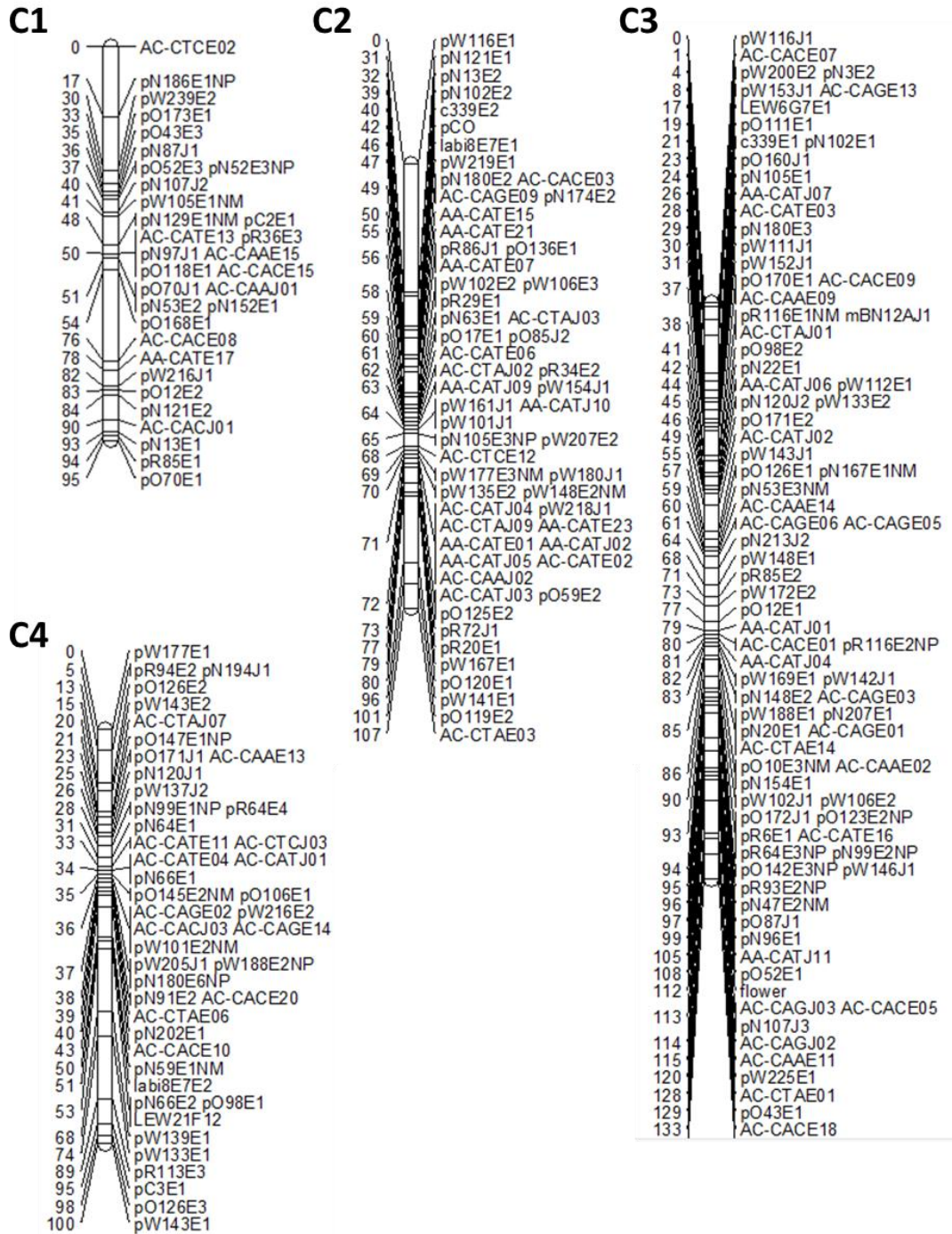


Figure 2.1 AFLP/RFLP Map of *B. Oleracea* chromosomes 1-4
Reprinted from Sebastian et al, 2010.

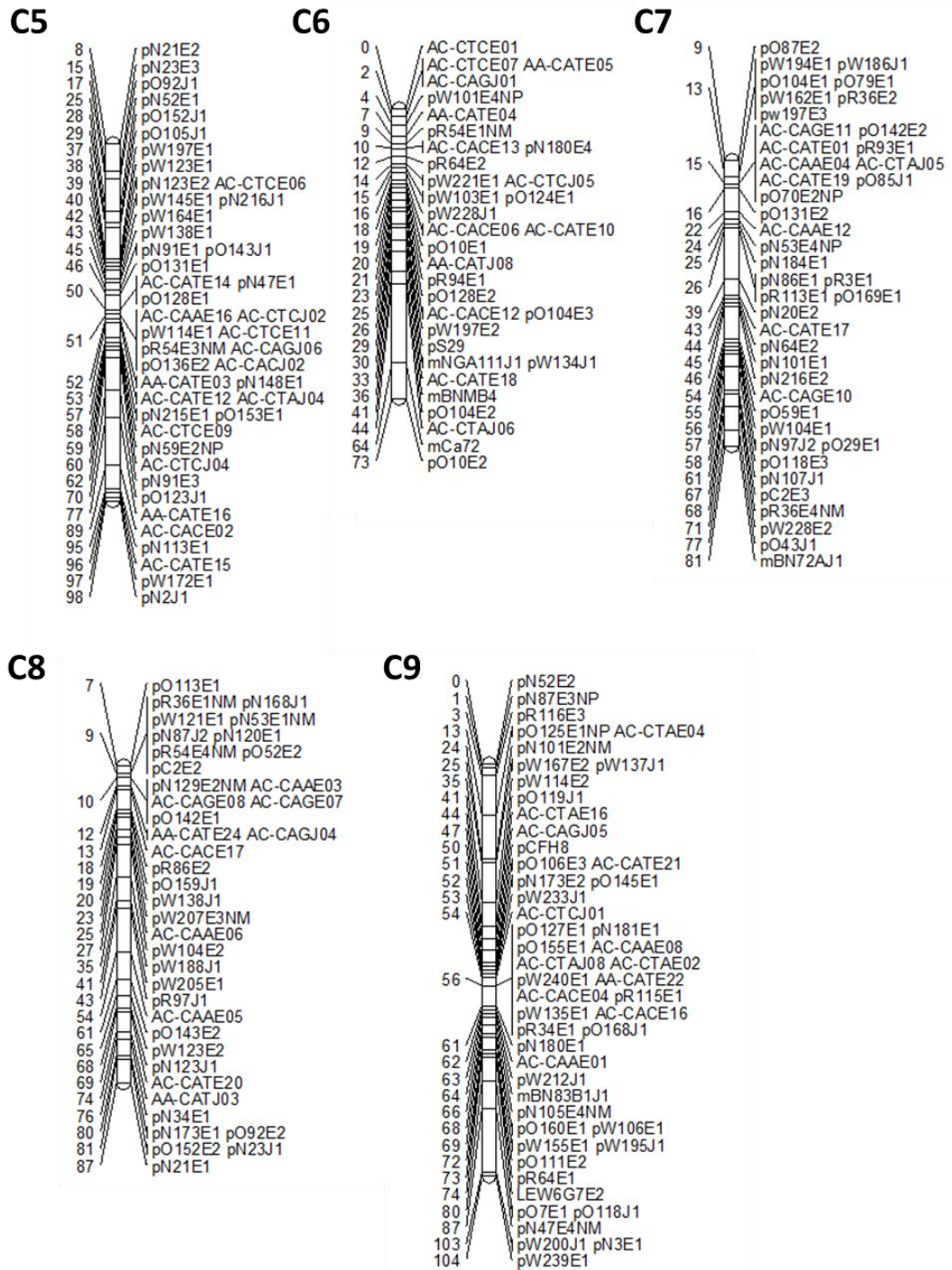


Figure 2.2 AFLP/RFLP map of *B. oleracea* chromosomes 5-9.
 Reprinted from Sebastian et al, 2010.

2.6.5 Sequence alignments

A number of different programs were used for the alignment of DNA and AA sequences. Extraction of specific unigene sequences, individual reads and predicted consensus sequence for A12 and GD mRNA seq was done in Tablet (version 1.13; Milne, 2013). Alignment of reads between *A. thaliana* and Brassica unigenes, prediction of codons and AA sequence prediction was done in Genious software (version 1.1; created by Biomatters), or Clustal X (version 2; Larkin, 2007).

2.6.6 Statistical Tests Used

The Specific statistical tests used are described in the text, and were primarily performed in either excel or genstat (Version 15.2). For mapping multiple repeats of the same trait, predicted means were generated for each line based on at least 4 complete experiments (each with at least 8 internal biological repeats). The predicted means were generated using a mixed linear model in Genstat taking line as a fixed variables, and experiment and plate (for PTO and ROS assays) as random variables.

2.6.7 Bioinformatics Tools Used

Table 4 summarises the bioinformatics tools, and associated websites used in this study.

Database/Tool	Description	Website	Reference
NCBI	Sequence database, BLAST	http://www.ncbi.nlm.nih.gov/	
TAIR	Gene annotation and GO-terms	http://www.arabidopsis.org/	
Genevestigator	Arabidopsis genome wide and micro array expression data	https://www.genevestigator.com/gv/plant.jsp	Hruz, 2008
Tassel	Creating Kinship Matrix for association mapping	www.maizegenetics.net	Bradbury, 2007
Tablet	Viewing and extracting mRNA seq data	http://ics.hutton.ac.uk/tablet/	Milne, 2013
BRAD	Blasts against <i>B. rapa</i>	http://brassicadb.org/brad/	
Brassica Genome Gateway	Blasts against unigenes, RFLP marker sequences	http://brassica.nbi.ac.uk/	
Brassica Info	Access to old maps	http://www.brassica.info/	
SALK Primer Design tool	SALK line Genotyping Primer design	http://signal.salk.edu/tdnaprimers.2.html	
NASC	Ordering SALK lines	http://arabidopsis.info/	
Primer 3	Primer Design	http://bioinfo.ut.ee/primer3/	Untergasser, 2012
Genstat	Statistical Analysis	http://www.vsni.co.uk/software/genstat	
GlimmerHMM	Codon use prediction	http://ccb.jhu.edu/software/glimmerhmm/	Kelley, 2012
R	Running Association Mapping Scripts	http://www.r-project.org/	

Table 4 Databases and bioinformatics tools used in this study.

Chapter 3 : Methods to Study PAMP- Triggered Immunity in *Brassica napus*

3.1. Aim

The research presented in this chapter had the aim of developing the techniques needed to investigate PTI in *Brassica* species. This was broken down into three main objectives. The first was the development of robust assays to explore PAMP responses in *B. napus* variety 'Temple' including early cell signalling events, transcriptional changes, physiological changes at the cell wall and the effects of PAMP treatment on development and pathogen resistance. The second objective was to characterise the genome wide transcriptional changes seen upon PAMP treatment using mRNA sequencing, including analysis of the genes and pathways that are up or down regulated by flg22 in *B. napus*, and to begin to understand how a genome-wide transcriptional response of this nature is coordinated within a complex genome. The final objective was to look at the natural variation of PAMP responses within a subset of genetically diverse lines and to assess the feasibility of QTL mapping and GWAS of PAMP responses in *Brassica*.

3.2. Introduction

Quantifying immune outputs downstream of PRRs are the primary means for assessing PTI. For example rapid MAP kinase (MAPK) phosphorylation, Ca²⁺ influx and an oxidative burst are PTI responses that occur within minutes following PAMP perception (Boller & Felix 2009). These PAMP responses have been demonstrated in species as diverse as grapevine (Dubreuil-Maurizi et al. 2010), barley (Proels et al. 2010), *B. oleracea* (Dunning et al. 2007), tomato (Nguyen et al. 2010) and soybean (Valdés-López et al. 2011).

Before modern PTI/ETI and PAMP/MAMP terminology became widely used, a number of early examples of responses to chitin or chitosan have historically been shown in rice cell cultures including measurement of plasma membrane ion fluxes, phytoalexin accumulation and chitinase expression (Kishimoto et al. 2010; Kuchitsu et al. 1997; Yamada et al. 1993; Nishizawa et al. 1999).

Substantial transcriptional changes occur rapidly upon PAMP treatment and specific marker genes can be used to quantify PAMP-responsiveness (Zipfel et al. 2004;

Navarro et al. 2004; Zipfel et al. 2006; Wan et al. 2008). PAMP responsive genes have not previously been published in *B. napus*, but there is a wealth of reported early induced marker genes for interactions with *Sclerotinia sclerotiorum* (Zhao, 2009; Yang, 2009) and *P. syringae* (Stearns, 2012) for example. These are likely to be effective PAMP response marker genes as well. Large scale transcriptome analysis is a powerful method for identifying novel PAMP-responsive genes, and has been carried out in *A. thaliana*, soybean and rice (Akimoto-Tomiyama et al. 2003; Navarro et al., 2004; Zipfel et al. 2004; Valdes-López et al. 2011). Microarrays developed for *B. napus* have been used to investigate genome wide transcriptional responses to pathogens including *Sclerotinia* (Zhao, 2009), and also one published study looking at the response of *B. napus* to chitosan (Yin, 2006).

Callose deposition has also frequently been used to evaluate PAMP responses. The role of callose deposition in resistance against important *Brassica* pathogens such as *Leptosphaeria maculans*, *Xanthomonas campestris pv. campestris* and *Sclerotinia sclerotium* is still largely unknown. Luna et al (2011) highlighted how variable callose deposition can be, with changes in temperature and growth conditions affecting the ability to mount the response. Its usefulness then as a discriminatory tool to investigate different brassica genotypes might be limited. Lignification is another pathogen response, but is relatively underrepresented in the literature because of a lack of durable assays for it. Lignification of *A. thaliana* roots mediated by isoxaben has been quantified using a phloroglucinol based assay (Deness, 2011), and flg22 treatment does increase vascular lignification in cotyledons (Adams-Phillips, 2010).

Assessing metabolome-wide changes after PAMP infiltration or pathogen infection is rare in the literature. Specific metabolites have been quantified after PAMP treatment however, including widespread measurement of the hormones ethylene and SA (Felix, 1999; Tsuda, 2008), and the reduction in auxin (Spoel, 2008; Navarro, 2006). Shenke et al (2011) reported flg22 to increase levels of the metabolites scopoletin, a phenolic compound, and camalexin, a phytoalexin. Glucosinolate production is also commonly studied as a resistance mechanism against pathogens

in *Brassicas* (Mithen, 1992), and it would be interesting to see the overlap between PAMP and pathogen-responsive glucosinolates.

An assay for PAMP responsiveness widely used is PAMP-induced resistance (PIR). The protective effect of PAMP treatment, or crude bacterial/fungal preparations, on subsequent pathogen growth has been demonstrated clearly in *A. thaliana*, where the application of flagellin or its derived peptide flg22 reduced the subsequent growth of the bacterial pathogens Pto DC3000 (Zipfel et al. 2004) and *Xanthomonas campestris pv. campestris* (Sun et al. 2006), the fungus *B. cinerea* (Ferrari et al. 2007) and the oomycete *Hyaloperonospora arabidopsidis* (Fabro et al. 2011). In other plant species, flg22 has been shown to induce resistance to Pto DC3000 on tomato (Nguyen et al. 2010) and *Sclerotinia sclerotiorum* on soybean (Valdés-López 2011). N-acetylchitooligosaccharides can induce resistance to *Magnaporthe grisea* on rice (Ning et al. 2004).

In order to assess the variability of some of the PAMP responses in *Brassica* varieties, lines from the OREGIN diversity set were used containing traits of interest to breeding programs (<http://www.oregin.info>). In this diversity panel the line Temple is the common female parent in multiple crosses (fig 1.5). As such it is the ideal background to develop PAMP response assays in, as any contrast in response between Temple and another line in the panel can be investigated in a mapping population.

3.3. Results

3.3.1 The Oxidative Burst in *Brassica napus*

Dose response curves were produced for flg22, elf18 and CSC to identify optimum concentrations of PAMP for the oxidative burst assay. The optimum concentrations for the bacterial peptide PAMPs was between 50 and 100nM, with no significant increase in ROS past this point (fig 3.1 A, B.). This is similar to previous findings in *A. thaliana* (Jeworutzki, 2010). The optimum concentration of CSC was 1mg/ml with significant inhibition of the responses seen at higher concentrations. This may be a result of long chain polysaccharides in the crude crab shell preparation inhibiting Ca^{2+} influx, a necessary prerequisite upstream of ROS signalling in *A. thaliana* (Segonzac, 2011). It's also possible that such high concentrations of variable length N-Acetyl Glucosamine sequester H_2O_2 itself or inhibit exogenous peroxidases necessary for quantification of the ROS. 100nM elf18 and flg22 and 1mg/ml CSC were utilised in most subsequent experiments unless otherwise stated.

The relative magnitude and timing of the oxidative burst varied between different PAMPs. flg22 consistently triggers a larger oxidative burst than elf18 at the same concentration. The relative abundance of the different PRRs in *B. napus* is unknown. Efficiency of RBOH activation and signalling output from various PRR complexes may also differ between cultivars. The peptide triggered ROS was between five and ten-fold more than the CSC triggered ROS (fig 3.2 A-B), likely a result of the impurities within the crude crab shell preparations as discussed above. In all three cases H_2O_2 levels returned to resting state levels within 45 minutes of PAMP treatment (fig 3.2 A-B).

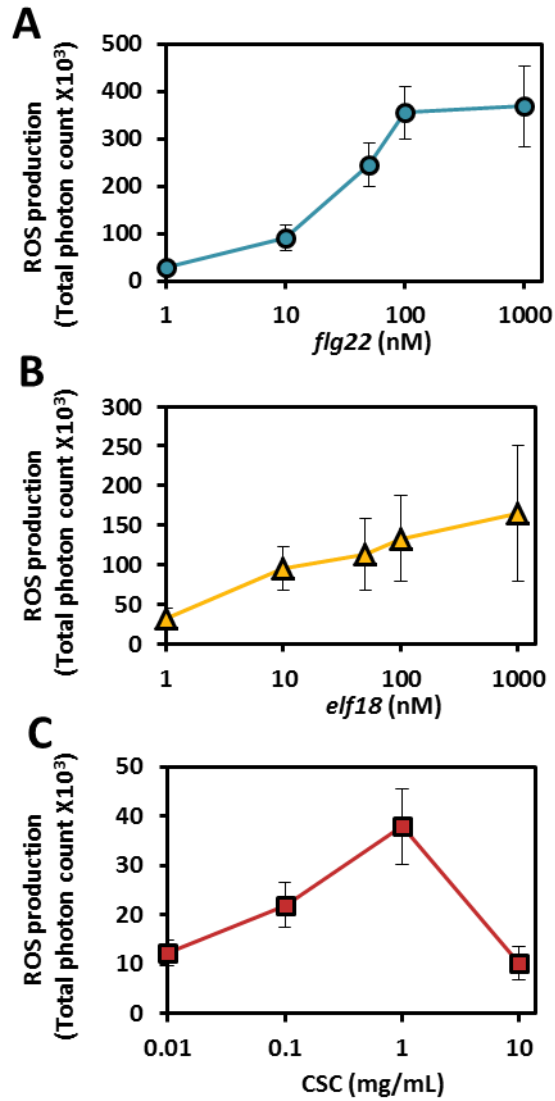


Figure 3.1 Dose response curves of the PAMP-triggered oxidative burst in *Brassica napus*. The oxidative burst dose response curves following treatment with(A) flg22 (B) elf18 or (C) CSC. Data is total RLU observed over 35 minutes in leaf discs following PAMP application at different concentrations. Data represent summation of RLU readings at 30 second intervals over a period of 35 minutes. Error bars are the standard error of 8 biological replicates.

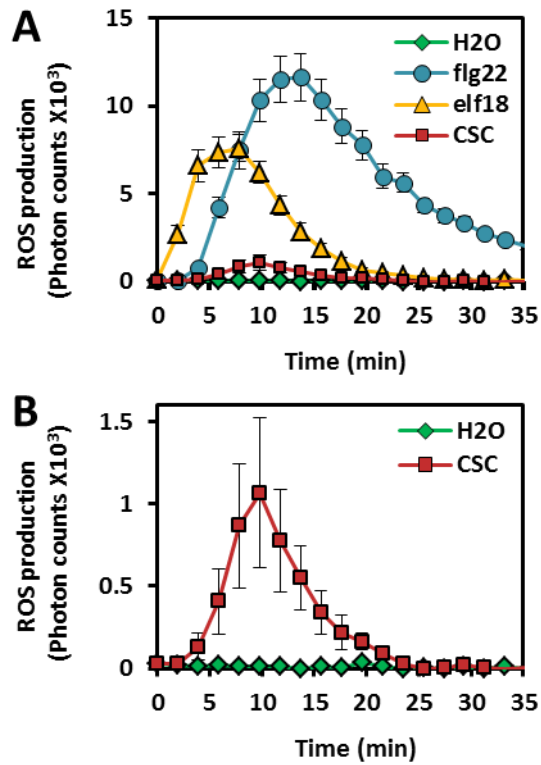


Figure 3.2 Relative ROS levels after PAMP treatment in *B. napus*.

Oxidative burst in response to flg22 (100 nM), elf18 (100 nM) or CSC (1mg/mL) over 35 minutes following PAMP application to leaf discs. Error bars are the standard error of 8 biological replicates. B) Oxidative burst in response to CSC (1 mg/mL).

In order to determine the best developmental stage for ROS assays leaf discs were taken from cotyledons, the first true leaf or second leaves of four week old Temple plants and treated with flg22 or CSC. There was no significant variation in total ROS observed between the different leaves in response to either PAMP (fig 3.3 A). In subsequent assays the second leaves were usually selected for all ROS assays.

Because leaf expansion and cell wall remodelling requires reducing environments and NADPH oxidase activity, it may have been that expanding regions of the leaf would have a different ROS response after PAMP treatment. To test this flg22 and CSC triggered oxidative burst was measured in leaf discs from four different regions of the leaf (proximal, distal, edge and middle). No significant difference between leaf disc sampling regions was seen for either PAMP (fig 3.3 B).

As the CSC preparation was not sterile, the effect of two different sterilisation methods on the efficacy of the CSC was tested. Autoclaving and filter sterilisation had no significant effect on the ROS produced after flg22 or CSC treatment. (fig 3.3 C). This result also indicates that the activity of the crab shell preparation is not a result of remaining bacterial peptide PAMPs (from bacteria in the crabs gut for example) as activity was maintained after autoclaving. All subsequent assays using CSC were performed with autoclaved solutions.

In order to understand the relative magnitude of the oxidative burst between Temple and the *A. thaliana* reference genotype Col-0 the oxidative burst between the two species was looked at in response to flg22, elf18 and CSC. There was no difference in the background H₂O₂ production in water treated samples between Temple and Col-0 (fig 3.4 A-C). There was a significant ($P < 0.05$) reduction in ROS in response to flg22 between Temple and Col-0 with the *B. napus* variety producing about 70% of the ROS seen in *A. thaliana* (fig 3.4 A). No significant difference was observed in total ROS produced in response to elf18 and CSC between the two genotypes (fig 3.4 A-C). The oxidative bursts observed in the reference genotype Temple are approximately equal in magnitude to those observed in Col-0.

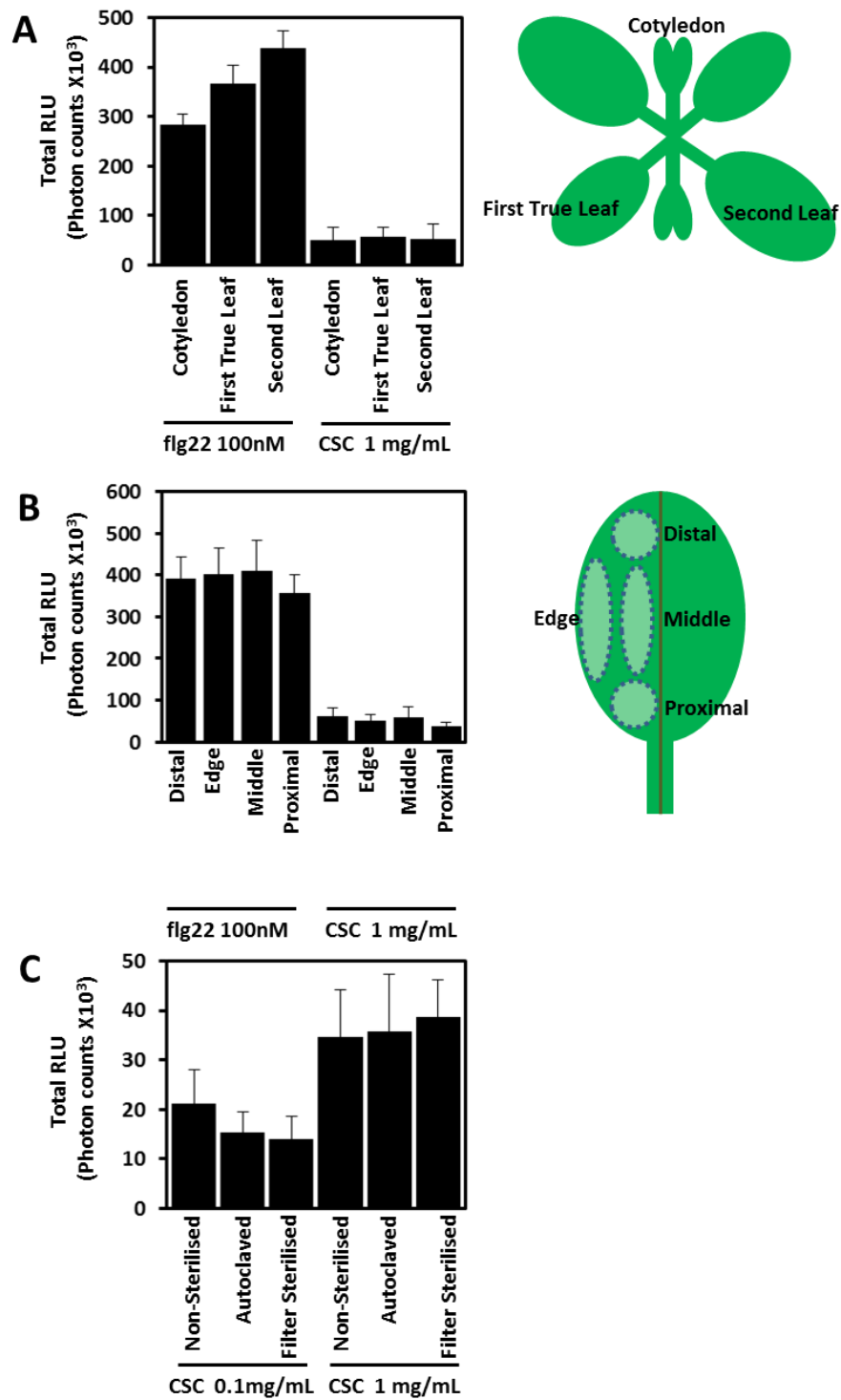


Figure 3.3 Optimising the oxidative burst in *Brassica napus*.

A) Comparison of the oxidative burst in response to flg22 (100nm) or CSC (1mg/ml) from the cotyledon, first or second true leaves in Temple. B) Comparison of the oxidative burst from leaf discs taken from different leaf regions in Temple. C) Comparison of methods to sterilise CSC chitin and there effect on the efficacy of the CSC triggered oxidative burst at two different CSC concentrations.

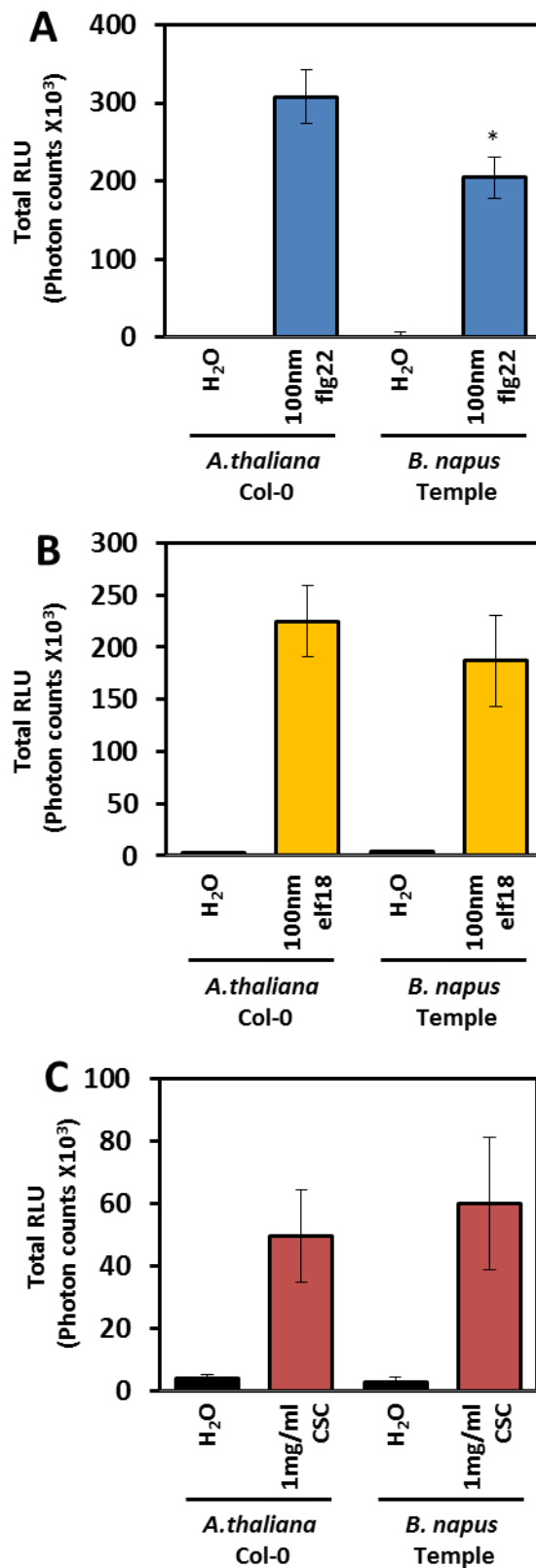


Figure 3.4 Comparison of the oxidative burst in *Brassica napus* and *Arabidopsis thaliana*. The oxidative burst between *B. napus* variety Temple and *A. thaliana* ecotype Col-0 in response to (A) flg22 (100nM), (B) elf18 (100nM) and (C) CSC 1mg/ml. * indicates a P value of <0.05 when compared to *A. thaliana* (T-test).

3.3.2 Map kinases are rapidly phosphorylated after flg22 treatment in *B. napus*

MAPK cascades are the sequential phosphorylation of MAPKKKs, MAPKKs and finally MAPKs (Tena et al. 2011). In *A. thaliana*, two distinct cascades are activated following flg22 treatment, namely *MEKKs-MKK4/5-MPK3/6* and *MEKK1-MKK1/2-MPK4/11* (Tena et al. 2011; Bethke et al. 2012). Using antibodies raised against human P-42/44 Erk1 the PAMP-dependant phosphorylation of MPKs in *B. napus* was investigated. MAPK activation could be observed within five minutes of flg22 treatment compared to water treated controls and was maintained at 15 minutes post flg22 treatment (fig 3.5). The approximate sizes of the phosphorylated proteins correspond to *MPK3* (44 kDa) and *MPK6* (48 kDa) in *A. thaliana*. However, there may only be very weak conservation of signalling roles, expression patterns and the interactions of MPKs between *A. thaliana* and *B. napus* (Liang, 2013).

3.3.3 PAMP-Induced Callose Deposition in *B. napus*

To investigate callose deposition in *B. napus*, leaf tissue was stained with aniline blue 24 h after infiltration with H₂O, flg22 or CSC. Significantly more callose deposits were seen after PAMP treatment than after water control in Temple (fig 3.6 A,B). As the number of deposits were less than and more sporadic across the leaf disc than in some published studies (Luna, 2011 for example) another *B. napus* genotype, POSH MC169 was also investigated. This line has a stronger ROS response to flg22 than Temple (fig 3.22) so more extensive callose deposition might also have been observed in it. Significantly more callose deposits were observed in POSH MC169 than Temple in response to both flg22 and CSC (fig 3.7 C,D). This might suggest that Temple has a partial impairment in Callose deposition, or potentially that there is very wide genotypic diversity in PAMP responsive callose deposition between *B. napus* genotypes.

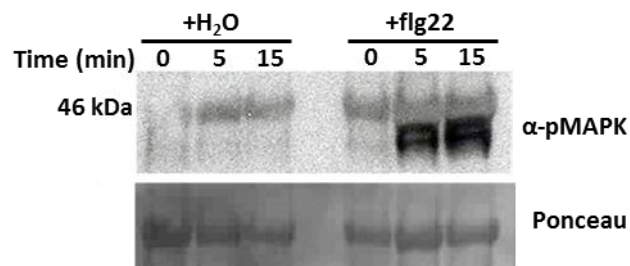


Figure 3.5 flg22-triggered MAPK phosphorylation.

MAPK activation following 1 μ M flg22 treatment in *B. napus* visualised with an immunoblot using a human anti-p42/44-ERK antibody. Lower panel: Ponceau stain of total protein.

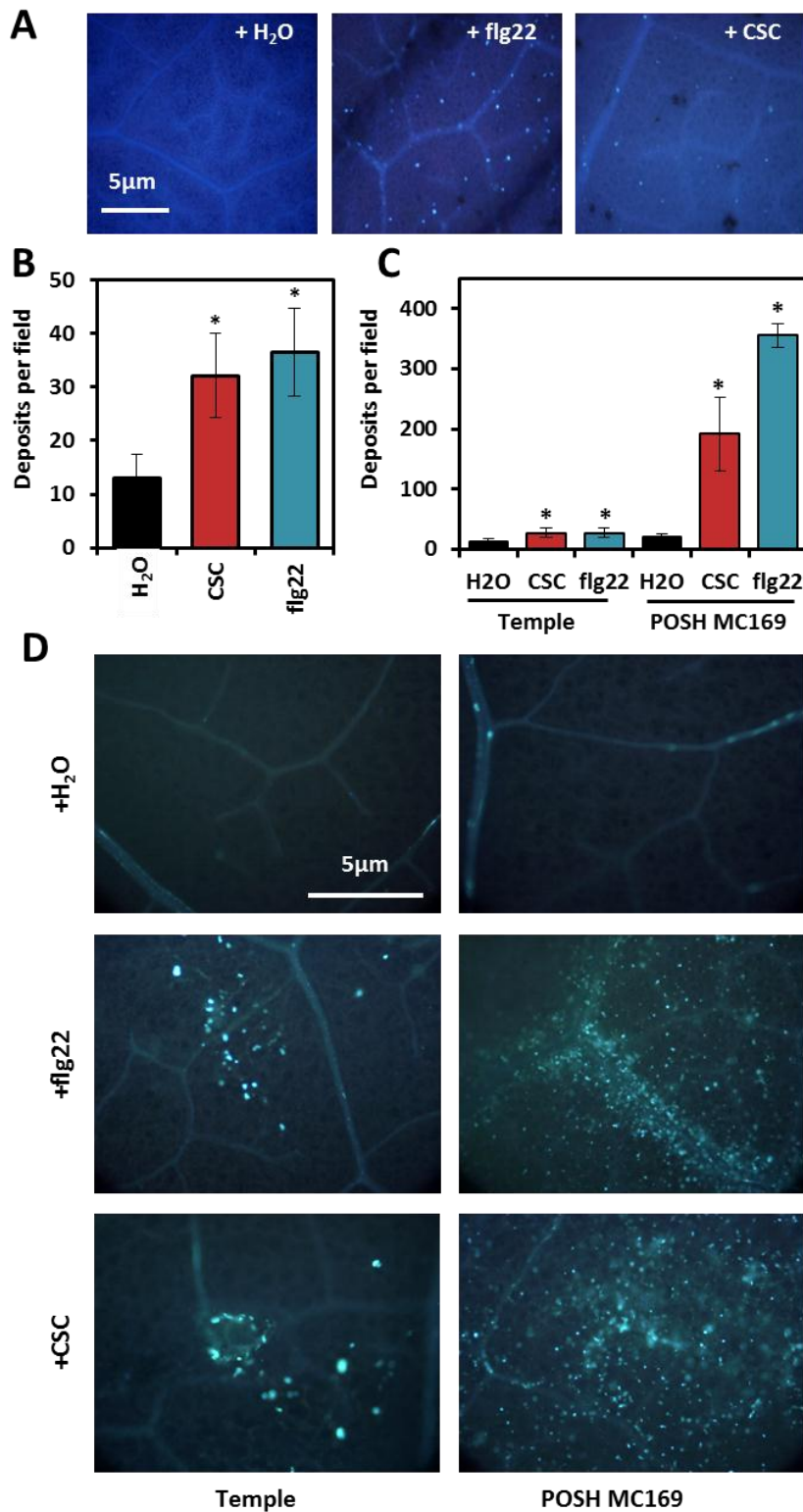


Figure 3.6 Callose deposition in *B. napus*

A) Microscopic comparison of callose deposits after PAMP infiltration and staining with aniline blue in Temple. B) Total number of callose deposits per field of view. C-D) comparison of PAMP induced callose between Temple and POSH MC169 by total deposit counts (C) and microscopic comparison (D). Error bars represent standard error of 10 biological replicates. * indicates $p < 0.05$ (T-test).

3.3.4 PAMP-Induced Seedling Growth Inhibition

PAMP application can inhibit seedling growth in *A. thaliana* and other *Brassicaceae* (Dunning et al., 2007; Vetter et al. 2012). In Temple significant growth inhibition can be seen in response to flg22, elf18 and CSC (fig 3.7 A, C), and the effect is dose-dependent (fig 3.7 B). Growth in PAMP media also often resulted in high anthocyanin deposition within the cotyledons compared to water treated controls (fig 3.7 C). This high-throughput assay could be readily applied to large-scale screens for quantifying PTI within *Brassica* populations.

3.3.5 PAMP-Induced Lignification

Lignin has been reported to accumulate during pathogen interactions (Lee, 2001, Mohr, 2007), and within the vasculature of *A. thaliana* cotyledons infiltrated with elf18 (Adams-Phillips, 2010). To investigate the possibility of PAMPs inducing lignin in the absence of a pathogen, PAMP infiltrated leaf strips were stained with phloroglucinol, a stain specific for cross-linked lignans (Pomar, 2002). PAMP treatment alone never resulted in observable lignin above water controls. In combination with wounding however, PAMP treatment did result in extensive lignin deposition around the wound sites more extensive than the wounding alone (fig 3.8 A, B).

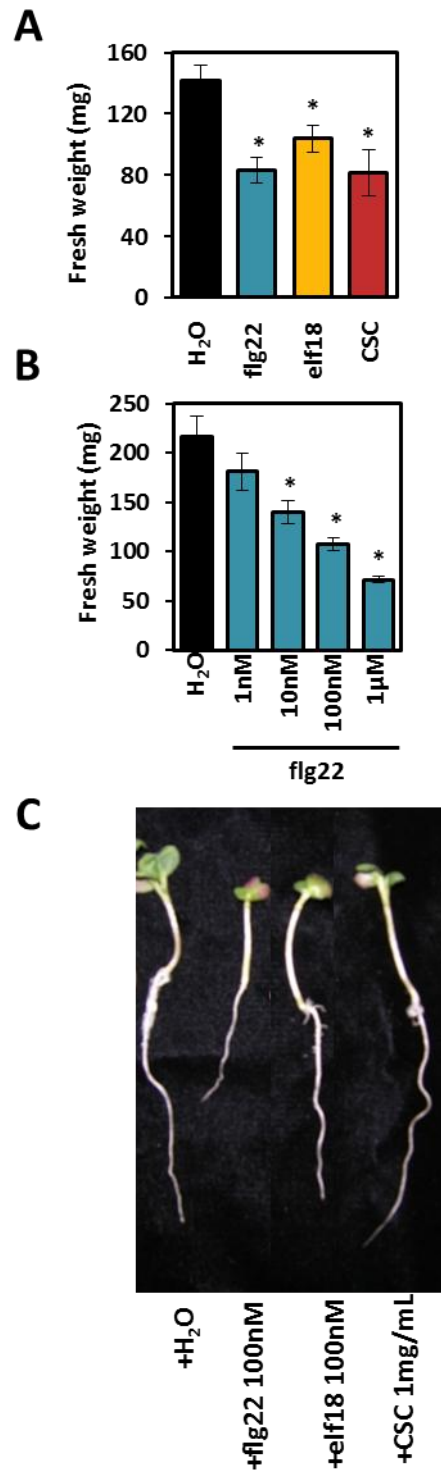


Figure 3.7 Seedling growth inhibition in *B. napus*.

A) Seedling growth inhibition of *B. napus* in liquid MS media containing H₂O, flg22 (100 nM), elf18 (100 nM) or CSC (4 g/L) 10 days after germination. B) Dose dependency of seedling growth inhibition. Error bars represent standard error of 12 biological replicates** indicates p<0.01 (T-test). C) Bright field photograph of *B. napus* seedlings 10 days post germination in H₂O, flg22 (100 nM), elf18 (100 nM) or CSC (4 g/L).

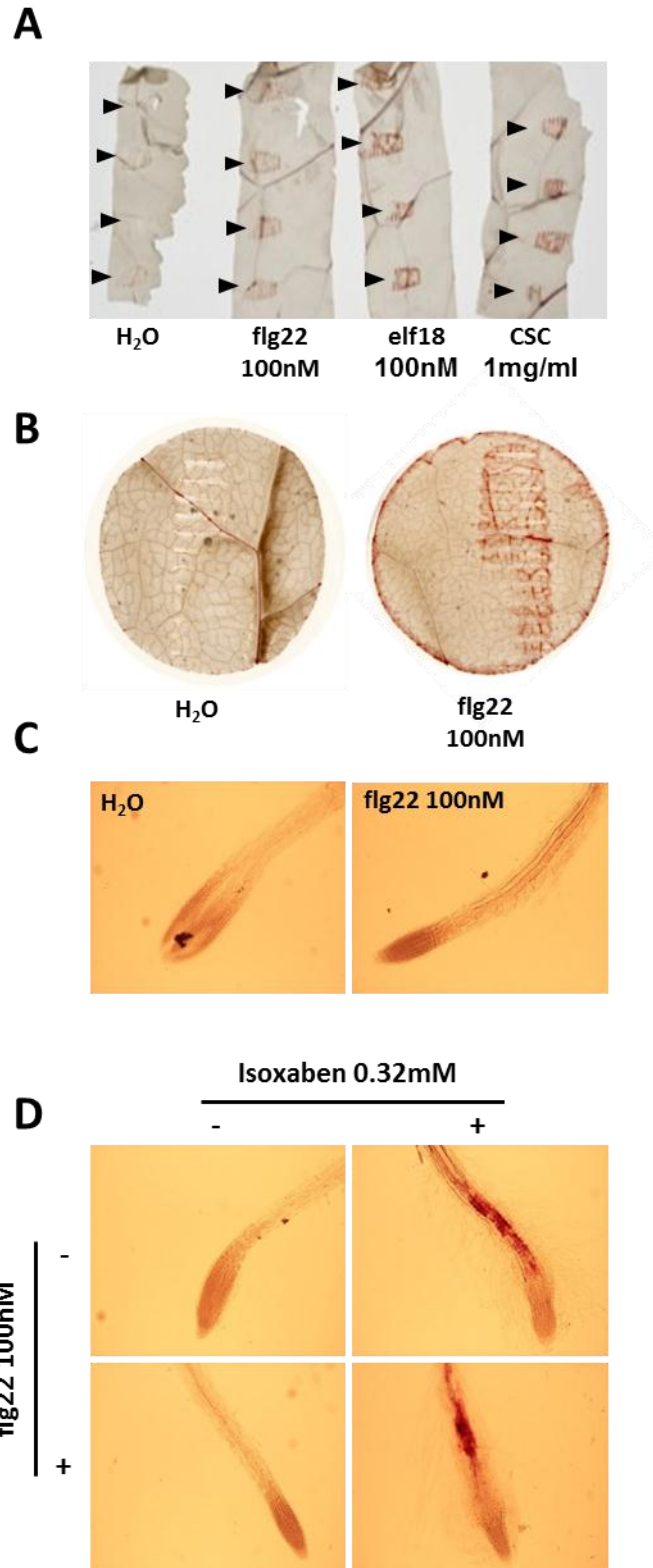


Figure 3.8 PAMP treatment enhances wound-induced lignification and vascular lignification staining in *B. napus*.

A) Leaf strips of Temple wounded with forceps and submerged in H₂O or PAMP solution for 24hrs before clearing and phloroglucinol staining. Wound sites are labelled with arrows. B) 20mm leaf discs wounded with forceps and treated with flg22 (100nM) before lignin staining with phloroglucinol. C) Phloroglucinol stain of 6 day old Temple seedlings submerged in H₂O and flg22 100nM for 24hours prior to staining. D) Phloroglucinol stain of 6 day old temple seedlings submerged in H₂O and flg22nM with or without Isoxaben 0.32mM for 24 hours prior to staining.

To investigate PAMP induced lignin in root tissues, seedlings germinated in liquid media and transferred to PAMP media for 24 hours prior to sampling were cleared and stained with phloroglucinol. Flg22 treated seedlings displayed vascular lignin deposition with very little lignin staining in cortical or epidermal root tissues (fig 3.8 C). It was reported that Isoxaben, a gluconase inhibitor that prevents normal cell wall development and mimics cell wall damage, could induce extensive root lignification and would serve as a good positive control for a root lignin phenotype (Deness, 2011). To see if PAMP treatment enhanced isoxaben-induced lignification of root tissues, Temple seedlings were treated with combinations of flg22 and Isoxaben 24 hours prior to sampling. Flg22 treatment did not increase isoxaben induced lignification (fig 3.8 D). Isoxaben-induced lignification had a different distribution to flg22 treatment being found extensively spread throughout different root tissues with the exception of the root tip (fig 3.8 D).

As phloroglucinol staining is a qualitative measurement it was necessary to try and get an accurate quantitation of PAMP-induced lignin observed in leaf discs. In order to quantify absolute lignin content a thiglycolic acid precipitation method was developed from (Mohr, 2007) et al. The method first extracts insoluble lignin, before acid hydrolysis results in the release of lignans, which can then be quantified by recording absorbance at 486nm. At 6 hours after PAMP infiltration there was significantly more flg22 and CSC induced lignin than water treatment or wounding (fig 3.9 A). Wounding alone did not result in increased lignin. Mohr et al (2007) identified the optimum time to record Pst DC3000 induced lignin was 72 hours post inoculation. To investigate this lignin quantification was performed on leaf discs at a later time point of 72 hours. At this time point flg22 treatment did result in higher levels of lignification (fig 3.9 B), but this was not observed for CSC treatment.

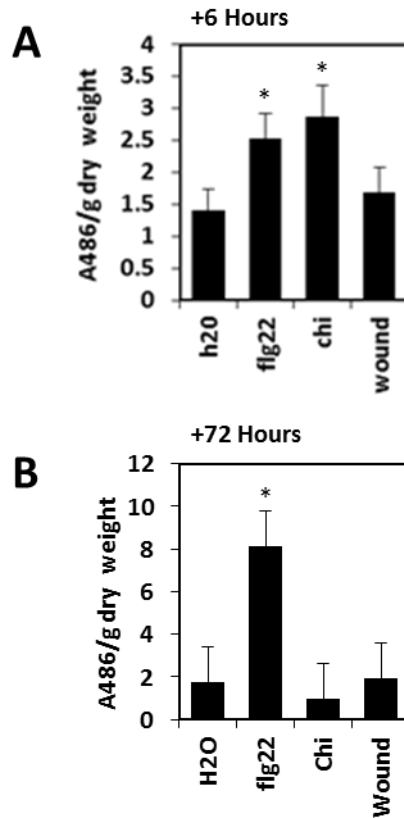


Figure 3.9 Lignin quantification in PAMP treated *Brassica napus* tissue. Quantification of absorbance at 486nm of acid hydrolysed lignin extractions stained with phloroglucinol. Leaf discs of temple were infiltrated with flg22 (100nM), elf18 (100nM) or CSC (1mg/ml) six (A) or 72 (B) hours prior to sampling. Error bars represent the standard error of 4 biological replicates. * indicates a P-value < 0.05 (T-Test).

3.3.6 Identifying PAMP-responsive marker genes in *Brassica napus*

Two different approaches were used to identify PAMP-responsive *B. napus* genes that could be used as PTI markers. A first approach was to focus on *Brassica* genes previously reported as being induced during the interaction of *B. napus* with *S. sclerotiorum* at early time points after infection (Zhao et al. 2009), or on *B. napus* orthologues of *A. thaliana* genes up-regulated upon treatment with flg22 (Zipfel et al. 2004). The expression of a range of candidate marker genes was assessed and of these *BnMPK3*, *BnMPK4* and *BnWRKY33* were consistently up-regulated upon flg22 and CSC treatment (fig 3.10 A-C) making them effective markers for PAMP responses in *Brassicac*s.

3.3.7 Genome wide changes upon PAMP treatment in *B. napus*

In a second approach, we investigated genome-wide changes in expression through Illumina sequencing of total RNA extracted from leaves treated for 0, 1 or 3 h with 100 nM flg22. mRNA sequence reads were aligned to the *B. napus* pseudomolecule assembly and quantified as the number of reads per kB per million mapped reads (RPKM) (Bancroft, 2011; Higgins et al 2012). There were 59,118 unigenes in the A genome and 61,594 unigenes in the C genome with sufficient expression (>0.002 RPKM) at all three time points to be included in the analysis (Appendix 1). Annotation of the *B. napus* unigenes was performed using BLASTN analysis of the unigene sequence against the TAIR 9 *A. thaliana* genome database using an E-value threshold of 1E-30. Substantial changes in gene expression were observed after flg22 treatment with approximately 35% of *B. napus* genes increasing or decreasing more than two fold after 3 h (Table 1). The number of unigenes up or down regulated was higher at 3 hours than 1 hour post PAMP treatment (Table 1). The list of flg22-regulated genes provides a valuable source of candidate marker genes for investigating PTI in *Brassicac*s.

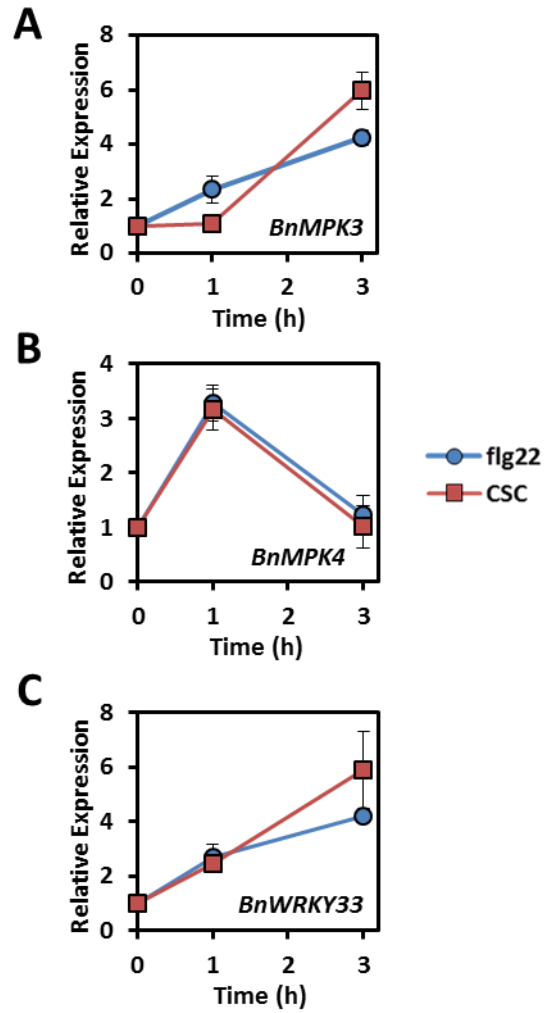


Figure 3.10 PAMP-responsive marker genes in *B. napus*.

Expression of *BnMPK3* (A), *BnMPK4* (B) and *BnWRKY33* (C) after treatment with CSC (0.4 g/L) or flg22 (100 nM) measured by qRT-PCR. Transcript levels were normalised against EF1a expression.

Fold Induction	A Genome		C Genome		Overall	
	T1/T0	T3/T0	T1/T0	T3/T0	T1/T0	T3/T0
>2 fold-up	5677 (9.6%)	8756 (14.8%)	5678 (9.2%)	8763 (14.2%)	11355 (9.4%)	17519 (14.5%)
>4 fold-up	3355 (5.6%)	5074 (8.6%)	3249 (5.2%)	5106 (8.3%)	6604 (5.4%)	10180 (8.4%)
>8fold-up	2498 (4.2%)	3659 (6.2%)	2389 (3.8%)	3641 (5.9%)	4887 (4%)	7580 (6.2%)
<2 fold-down	8319 (14%)	12257 (20.1%)	8437 (13.7%)	12339 (20%)	16756 (13.8%)	24596 (20.4%)
<4 fold-down	5025 (8.5%)	9039 (15.3%)	5159 (8.3%)	9116 (14.8%)	10184 (8.4%)	18155 (15%)
<8 fold-down	3773 (6.3%)	6891 (11.6%)	3807 (6.2%)	6875 (11.6%)	7580 (6.2%)	13766 (11.4%)
Total unigenes	59,118		61,594		120,712	

Table 5 Genome wide changes in gene regulation after flg22 treatment in *B. napus*.

Gene expression changes measured as fold induction at 1 or 3 hours compared to 0hrs after PAMP treatment. Data is sorted into both A and C genome specific lists and overall expression changes.

3.3.8 Co-ordination of PAMP-Responsive Transcription Between the A and C Genomes

As a tetraploid *B. napus* contains the complete A and C genomes of ancestral *B. rapa* and *B. oleracea* resulting in multiple copies of the same gene found between orthologous chromosomes. In order to understand better how a tetraploid coordinates a specific transcriptional response to an external stimuli, a comparison of the expression profiles was made between the A and C orthologs of flg22-induced genes. Most unigenes that were up-regulated more than 4-fold on PAMP treatment had a similar expression pattern between orthologous copies, and there was a highly significant ($p < 0.0001$) correlation between A and C genome orthologous gene expression (fig 3.11 B). The correlation is greater three hours compared to one hour post PAMP treatment (fig 3.11 A, B). A large number of flg22 responsive unigenes were still genome specific however, with predicted homeologous copies not being co-expressed together (fig 3.11 C). This might be due to the higher false positive rate at two fold expression changes, or mis-annotation of unigenes after BLAST analysis however.

3.3.9 Functional Characterisation of up-regulated unigenes in *B. napus*

Consistent with their phylogenetic relationship, the high degree of synteny between the two species allows annotation of the *B. napus* unigenes with *A. thaliana* accession numbers. This allows the characterisation of unigenes using bioinformatics resources that have been developed around the model species. In order to understand the functional roles of flg22 responsive genes the *A. thaliana* gene-ontology (GO) terms database was used to annotate the *B. napus* unigenes. In the up-regulated unigenes there was an enrichment of genes associated with transport, response to stress and signal transduction (fig 3.12 A, B). GO-terms more often associated with the genes down regulated by flg22 were linked to electron transport, cell organisation and biogenesis, development and DNA or RNA metabolism (fig 3.12 A, B).

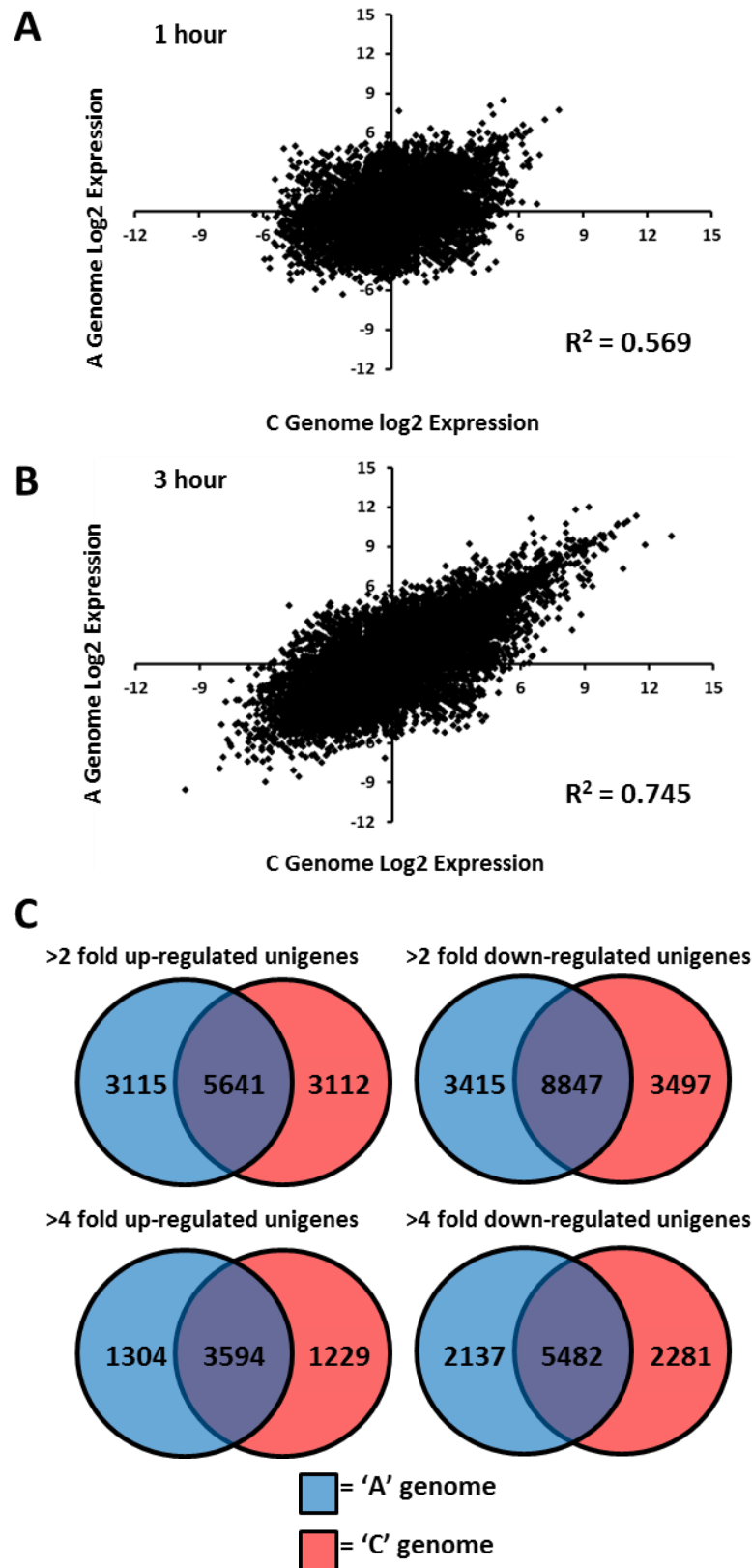


Figure 3.11 Co-expression of homologous genes after *flg22* treatment in *Brassica napus*.

Correlation of log₂ fold expression for *B. napus* unigenes present in both the A and C genomes at (A) one hour and (B) three hours after PAMP treatment. (C) Genome specific up regulation of *B. napus* unigenes. Numbers indicate number of unigenes two or four fold up or down-regulated three hours after *flg22* treatment in *B. napus*. Unigenes are grouped into A genome specific (blue), C genome specific (red) or unigenes co-up or down regulated between orthologous copies (purple).

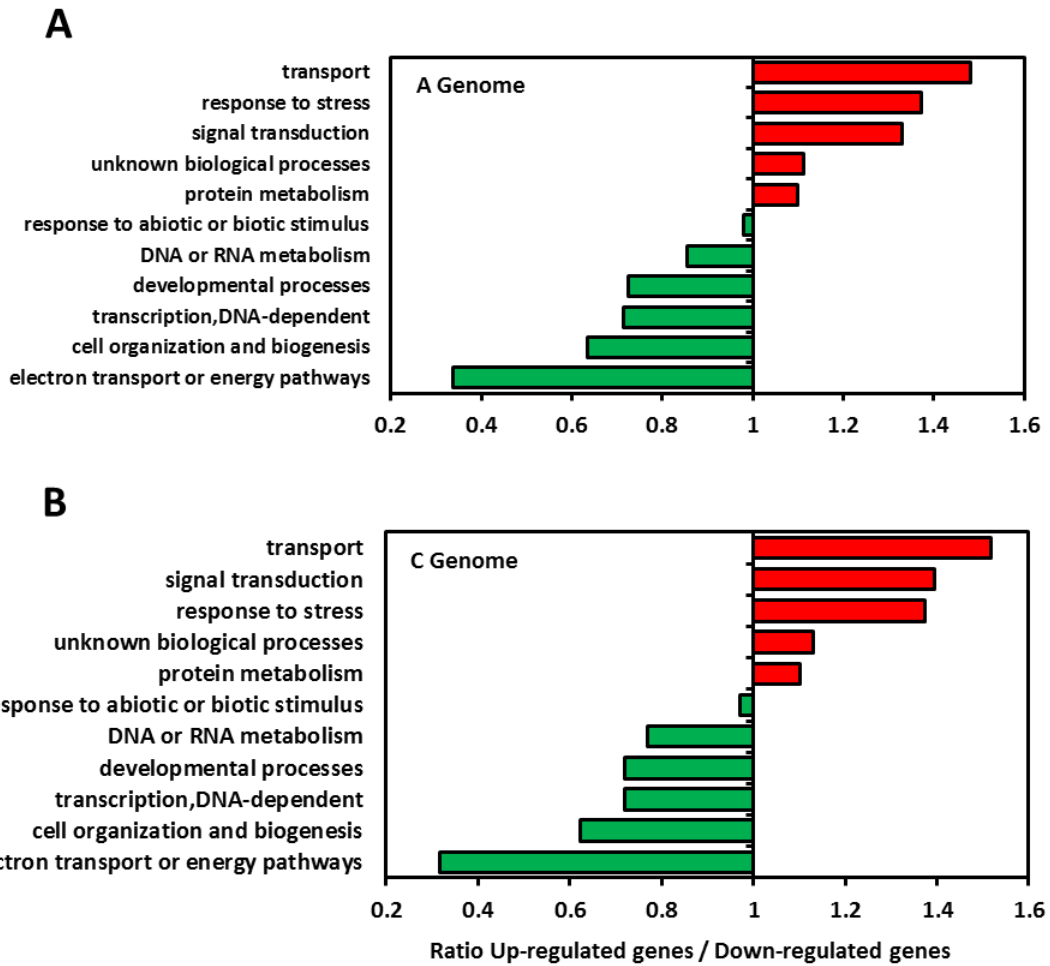


Figure 3.12 Functional characterisation of flg22 responsive genes in *Brassica napus*.

Ratio between flg22 up-regulated and down-regulated unigenes within specific GO-Term categories. Bars in red indicate categories that are enriched in the up-regulated genes. Bars in green indicate categories that were enriched in the flg22 down regulated genes.

The annotation of *B. napus* unigenes with *A. thaliana* GO-Terms also allowed the sub-cellular location of the associated protein to be identified. Unigenes up-regulated by flg22 compared to down regulated genes saw an enrichment of proteins localising to the nucleus, extracellular space and golgi apparatus (fig 3.13). This perhaps indicates that a large number of transcription factors are being expressed at this time (including many *WRKY* transcription factors (Appendix 1)) as well as the secretion of defence linked genes such as chitinases into the apoplast, many examples of which are up-regulated in *B. napus* by flg22 (Appendix 1). Over represented in the down-regulated genes are proteins localising to the chloroplast (fig 3.13), which is a consistent observation amongst whole genome expression analysis after PAMP treatment (Navarro, 2004).

Using the *B. napus* unigenes and *A. thaliana* annotations, Mapman (Thimm et al. 2004) was used to identify processes and gene families that were expressed or down-regulated by flg22. Notable clusters of up-regulated genes correspond to enzymes involved in phenylpropanoid lignin and glucosinolate metabolic pathways (fig 3.14 A). The *WRKY* transcription factor family was also strongly up-regulated by flg22 (fig 3.15 B). There was a down-regulation of pathways involved in photosynthesis, starch regulation and carotenoid synthesis (fig 3.14 A, B).

Significant up-regulation of LRR-RLKs was observed, including most of family XII (fig 3.15 A). The orthologues of the LRR-RLKs *FLS2*, *EFR*, *BAK1*, as well as the LysM-RLP *LYM2* and LysM-RLK *CERK1* were all up-regulated to a similar extent after flg22 treatment, whereas the LRR-RLK *BRI1* (the brassinosteroid receptor) was not affected in its expression (fig 3.15 A, 3.16).

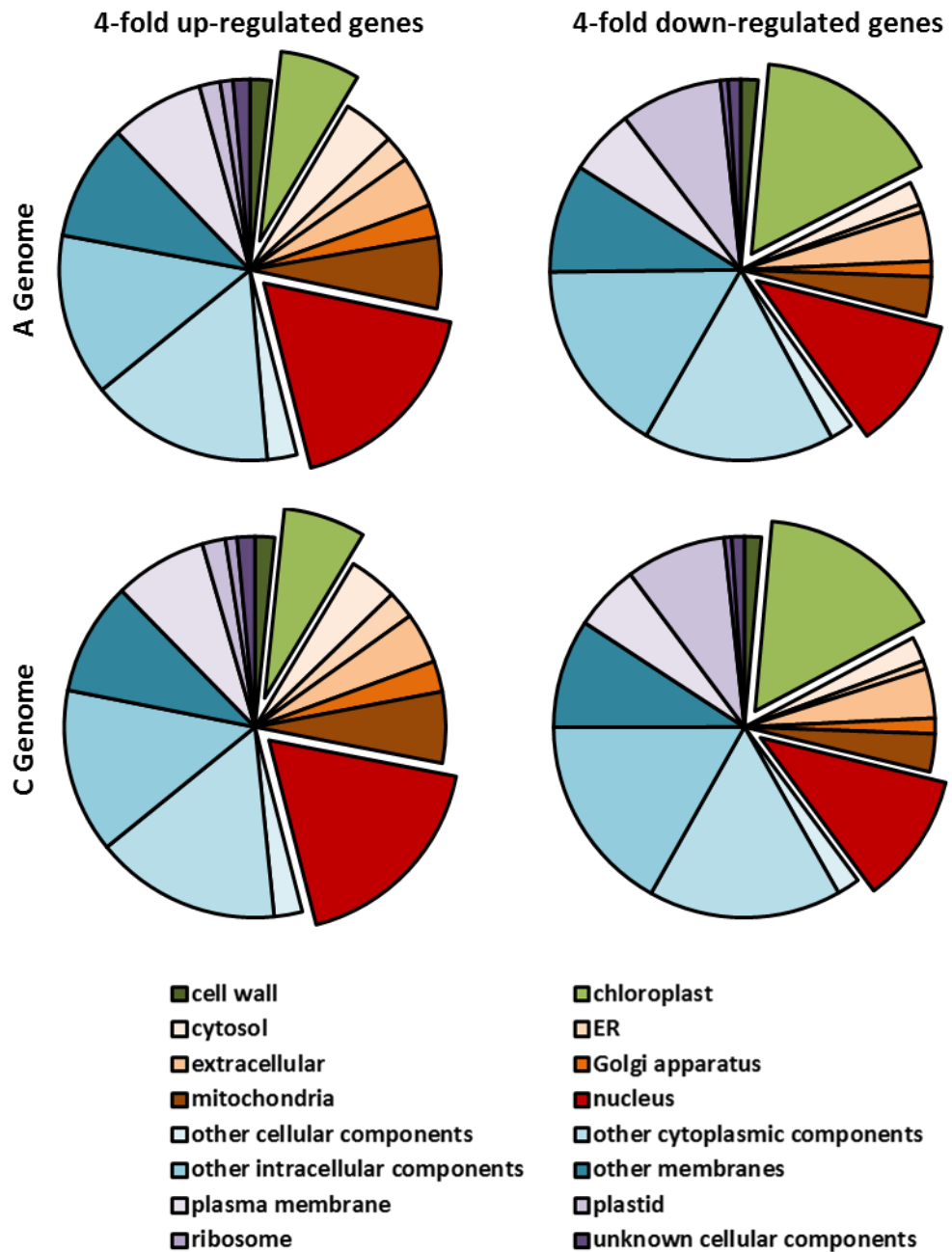


Figure 3.13 Subcellular location of products of PAMP responsive genes in *Brassica napus*.

Relative number of genes annotated with different localisation GO-terms in unigenes with >4 fold up or down regulation in the A and C genomes. Cut away sections highlight genes linked to the Chloroplast (Green) and nucleus (red).

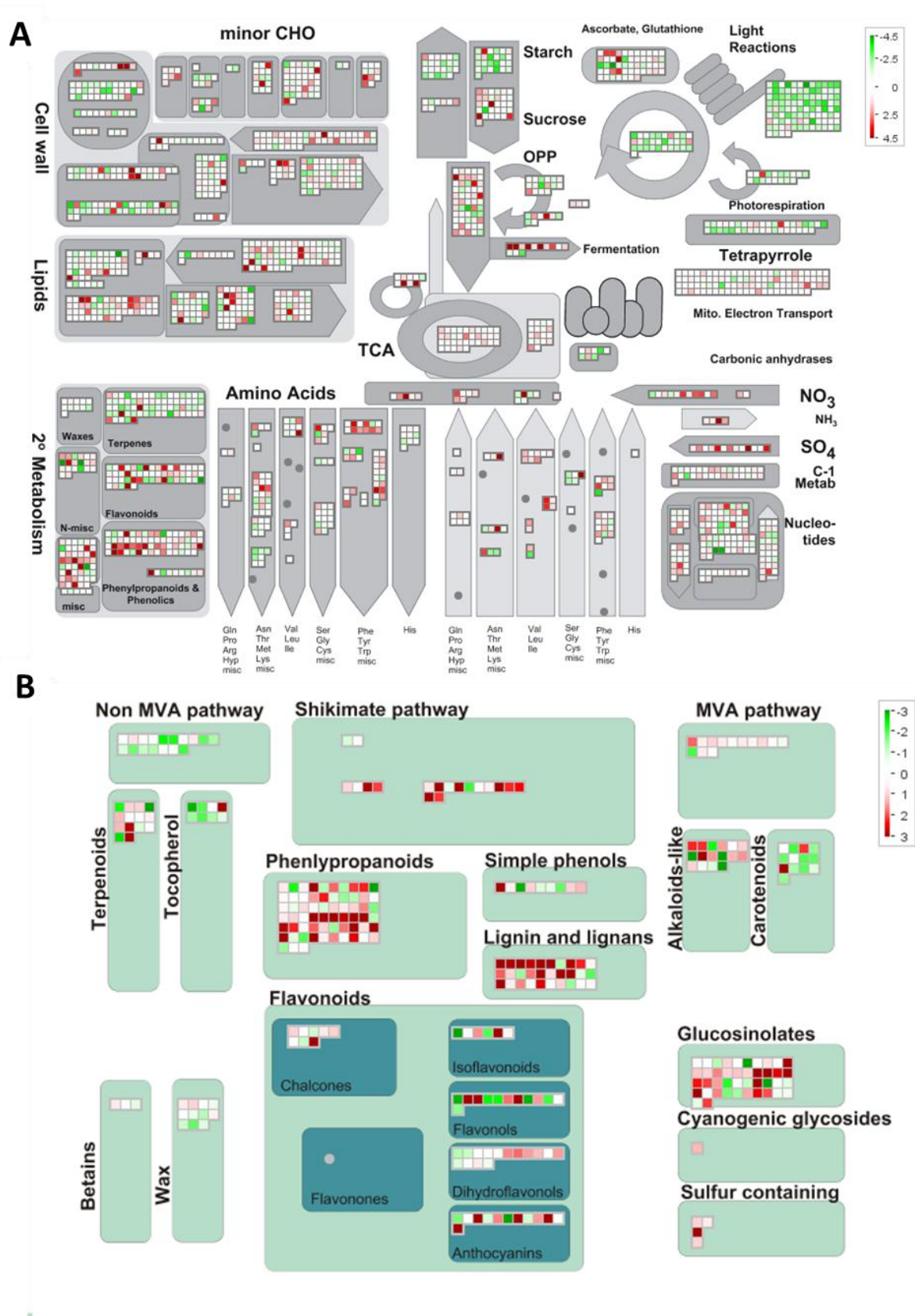


Figure 3.14 Metabolomic pathways up and down regulated by flg22 in *Brassica napus*.

Mapman analysis of flg22 responsive genes in *Brassica napus*. Outputs listed are (A) global metabolism and (B) Secondary Metabolites.

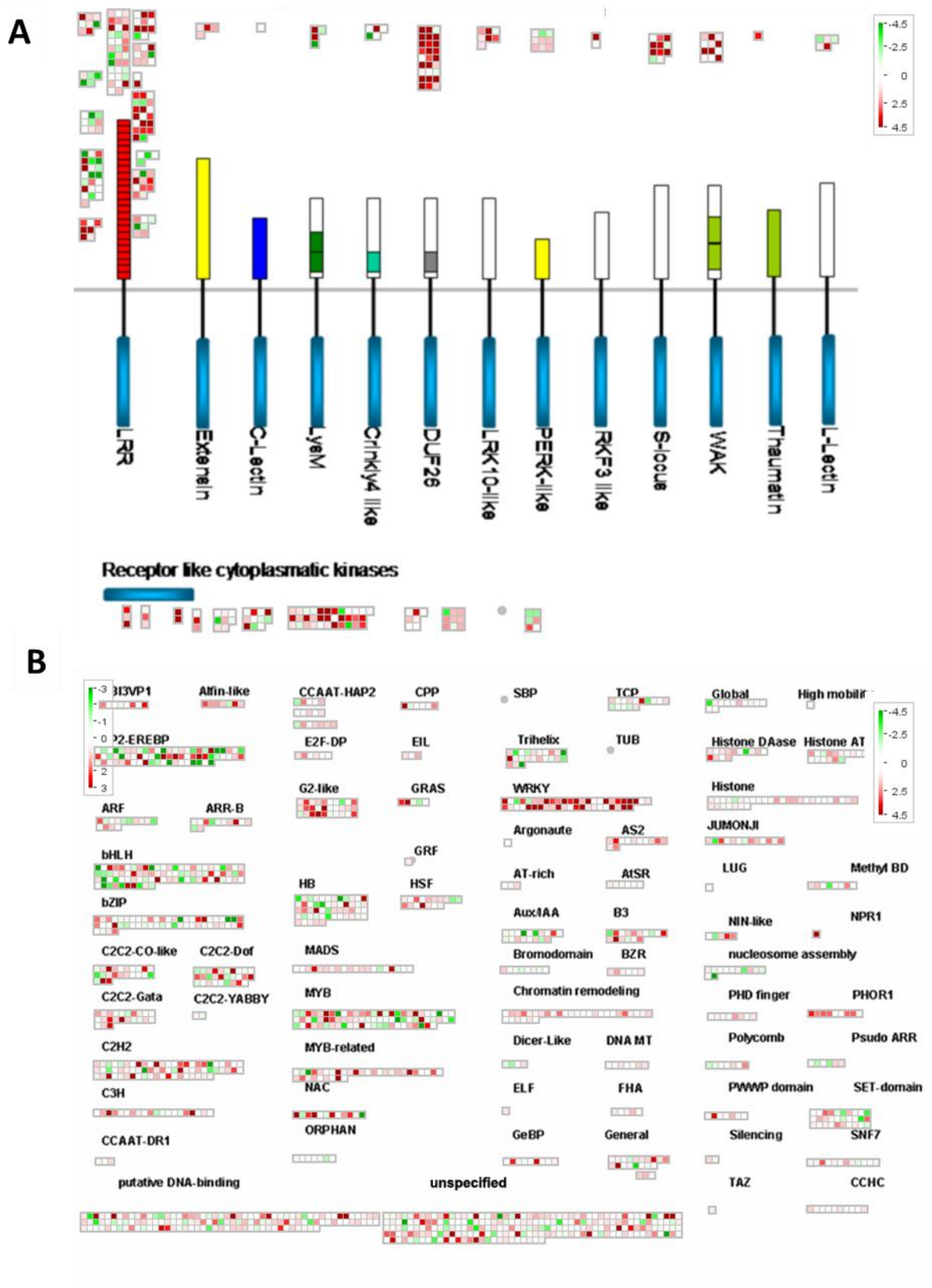


Figure 3.15 RLKs and transcription factor families up and down regulated by *flg22* in *Brassica napus*.

Mapman analysis of *flg22* responsive genes in *Brassica napus*. Outputs listed are (A) RLKs and (B) Transcription factors.

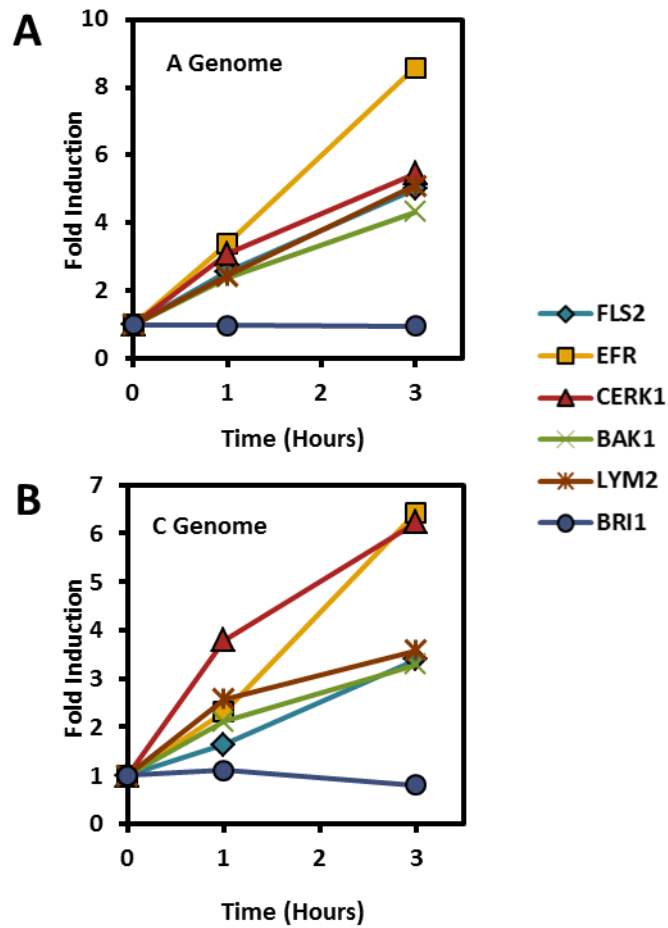


Figure 3.16 RLK Expression in *Brassica napus* after PAMP treatment. Fold expression of the LRR-RLKs FLS2, EFR, BAK1 and BRI1 and the LYS-M containing CERK1 and LYM2 in *B. napus* at 1 and 3 hours post flg22 treatment in the (A) A and (B) C genomes.

3.3.10 PAMP Induced Resistance in *B. napus*

The restriction of pathogen growth following PAMP infiltration is a common assay in many different systems including *A. thaliana* (Zipfel, 2004), *Nicotiana benthamiana* (Hann, 2007), tomato (Nguyen, 2010), soybean (Valdés-López 2011) and rice (Ning et al. 2004). To assess the role of PAMP application in inducing disease resistance in *B. napus*, we developed assays around the use of three different pathogens, *P. syringae*, *B. cinerea* and *Sclerotinia sclerotiorum*.

P. syringae DC3000 is a commonly studied bacterium in model systems and a strain that constitutively expresses the LUXCDABE operon (LUX-hrcC-) has been developed and used in high-throughput disease resistance screens in *A. thaliana* (Fan et al. 2008). To avoid potential ETI responses in bacterial assays a Pto DC3000 hrcC- strain lacking a functional type-three secretion system was generated in the LUXCDABE background. Both strains are luminescent and quantifiable with a photometer, although the HrcC- does have a slightly lower of luminescence for the same number of bacteria (fig 3.17 A). There was a very clear similarity between the luminescence and bacterial number in *B. napus* leaves over a three-day time-course following the inoculation of both strains (fig 3.17 B, C). There was an approximately 50-fold increase in LUX HrcC- photon counts over 3 days, similar to that previously reported for the HrcC- mutant in *A. thaliana* (Hauck et al.2003). Growth was significantly reduced after 100 nM flg22 treatment compared to the water-infiltrated control (fig 3.18 A, B).

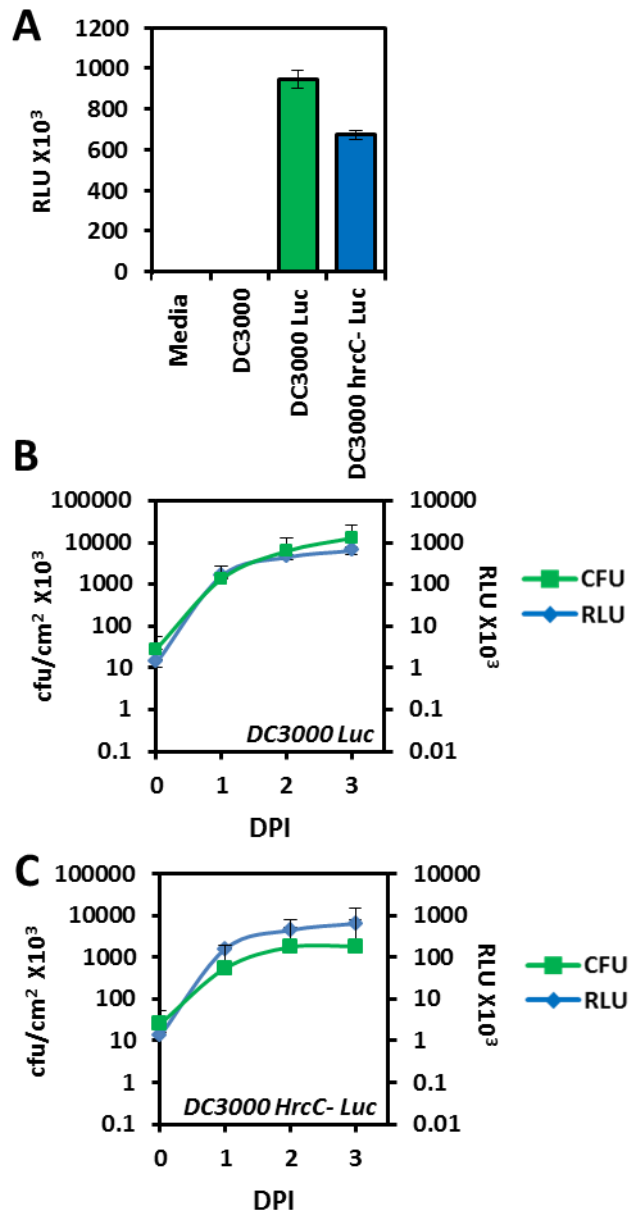


Figure 3.17 Luminoimetric quantification of *Pseudomonas syringae* growth in *Brassica napus*

(A) Luminescence of bacterial suspensions (OD 0.02) or liquid media. (B) Growth of Pto DC3000 LUXCDABE in Temple over three days. The correlation between CFU and RLU was highly significant ($R^2 = 0.8972$). (C) Growth of Pto DC3000 LUXCDABE hrcC- in Temple over three days. The correlation between CFU and RLU was highly significant ($R^2 = 0.9412$). Error bars on the RLU are the standard error of 16 biological replicates. Error bars on the CFU are the standard error of 6 biological replicates.

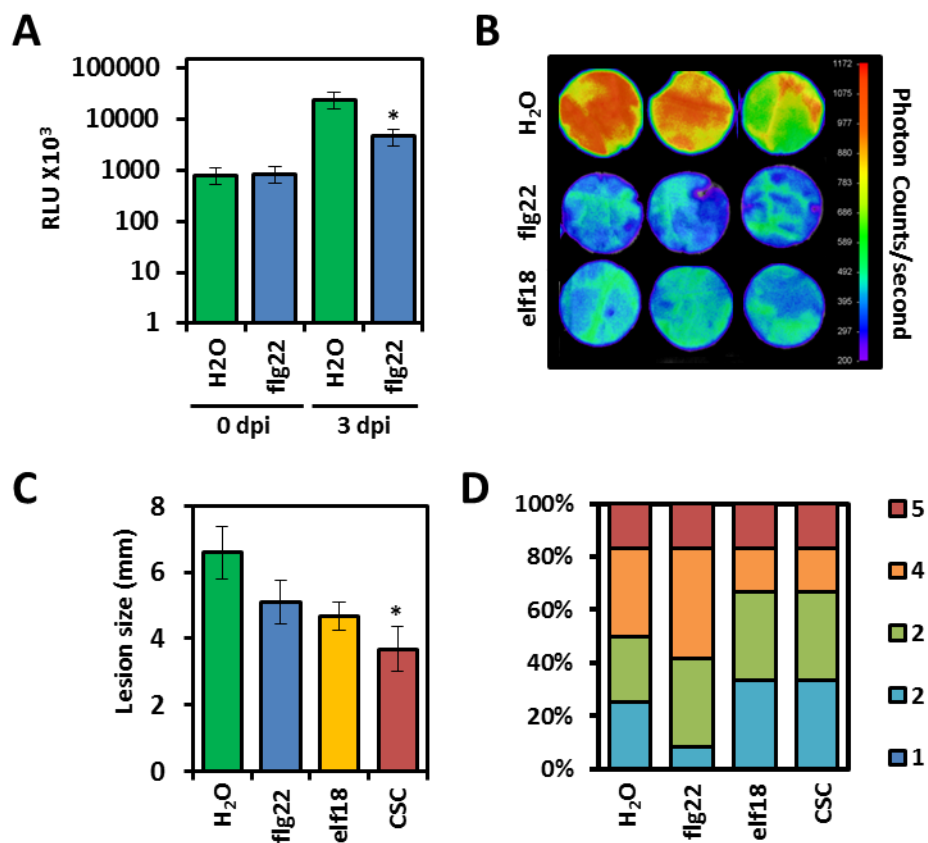


Figure 3.18 PAMP-Induced resistance in *Brassica napus*.

A) Growth of *Pto* DC3000 hrcC- luxCDABE after PAMP treatment by measuring total photons recorded over 5 seconds of sampling. B) Heat map of *Pto* DC3000 hrcC- luxCDABE infiltrated Temple leaf discs (D=20mm) three days after infiltration recorded by NightOwl Imaging software. The scale of the fluorescence is indicated on the bar on at the side. C) flg22- (100 nM), elf18- (100 nM) and CSC- (1 g/L) treatments reduce symptoms caused by *Botrytis cinerea*. D) Symptoms caused by *Sclerotinia sclerotiorum* were not reduced after infiltration with flg22 (100 nM), elf18 (100 nM) or CSC (1 g/L). Scale corresponds to 1-No lesion, 2-no spreading lesion, 3-lesion \leq 10mm, 4 lesion >10mm, 5- Leaf disc fully consumed with extensive aerial hyphae. * indicates a significance ($p < 0.01$) by t-test between PAMP and water treatment.

In order to investigate the effect of PAMP pre-treatment on fungal pathogens of *B. napus*, the ability of flg22, elf18 and CSC to restrict symptom development of *B. cinerea* and *S. sclerotiorum* was determined. Consistent reduction in disease symptoms caused by *B. cinerea* after PAMP treatment was measured, and this was always greatest after CSC application (fig 3.18 C). No decrease in symptoms caused by *S. sclerotiorum* could be observed after PAMP treatment (fig 3.18 D), which may be due to the strong virulence of the strain used on Temple. It will be interesting to test if PAMP treatment can affect disease caused by less virulent strains of *S. sclerotiorum*. Our results nevertheless demonstrate that PAMP-induced resistance provides a quantifiable measure of PTI in *B. napus*, which could be extended to screening with other PAMPs and/or pathogens.

3.3.11 PAMP Induced Metabolome Changes in *B. napus*

Quantifying the increase in defence related metabolites could be used to assess the innate immune response in brassicas. A preliminary investigation was carried out on PAMP induced metabolites in *B. napus*. In order to understand the effect of flg22 treatment on the metabolome as a whole, HPLC and mass spectrometry was performed on flg22 treated or untreated *B. napus* tissue at 6 and 48 hours post infiltration. Metabolites were extracted in organic phase solution (free metabolites) and aqueous phase after acid hydrolysis (for phenolic compounds, glycosides and other conjugates). After flg22 treatment nearly 10% of all unique peaks identified by mass spec were two fold greater or less after PAMP treatment at 6 hours in both organic and aqueous extractions (table 6). The effect of PAMP treatment was greatest at 48 hours, with 12.4% and 9.3% individual peaks more than two fold greater in organic and aqueous respectively, with 16 and 18.1% down regulated more than two fold (table 6). This suggests that flg22 treatment does trigger large metabolome changes in *B. napus*, and it would be interesting to identify some of the induced or repressed metabolites.

<i>Fold Induction</i>	<u>Organic Extract</u>		<u>Aqueous Extract</u>	
	6 hours	48 hours	6 hours	48 hours
<i>>5 fold-up</i>	18 (4.7%)	25 (6.5%)	23 (5.0%)	14 (3.0%)
<i>>2 fold-up</i>	36 (9.3%)	48 (12.4%)	54 (11.6%)	43 (9.3%)
<i>>2 fold-down</i>	37 (9.6%)	62 (16.0%)	74 (15.9%)	84 (18.1%)
<i>>5 fold-down</i>	17 (4.4%)	20 (5.2%)	26 (5.6%)	59 (12.7%)
total peaks		387		464

Table 6 PAMP-Induced Metabolites in *B. napus*.

Number of unique HPLC peaks that showed greater than 2 or 5 fold up or down regulation at 6, 24 and 48 hours post PAMP for aqueous and organic extractions. Peaks were quantified as area under the curve before fold induction was measured comparing PAMP treated samples to water controls at the same time points

As well as looking at metabolome wide changes, the induction of specific metabolites previously reported to be flg22-responsive was also investigated. SA has been reported to be induced at the earliest stages of PAMP response in *A. thaliana* (Mishina, 2007, Tsuda, 2008). In *B. napus*, flg22 did induce an increase in SA levels at 6 hours post flg22 treatment, an over three-fold increase over water controls (fig 3.19 A, B). This is consistent with the level of induction previously reported in *A. thaliana* by Tsuda et al, 2008. Interestingly, there was also an increase in the level of SA in the aqueous extraction, suggesting that the level of SA might be a result of *de novo* synthesis instead of the hydrolysis of stores of glycosylated SA (fig 3.19 B). By 48 hours post PAMP treatment, SA levels returned to the background level seen in non-treated samples, suggesting a transient SA burst after flg22 perception.

Camalexin and scopoletin are two other compounds previously reported to be induced by flg22 (Shenke, 2011). Higher levels of camalexin in the organic phase were observed at 6 and 48 hours post flg22 treatment (fig 3.20 A). No change in camalexin in aqueous samples was observed (fig 3.20 A). Despite clear peaks being identified in the water controls, there was no observable scopoletin in any of the flg22 treated samples (fig 3.20 B). This might be a result of its consumption during the oxidative burst (Levine, 1994). There was no increase in glycosylated scopoletin (scopolin) at 6 hours post flg22 treatment, but there was approximately 50% more hydrolysed scopoletin at 48 hours post flg22 treatment compared to water controls (fig 3.20 B).

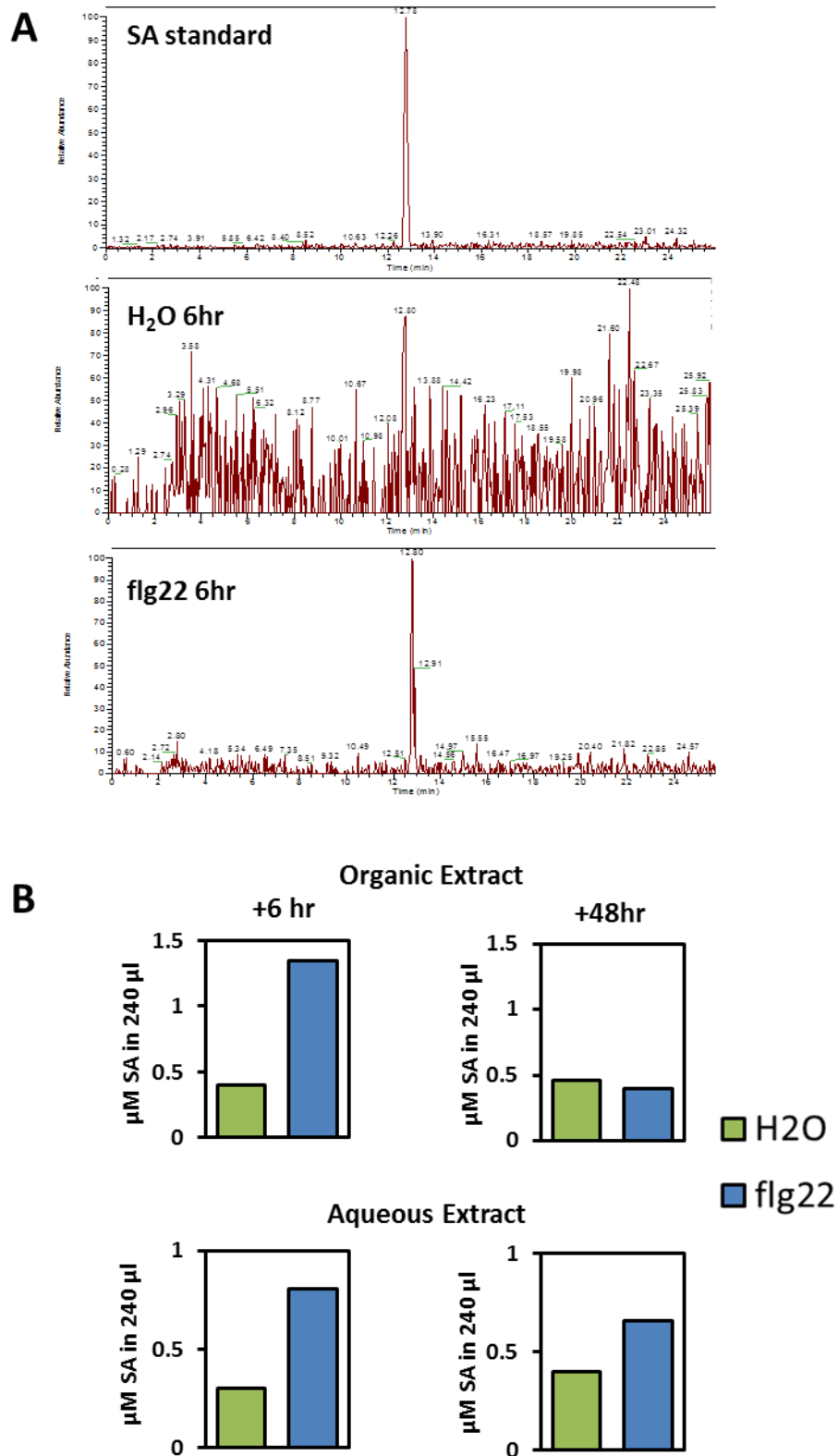


Figure 3.19 Salicylic acid is induced by flg22 treatment in *Brassica napus*.

(A) Mass spec peaks of an SA standard and corresponding peaks in organic extractions from *B. napus* leaf discs 6 hours after infiltrated with H₂O or flg22 100nm. (B) Quantification of SA in 6 hour and 48 hour organic and aqueous extractions. SA was quantified by comparison of peak area to a SA standard. Data is the mean of 4 samples at each time point.

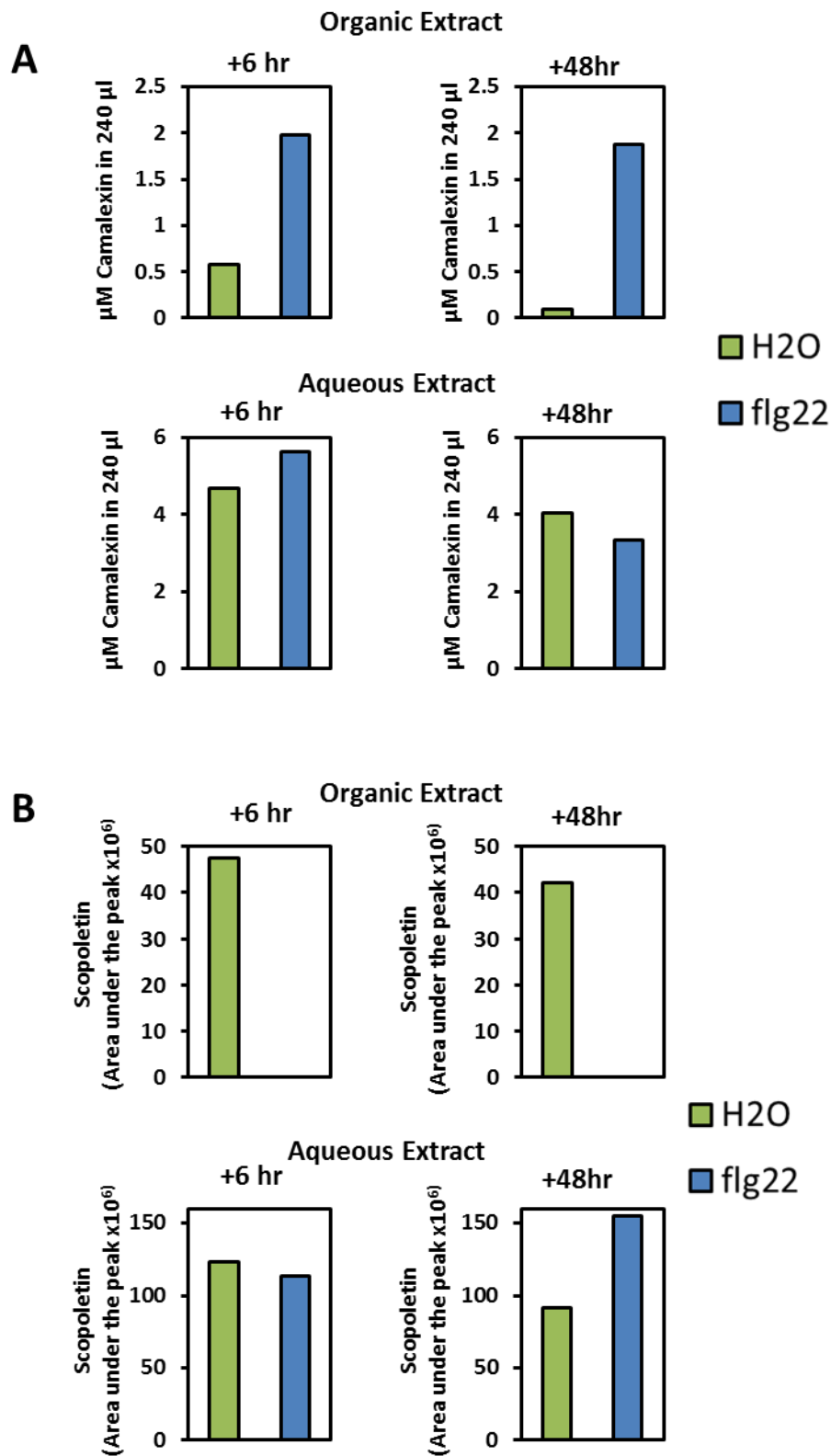


Figure 3.20 Quantification of camalexin and scopoletin after flg22 Treatment.
 Quantification of (A) camalexin and (B) scopoletin in 6 hour and 48 hour organic and aqueous extractions. Camalexin was quantified by comparison of peak area to a camalexin standard. As no scopoletin standard was available, data is presented as area under the peak. Data is the mean of 4 samples at each time point.

In order to see any direct fungi-toxic effect of extracted metabolites from PAMP-treated samples compared to control extractions, the growth of *B. cinerea* in the extracts was recorded for three days post inoculation. Germinating spores of GFP tagged *B. cinerea* in the absence of metabolites rapidly grew in the liquid media with increasing fluorescence observed until 3dpi (fig 3.21 A, B). All extracted metabolite solutions, at both 1 and 0.01% concentration, saw limited or no growth of *B. cinerea* past germination (fig 2.21 A, B). There was no discernible difference in the effect of metabolites from PAMP treated extracts and water treated controls on the growth of *B. cinerea*. The presence of EtOH at equivalent volume to the extracts slowed the growth of *B. cinerea* at both 1 and 0.01% (fig 3.21 A, B). In order to see an effect of PAMP treated metabolites compared to water controls it may be necessary to lower the concentration of the metabolites even further below that used. A difference may also be seen when the metabolites are applied only after spores have germinated, as there maybe metabolites expressed at a basal level that inhibit germination, as opposed to growth of the pathogen.

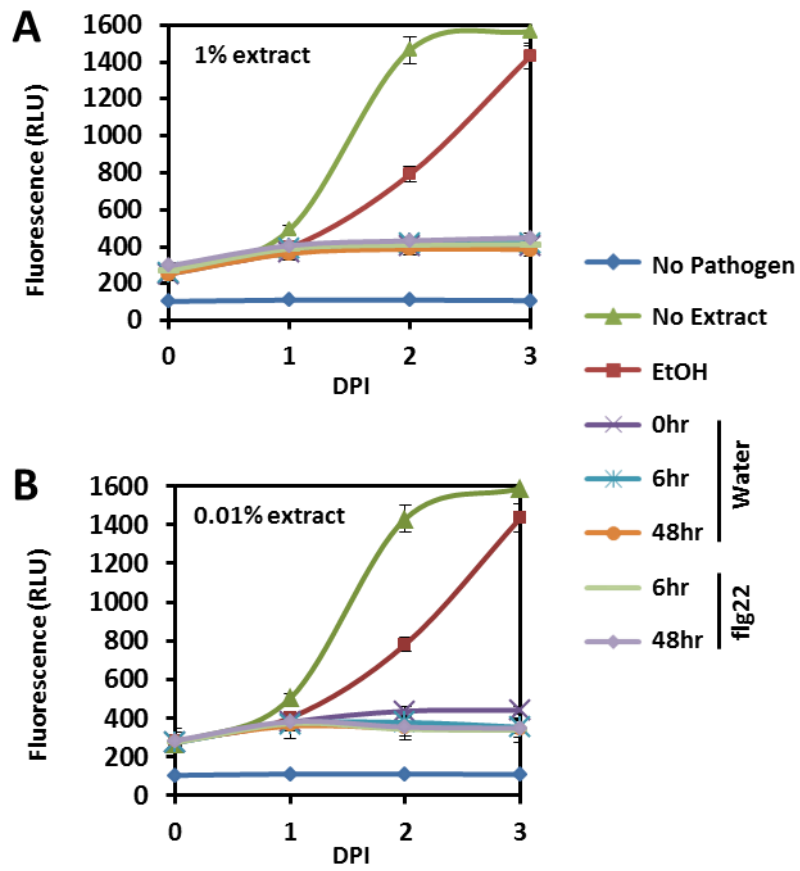


Figure 3.21 Growth of *B. cinerea* in metabolite extractions after fig22 treatment.

Fluorescence of germinating *B. cinerea* spores (2.5×10^6 spores/ml) in MS media in a 96-well plate over three days in a range of different metabolite solutions.

3.3.12 Natural Variation in PAMP Responsiveness in *B. napus*

Further to the demonstration that the *B. napus* variety POSH MC169 had significantly higher PAMP inducible callose than the variety Temple (fig 3.6 C, D), the variation in the oxidative burst between *B. napus* lines was investigated. The *B. napus* cultivars investigated are present in the genetic diversity set OREGIN containing traits of interest to breeding programs (<http://www.oregin.info>). Substantial variation was found between cultivars in the oxidative burst response to flg22, elf18 and CSC (fig 3.22 A-D). Some cultivars such as POSH MC169 gave a consistently strong response to all three PAMPs (fig 3.22 A-C, red bar). Notably, cultivars with a strong response to one PAMP did not necessarily give a strong response to other PAMPs. Ningyou, a cultivar that is very susceptible to *L. maculans* (Fitt et al. 2008), had a high response to flg22 and very low responses to elf18 and CSC (fig 3.22 A-C, yellow bar). In contrast, Capitol responded strongly to elf18 and CSC but very weakly to flg22 (fig 3.22 A-C, green bar). No significant variation was found in the background levels of H₂O₂ between accessions (fig 3.22 D).

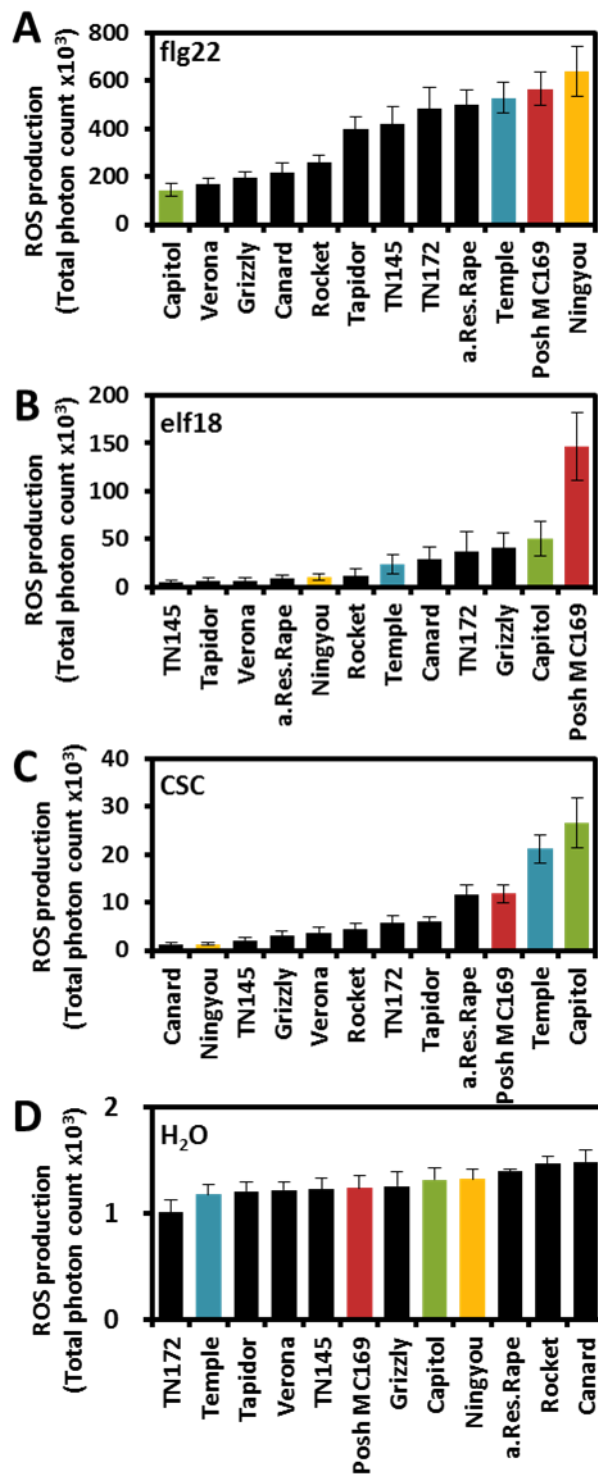


Figure 3.22 Variation in PAMP responses between *B. napus* cultivars. A-D Oxidative burst in response to flg22 (100 nM), elf18 (100 nM) or CSC (4 g/L) or H₂O treatment. Data is expressed as total photon counts over 40 minutes with error bars representing the standard error of 8 biological replicates. Cultivars discussed in the text are highlighted in the following colours: Temple (blue), POSH MC169 (red), Capitol (green), Ningyou (yellow).

3.4. Discussion

In this chapter a range of techniques have been developed to enable characterisation of the PAMP response in *B. napus*. The assays cover early molecular events occurring within the first hour of PAMP perception, transcriptional and metabolomic changes within three hours, cell wall reinforcement observed over days and methods to investigate the increase in pathogen resistance PAMP perception causes. The assays developed here have wide applicability in many different future studies, and it is hoped that tools such as the PAMP induced transcriptome will be a valuable resource to the brassica research community in the future. The remainder of this project is to take some of these assays and assess the natural variation between brassica genotypes, and to investigate the genes giving rise to this variation. As such only a few of these assays are used again within this project, and their suitability as mapping tools is discussed here.

The observation that the oxidative burst is highly polymorphic between cultivars of oilseed rape (fig 3.22) is important. As a high throughput response, quantitation of the oxidative burst lends itself well to large population genetics, including QTL mapping and associative transcriptomics. This approach has been demonstrated in soybean, where Valdez-Lopez et al (2011) used the oxidative burst in response to flg22 to map four QTL between parents with variation in quantitative resistance. With a wealth of mapping populations with segregating quantitative resistance in brassica species, including the recently fine mapped Tapidoor x Ningyou cross (Qiu, 2006), it would be interesting to see how diverse these lines are in PAMP response.

At least two separate MAPKs are phosphorylated within five minutes of PAMP treatment and the two bands correspond in size to AtMPK3 and AtMPK6. It has been suggested by Liang et al (2013) that the functions of MAPKs between *A. thaliana* and *Brassicacae* may not be entirely conserved. Identifying the exact MAPKs that have been phosphorylated in our study then, would require significantly more work. It would be interesting to see if elf18 and CSC also lead to a similar response.

The assay is not high-through-put and therefore not amenable to QTL or GWAS studies.

PAMP induced callose deposition has been observed in many different systems, but may not be suitable when handling multiple genotypes. It is high throughput, but the assay is unreliable with large within-genotype variation (fig 3.6, a-d). Luna et al 2011 reported that callose deposition varied substantially with environmental conditions and the timing of sampling and warned of drawing conclusions on defence related signalling based on callose alone. Although an attempt has been made to quantify the callose here (fig 3.6 b, c), it is ultimately a qualitative measurement based on the presence or absence of callose. As variation existed in the size of individual deposits, a measure of “total deposits” may be redundant, as fewer, larger deposits might be more physiological relevant than many smaller ones. This issue may be solved by assessing the relative intensity of the callose stain across samples instead of total deposits (as seen in Luna, 2011 for example). Nevertheless, the difference between Temple and POSHMC169 is striking, potentially indicating impairment in PAMP and wound induced callose in the line Temple, which should be considered if any of the mapping populations where it is parent are to be screened.

Examples of PAMP-induced lignification are rare in the literature (Adams-Phillips 2010 is an example), but it is more frequently observed during pathogen interactions (Mohr, 2007, Lee, 2001). Three different methods were developed here for assessing PAMP-induced lignin. The phloroglucinol staining used here did capture PAMP-induced lignification, but this is difficult to quantify directly. Fluorometric measurements of the red stain are difficult, not least because of the insolubility of lignin resulting in a suspension of insoluble lignans instead of a consistent solution. Phloroglucinol staining of wounded leaf tissue did reveal enhanced lignification after PAMP treatment, but only in conjunction with wounding (fig 3.8, A, B). It is unclear if the combination of PAMP plus wounding resulted in higher lignification because of the cumulative effect of wound and PAMP signalling, or a result of increased penetration of the PAMPs after cuticle damage. This result might suggest that PAMP perception is involved in the normal

wound responses in leaf tissue, as any open wound in natural environments would be flooded with flagellin expressing microbes. The interaction between JA mediated wound responses and FLS2 signalling is unclear, with Dennes et al (2011) reporting JA as having an inhibitory effect on cell wall damage (CWD) mediated lignification. In the same study RBOHD mutants were reported to have decreased CWD induced lignification, suggesting a complex interplay between ROS and JA mediated responses at wound sites. How PAMP perception or PAMP-triggered ROS production interacts with lignification processes remains to be studied in model systems.

Absolute quantification of lignin through a thioglycolic acid precipitation method did show an increase in flg22 triggered lignin production at 24 and 72 hours post PAMP treatment, but this was not consistent with CSC application, which might be a result of the lower efficacy of the CSC preparation used (as seen in fig 3.2A). If the assay were to be developed further, investigating the temporal dynamics of the response would be necessary to identify optimum sampling conditions. All three methods of assessing lignin trialled here would be amenable to high throughput study in *Brassica* populations. As lignification responses have been suggested to be essential in resistance to *L. maculans* (Fitt, 2008), looking at the diversity of pathogen, PAMP or wounding induced lignification in segregating populations displaying quantitative resistance (for example Darmor x Eurol (Huang, 2009)) might be fruitful. As ROS is reported to enhance wound induced lignin (Denness 2011), it would also be interesting to observe the lignification phenotype of POSH MC169, which produces high H₂O₂ in response to all PAMPs (fig 3.22) and has a high pod shatter score, a result of elevated lignification between the valve margins of seed pods (Ostergaard, 2006).

Identifying PAMP responsive marker genes was essential, and genes previously reported as being up-regulated early in the interaction with *Sclerotinia* (Zhao, 2009) did show a similar expression pattern on flg22 and CSC treatment at 1 and 3 hours after application (fig 3.10). *MPK3*, *MPK4* and *WRKY33* have all been reported previously as being up-regulated by flg22 in *A. thaliana*, (Navarro, 2004). Although we saw moderate levels of induction of 4 to 8 fold for these genes, some genes

have been reported with significantly higher levels of induction which might serve as better markers including *FRK1*, *At2g17700* and *NHL10* (Albrecht, 2012 ,Lozano-Duran, 2013). All three of the marker genes selected are core components of PTI signalling and might be expected to have a similar level of induction between flg22 and CSC (fig 3.10).

The genome-wide transcriptomics of PAMP treated *B. napus* tissue has produced a valuable resource for the *Brassica* research community. Such extensive changes to the expression profile of *B. napus*, where approximately 25% of all genes were more than four fold up or down regulated by flg22, are similar to what has been reported before in *A. thaliana* (Navarro, 2004). The list of up and down regulated genes annotated with TAIR descriptions of their closest *A. thaliana* BLAST hit might be useful for identifying new marker genes. From the list *WRKY28* appears to be a very strong candidate – all 6 copies across the two genomes are up-regulated more than 1000 fold, suggesting it is strongly induced and consistent between copies (Appendix 1). Other good candidates include *ATNRT2.6*, annotated as a nitrate transporter in *A. thaliana*, and *AT1G51800.1*, a LRR-RLK. The expression profiles of these putative marker genes need to be studied further under a wider range of time points and PAMP / pathogen treatments.

The genes showing induction or repression by flg22 treatment broadly agree with the transcriptional changes reported in *A. thaliana* and rice: a general down regulation of photosynthetic and energy pathways is consistently observed, as is the high expression of genes functionally annotated as being involved in transport and stress response (Akimoto-Tomiyama et al. 2003; Navarro et al., 2004;). The observation that many nuclear localised proteins are induced at early time points (fig 3.13) is another hall mark of early flg22-triggered expression changes (Navarro, 2004).

The expression dataset as it is presented here can also be used for further analyses. The observation that the PRRs *FLS2*, *EFR* and *CERK1* are all similarly up-regulated while *BRI1* is not (fig 3.16) might be used to identify other novel PRRs. Any LRR-RLK

or LYS-M RLK showing a similar expression pattern to these PRRs could be identified and studied further.

The annotation of the *B. napus* unigene models with *A. thaliana* identifiers has allowed for functional analysis, but care must be taken that similar function is not assumed for homologous genes between the two species (Liang, 2013). It is likely that many BLAST hits of *B. napus* genes are not hitting the most functionally related target, especially for large gene families like the WRKY transcription factor. The annotations must be taken as a guide until proper alignments of *B. napus* genes of interest and *A. thaliana* sequence is performed. Other potential issues arise from functionally annotating a brassica expression set with *A. thaliana* data. In the case of using MAPMAN analysis for example, homoeologous copies within the A or C genome were discarded – a huge loss of potentially valuable candidate genes. Approximately 10% of the genes showing greater than 5-fold up-regulation have no clear homology to *A. thaliana* genes (Appendix 1).

As a tetraploid, the genetics of *B. napus* is more complicated than *A. thaliana*, and to begin to understand how complex transcriptional responses are mounted across a polyploidy organism a correlation of the expression level of homologous genes between the A and C genome was carried out (fig 3.11). Most homologous pairs were up or down regulated together, suggesting a high conservation of the regulation between homologous genes. This analysis could be taken a lot further in subsequent work, including the conservation and polymorphism of key nodes in PTI signalling such as *FLS2*, potentially looking at homologous expression level and gene or promoter sequence divergence. PAMP-induced expression changes might be a great model system for investigating transcriptional regulation in *B. napus* because of the high selection pressures on PRRs (Monaghan, 2012) and the potential benefit of diversification of PAMP recognition domains between redundant homeologous copies. It would also be interesting to investigate the handful of genes that show opposing levels of expression between homologs, although many of these may be false positives as a result of extremely low basal expression (Appendix 1).

PAMP-induced resistance was assessed in three brassica pathogens *P. syringae*, *B. cinerea* and *S. sclerotiorum*. *P. syringae* has the advantage of being heavily studied in *A. thaliana* and genetic resources exist for it. The DC3000 LUXCDABE HrcC- strain is ideal for assessing PIR in brassica, lacking a TTSS and growing relatively well on the crop. Quantifying luminescence is a rapid means to measure bacterial growth that lends itself well to large scale mapping programs. Significant reduction in the growth of this pathogen was observed after treatment with flg22 (fig 3.18). Assessing *B. cinerea* lesion size is another high throughput technique, although quite variable between biological replicates. Significant reduction in symptoms was observed after PAMP treatment, particularly after CSC application (fig 3.18). No increase in resistance to *S. sclerotiorum* was observed however after any PAMP application. This may be a result of experimental conditions, where the *S. sclerotiorum* was at optimum virulence and growing too rapidly to observe moderate increases in resistance after PAMP treatment. A range of *S. sclerotiorum* isolates exist however and it may be possible to find less virulent isolates. Alternatively, it might be that the variety Temple worked on here is particularly susceptible to the strain, and assessing PIR to *S. sclerotiorum* might be successful on a more resistant line. Ideally *L. maculans* would also have been included, as the most destructive pathogen of Brassicas worldwide (Fitt, 2008), but no viable PAMP induced resistance assay could be developed for the pathogen. As *L. maculans* also takes a long time to develop, over a period of weeks, the impact an isolated dose of PAMPs at a very early time point on the ultimate phenotype recorded remains to be seen.

From the initial pilot experiment into PAMP-induced whole metabolome changes, there is potential to expand further and begin to characterise many of the up regulated compounds. It is encouraging that the metabolites SA and camalexin, both known to be up-regulated by PAMPs, were found in the extracted metabolites (fig 3.19, 3.20). The dataset does however contradict the previously published result that scopoletin is induced by flg22 (Shenke, 2011). Although an increase in PAMP treated aqueous samples at 48hours was observed, which is likely to be a combination of scopoletin and acid-hydrolysed scopolin. In the organic extractions

there was no detectable scopoletin present in any flg22 treated sample, despite producing clear peaks in the water control. Levine et al (1994) suggest that the cellular scopoletin is consumed in the oxidative burst by peroxides, but we still see no scopoletin at 48 hours after PAMP treatment, when H₂O₂ levels are assumed to be much lower. Differences between the study presented here and the Shenke (2011) experiments are the timing of recording at 24 hours post treatment, and the extraction method which used solid phase extraction cartridges, which may result in higher retention rates of scopoletin. As they did not partition the scopoletin into organic and aqueous phases, it might be that if the aqueous and organic data were combined a single extraction of our samples would reveal an increase in total scopoletin in flg22 treated samples.

The very large difference in PAMP responses measured between *B. napus* cultivars indicates that PTI could readily be mapped to test associations with quantitative disease resistance. The identification of molecular markers associated with quantitative disease resistance would be of considerable benefit in *B. napus* breeding programs.

There are many different assays that have been reported in the literature that have not been developed here, but may well be applicable to *Brassicas*. Ethylene biosynthesis is one of the classic methods to measure flg22 response, (Felix, 1999). Similarly Ion fluxes and early Ca²⁺ influx are key assays for PTI in *A. thaliana* (For example, Segonzac 2011). These are only possible once aqueroir transformed *Brassica* lines are available, and this was not within the scope of this project. It would also be possible to screen a range of different PAMPs outside of flg22, elf18 and CSC. Peptidoglycan and oligogalacturonides could be easily screened in brassicas as well as different preparations of chitin or chitosan.

A range of assays have been developed in *B. napus* that dissect the PAMP response at multiple levels, from early signalling to the induction of resistance. The tools described here can have widespread applicability in the brassica research and breeding community. Some of these tools have high throughput applicability and

will be used in the following chapters to characterise PAMP responsiveness and resistance in different brassica populations.

**Chapter 4 : Association Transcriptomics of
PAMP Responses and Pathogen Resistance
in *Brassica napus***

4.1. Aim

The objective of the research presented in this chapter was to perform a genome wide association study (GWAS) of PAMP responses and resistance within the *B. napus* association genetics panel developed by Ian Bancroft and Andrea Harper (Harper, 2012). The four traits to be mapped were the oxidative burst in response to flg22 and elf18, and resistance to the pathogens *B. cinerea* and *P. syringae*. These traits were phenotyped in 84 lines before previously identified Single Nucleotide Polymorphism (SNP) and Gene Expression Markers (GEMs) in the population were used in a GWAS to identify significant associations with the observed phenotypic variation. Finally the correlation between PAMP responses and resistance is discussed as well as initial description of significantly associated genes.

4.2. Introduction

Association genetics is emerging as a powerful tool to identify the genetic basis of phenotypic diversity. The approach takes underlying polymorphism within a large population and correlates the SNPs within to quantitative traits of interest. Since the first GWAS study investigating age-related macular bone degeneration in 2005 (Klein, 2005), the approach has become very common in human genetics studies. High profile examples include investigations into human evolutionary origins (Lim 2008; Garrigan 2006), success in school (Rietveld, 2013) and resistance to infectious disease (Chapman, 2012). These studies typically investigate a high number of sequenced individuals ranging from around 100, for example the population of 96 used in Klein et al (2005), to over 100,000, such as the 126,559 transcriptomes used in Rietveld et al (2013), allowing powerful statistical associations to be identified.

GWAS are increasingly being applied in plant research. Atwell et al (2010) published a GWAS of 107 different phenotypes in *A. thaliana*, including 23 defence related traits such as recognition of the effector *AvrRPM1*, *Pst* DC3000 growth and aphid fecundity. The results demonstrated that GWAS was possible within relatively

complex plant genomes, although issues including polyploidy and population structure between related lines are likely to complicate studies in plants.

GWAS have also been applied in crop plants. In Rice, an Affymetrix SNP array of 44,100 SNPs used to genotype 413 individuals was used in a GWAS to find loci involved in phenotypes as diverse as flowering time, plant height and *Magnaporthe grisea* resistance (Zhao, 2011). In maize, GWAS of traits such as leaf architecture, kernel oil content and resistance to southern leaf blight have been performed (Tian, 2011; Li, 2013; Kump, 2012). In the latter study, Kump et al (2012) identified 6 RLKs associated with defence within previously identified QTLs for quantitative resistance, potentially indicating the power of the method to identify novel PRRs within crop species. In barley, 500 diverse cultivars were genotyped using an array of 1,536 SNPs across a number of barley expressed sequence tags (ESTs) and used in a GWAS to identify variation behind morphological characteristics including anthocyanin colouration and ear altitude (Cockram, 2010). Both the maize and barley studies have been run using a relatively small number of SNP markers however, limiting the ability to find novel associations.

The further refinement of GWAS studies in these crops, and the development of new GWAS populations, is limited by a low number of identified SNP markers and the lack of reference genomes to order them against. Advances in mRNA sequencing technologies may help here as they are enabling high throughput SNP identification protocols coupled with relatively rapid assembly of reference sequences. mRNA-seq has another advantage of quantifying variation in transcript abundance as well as in nucleotide sequence, providing another potential source of association to phenotypic data. This was termed 'associative transcriptomics' by Harper et al (2012) who first used the method in a GWAS of oil quality traits in *B. napus*, a plant with no previously published genome.

In the Harper *et al* study, a pseudomolecule reference sequence for *B. napus* was produced by ordering the illumina reads from the mRNA-seq data against unigene sequences arranged on a pre-existing SNP map. A panel of 84 lines was sequenced, relatively few for a GWAS study, and these were selected from diverse genetic

backgrounds representing seven different crops types. The reads had an average depth of coverage of 34.9 reads and 101,644 SNPs were identified across 11,743 unigenes in total. However, with such a small population it was necessary to only run GWAS using alleles found in greater than 5% of the population in order to prevent excessive false positives, reducing the number of SNPs that could be mapped to 62,980. Using this SNP reference and unigene expression data they were able to map loci known to be important for low erucic acid content (the genes ERU1 and ERU2) and low glucosinolate content (HAG1), demonstrating a successful proof of concept for using associative transcriptomics in a polyploid crop species.

Many questions still remain about using the *B. napus* association genetics panel developed by Harper et al however. The two phenotypes investigated are both relatively simple, conferred by single loci in the A and C genomes. Furthermore both traits have artificially selected allelism present within the sequenced population as deletions in ERU1, ERU2 and HAG define 'canola', the oilseed crops with superior quality oil found in most modern varieties. As such the robustness of this mapping population to identify novel markers has not been tested using a genuinely quantitative phenotype with no previously characterised allelism. In this study then, the association genetics panel developed by Harper et al will be used to try and identify the genetic variation, both in sequence and expression, that underlies quantitative variation in PAMP response and pathogen resistance.

4.3. Results

4.3.1 Overview of Associative Transcriptomics Method

Four high throughput defence related traits were studied using GWAS: the flg22 and elf18 triggered oxidative bursts; resistance to *Pseudomonas syringae* DC3000 LUXCDAB *hrcC*-; and resistance to *B. cinerea*. Phenotyping was performed four times for each trait, and the final GWAS was run using the predicted mean from a mixed linear model in GENSTAT, taking line as a fixed model, and experiment and plate (for ROS and DC3000 assays) as random variables. Error bars in figures depicting the predicted mean show the standard error of that mean. For each trait a GWAS was performed using both SNP and GEM data, with results for each presented separately.

4.3.2 Associative Transcriptomics of the flg22 Triggered Oxidative Burst In *B. napus*

Significant variation in the oxidative burst was observed in the lines of the association genetics panel (fig 4.1). There was generally good reproducibility between phenotyping repeats, however one of the repeats had higher than usual variability between biological replicates. The strongest responding line, N01D-1330, had approximately ten-fold more total luminescence than the weakest responders Rocket x Lizard and Primor (fig 4.1).

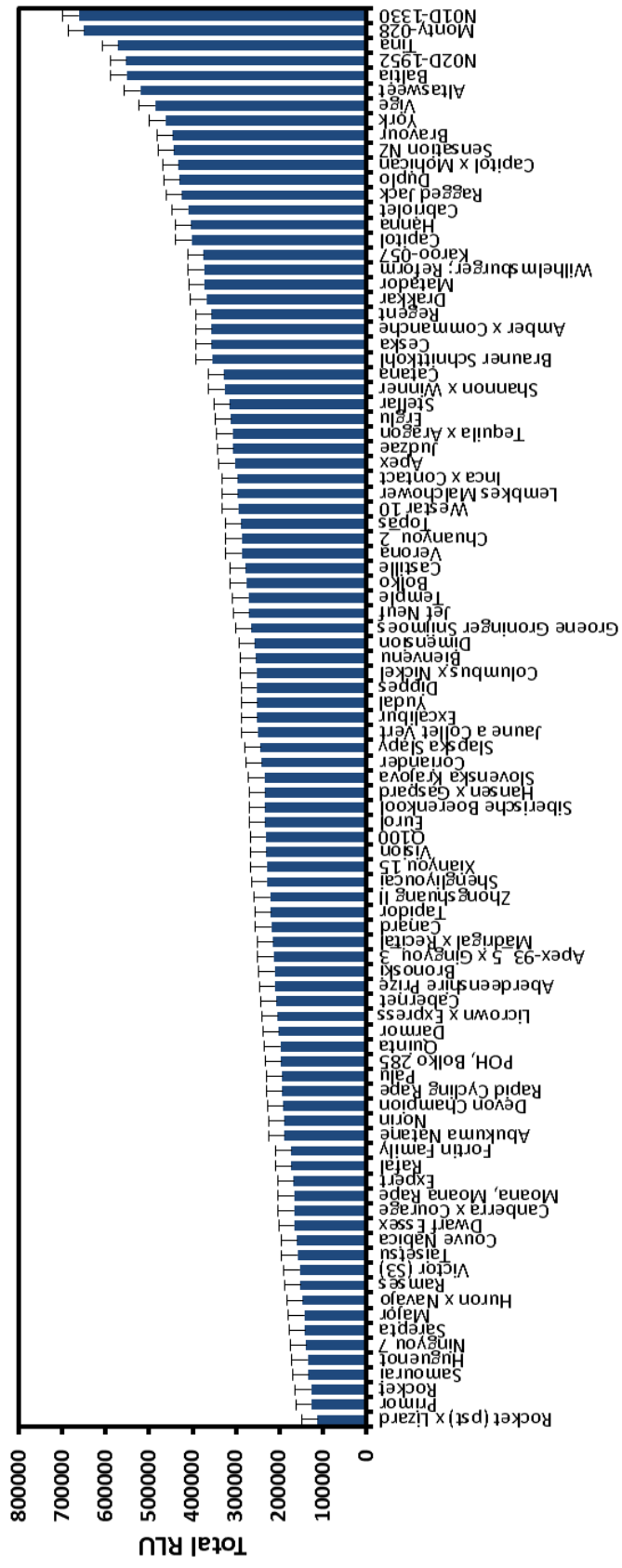


Figure 4.1 The fig22 triggered oxidative burst in the association genetics mapping panel of *Brassica napus*. Total RLU observed over a 40 minutes time period. Data represent the predicted mean of 4 separate experiments each with eight biological repeats. Error bars show standard error of the predicted mean.

A GWAS was run on the phenotypic data using the SNP and GEM information to identify the most significant markers. Significant peaks were observed for both SNP (fig 4.2) and GEM markers for this phenotype (fig 4.3). SNP markers can achieve significance through linkage to a causative gene, so true SNP markers must be clustered together around a given locus. We see this effect here with clusters seen on A3, A6, A7, C3 and C4, although their significance is lower than the other traits studied (fig 4.2). There were over 230 SNP associations to this phenotype with significance above 0.005 (Appendix 3, table 15). The top 50 significantly associated SNPs are summarised in table 6.

Because expression can vary greatly between closely linked genes, a clustering effect is not expected with GEM markers, as seen in fig 4.3. Furthermore the candidates identified through the GEM GWAS may be the causative gene of interest. Amongst the top 50 significantly associated GEM markers are *CPK34* and *TIR1*, defence related genes previously studied in *A. thaliana* (table 8). Also within this list are *PTR3* involved in defence against bacteria, and *WRKY21* (Appendix 4). The expression of *CTR1*, a negative regulator of ethylene signalling, was also significantly associated with ROS response. This perhaps indicates that ethylene is as essential for PTI in *B. napus* as it is in *A. thaliana* (Boutrot, 2012).

Although no SNP in *FLS2* or *RBOHD* was found at high enough abundance in the population (>5%) to be included as a SNP markers, the expression variation in *FLS2*, the receptor for flagellin, is significantly associated with the magnitude of the oxidative burst with a p-value of 0.0037 (Appendix 4). This can be seen in greater detail in figure 4.4 which plots expression against the flg22 triggered ROS score.

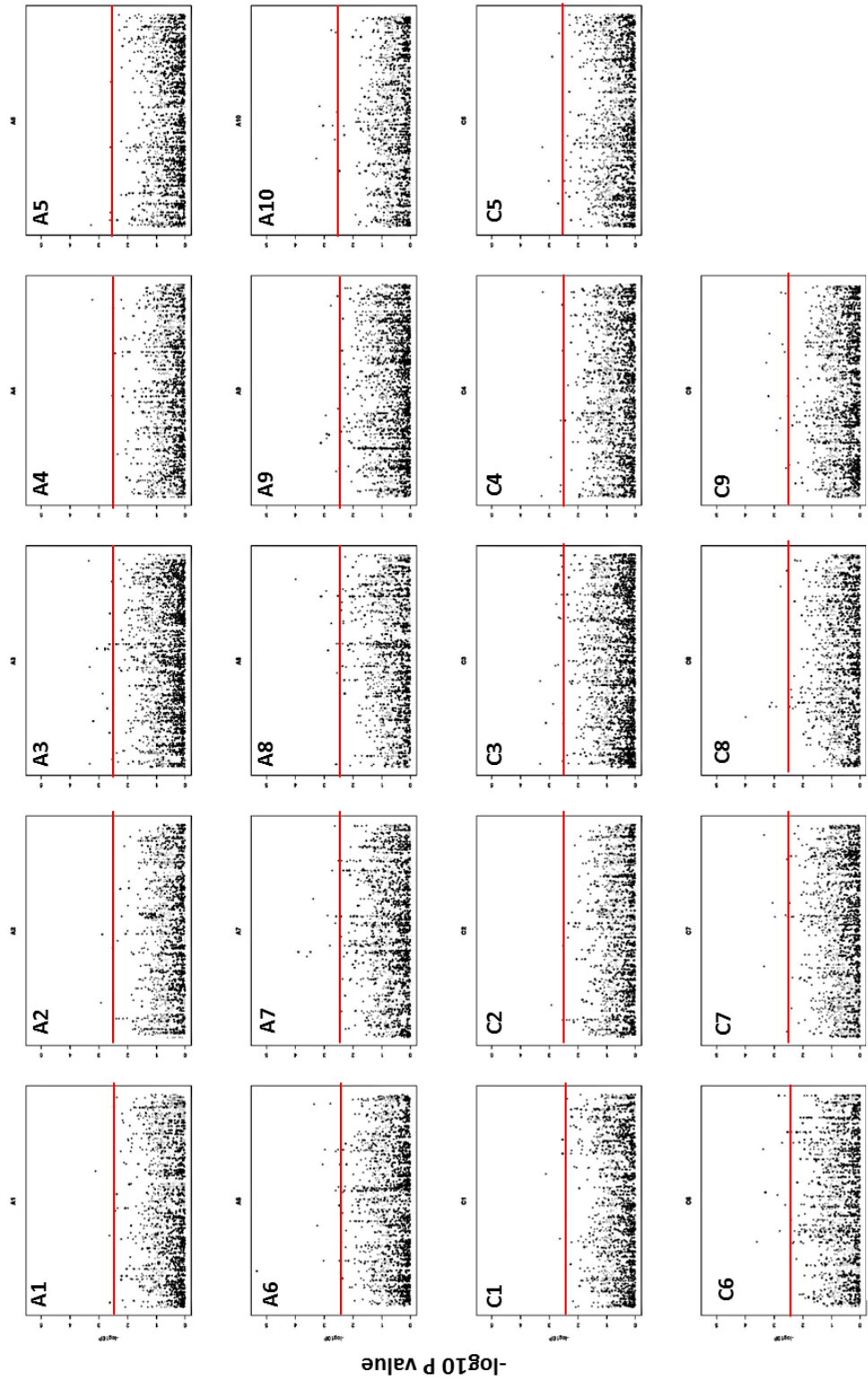


Figure 4.2 SNP markers associated with the fig22-triggered oxidative burst in *Brassica napus*

Manhattan plots for each *B. napus* chromosome plotting significance of SNP against its predicted unigene position. Significance ($-\log_{10} P$ value of >2.5) is marked with a red line. Grey dots represent SNPs in illumina reads that could not be assigned conclusively between the A and C genome homeologous copies of the unigene scaffold, and are represented twice here at both possible loci.

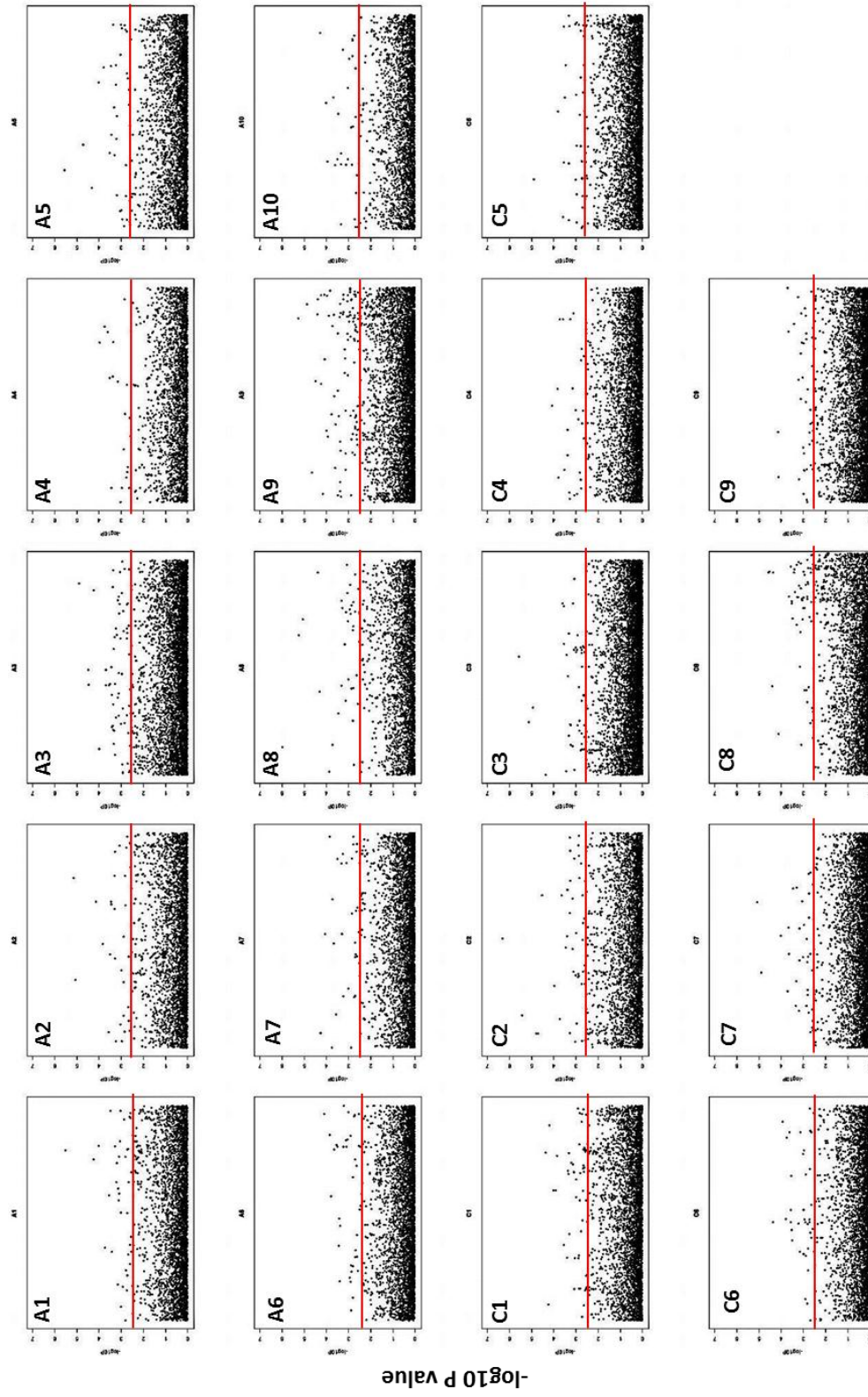


Figure 4.3 GEM markers associated with the flg22-triggered oxidative burst in *Brassica napus*
 Manhattan plots for each *B. napus* chromosome plotting significance of SNP against its predicted unigene position. Significance ($-\log_{10} P$ value of >2.5) is marked with a red line.

SNP	Significance (p)
JCVI_12463:129	4.63805E-06
JCVI_30759:518	1.72962E-05
JCVI_14795:1676	6.0592E-05
JCVI_30759:467	7.03307E-05
JCVI_33304:460	9.7997E-05
JCVI_30759:465	0.000100777
JCVI_10078:234	0.000103876
JCVI_2719:644	0.000119581
JCVI_7991:117	0.000126515
JCVI_12463:180	0.000188997
JCVI_12463:46	0.000210779
JCVI_33238:546	0.000235035
JCVI_11365:304	0.000251921
JCVI_13874:348	0.000272146
EX103538:405	0.00032358
JCVI_15947:250	0.000329204
JCVI_7991:149	0.000333365
CX192962:751	0.000387208
JCVI_3665:541	0.000414794
JCVI_29979:45	0.000447605
JCVI_1857:838	0.000454572
JCVI_23132:470	0.000454814
JCVI_3059:300	0.000476159
JCVI_8179:311	0.00048658
JCVI_20940:51	0.000487824
JCVI_7974:322	0.000499072
JCVI_2942:202	0.000501406
JCVI_6684:249	0.000506844
JCVI_14575:174	0.000530956
JCVI_2097:359	0.000541575
JCVI_583:233	0.000568781
JCVI_3961:297	0.000570532
JCVI_5214:926	0.000575748
JCVI_16241:957	0.000591545
JCVI_7974:498	0.000605492
JCVI_6767:295	0.00060789
JCVI_34009:584	0.000641444
JCVI_26740:389	0.000648
JCVI_36253:302	0.000657875
JCVI_27578:176	0.000672756
JCVI_14056:572	0.000696867
JCVI_12748:700	0.000709697
JCVI_17868:1294	0.000715694
JCVI_36898:123	0.000745433
JCVI_7541:361	0.000762134
JCVI_9864:532	0.000763114
JCVI_22578:590	0.00076909
EV196300:116	0.000777252
JCVI_10269:592	0.000787063

Table 7 The 50 SNP markers most significantly associated with the flg22-triggered oxidative burst.

Unigene	At Accession	Tair 10 Annotation	Significance (p)
C_JCVI_27731	AT3G58680.1	DNA binding / transcription coactivator	5.03852E-07
A_EV025046	AT5G19360.1	CPK34	1.05455E-06
C_ES914047	AT5G55940.1	EMB2731	1.65894E-06
C_JCVI_21002	AT2G26990.1	FUS12 (FUSCA 12)	2.7296E-06
A_ES914047	AT5G55940.1	EMB2731	2.85154E-06
C_EV025046	AT5G19360.1	CPK34	2.88844E-06
A_JCVI_23682	AT3G17465.1	RPL3P	3.0706E-06
C_JCVI_9798	AT5G15450.1	ATP binding / ATPase/ nucleoside-triphosphatase	3.83963E-06
A_JCVI_21002	AT2G26990.1	FUS12 (FUSCA 12)	5.21696E-06
A_EX096842	AT5G01750.2	unknown protein	5.53029E-06
A_EV085469	AT5G57890.1	anthranilate synthase	5.794E-06
A_JCVI_18851	AT3G26170.1	CYP71B19	7.30209E-06
C_JCVI_19563	AT2G33585.1	unknown protein	7.59054E-06
A_JCVI_15910	AT1G20670.1	DNA binding	8.94854E-06
A_EV174841	AT3G60245.1	structural constituent of ribosome	9.33652E-06
C_JCVI_17889	AT1G65790.1	ARK1 (A. THALIANA RECEPTOR KINASE I)	1.17288E-05
C_EX115551	AT4G15030.1	unknown protein	1.25555E-05
C_CD826806	AT5G07300.1	BON2 (BONZAI 2)	1.27226E-05
A_JCVI_26945	AT4G28025.1	unknown protein	1.29215E-05
A_JCVI_6339	AT5G64370.1	PYD3	2.3193E-05
C_EE424660	AT1G08510.1	FATB	2.76187E-05
C_JCVI_26802	AT1G08220.1	unknown protein	3.06004E-05
A_JCVI_7256	AT2G25730.1	unknown protein	3.52152E-05
A_JCVI_28242	AT1G48920.1	nucleic acid binding	3.74878E-05
A_AM389775	AT2G26990.1	FUS12 (FUSCA 12)	3.85741E-05
C_JCVI_19110	AT1G23190.1	intramolecular transferase, phosphotransferases / phosphoglucomutase	3.97447E-05
A_JCVI_31949	AT1G16040.1	unknown protein	4.0678E-05
C_AM389775	AT2G26990.1	FUS12 (FUSCA 12)	4.07758E-05
A_JCVI_2920	AT1G06460.1	ACD32.1	4.21348E-05
A_EE424660	AT1G08510.1	FATB	4.25751E-05
C_JCVI_23682	AT3G17465.1	RPL3P	4.36266E-05
C_JCVI_26123	AT1G08510.1	FATB	4.46127E-05
C_EX096842	AT5G01750.2	unknown protein	4.5128E-05
A_DY009852	AT2G38140.1	PSRP4 (PLASTID-SPECIFIC RIBOSOMAL PROTEIN 4)	4.76562E-05
A_JCVI_17151	AT2G16570.1	ATASE (GLN PHOSPHORIBOSYL PYROPHOSPHATE AMIDOTRANSFERASE 1)	5.61029E-05
A_JCVI_117	AT1G06400.1	ARA2	5.72757E-05
A_JCVI_28763	AT4G24920.1	protein translocase	5.77192E-05
A_JCVI_13023	AT1G27330.1	unknown protein	5.80481E-05
C_EX099001	AT4G35290.2	GLUR2	5.82597E-05
A_DY013286	AT3G20000.1	TOM40	5.88256E-05
A_JCVI_8950	AT4G02980.1	ABP1 (ENDOPLASMIC RETICULUM AUXIN BINDING PROTEIN 1)	7.10612E-05
C_JCVI_11858	AT2G44450.1	hydrolase, hydrolyzing O-glycosyl compounds	7.40008E-05
A_JCVI_41863	AT4G19110.1	ATP binding / protein kinase/ protein serine/threonine kinase	7.43966E-05
C_JCVI_2920	AT1G06460.1	ACD32.1	7.89312E-05
A_JCVI_25962	AT2G31650.1	DNA binding / nucleic acid binding / protein binding / zinc ion binding	8.22618E-05
C_JCVI_36897	AT1G30510.2	oxidoreductase	0.000158275
C_EV225069	AT5G09250.1	KIWI	0.000204063
C_JCVI_29480	AT5G15970.1	KIN2 (COLD-RESPONSIVE 6.6)	0.00022008
C_JCVI_30615	AT3G62980.1	TIR1 (TRANSPORT INHIBITOR RESPONSE 1)	0.000251224

Table 8 The 50 most significantly associated GEM markers for the flg22-triggered oxidative burst.

Unigenes in the A or C genome are annotated with their predicted *Arabidopsis* homolog accession number and Tair 10 annotation.

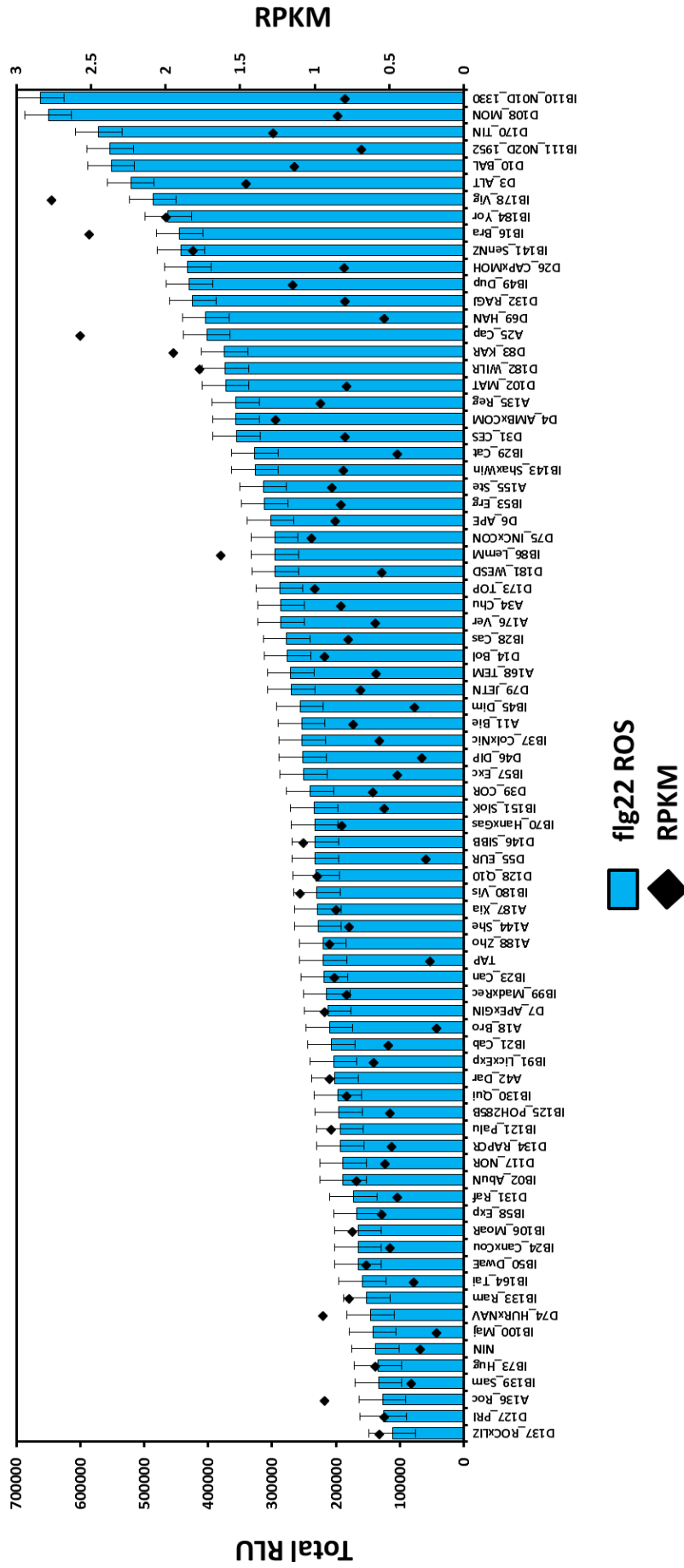


Figure 4.4 FLS2 expression correlates with the flg22 triggered ROS burst in different *Brassica napus* varieties

Phenotyping scores represent the predicted mean of four separate experiments, each with 8 biological repeats. Error bars indicate the standard error of that mean. RPKM is the expression of the unigene JCVI-12710 (FLS2) in reads per million as calculated in the mRNA-seq of every line in the association mapping panel.

A number of significant GEM markers include genes related to auxin signalling and flowering time. *FUSCA12/COP12/CSN2*, a negative regulator of photomorphogenesis, and *ABP1*, an auxin binding protein are both significantly associated with ROS production. The expression of the negative regulator of auxin signalling, *AXR3*, is also significantly associated with ROS. Auxin signalling and PTI are well known to be antagonistic pathways (Navarro, 2006), but it is interesting that mRNA level of these developmental related genes at the seedling stage is associated with a defence related phenotype within the adult plants (5-6 weeks old). The flowering time associated genes *ARA2*, *FRIGIDA* and *MAF4* are also significantly associated with the flg22 triggered oxidative burst (Appendix 4). *BON2* (BONZAI 2), a gene previously identified as promoting growth and repressing cell death pathways (Yang, 2005), is also significantly associated. The presence of many genes like *BON2*, *AXR3* and *ABP1* in the associations suggests that interplay and antagonism between development and defence might be a major determinant behind the variability in PTI observed between brassica varieties.

4.3.3 Associative transcriptomics of the elf18 triggered oxidative burst In *B. napus*

Significant variation in the elf18 triggered oxidative burst was observed in the lines of the association genetics panel (fig 4.5). There was strong reproducibility between phenotyping repeats. The strongest responding line, York, had approximately 20 fold more total luminescence than the weakest responder Bienvenue (fig 4.5).

Many significant peaks were observed for both SNP (fig 4.6) and GEM markers for this phenotype (fig 4.7). Significant clusters of SNP markers can be seen on most chromosomes, but standout peaks are observed on A1, A5, A9 and C1, C5, C8 and C9 (fig 4.6). There were over 1686 significant SNP associations to this phenotype with significance above 0.005 (Appendix 3, table 15). This is a lot higher than the flg22 triggered oxidative burst (fig 4.3, table 15), most likely a result of extremely high similarity between the phenotype scores over the four repeats. The top 50 significantly associated SNPs can be seen in table 9.

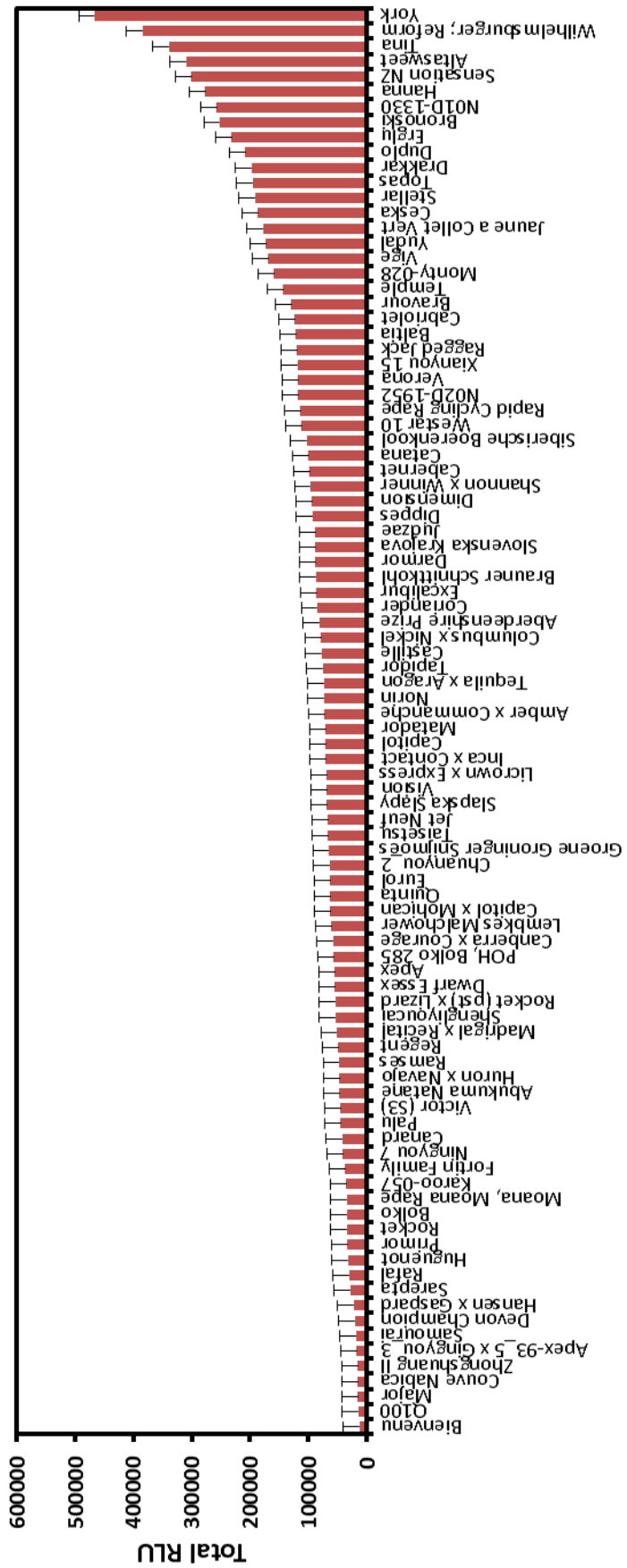


Figure 4.5 The elf18 triggered Oxidative Burst in the Association Genetics Mapping Panel.

Total RLU observed over a 40 minutes time period. Data represent the predicted mean of 4 separate experiments each with 8 biological repeats. Error bars show standard error of the predicted mean.

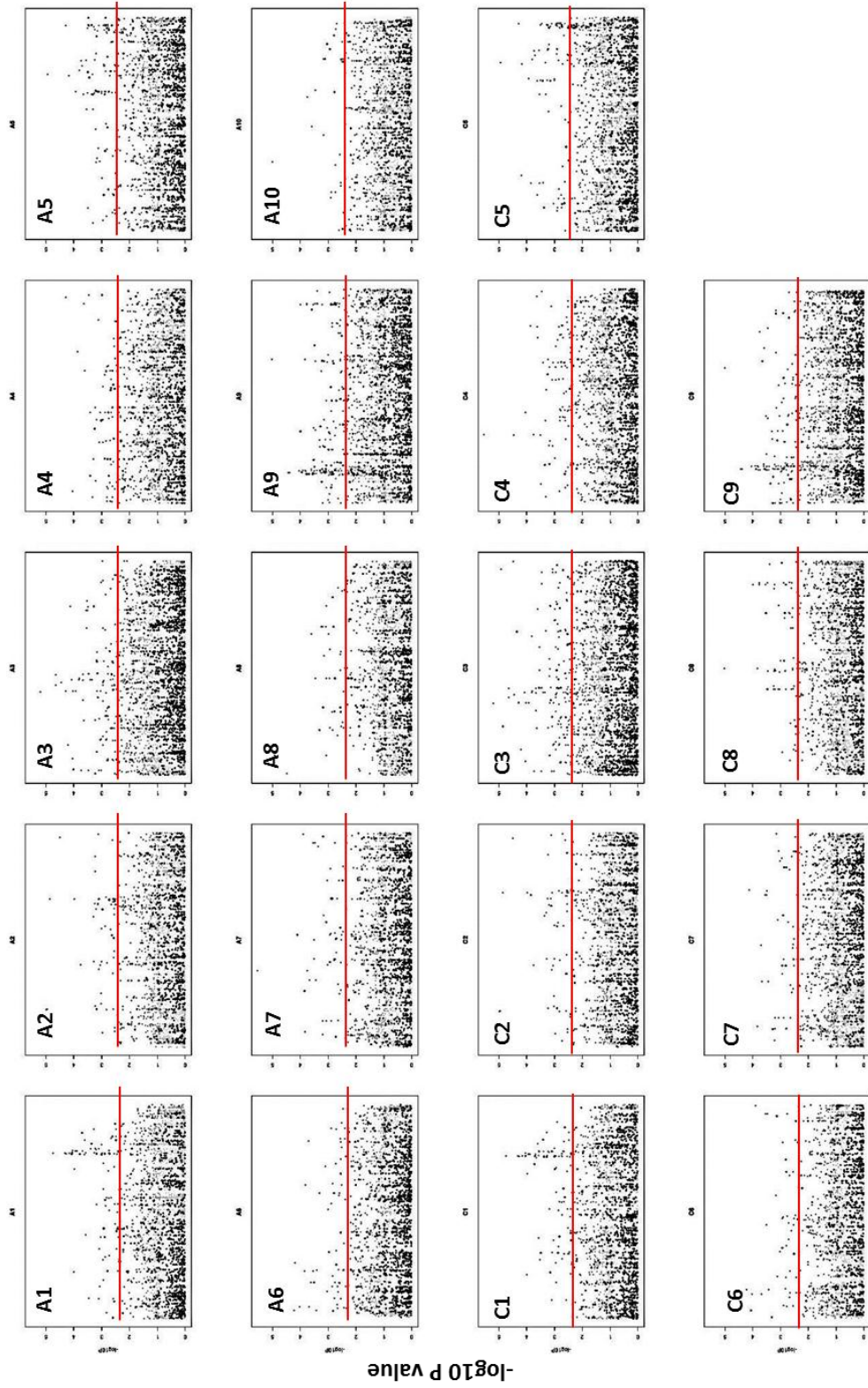


Figure 4.6 SNP markers associated with the elf18-triggered oxidative burst. Manhattan plots for each *B. napus* chromosome plotting significance of SNP against its predicted unigene position. Significance ($-\log_{10} P$ value of >2.5) is marked with a red line. Grey dots represent SNPs in illumina reads that could not be assigned conclusively between the A and C genome homeologous copies of the unigene scaffold, and are represented twice.

Like the GEM associations found with flg22 ROS, there are many defence related candidates significantly associated with the elf18 ROS. Among the most significant include *PLDALPHA 1*, implicated in response to bacterial and fungal pathogens (Zhao, 2013; Pinoso 2013), *RPS5*, RESISTANT TO PSEUDOMONAS SYRINGAE 5, a well-studied R gene in *A. thaliana*, and *FLS2* (table 10, Appendix 4). Many genes linked with development and auxin signalling are associated including *EMB2731*, *AIR12* and *ARA2* again (table 10).

Like with the flg22 triggered ROS associations, many genes reported to be at the interface between development and defence trade-offs have been found here. These include *BON2* again and *ASB1/WEI7*, involved in ethylene sensitivity and regulating auxin signalling in root formation (Ivanchenko, 2008).

Quite striking in the list of significant associations with the elf18 triggered ROS phenotype is the number of homeologous genes with similar significance. Homeologous copies of *EMB2731*, *MAF4*, *AT1G45100* and *At4G21910* are both in within the top 50 most significant genes (table 10), and this trend is consistent amongst many of the significantly associated GEM markers (Appendix 4). This is probably a result of reads that cannot definitively be sorted to a specific homeologue, and are counted twice. This would bring a homeologous copy up to the same level of significance as the true association.

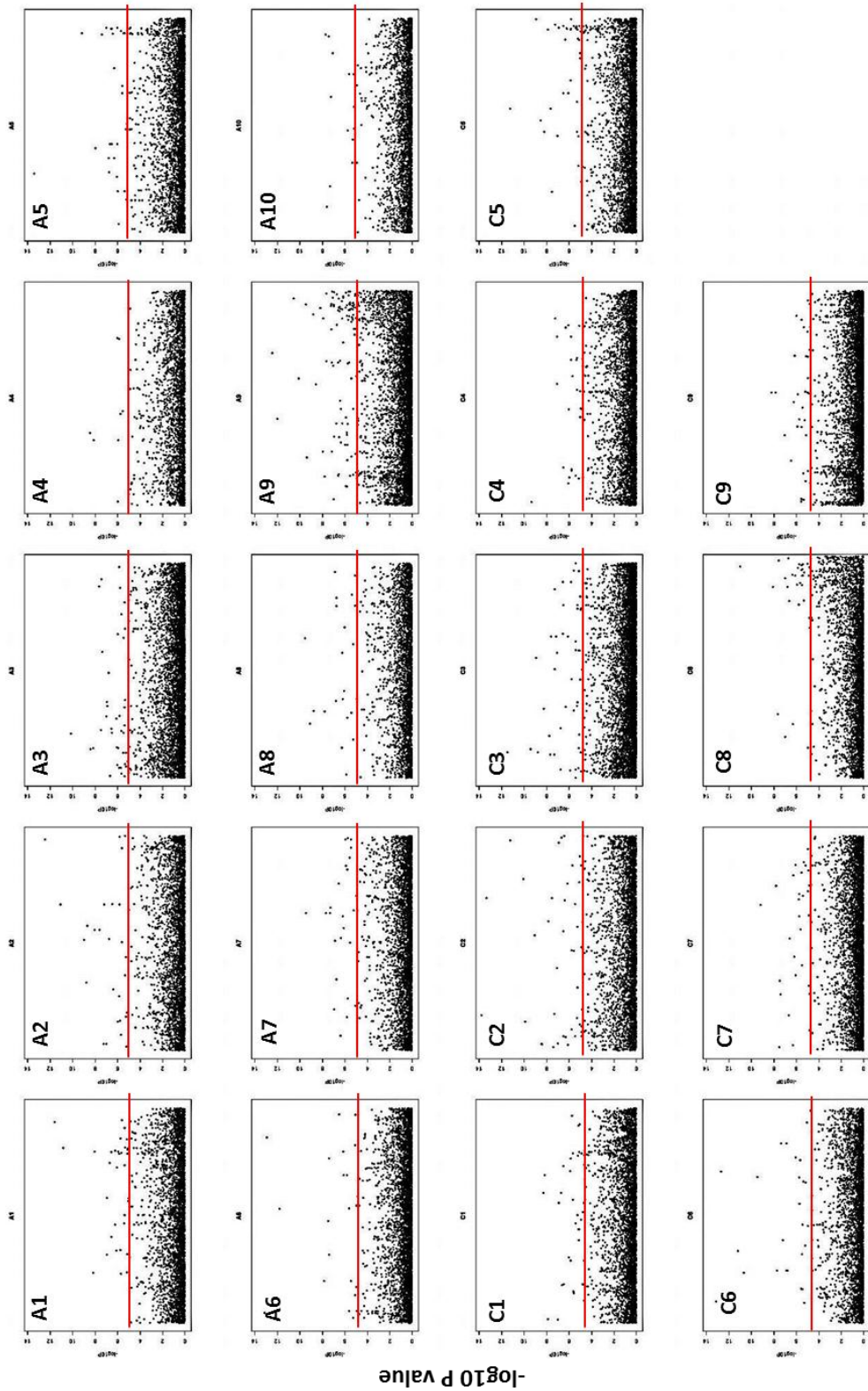


Figure 4.7 GEM markers associated with the elf18-triggered oxidative burst.
 Manhattan plots for each *B. napus* chromosome plotting significance of SNP against its predicted unigene position. Significance ($-\log_{10} P$ value of >2.5) is marked with a red line.

SNP	Significance (p)
JCVI_5426:540	2.93087E-06
JCVI_1025:584	4.50754E-06
JCVI_28348:789	5.12596E-06
JCVI_29522:293	5.56471E-06
JCVI_5247:487	6.2173E-06
JCVI_13361:82	6.42292E-06
JCVI_15377:1688	6.69973E-06
JCVI_38356:525	7.31677E-06
JCVI_2212:243	8.6665E-06
JCVI_23376:695	9.63102E-06
JCVI_36053:423	1.00229E-05
JCVI_681:120	1.02311E-05
JCVI_5290:556	1.02804E-05
JCVI_8575:309	1.12247E-05
JCVI_23722:450	1.13565E-05
EV177399:325	1.16122E-05
JCVI_1808:875	1.21808E-05
JCVI_3889:520	1.21953E-05
JCVI_681:123	1.23611E-05
JCVI_3212:212	1.28127E-05
JCVI_3899:441	1.37983E-05
JCVI_23130:527	1.42493E-05
JCVI_3889:483	1.57841E-05
JCVI_5247:383	1.75291E-05
JCVI_19553:415	1.79794E-05
JCVI_13518:295	1.85222E-05
JCVI_5094:417	1.87421E-05
JCVI_12883:369	1.92393E-05
JCVI_3551:1149	2.19148E-05
JCVI_21901:84	2.23527E-05
JCVI_2264:609	2.24584E-05
JCVI_25931:123	2.32199E-05
JCVI_29040:87	2.48486E-05
JCVI_2663:639	2.51861E-05
JCVI_10273:403	2.594E-05
JCVI_2252:631	2.81779E-05
JCVI_21063:1013	3.07329E-05
JCVI_5259:761	3.09681E-05
JCVI_7772:797	3.16895E-05
JCVI_3889:384	3.27666E-05
JCVI_22224:496	3.34445E-05
JCVI_11571:333	3.36876E-05
EE443270:357	3.41695E-05
JCVI_38604:822	3.43997E-05
JCVI_21141:402	3.4431E-05
EX088011:31	3.48116E-05
JCVI_16818:353	3.49917E-05
JCVI_3734:127	3.50523E-05
JCVI_58:655	3.55971E-05

Table 9 The 50 SNP markers most significantly associated with the elf18-triggered oxidative burst.

Unigene	At Accession	Tair 10 Annotation	Significance (p)
C_EX091048	AT3G54730.1	unknown protein	1.71904E-14
C_ES914047	AT5G55940.1	EMB2731	1.80926E-14
A_ES914047	AT5G55940.1	EMB2731	3.76229E-14
C_ES268132	AT1G45100.1	RNA binding / nucleic acid binding	7.32148E-14
A_ES268132	AT1G45100.1	RNA binding / nucleic acid binding	7.73893E-14
A_JCVI_40926	AT2G02790.1	calmodulin binding	1.21328E-13
A_JCVI_671	AT5G65070.1	MAF4 (MADS AFFECTING FLOWERING 4)	3.54364E-13
A_JCVI_11056	AT3G07390.1	AIR12	2.59681E-12
C_JCVI_671	AT5G65070.1	MAF4 (MADS AFFECTING FLOWERING 4)	6.24476E-12
A_JCVI_1851	AT3G15730.1	PLDALPHA1 (PHOSPHOLIPASE D ALPHA 1)	1.5042E-11
C_ES266017	AT1G53290.1	transferase	2.2318E-11
A_JCVI_117	AT1G06400.1	ARA2	3.00854E-11
C_EE470178	AT1G25220.1	ASB1 (ANTHRANILATE SYNTHASE BETA SUBUNIT 1)	7.77244E-11
A_EV091400	AT3G21350.1	transcription regulator	8.05593E-11
A_EV085469	AT5G57890.1	anthranilate synthase	2.94776E-10
A_JCVI_2237	AT1G09560.1	GLP5 (GERMIN-LIKE PROTEIN 5)	3.53722E-10
C_DY017708	AT2G47240.1	catalytic/ long-chain-fatty-acid-CoA ligase	4.94744E-10
A_JCVI_13747	AT3G04830.1	unknown protein	6.65704E-10
A_EV176450	AT2G47400.1	CP12-1	1.03983E-09
A_JCVI_20466	AT4G05530.1	oxidoreductase	1.70143E-09
A_JCVI_19685	AT5G39990.1	acetylglucosaminyltransferase	3.64933E-09
A_JCVI_29249	AT5G17090.1	unknown protein	4.18488E-09
C_EV223893	AT3G15640.1	cytochrome-c oxidase	4.65741E-09
C_JCVI_12512	AT1G70090.1	transferase, transferring glycosyl groups	6.33108E-09
A_DW997756	AT1G11750.1	CLPP6	7.12515E-09
A_EE550992	AT5G17600.1	protein binding / ubiquitin-protein ligase/ zinc ion binding	7.40341E-09
C_EV098999	AT1G12220.1	RPS5 (RESISTANT TO P. SYRINGAE 5)	8.87237E-09
A_JCVI_7814	AT3G17000.1	ubiquitin conjugating enzyme	9.05235E-09
A_ES908224	AT1G62660.1	hydrolase, hydrolyzing O-glycosyl compounds	1.16419E-08
A_JCVI_9934	AT1G16445.1	S-adenosylmethionine-dependent methyltransferase	1.29198E-08
C_EE481041	AT5G58340.1	DNA binding	1.42845E-08
A_JCVI_27469	AT1G11790.1	amino acid binding / prephenate dehydratase	1.56064E-08
A_JCVI_25395	AT5G64140.1	RPS28 (RIBOSOMAL PROTEIN S28)	1.58125E-08
C_CV432194	AT4G21910.2	antiporter/ drug transporter/ transporter	1.59674E-08
A_JCVI_2288	AT5G16310.1	ubiquitin thiolesterase	1.65854E-08
A_JCVI_21967	AT4G21910.2	antiporter/ drug transporter/ transporter	1.70819E-08
C_JCVI_18490	AT5G54970.1	unknown protein	1.80783E-08
C_JCVI_3099	AT1G52400.1	BGL1 (BETA-GLUCOSIDASE HOMOLOG 1)	1.89881E-08
A_EE432561	AT5G04480.1	unknown protein	1.93631E-08
A_DY003910	AT2G17430.1	calmodulin binding	1.99908E-08
C_JCVI_1094	AT5G16330.1	unknown protein	2.15685E-08
A_JCVI_21419	AT2G42470.1	unknown protein	2.32729E-08
C_JCVI_20724	AT3G06700.1	structural constituent of ribosome	2.33359E-08
A_JCVI_4113	AT3G54400.1	pepsin A	2.34432E-08
C_JCVI_16168	AT1G13930.1	unknown protein	2.39287E-08
A_JCVI_26945	AT4G28025.1	unknown protein	2.45331E-08
A_JCVI_6138	AT1G75380.1	unknown protein	2.55095E-08
A_JCVI_38115	AT1G05210.1	unknown protein	2.59932E-08
C_JCVI_21419	AT2G42470.1	unknown protein	2.94059E-08

Table 10 Top 50 most significantly associated GEM markers for the elf18-triggered oxidative burst.

Unigenes in the A or C genome are annotated with their predicted *Arabidopsis* homolog accession number and Tair 10 annotation.

4.3.4 Associative Transcriptomics of *B. cinerea* resistance in *B. napus*

Identifying novel genes responsible for resistance to *B. cinerea* is traditionally very difficult. No typical R genes are known to work against this necrotrophic pathogen and the majority of resistance is described as polygenic, quantitative resistance. As such, previous QTL mapping experiments have rarely found any genes which contribute in a significant way to a resistance phenotype. Because of this, association genetics, which finds an abundance of associations each with a small phenotypic effect, might be an ideal method to understand the allelic variation that gives rise to *B. cinerea* resistance in crops.

We see significant variation in the symptoms caused by *B. cinerea* across the lines of the association mapping panel (fig 4.8). The most resistant lines were Victor, Ragged Jack and Quinta, with Karoo-057 and Westar 10 the most susceptible. Westar10 has previously been published as being susceptible to *L. maculans* stem canker development, another fungal pathogen with necrotrophic life cycle stages (Zhao, 2009).

Significant SNP clusters could be found across the genome, with well-defined clear peaks observed on A1, A2, A5, A8, C1 and C5 (fig 4.9). In total over 341 SNP markers were significant (table 11, table 15, Appendix 3). 913 significantly associated GEMs were identified (fig 4.10, table 15, Appendix 4). A very high number of genes associated with flowering time are found amongst the GEM associations including *FT* (FLOWERING LOCUS T), *AGL20* (AGAMOUS LIKE-20) and *AP1* (APETALA 1) (table 14). This might perhaps be expected, as JA responsive related genes are often linked with the induction of flowering, and many significantly associated GEMs are linked directly to JA or ET signalling including *AALP*.

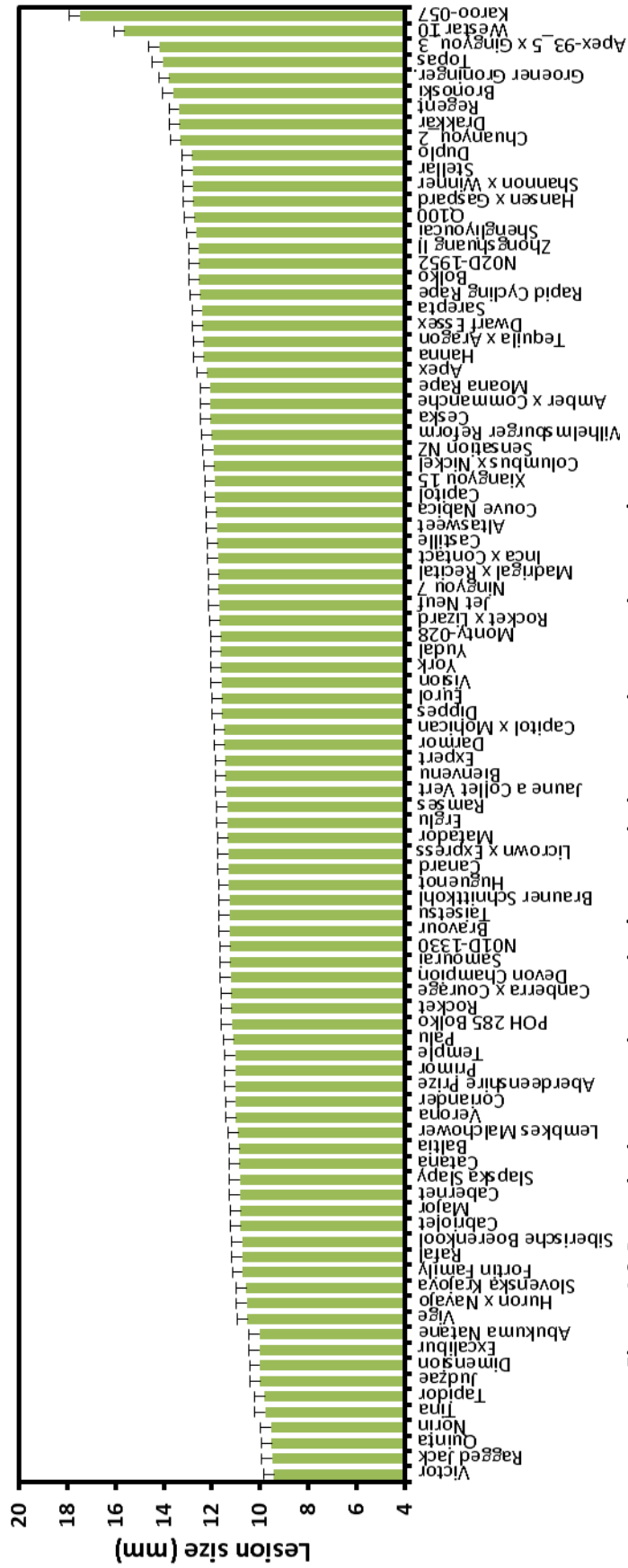


Figure 4.8 Botrytis cinerea resistance in the association genetics mapping panel.

Lesion size 3dpi with agar plugs of *Botrytis cinerea* in 20mm leaf discs. Data represent the predicted mean of 4 separate experiments each with between 8 and 16 biological repeats. Error bars show standard error of the predicted mean.

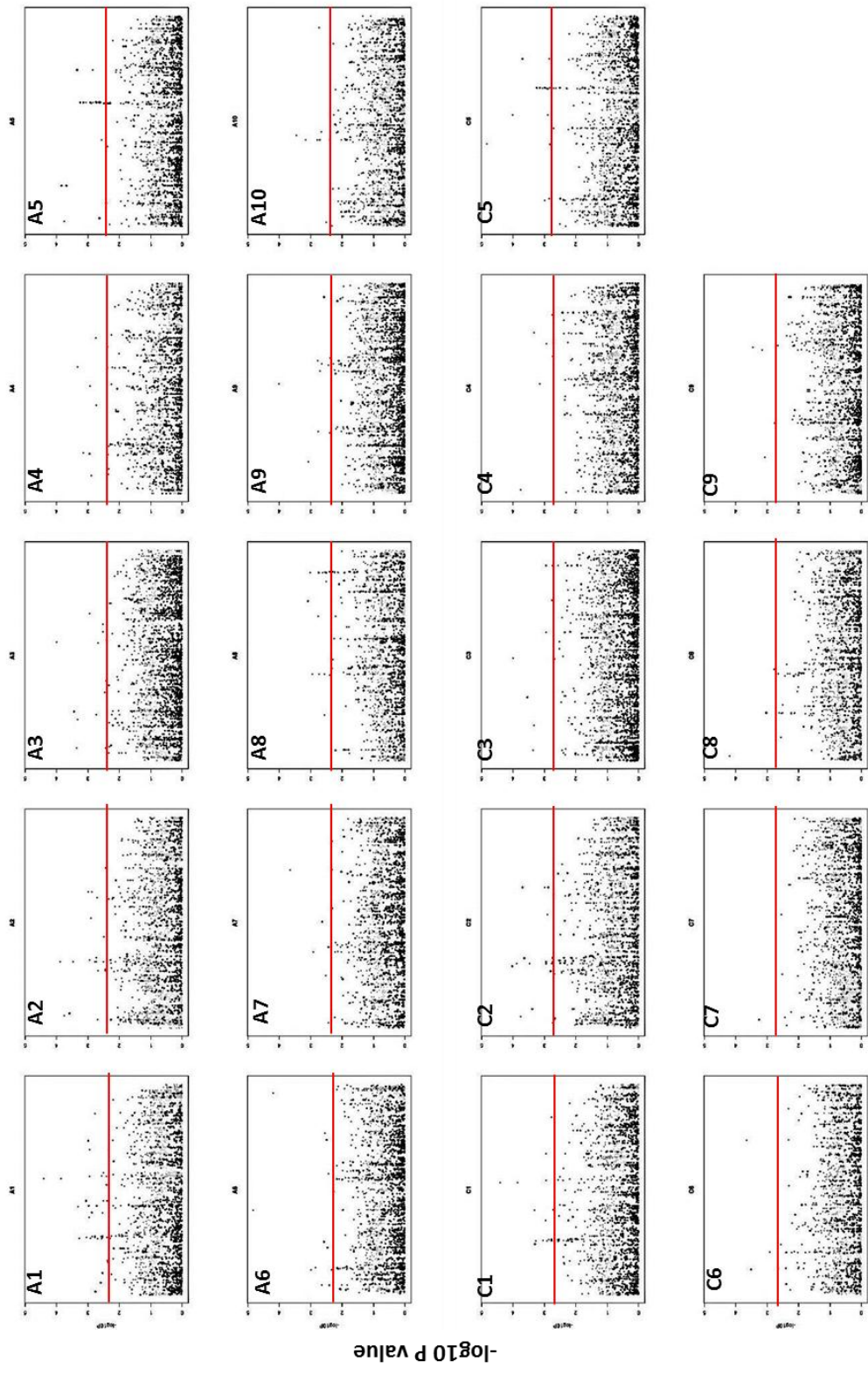


Figure 4.9 SNP markers associated with *Botrytis cinerea* resistance. Manhattan plots for each *B. napus* chromosome plotting significance of SNP against its predicted unigene position. Significance ($-\log_{10} P$ value of >2.5) is marked with a red line. Grey dots represent SNPs in illumina reads that could not be assigned conclusively between the A and C genome homeologous copies of the unigene scaffold, and are represented twice here.

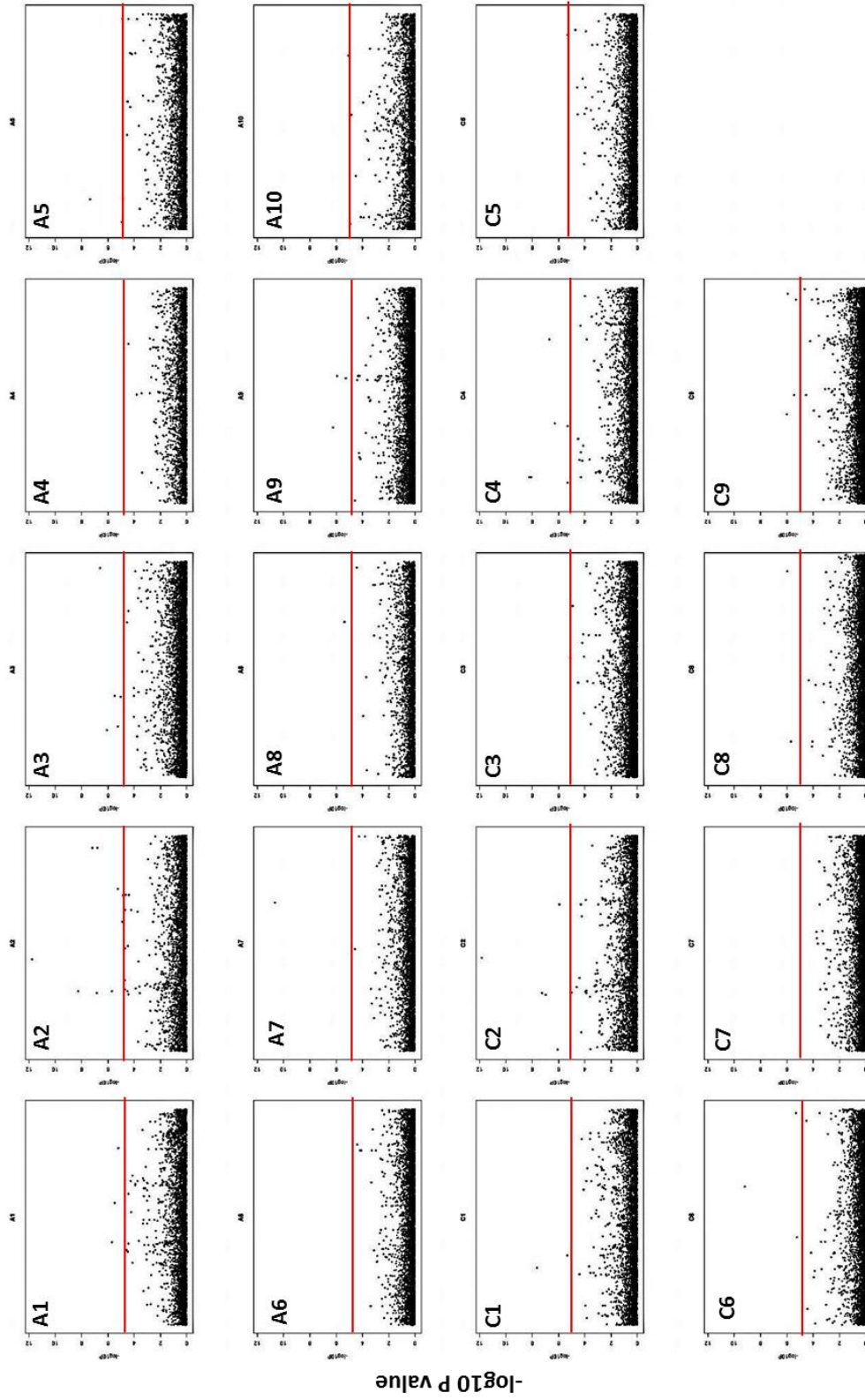


Figure 4.10 GEM markers associated with *Botrytis cinerea* resistance

Manhattan plots for each *B. napus* chromosome plotting significance of SNP against its predicted unigene position. Significance ($-\log_{10} P$ value of >2.5) is marked with a red line.

SNP	Significance (p)
JCVI_28491:830	1.50517E-05
JCVI_20199:88	3.28878E-05
JCVI_40480:1060	3.3126E-05
JCVI_27253:128	3.97008E-05
JCVI_2306:434	4.39665E-05
JCVI_2306:440	4.39665E-05
JCVI_2306:507	4.39665E-05
JCVI_2066:257	5.03472E-05
JCVI_35224:178	6.48976E-05
JCVI_2066:85	6.66713E-05
JCVI_3124:419	6.709E-05
JCVI_35224:143	7.14014E-05
JCVI_41844:798	7.39818E-05
JCVI_18398:579	8.31989E-05
JCVI_3670:857	9.64896E-05
JCVI_4689:182	9.64896E-05
JCVI_4689:299	9.64896E-05
JCVI_18006:1587	0.0001006
DY015167:397	0.000102614
JCVI_25167:62	0.000103108
JCVI_2306:384	0.000105947
JCVI_6942:539	0.000131825
JCVI_6942:466	0.00013414
JCVI_6942:481	0.00013414
JCVI_6258:761	0.000138379
JCVI_26002:1218	0.000140836
JCVI_6942:991	0.000146946
JCVI_35899:1603	0.000148665
JCVI_6942:640	0.000154251
JCVI_11003:171	0.000164753
JCVI_4992:323	0.000166292
JCVI_26441:775	0.000178779
JCVI_25470:556	0.000179601
JCVI_11003:666	0.000180566
JCVI_6942:196	0.000183721
JCVI_6942:198	0.000183721
JCVI_26002:39	0.000190496
JCVI_4854:693	0.000194088
JCVI_11015:1886	0.000201093
JCVI_29656:461	0.000204223
JCVI_8133:335	0.000206322
JCVI_35899:1597	0.000208647
JCVI_22084:521	0.00021456
JCVI_5376:523	0.000224081
JCVI_4992:314	0.000225451
JCVI_3933:110	0.000234189
JCVI_2306:536	0.000236624
JCVI_12766:101	0.000237403
EV145122:279	0.000259139
JCVI_5840:1477	0.000263849

Table 11 The 50 SNP markers most significantly associated with the *Botrytis cinerea* resistance

Unigene	At Accession	Tair 10 Annotation	Significance (p)
C_JCVI_40108	AT1G65480.1	FT (FLOWERING LOCUS T)	1.52394E-12
A_JCVI_40108	AT1G65480.1	FT (FLOWERING LOCUS T)	1.80287E-12
A_JCVI_31384	AT5G60360.1	AALP	5.53002E-09
C_JCVI_2518	AT2G45660.1	AGL20 (AGAMOUS-LIKE 20)	6.21268E-09
C_ES989775	AT4G19350.1	EMB3006 EMBRYO DEFECTIVE 3006	2.45756E-08
A_EV091356	AT2G45660.1	AGL20 (AGAMOUS-LIKE 20)	4.70707E-08
C_JCVI_31384	AT5G60360.1	AALP	5.91898E-08
A_JCVI_39987	AT5G19010.1	ATMPK16	6.51164E-08
C_JCVI_16293	AT5G60710.1	protein binding / ubiquitin-protein ligase/ zinc ion binding	1.10967E-07
A_EX100045	AT5G22850.1	pepsin A	1.46354E-07
C_EV145529	AT5G59880.1	ADF3 (ACTIN DEPOLYMERIZING FACTOR 3)	4.35267E-07
C_JCVI_5007	AT5G37740.1	unknown protein	5.26445E-07
A_JCVI_4782	AT2G01520.1	unknown protein	5.69856E-07
A_JCVI_26231	AT5G55990.1	CBL2	8.88772E-07
C_JCVI_4782	AT2G01520.1	unknown protein	1.0176E-06
C_JCVI_42533	AT1G07600.1	MT1A (METALLOTHIONEIN 1A)	1.07723E-06
C_EL589622	AT4G02425.1	unknown protein	1.16037E-06
C_EV195750	AT5G03910.1	ATATH12	1.17811E-06
A_JCVI_6943	AT1G23860.1	SRZ-21	1.21813E-06
C_JCVI_13458	AT1G04400.2	CRY2 (CRYPTOCHROME 2)	2.15941E-06
A_DW998159	AT5G60370.1	unknown protein	2.18403E-06
A_JCVI_11438	AT4G24730.2	hydrolase/ protein serine/threonine phosphatase	2.19441E-06
A_JCVI_18380	AT2G43820.1	UDP-glycosyltransferase/ transferase, transferring glycosyl groups	3.35929E-06
A_JCVI_23335	AT3G11520.1	CYCB1	3.48492E-06
C_EV163457	AT4G34590.1	GBF6	3.48689E-06
C_DY026614	AT4G22890.5	unknown protein	4.8461E-06
C_JCVI_28976	AT5G05610.1	DNA binding / protein binding / zinc ion binding	4.94209E-06
C_JCVI_29467	AT2G44230.1	unknown protein	5.04202E-06
C_JCVI_7295	AT3G07310.1	unknown protein	5.11867E-06
C_EE558140	AT1G79570.1	ATP binding / protein kinase/ protein serine/threonine kinase	5.12351E-06
C_JCVI_26073	AT2G04350.1	catalytic/ long-chain-fatty-acid-CoA ligase	5.1783E-06
A_JCVI_24096	AT1G26930.1	unknown protein	5.35296E-06
A_JCVI_18970	AT5G53440.1	unknown protein	5.78395E-06
A_JCVI_5649	AT3G15510.1	ATNAC2	6.72174E-06
C_EV110599	AT4G21910.1	antiporter/ drug transporter/ transporter	8.42444E-06
C_JCVI_33010	AT3G18295.1	unknown protein	8.51336E-06
A_EE447559	AT5G08520.1	DNA binding / transcription factor	9.23496E-06
A_EV049523	AT2G43370.1	RNA binding / nucleic acid binding	9.77757E-06
C_DY020927	AT5G60120.1	TOE2	1.05277E-05
A_JCVI_13341	AT4G01480.1	inorganic diphosphatase/ magnesium ion binding / pyrophosphatase	1.19053E-05
C_JCVI_39987	AT5G19010.1	ATMPK16	1.22561E-05
A_JCVI_40790	AT1G78130.1	carbohydrate transporter/ sugar porter/ transporter	1.28833E-05
A_JCVI_17091	AT3G01470.1	ATHB-1	1.32174E-05
A_JCVI_19610	AT5G18660.1	PCB2 (PALE-GREEN AND CHLOROPHYLL B REDUCED 2)	1.41322E-05
A_JCVI_33137	AT1G55160.1	unknown protein	1.43844E-05
A_EV054282	AT2G45740.1	unknown protein	1.46954E-05
C_EE425481	AT3G06145.1	unknown protein	1.90548E-05
A_JCVI_28953	AT5G59660.1	ATP binding / kinase/ protein serine/threonine kinase	1.94059E-05
A_JCVI_13763	AT1G69120.1	AP1 (APETALA1)	2.0978E-05
A_JCVI_24083	AT4G02450.1	unknown protein	2.22149E-05

Table 12 Top 50 most significantly associated GEM markers for *Botrytis cinerea* resistance.

Unigenes in the A or C genome are annotated with their predicted *Arabidopsis* homolog accession number and Tair 10 annotation.

4.3.5 Associative Transcriptomics of *Pseudomonas syringae* resistance in *B. napus*

The lines of association genetics panel were next inoculated with *Pto DC3000 LUXCDAB HrcC-*. The assay measured the luminescence of the strain in the liquid media surrounding each leaf disc (eight per repeat) with fluorescence recorded at day 0, 1, 2 and 3. The trait that was mapped was the predicted mean fold increase of luminescence for each line between day 0 (within an hour of inoculation) and day 3. Increases in luminescence between two and twenty eight-fold was observed within the association mapping panel. Darmor, Slapska Slappy and Rocket were highly resistant to the pathogen and Siberische Boerenkool and Brauner Schnittkohl were the most susceptible.

There are relatively fewer distinct SNP peaks associated with *P. syringae* resistance compared to other traits, but peaks on A4, A10, C4 and C9 are SNP-dense and well defined (fig 4.12, table 13, table 15). In total 202 SNPs were significantly associated with the trait. GEM markers were also relatively sparse across the genome with 512 significant hits found (table 14). This is likely a result of the variability within the phenotyping.

In the absence of a TTSS, and a significant reduction in the delivery of effectors, we expect to be identifying candidate GEMs not linked to any specific R gene, as was the case when Pst resistance was mapped using GWAS in *A. thaliana* (Atwell, 2010). Defence related candidates including *AtMKK6* and *UDP-Glucosyltransferase* are amongst the most significantly associated, and again, like the other traits studied, there is an abundance of genes linked to development and flowering, including *BON2*, *TMP-C* and *SPA3* (Table 14).

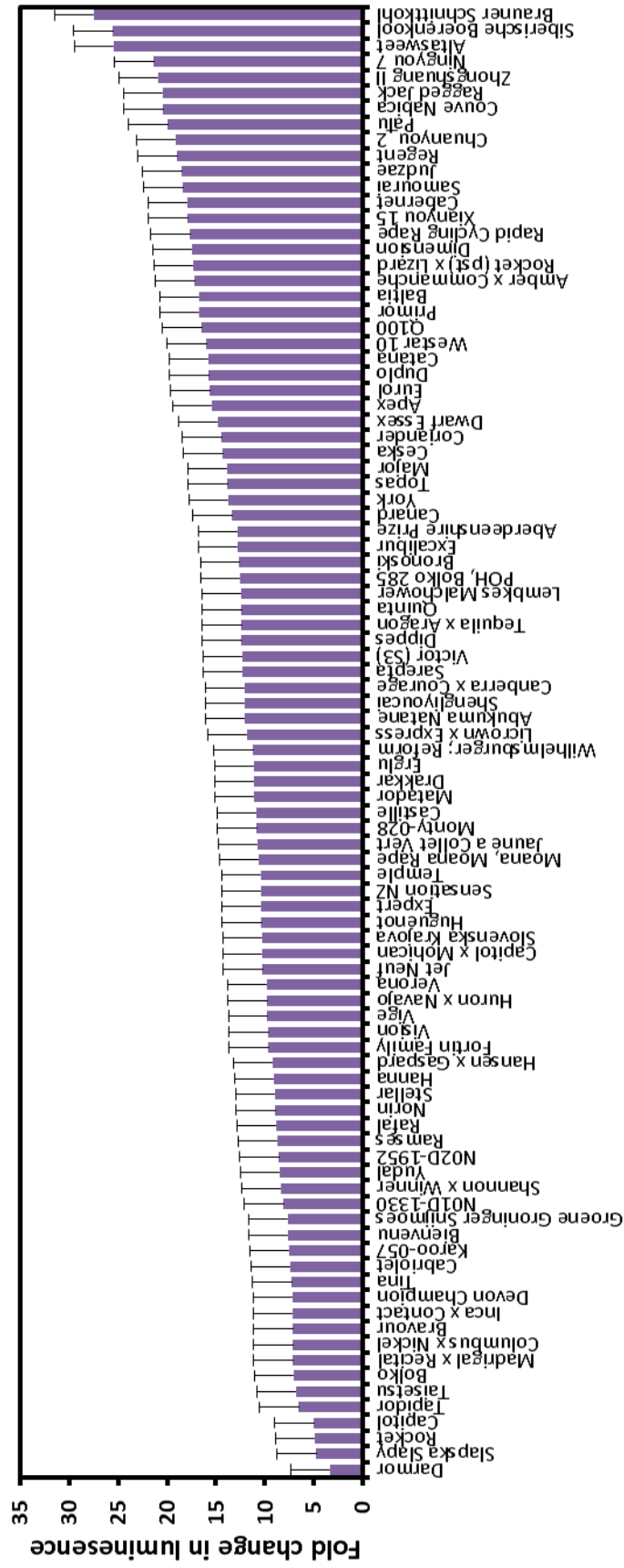


Figure 4.11 *Pseudomonas syringae* resistance in the association genetics mapping panel.

Fold increase in luminescence between inoculation and 3DPI. Data represent the predicted mean of 3 separate experiments each with 8 biological repeats. Error bars show standard error of the predicted mean.

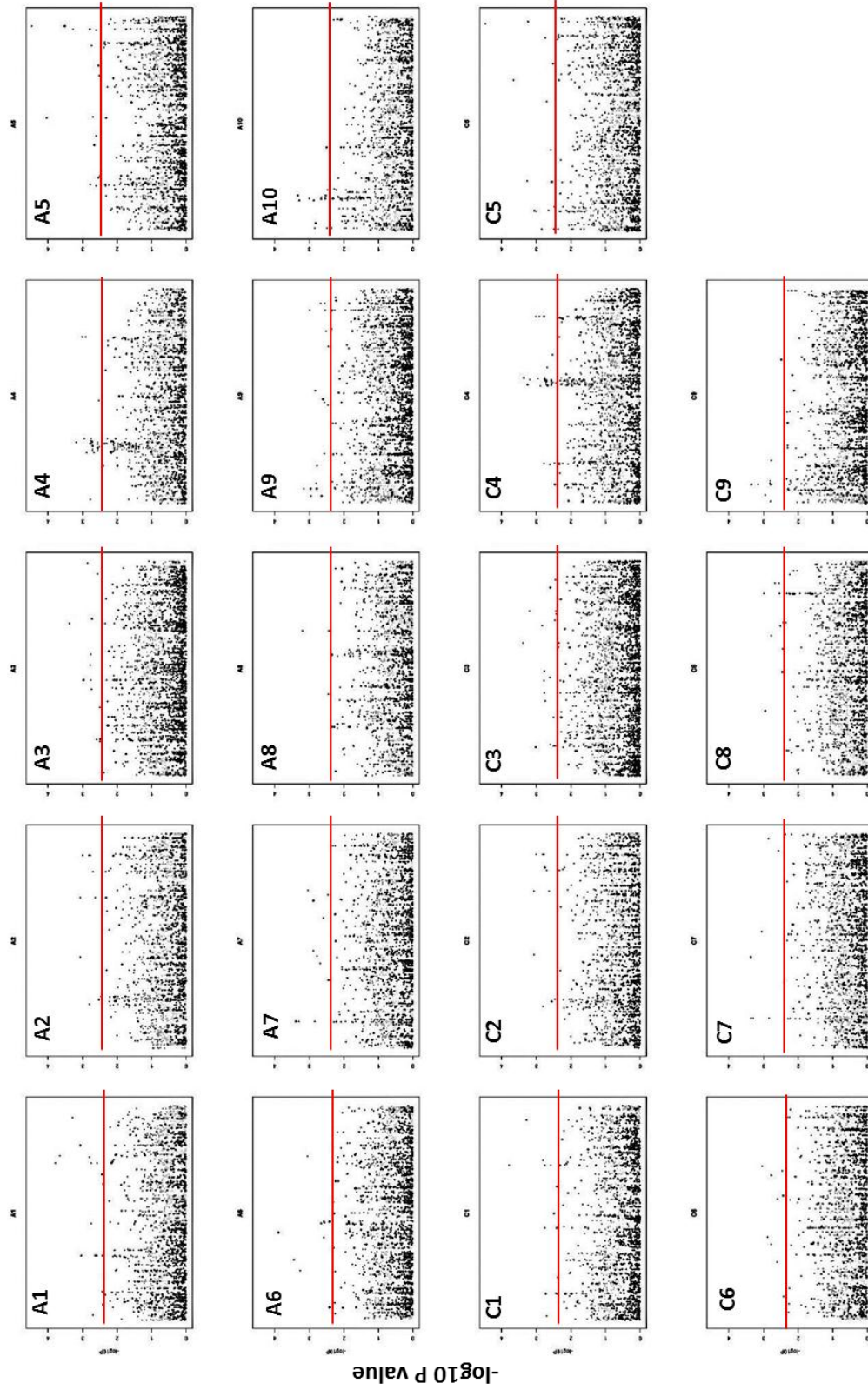


Figure 4.12 SNP markers associated with *Pseudomonas syringae* resistance.

Manhattan plots for each *B. napus* chromosome plotting significance of SNP against its predicted unigene position. Significance (a $-\log_{10} P$ value of >2.5) is marked with a red line. Grey dots represent SNPs in illumina reads that could not be assigned conclusively between the A and C genome homeologous copies of the unigene scaffold, and are represented twice here.

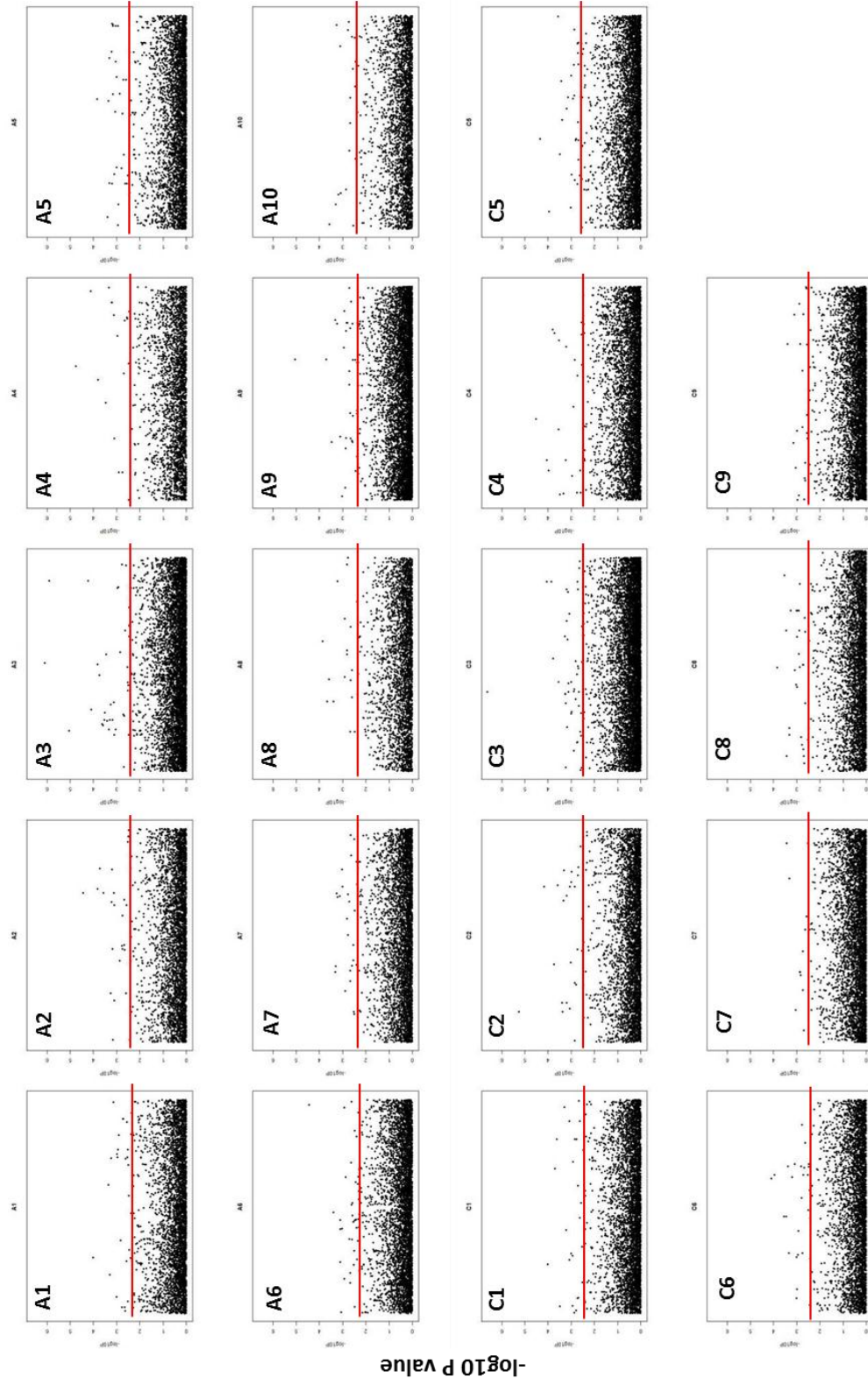


Figure 4.13 GEM markers associated with *Pseudomonas syringae* resistance
 Manhattan plots for each *B. napus* chromosome plotting significance of SNP against its predicted unigene position. Significance ($-\log_{10} P$ value of >2.5) is marked with a red line.

SNP	Significance (p)
JCVI_4204:540	3.4431E-05
JCVI_8960:449	9.3077E-05
JCVI_2530:498	9.36275E-05
JCVI_8995:88	0.00013105
JCVI_28210:442	0.000161668
JCVI_40644:657	0.000164051
JCVI_23343:722	0.000199501
JCVI_21874:1169	0.000216854
JCVI_5290:158	0.000222339
JCVI_12082:330	0.0002708
JCVI_4204:465	0.000315183
JCVI_40644:449	0.000332467
EV100221:539	0.000356429
JCVI_8852:181	0.000363027
JCVI_2401:220	0.000372856
JCVI_12082:312	0.000390013
JCVI_4699:454	0.000402395
JCVI_17859:448	0.000421973
JCVI_41215:114	0.000427371
EV090686:679	0.000428366
JCVI_845:690	0.000437661
JCVI_42386:401	0.000444498
JCVI_1058:341	0.000446772
JCVI_18836:122	0.000469721
JCVI_27146:678	0.000487759
EV090686:450	0.000500187
JCVI_4699:653	0.000500187
JCVI_38271:366	0.000517804
JCVI_4800:90	0.000520274
JCVI_11768:887	0.000530044
JCVI_5736:1200	0.000533075
JCVI_40644:263	0.000544672
JCVI_9903:55	0.000548353
JCVI_1522:361	0.000569083
JCVI_5120:494	0.000577404
JCVI_7105:212	0.000581504
JCVI_7105:230	0.000581504
JCVI_4143:969	0.000612699
JCVI_40644:477	0.000618559
EV090763:143	0.000632366
JCVI_29601:945	0.000635269
ES979151:121	0.000660314
JCVI_5089:187	0.000665013
EV193645:611	0.000668755
JCVI_26722:390	0.00069132
JCVI_1058:281	0.000704179
JCVI_9655:73	0.000710851
JCVI_19215:859	0.00076774
JCVI_14280:1324	0.000774418

Table 13 The 50 SNP markers most significantly associated with *Pseudomonas syringae* resistance.

Unigene	Arabidopsis Accession	Tair 10 Annotation	Significance (p)
C_JCVI_2426	AT4G00430.1	TMP-C	2.45877E-07
A_JCVI_2426	AT4G00430.1	TMP-C	8.22657E-07
A_EV095607	AT4G28080.1	unknown protein	1.2865E-06
C_EV096109	AT5G14740.3	CA2 (CARBONIC ANHYDRASE 2)	5.5437E-06
A_JCVI_4638	AT3G53420.1	PIP2A	9.06573E-06
A_EV199111	AT5G59580.1	UDP-glycosyltransferase	9.28479E-06
A_JCVI_20750	AT2G30490.1	ATC4H (CINNAMATE-4-HYDROXYLASE)	1.76218E-05
C_JCVI_24275	AT5G42760.1	unknown protein	3.00673E-05
A_JCVI_24148	AT5G46800.1	BOU (A BOUT DE SOUFFLE)	3.58519E-05
A_JCVI_24275	AT5G42760.1	unknown protein	3.70423E-05
C_JCVI_5107	AT3G47430.1	unknown protein	4.65754E-05
A_EV194157	AT4G28080.1	unknown protein	6.07427E-05
C_JCVI_24148	AT5G46800.1	BOU (A BOUT DE SOUFFLE)	6.83578E-05
A_JCVI_7843	AT2G46800.1	ZAT1	7.75493E-05
A_EV046845	AT5G07300.1	BON2 (BONZAI 2)	8.00302E-05
C_JCVI_12734	AT2G14247.1	unknown protein	8.1729E-05
C_EV190519	AT2G37050.2	kinase	8.77655E-05
C_JCVI_20549	AT5G53045.1	unknown protein	8.97652E-05
C_JCVI_12696	AT4G35090.1	CAT2 (CATALASE 2)	9.12675E-05
C_JCVI_31697	AT2G39980.1	transferase	0.000109028
C_EV177418	AT2G02010.1	calmodulin binding	0.00011692
C_JCVI_26735	AT1G05560.1	UGT1	0.000113565
C_JCVI_16478	AT4G35090.1	CAT2 (CATALASE 2)	0.000137116
A_EE531724	AT1G28510.1	unknown protein	0.000138618
C_JCVI_4638	AT3G53420.1	PIP2A	0.000145958
A_JCVI_30402	AT3G19270.1	CYP707A4	0.000147492
A_EX078810	AT4G01150.1	unknown protein	0.000152428
A_JCVI_25775	AT5G47770.1	FPS1 (FARNESYL DIPHOSPHATE SYNTHASE 1)	0.000156012
C_JCVI_39168	AT2G31750.1	UDP-glycosyltransferase/ transferase	0.000158085
A_JCVI_18201	AT2G27860.1	AXS1 (UDP-D-APIOSE/UDP-D-XYLOSE SYNTHASE 1)	0.000160891
C_EH422975	AT3G14420.1	glycolate oxidase/ oxidoreductase	0.000168324
C_JCVI_3671	AT5G53970.1	1-aminocyclopropane-1-carboxylate synthase/ transaminase/ transferase	0.000179127
A_JCVI_8442	AT4G09620.1	unknown protein	0.000184089
A_JCVI_4089	AT3G27210.1	unknown protein	0.000193342
C_JCVI_28363	AT3G24140.1	DNA binding / transcription	0.000200869
A_JCVI_16478	AT4G35090.1	CAT2 (CATALASE 2)	0.000214295
A_JCVI_27462	AT5G55630.1	KCO1	0.000239941
C_EV100364	AT3G15354.1	SPA3 (SPA1-RELATED 3)	0.000243109
C_EGO19931	AT4G04540.1	kinase	0.000257761
A_JCVI_24381	AT4G28290.1	unknown protein	0.000263575
A_JCVI_24811	AT1G15100.1	RHA2A	0.000264046
A_JCVI_41403	AT5G56580.1	ATMKK6 (ARABIDOPSIS NQK1)	0.000264809
C_EX055536	AT3G02450.1	ATP binding / ATPase	0.000267651
A_JCVI_15529	AT1G01180.1	unknown protein	0.000273761
A_EV099224	AT5G46800.1	BOU (A BOUT DE SOUFFLE)	0.000278687
C_JCVI_41469	AT4G11220.1	unknown protein	0.00028047
C_JCVI_2037	AT2G28470.1	BGAL8	0.000281189
C_JCVI_3650	AT3G61610.1	aldose 1-epimerase	0.000285528
C_JCVI_24811	AT1G15100.1	RHA2A	0.000295431

Table 14 Top 50 most significantly associated GEM markers for *Pseudomonas syringae* resistance.

Unigenes in the A or C genome are annotated with their predicted *Arabidopsis* homolog accession number and Tair 10 annotation.

Trait	Significant SNP Associations	Significant GEM Associations
flg22-triggered ROS	230	1092
Elf18-triggered ROS	1686	5654
<i>Botrytis cinerea</i> resistance	341	913
<i>Pseudomonas syringae</i> resistance	202	521

Table 15 Summary of significant associations found in the GWAS of four defence related traits

4.3.6 Correlation of phenotypes

Whether or not a high oxidative burst can predict resistance to a pathogen is unknown. In order to assess the relationship between the phenotypes, the phenotypic scores for each line were correlated with all other phenotypes assessed. Only the oxidative burst in response to flg22 and elf18 was significantly ($p < 0.001$) correlated with each other (fig 4.14 A, B). The oxidative burst in response to either PAMP was not strongly correlated with resistance to *P. syringae* (which expresses both flagellin and EF-TU) or *B. cinerea* (fig 4.14 A, B).

4.3.7 Correlation of GEMS

The oxidative burst in response to flg22 shared many significant GEMs with the elf18 triggered oxidative burst. The significance of association to flg22 ROS against the significance to elf18 ROS traits was plotted for every GEM marker. A significant ($p < 0.001$) correlation was seen between these scores (fig 4.15). This was consistent in both the A and C genomes. No significant correlation of GEM significance was observed between any other pair of traits.

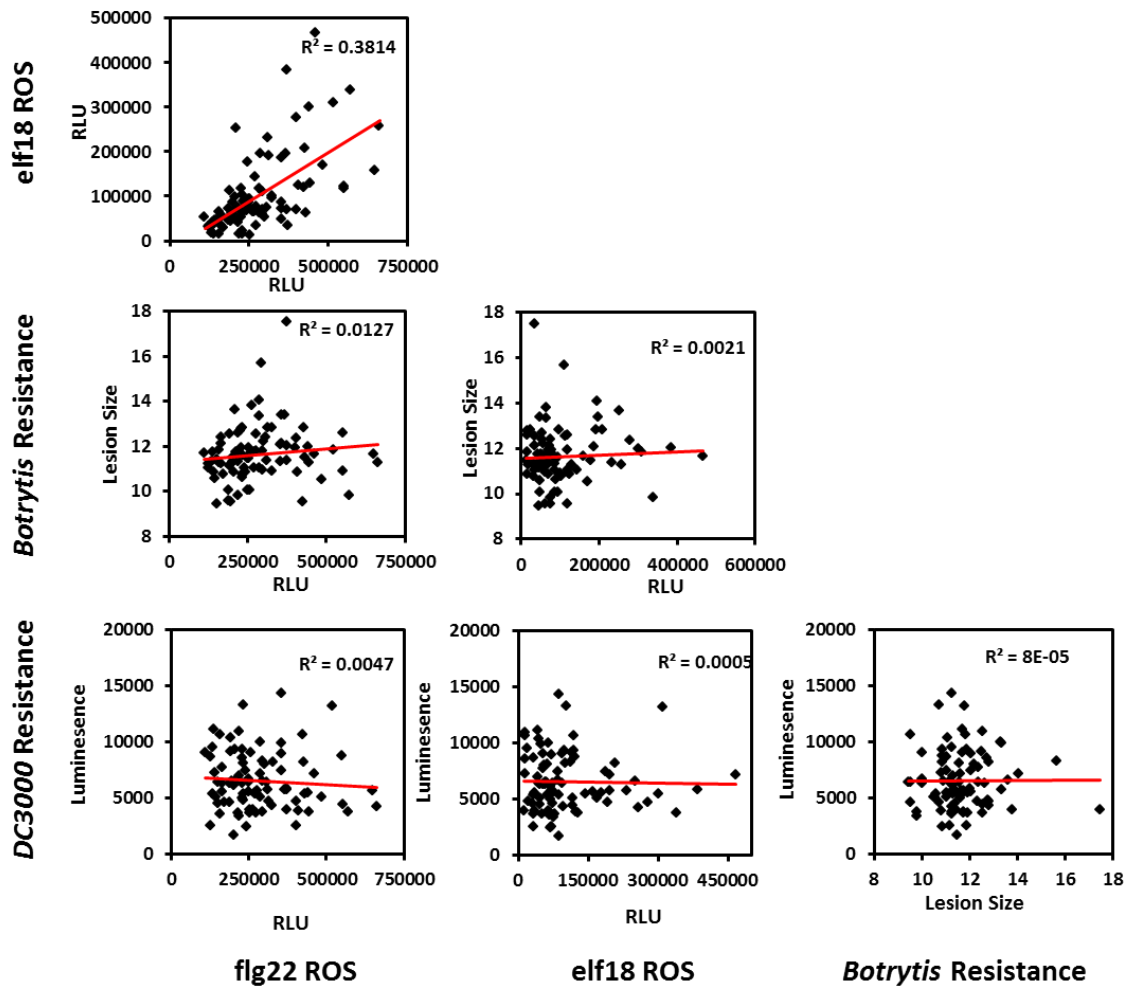


Figure 4.14 Correlations between pathogen resistance related phenotypes in the association mapping panel.

Scatter plots of four phenotypes (flg22 oxidative burst RLU, elf18 oxidative burst RLU, *Botrytis* lesion size, *Pseudomonas syringae* luminescence) for each line of the association genetics panel.

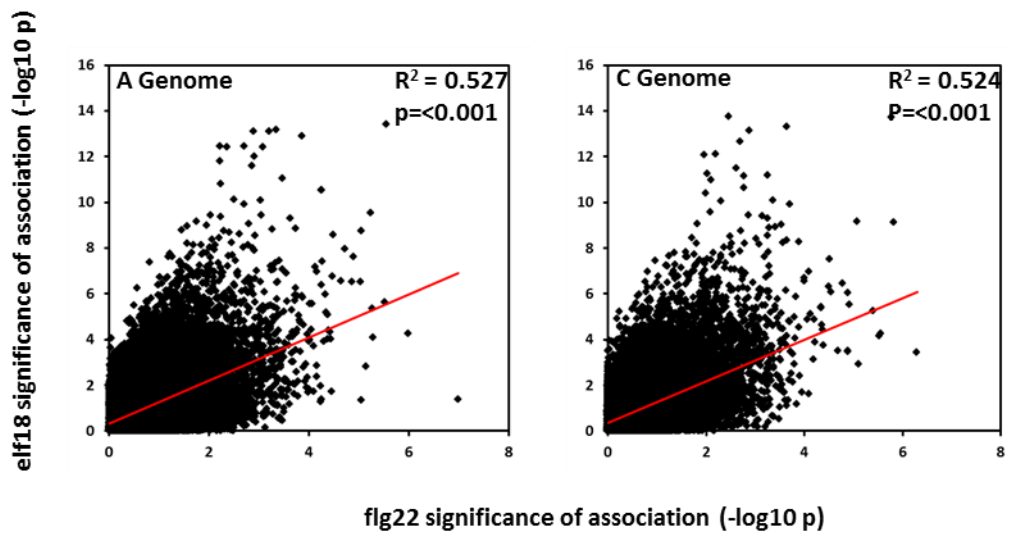


Figure 4.15 Correlation of GEM association significance between the flg22 and elf18 triggered oxidative burst phenotypes for the A and C *B. napus* genomes.

4.3.8 Functional Annotation of Significantly Associated GEMs

In order to get an overview of the function of the genes with expression significantly associated with defence traits, the GEMs were functionally annotated using *A. thaliana* GO-Terms. This produced a percentage of GEMs within each GO-Term category. As a reference to compare this to, every GEM marker used in the GWAS was also functionally annotated. An enrichment of genes linked to biotic stimuli and stress response were found amongst GEMs associated with a defence phenotype (fig 4.16). This is particularly true of *P. syringae* resistance, which might just be a bias resulting from the relatively small sample size (only 202 significant GEMs).

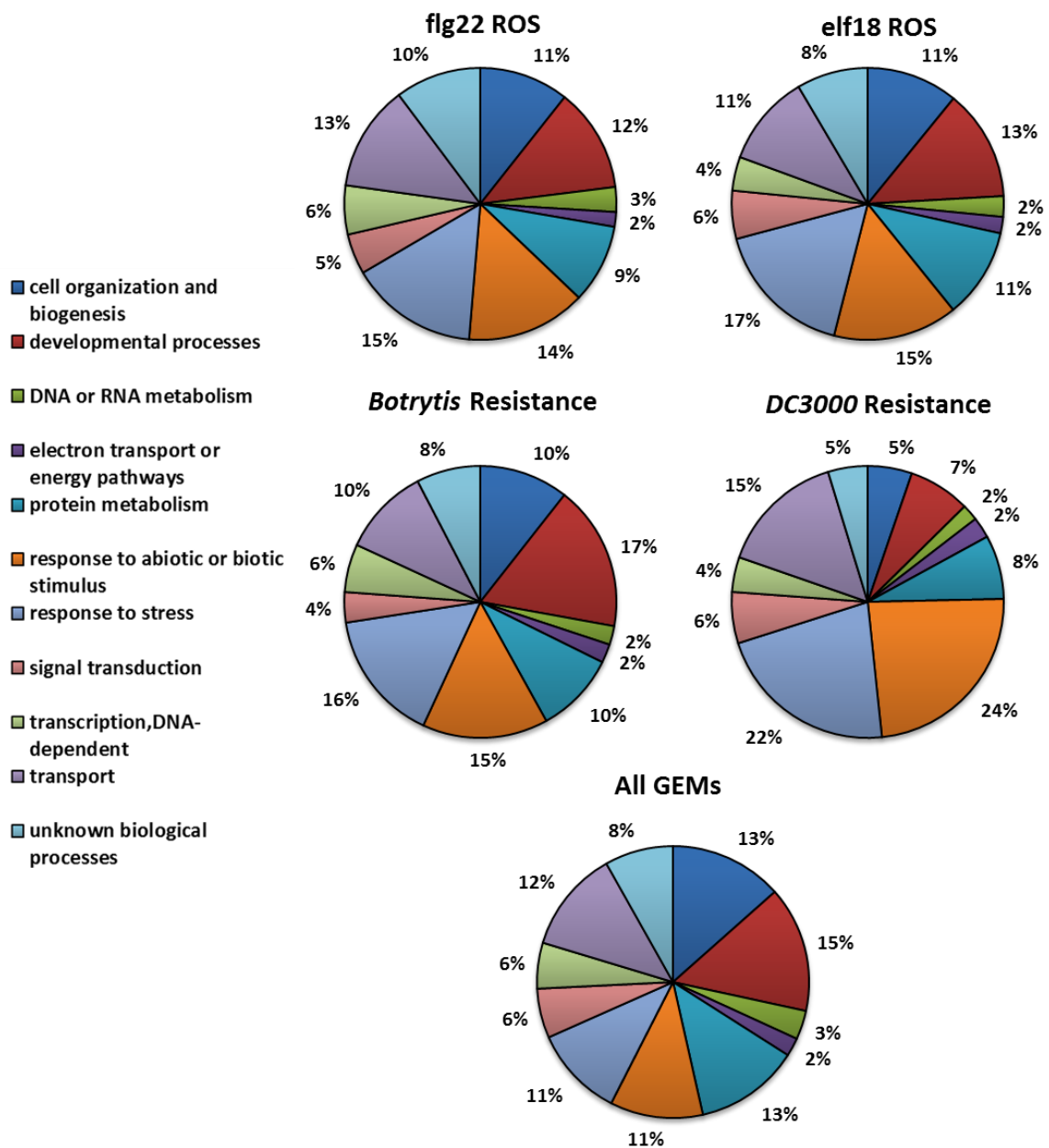


Figure 4.16 *Arabidopsis* GO-term annotation of GEM markers significantly linked to defence phenotypes

Numbers indicate percentage of GEMs that fall into the specified Biological Processes GO-Term. All GEMs refers to the GO-Term annotation of every GEM used in the GWAS.

4.4. Discussion

The work presented in this chapter is a pilot study for using associative transcriptomics to identify regulators of defence in a crop species. The SNPs and gene expression differences between 84 *B. napus* varieties were correlated with four different defence traits to identify the genetic loci implicated in the phenotypic variability. The loci identified include many genes involved in pathogen detection and resistance and a number of developmental regulators. It is a promising pilot study with huge potential for future research and *Brassica* pre-breeding, but many fundamental issues still remain with the population as it stands.

The power of GWAS depends on multiple factors including population size, SNP density, read depth and phenotypic variability. Improving each of these within the panel is a clear goal for the future. The panel currently consists of 84 lines, a very small number of lines for a GWAS. This limits the potential of the panel by reducing the number of potential SNP markers, reducing the phenotypic diversity covered and potentially allowing a greater effect of population structure bias (although this has been corrected for as much as possible).

The low population number has resulted in a very high cut off of 5% allelism for a SNP to be included in the study. The 5% cut off is essential in a population this small to remove excessive false positives. This reduces the number of useable SNPs in the population from over 100,000 potential SNPs to 62,000 (Harper, 2012). This limits the representation of SNPs with major phenotypic effects. For example, despite many SNPs appearing in FLS2, EFR and other PRRs in the population, none of these were found in 5% of the lines. For conserved genes with major phenotypic impacts, like PRRs, that are under strong negative selection a 5% allelism rate will be extremely rare. With increasing population size, and a lowering of the percentage allelism cut off for SNPs, major impact genes with severe deleterious or beneficial effects have a higher chance of being captured.

The average read depth of the population may be limiting the power of the GEM markers identified. An average read depth of 34.9 was considered good a few years ago, but still misses out coverage on many important genes. For example, coverage of EFR is incomplete in many of the lines. Genes that have low basal expression but contribute meaningfully to a phenotype can often be excluded due to low transcript abundance. A greater depth of sequencing would greatly improve the number of potential GEM candidates as well as increase the accuracy of the expression variation between cultivars. As the population was sequenced in 2009 using emergent technologies that are improving all the time, the 80bp reads originally used to identify the markers and construct the reference maybe less effective than modern methods. Using longer reads, for example, limits the problem of ambiguous callings between homeologues due to a higher chance of a loci-specific SNP being present in any given read.

The phenotypic range observed within the panel has been very good, with large quantitative differences observed for each of the traits. There is no obvious bias towards different crop types, for example Winter OSR lines do not cluster together separately from swedes for example, and the assaying methods used have captured meaningful biological variation in the traits. Despite the truly quantitative nature of the phenotypes studied significant GEM and SNPs were commonplace, suggesting that the population can be used to dissect complex resistance traits as opposed to the single loci effects previously studied using it.

Scores for *B. cinerea* resistance and elf18 oxidative bursts are reliable datasets which had very little in-line variability between repeats. This explains why better SNP clustering and SNP and GEM marker significance was observed for these traits. The flg22-triggered oxidative bursts were too variable, particularly with one of the phenotyping rounds using older plants (8 weeks instead of 5). As such, some of the individual repeats had more significant markers identified than the predicted mean of the four experiments together. Further phenotyping of this trait would be necessary for a thorough analysis. Similarly, the quantification of *P. syringae* resistance was problematic. Maintaining a similar level of growth and viability of the inoculum for hundreds of infections in a limited period of time was difficult to

manage. Similarly quantifying luminescence of the surrounding media is not a direct measure of infection, and is subject to variability as a result of factors not directly relevant for resistance, for example variation in rate of sugar loss into surrounding media, wound response or suberification and viability of leaf discs after detachment. As such the *P. syringae* phenotyping is highly variable and is not the best possible means of scoring resistance to this pathogen in the population. Even with clear difficulties in the phenotyping for these two traits, significant and meaningful SNP and GEM associations were still found.

In total over 2459 SNPs markers were found to be significantly associated with the defence traits studied (table 15). This is a relatively high number of associations, especially for the more reliable elf18 ROS and *B. cinerea* GWAS. All four traits produced clear SNP clustering with peaks achieving significance on different chromosomes across the genome (fig 4.3, 4.6, 4.7,4.8).

In order to take the SNP analyses further, genes found within the mapped SNP clusters would need to be characterised. This would require identifying the significantly associated SNPs within a *B. oleracea* genomic reference and extracting all the genes within that that region for further study. This is possible using the current pseudomolecule assembly, but determining the gene of interest from what can be large genomic regions underlying the peak is highly subjective. As the SNP markers can achieve significance through linkage to any form of genetic polymorphism (SNPs, expression differences, epigenetic differences or regulatory element changes for example) using mRNA-Seq data may not be an effective means to narrow the genes down. If the reads could be aligned to the A genome reference (from Rapa) the full genomic region underlying the SNP cluster could be identified for candidate searching.

As such a large number of SNP markers were significant it would perhaps help to only focus on loci involved in multiple defence responses. Good candidates for this include the cluster observed in the middle of A8 for all traits and A3 which appears to be conserved across the flg22, elf18 and *P. syringae* resistance traits.

8180 GEMs were found to be significant across the four traits studied (table 15). As the GEMs are likely to be the gene responsible for the association characterising them is more straightforward. Errors in the annotation of the *B. napus* unigenes are likely to be commonplace however, and this should be borne in mind when analysing the datasets. Many of the identified GEMs have previously identified roles in defence, including *FLS2*, *RPS5*, *TIR1*, *CTR1*, *AALP*, *WRKY21* and *WRKY33*. These are all well-established resistance genes involved in different aspects of defence signalling, and their abundance within the significant GEMs does suggest an associative transcriptomics approach can identify key regulators of defence.

It is interesting that we often see clustering of GEMs as well as SNPs. For example, GEM clusters can be seen on A5 and C5 of figure 4.7. These clusters may represent gene duplication events or large gene families all with a role in defence, such as a clade of WRKY transcription factors or a cluster of defence genes.

The most striking observation here is perhaps that resistance phenotypes of adult tissues is often associated with the expression of genes that regulate the interplay between defence and growth at the seedling stage. The expression of *BON2*, a calcium dependent membrane binding protein, is linked to development and cell death with knockouts displaying constitutive ethylene dependant cell death (Yang, 2006). *BON2* expression is significantly associated with all the defence traits studied here. Similarly *ABP1*, *AXR3* and *ARA2* have all previously been reported to either promote or repress auxin mediated signalling, which might have direct consequences on adult resistance (Tomas, 2009; Perez-Perez 2010; Navarro, 2006). The expression of these global promoters of growth and development at the seedling stage are major determinants of the variation in resistance observed in adults. Finding candidates that regulate global and long lasting growth / defence trade-offs could be future work from this project.

Although the magnitude of the flg ROS burst was significantly correlated with the magnitude of the elf ROS burst, no correlation was observed between the oxidative bursts and the two pathogen growth phenotypes. This is perhaps expected for *B. cinerea* growth, which does not express flg22 and elf18, but *P. syringae* expresses

both PAMPs. Looking at the effects of individual PAMPs in isolation may not accurately represent a real infection, in which multiple PAMPs (including unidentified ones) are being perceived alongside other 'danger signals' such as cell wall integrity changes, DAMP signalling and potential effector recognition. As such the complexity of a real interaction may not be predictable from one single component of it. The ROS burst is also only a very early part of PTI. It's possible that lines with a strong ROS burst and strong early immune signalling may then be unable to mount an effective response because of impairment or weak downstream defence signalling, such as limited metabolite excretion. Conversely lines with low early PTI might have strong constitutive defences, such as a thicker cuticle, or stronger late stage responses. Using an early stage of the immune response as a predictor of the final outcome is not taking into account the huge variation that may exist downstream of the initial ROS burst itself.

The population can be used for surveying multiple defence traits in the future. Chitin triggered ROS could be correlate with *B. cinerea* resistance, PAMP-induced lignification, seedling growth inhibition and resistance to *Sclerotinia sclerotiorum* or *L. maculans* are other phenotypes that could be added to the GWAS. Pathways analysis is another method that could be applied with multiple phenotypes. In the approach linked traits are mapped together to identify regulatory loci involved in multiple phenotypes.

The associative transcriptomics pilot study presented here has definite potential to be expanded in the future. Although the small number of lines within the population, and shortcomings in annotation and read depth limits its thoroughness at present, more lines are being sequenced and added to the panel all the time. Even with a limited number of lines meaningful associations to defence genes and developmental regulators have been found. With an expanding population the statistical power available for these studies also increases, as does the number of potential SNP markers. This also opens up a number of interesting possibilities for using the data. For example, with more lines sequenced it might be possible to locate potential PRRs by searching for polymorphism in any LRR-RLK significantly associated with a defence phenotype. As we have found FLS2 expression associated

with flg22 triggered ROS bursts, *B. cinerea* and *P. syringae* resistance this approach might be feasible. The approach could also be used to identify receptors of 'orphan PAMPs' such as ergosterol. In this example any sterol binding domain containing protein associated with an ergosterol ROS burst might be a good candidate receptor.

Associative transcriptomics in *B. napus* is in it's infancy. The pilot study presented here suggests that as a means to characterise the genetic variation behind complex traits it has great potential.

**Chapter 5 : QTL Mapping of PAMP
Responses in the A12 x GD *B. oleracea*
Cross**

5.1. Aim

The objective of the research presented in this chapter is to characterise and map PAMP responses in the *B. oleracea* A12 x Green Duke cross. This *B. oleracea* mapping population has previously reported segregating susceptibility to *Agrobacterium tumefaciens*, and as such the causative genes of interest may be in core components of PTI. The flg22 and elf18 triggered oxidative burst, *P. syringae* and *B. cinerea* resistance will be mapped to see if QTLs co-localise with *Agrobacterium* QTL previously identified.

Markers from the genetic map will be transferred to the pseudomolecule assembly to identify the physical coordinates of the significant markers, and mRNA-seq of A12 and GD will be used to identify the genetic variation within the QTL. Identifying non-synonymous SNPs between the parents and expression profiling of all genes within the QTL will be utilised to produce a candidate list. The SNP identification will allow the addition of KASPar markers within the cross to fine map and delineate any QTL identified further.

5.2. Introduction

QTL mapping is the identification of genetic loci that co-segregate with a quantitative phenotypic trait of interest within a related population. It has been used for decades as a means of identifying the markers linked to agronomically important traits of interest, and these can be used in marker-assisted breeding in crop improvement.

PAMP responses have been used as mapping traits previously. For example, in the identification of the flagellin receptor, flg22-induced seedling growth inhibition was the phenotypic trait used to identify the *FLS2* locus (Gomez-Gomez, 2000). QTL mapping of the flg22 triggered oxidative burst and the induction of a PAMP responsive marker genes led to the identification four QTL for PAMP responses in a soybean population (Valdez-Lopez, 2011). There are also numerous examples of QTL mapping used to identify non-host resistance, for example resistance to *P.*

syringae pv. *phaseolicola* in *A. thaliana* (Forsyth, 2010), powdery mildew resistance in barley (Aghnoum, 2010) and downy mildew resistance in lettuce (Zhang, 2009).

The mapping population used in this study is a double haploid (DH) population derived from the cross of *B. oleracea* ssp *italica* Green Duke and *B. oleracea* ssp *alboglabra* A12. The original map was composed of 303 restriction fragment length polymorphism (RFLP) markers, published by Bohuon et al (1996). This map was later used to create an integrated map adding 204 amplified fragment length polymorphism (AFLP) markers (Sebastian et al 2000). The population consists of 210 double haploid lines, of which 60 were used in the Sparrow et al (2004) study.

Susceptibility to *Agrobacterium tumefaciens* was mapped in the A12xGD cross, with a major QTL identified by Sparrow et al (2004) found in the middle of C9. The peak of this QTL was 41 cM on the genetic map, and susceptibility to three different strains of *A.tumefaciens*, ACH5, T37 and C58 all mapped to this locus (Sparrow, 2004). As this QTL conferred susceptibility to a non-host pathogen, it may represent impairment in aspects of PTI, which is assumed to be a major contributing factor to non-host resistance. However, as the phenotype scored in this study was emergence of crown gall not a direct measure of bacterial growth, it's possible that the QTL contains genes vital for T-DNA integration instead of resistance to the bacterium directly. This was the case in Mysore et al (2000) where *A. tumefaciens* susceptibility mapped to histone H2A, RESISTANCE TO AGROBACTERIUM 5 (*RAT5*) that was required for T-DNA integration.

A direct result of the mapping project in Sparrow et al 2004 was the identification of the line AG1012 as a promising candidate for a standard *B. oleracea* transformant line. AG1012 is highly susceptible to *A. tumefaciens* and has very good regeneration rates in vitro. As such it has been adopted as a readily transformable line for many studies in *B. oleracea*. The genetic basis of the agrobacterium susceptibility remains unclear. Whether or not there is segregating susceptibility to other non-host pathogens in the A12xGD population is unknown, and we do not yet know if PAMP responses are impaired in this population.

5.3. Results

5.3.1 There is segregating variation in oxidative burst in the A12xGD cross.

Whilst surveying different brassica populations for potential to map PAMP responses in, the transformant line AG1012's ROS response to flg22 and CSC was tested. The ROS burst in AG1012 was remarkably low in response to both PAMPs (fig 5.1 A). Compared to the ROS burst in Temple, there was hardly any ROS produced at all in this line (fig 5.1 A). H₂O₂ production above baseline was observed in response to both PAMPs however, suggesting that there is at some least some recognition of flg22 and CSC in the line.

To investigate the very low ROS observed in AG1012 further the oxidative burst in its two parental lines A12 and GD was measured. The parental line GD had significantly lower ROS at 10nM and 100nM than the line A12 (fig 5.1 B). There is no difference between A12 and GD ROS production at 1 µM flg22 however. The normal ROS burst observed at 1 µM suggests that PAMP sensitivity and early signalling are affected, as opposed to the ability to produce H₂O₂ in this line. In two of six repeats looking at 100nm flg22 triggered ROS in A12 and GD, there was no significant difference between A12 and GD, potentially suggesting that the observed impairment is a threshold effect and that 100nm is close to that threshold, or that the response is subject to environmental variability. No significant difference was observed in the elf18 or CSC triggered oxidative burst between the two parents at 100nM and 1mg/mL, even though the offspring AG1012 is impaired at this concentration.

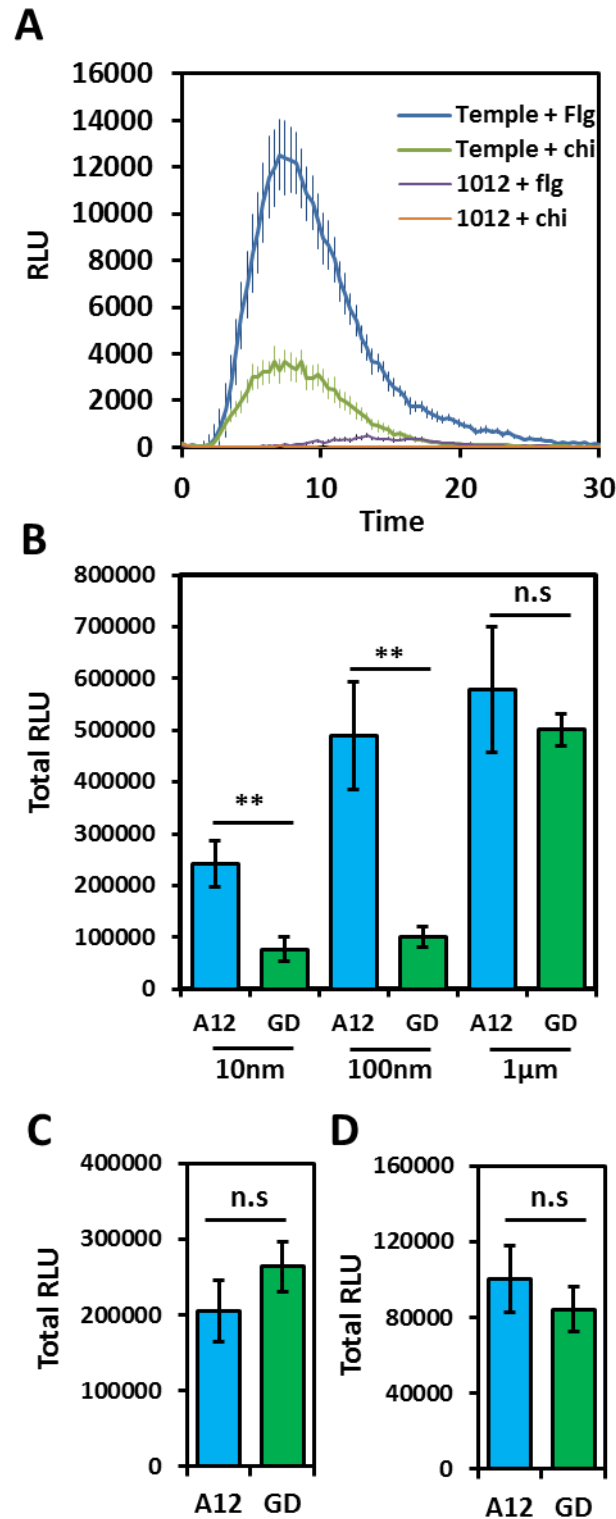


Figure 5.1 Oxidative burst phenotypes in *Brassica oleracea* lines A12, GD and AG1012.

A) Oxidative burst in response to flg22 (100nM) and CSC (1mg/ml) in Temple and AG1012 over 35 minutes following PAMP application. Error bars are the standard error of 8 biological replicates. B) ROS response of A12 and GD to different doses of flg22. Data represent total RLU read over a period of 35 minutes. Error bars are the standard error of 8 biological replicates. C,D) Total RLU observed in A12 and GD after treatment with elf18 100nM (c) and CSC (D) 1mg/ml.

5.3.2 The parental lines A12 and GD have contrasting resistance phenotypes to *P. syringae* and *B. cinerea*

After the observation that PAMP responses are impaired in GD, its susceptibility to pathogens was then tested. As A12 and GD have already had contrasting susceptibilities to *A. tumefaciens* described, the level of resistance to the pathogens *P. syringae* and *B. cinerea* was investigated. A significant increase in the growth of *Pseudomonas syringae* was observed in GD compared to A12 (fig 5.2 A). Furthermore, whilst clear PIR was seen in A12, with flg22 pre-treatment restricting pathogen growth, no PIR was observed in GD. Similarly, A12 was resistant to *B. cinerea* whereas GD was susceptible with almost double the average lesion size compared to A12 at 3dpi (fig 5.2 B). Flg22 pre-treatment did not significantly decrease growth of *B. cinerea* in either parent.

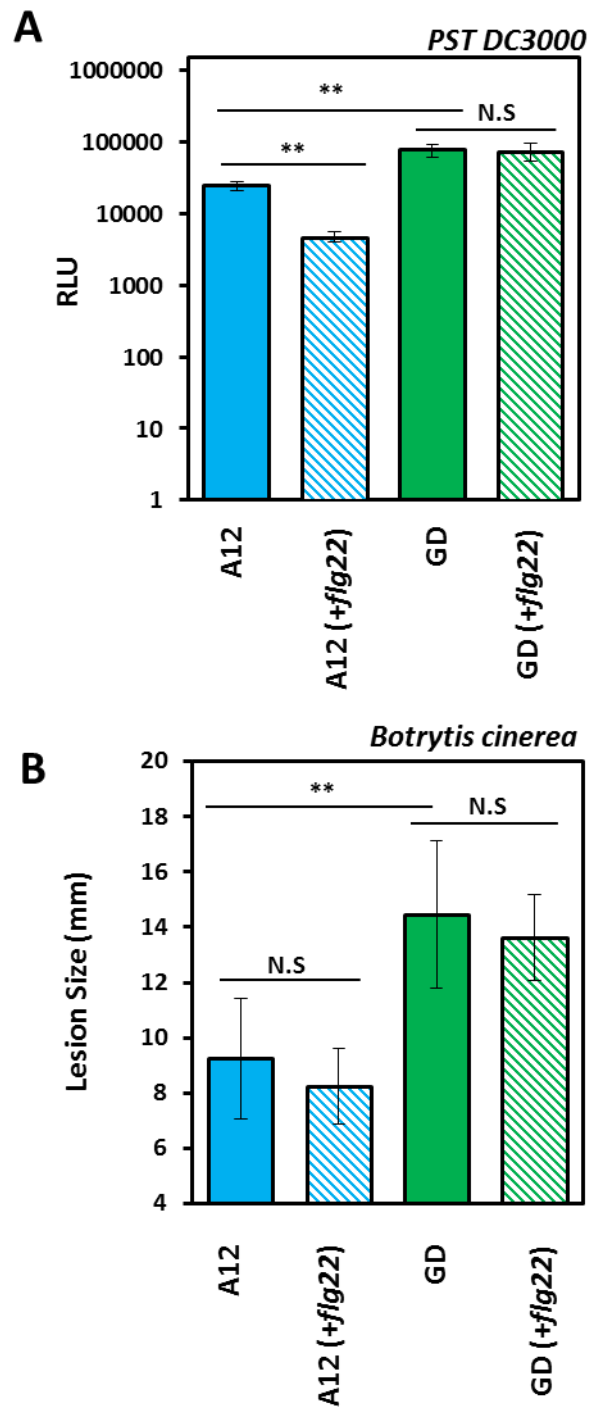


Figure 5.2 Resistance of A12 and GD to *Pseudomonas syringae* and *Botrytis cinerea*.

A) Growth of Pto DC3000 hrcC- luxCDABE with or without a flg22 100nm pre-treatment 24 hours before infection. PST levels were measured as total photons recorded over 5 seconds of sampling. Error bars are the standard error of 16 biological replicates. ** indicates a p-value < 0.001. B) lesion size of *Botrytis cinerea* infections on A12 and GD leaf discs 3dpi with or without a flg22 100nm pre-treatment 14 hours earlier. Error bars represent standard error of 16 biological replicates. ** indicates a p-value < 0.001.

5.3.3 Offspring of the A12xGD cross are highly polymorphic in ROS responses and resistance to *B. cinerea* and *P. syringae*

Clear differences were observed between the parents A12 and GD for a range of defence traits. In order to map these traits, and to see the segregation of them within the offspring, the flg22 and elf18 triggered ROS bursts and resistance to both pathogens were phenotyped in 55 individuals from the population. The four responses were scored multiple times across the population, and good reproducibility between experiments was observed.

All four responses were highly variable across the population (fig 5.3 A-D). Some of the lines displayed consistently low ROS and high susceptibility, including AG1012 and AG2072. In general however, there is no clear correlation between high ROS and resistance (fig 5.3), suggesting that the loci underlying the traits are genetically distinct. For the elf18 oxidative burst, it appears there is transgressive segregation from the parental phenotypes, which were observed to have no significant difference between them despite the offspring being highly polymorphic for the trait.

Of the four traits only *B. cinerea* resistance was observed to be normally distributed in the population (fig 5.4). The log₁₀ of the raw data for the ROS bursts and PST resistance was closer to normal distribution, and it is the log₁₀ of the raw data that was used for QTL mapping.

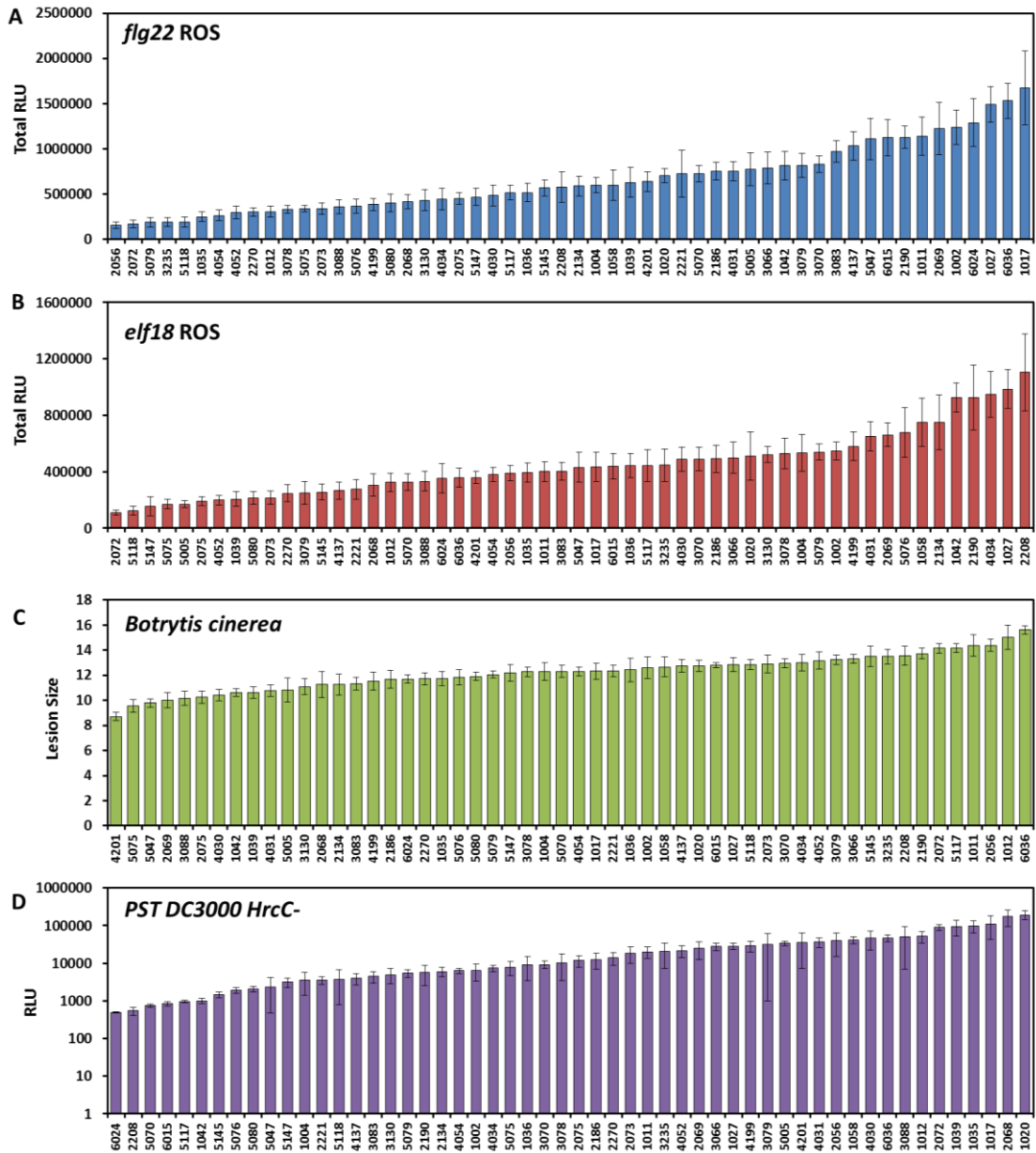


Figure 5.3 Phenotyping the A12xGD cross of *B. oleracea* for response to flg22, elf18 and disease resistance to *P. syringae* and *B. cinerea*

Variation of the oxidative burst in response to flg22 100nm (A) and elf18 100nm (B), resistance to *Botrytis cinerea* (C) and resistance to *Pseudomonas syringae* (D) in the A12 x GD cross. Data shown are a typical example of one of up to four different repeats. Error bars are the standard error of 8 biological replicates for ROS bursts, and 8-16 biological replicates for disease assays.

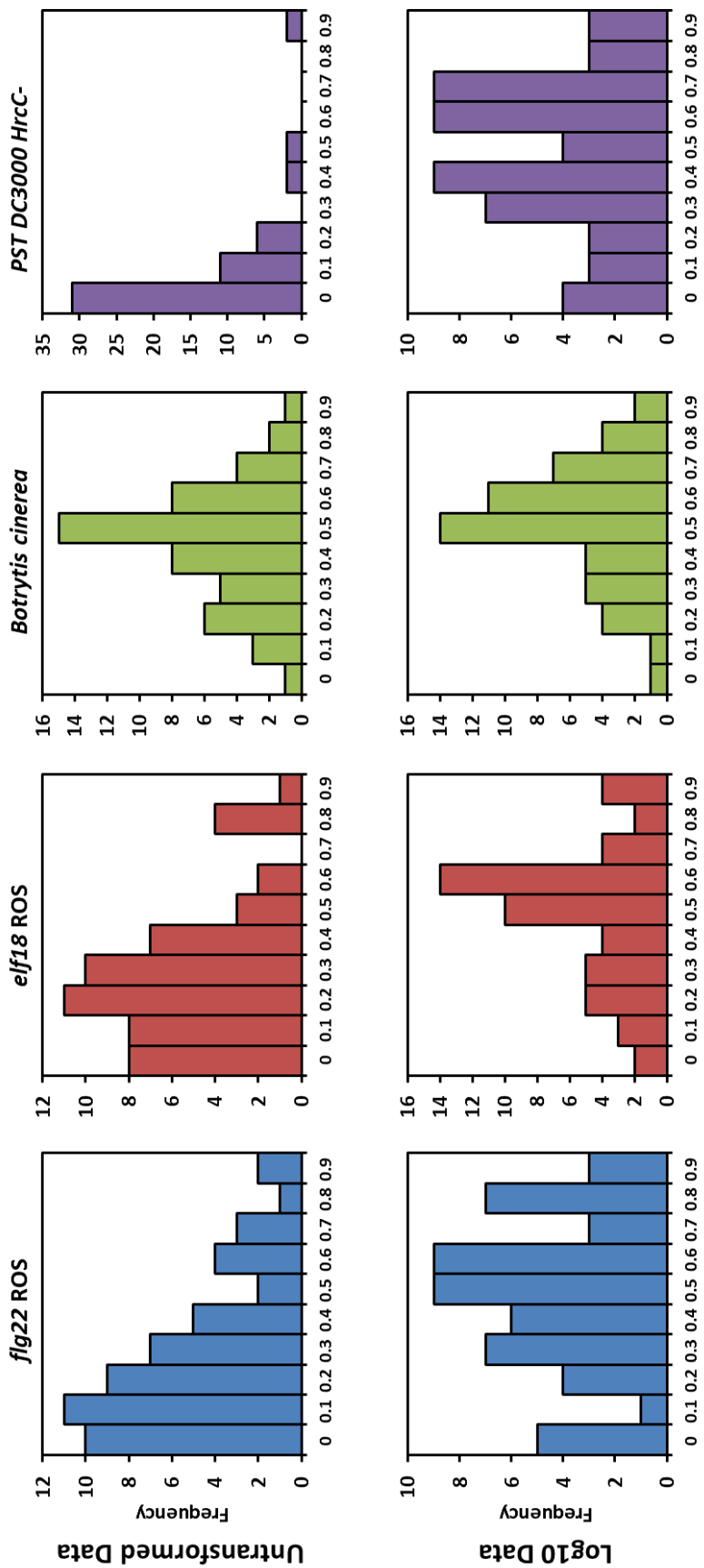


Figure 5.4 Distribution frequencies of variation in defence phenotypes in the *B. oleracea* A12 x GD cross.

5.3.4 A significant QTL on C9 was found for the flg22 triggered ROS burst

The phenotyping scores, along with genotype data for the lines used and the genetic map of A12 x GD produced by Sebastian et al (2000) were run in MAPQTL for interval mapping analysis. For the flg22-triggered oxidative burst four different phenotyping repeats and the predicted mean across all four experiments were mapped.

A significant (LOD > 2.5) QTL on the middle of C9 was observed in all repeats (fig 5.5). The reproducibility and consistency of the QTL does suggest that a major determinant of the flg22-triggered ROS burst in this population is present on C9. The highest LOD score observed in the predicted mean was 5.94, seen at 65 cM along the genetic map at the marker pN105E4NM. LOD scores above 3 were seen between the markers AC-CATE21 and LEW6G7E2, representing a wide interval of 22.8 cM. To narrow the interval further, a LOD drop approach was used with the QTL delineated by a reduction in LOD of >1.5 from the peak. This results in a smaller interval between the markers pN180E1 and pW106E1 of 6.9cM consisting of markers all above a LOD score of 4.44 (fig 5.6).

The GD allele of the most significant marker, pN105E4NM, was responsible on average for 45% of the phenotypic variation in the cross. Lines with the GD allele at this position had an average total RLU of 451, 453, with the A12 allele having an average total RLU of 1,177,050.

Like the *Agrobacterium* susceptibility QTL identified by Sparrow (et al 2004), an allele from GD on the middle of C9 was a major determinant of the trait. Unexpectedly however, the flg22 QTL and the QTL for *Agrobacterium* susceptibility are not at the same locus. The most significant peak for flg22 ROS is nearly 20cM distal from the *Agrobacterium* peak, the marker pW233 (Sparrow, 2004) (fig 5.7).

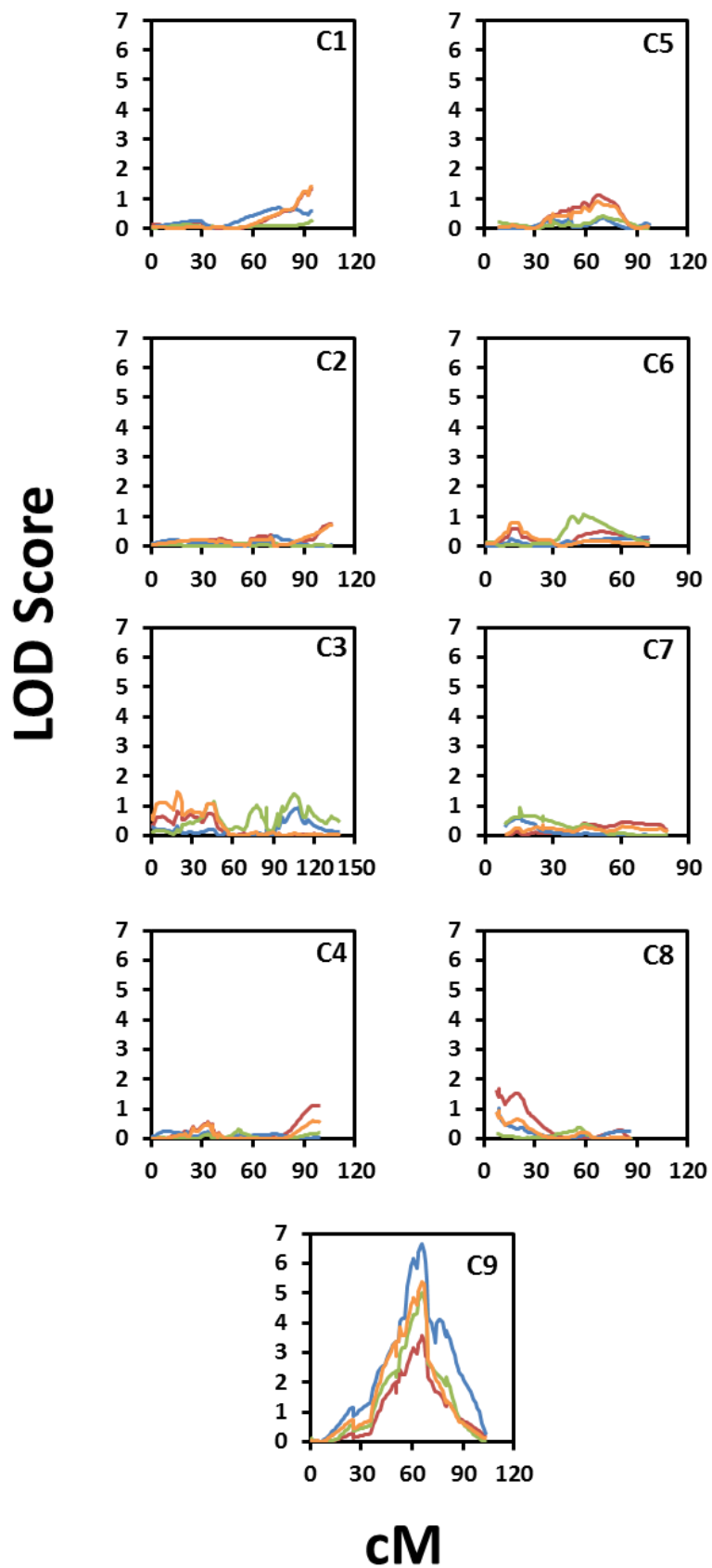


Figure 5.5 QTL profiles of the flg22 triggered ROS burst in A12 x GD.
 Interval mapping output from MAPQTL for four different experiments scoring the flg22 triggered ROS burst in *B. oleracea* A12xGD.

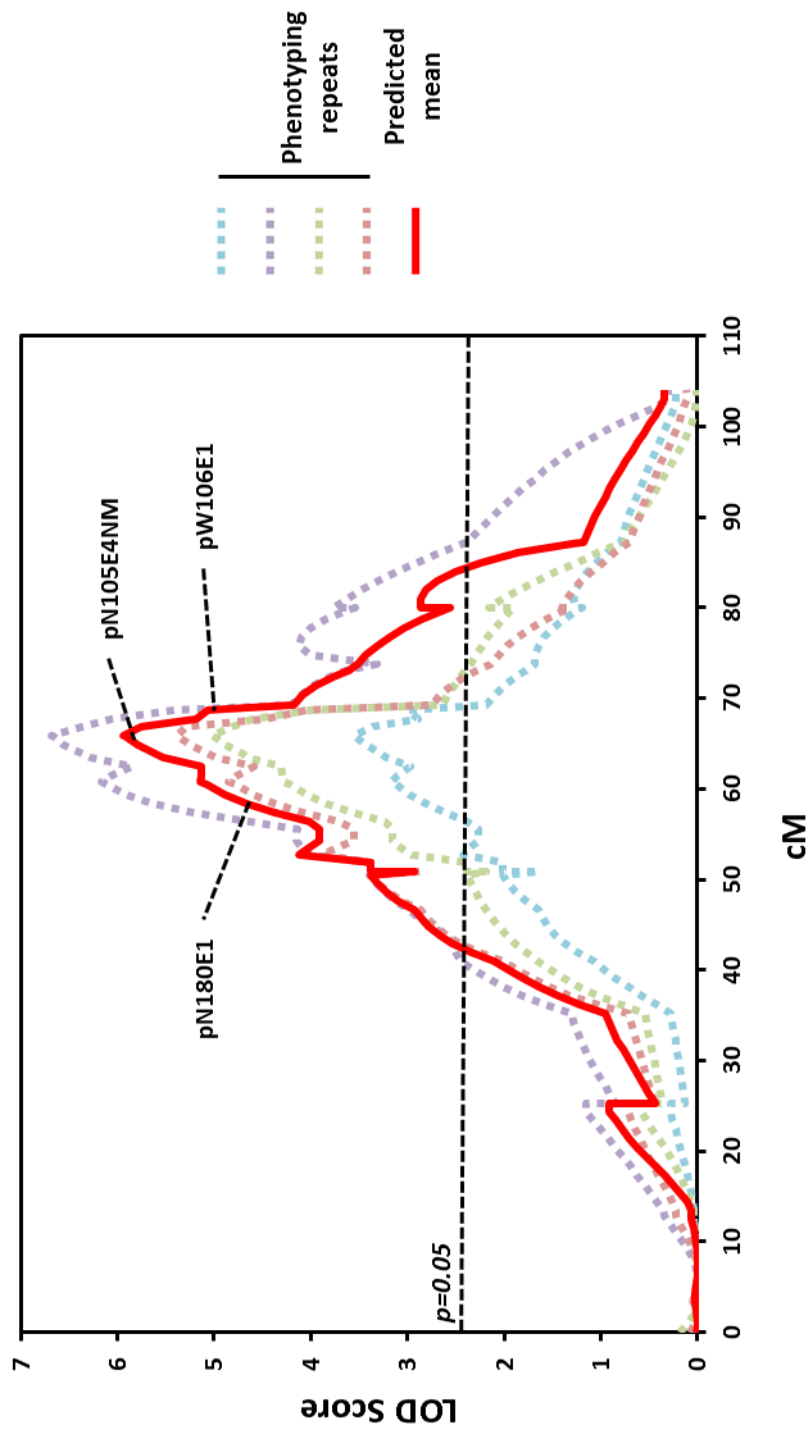


Figure 5.6 The C9 QTL controlling the flg22 triggered ROS burst in A12 x GD *B. oleracea* cross

Data shows the QTLs from four different experiments (dotted lines) and the QTL from the predicted mean of the four repeats. The markers representing the peak, and those that delineate

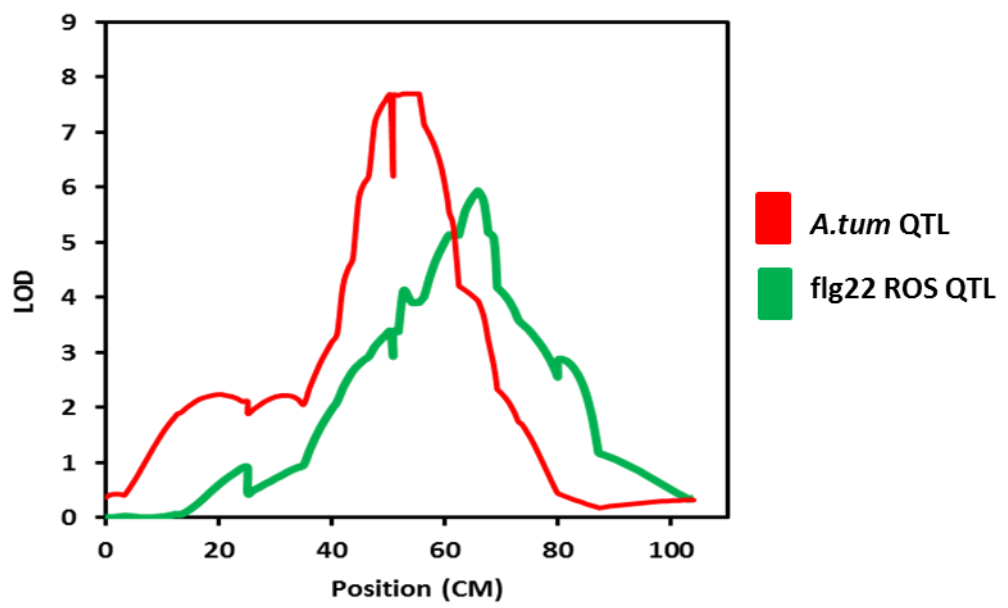


Figure 5.7 The flg22 and *Agrobacterium* QTL peaks in A12xGD do not overlap.

5.3.5 No significant QTLs for elf18 ROS, *B. cinerea* resistance or *P. syringae* resistance were found in A12 x GD.

No Major QTLs (LOD > 2.5) were observed consistently for elf18 ROS, *B. cinerea* resistance or *PST DC3000* resistance in the A12 x GD cross.

For the elf18 triggered oxidative burst a significant QTL was seen on C5 in one repeat, but this was not observed again (Appendix 4). There are possible minor QTLs on C3 and C4 that appear to be consistent between repeats. No QTL was found on C9 overlapping with the flg22-triggered ROS QTL. This suggest that the genetic regulation of the flg22 and elf18 triggered ROS busts in A12 x GD is separate, and potentially that core shared components of H₂O₂ production and PTI signalling, such as RBOHD or BAK1 for instance, are not the causative genes of interest underlying the QTL. Alternatively, the QTL on C9 might only be relevant at lower concentrations of PAMP, and 100nM elf18 might be beyond the threshold for observing any inhibition. This is consistent with the different dose response curves to elf18 and flg22 observed in *B. napus* (Fig 1. 1 A-C).

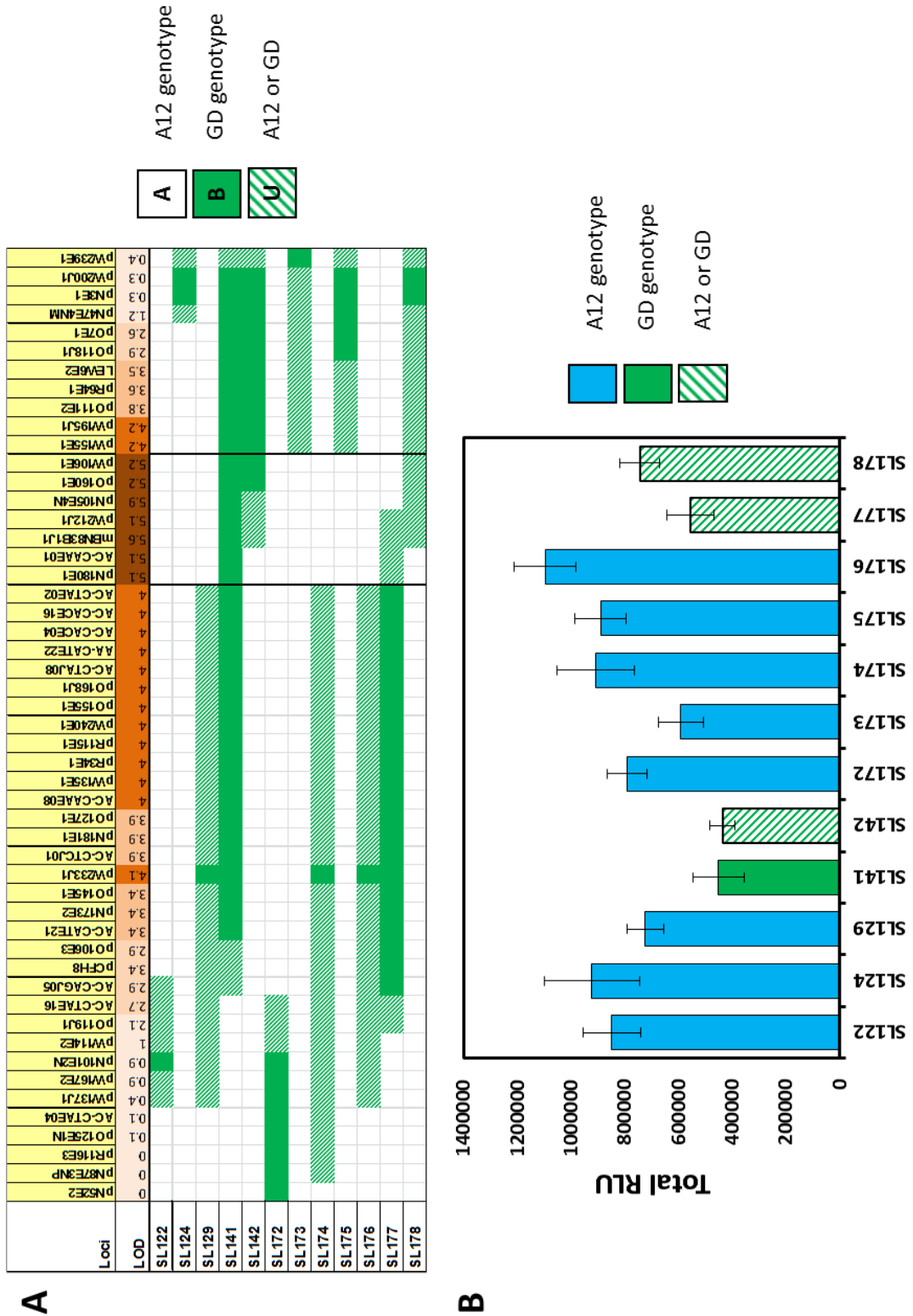
Two potentially interesting minor QTLs for *B. cinerea* resistance were found on C9 and C4 (Appendix 4). They are consistent between the two phenotyping repeats performed thus far. Major gene effects contributing to *B. cinerea* resistance are rare in the literature, so these QTLs may be worth investigating further. There is no overlap between the *B. cinerea* C9 QTL and the flg22 and *Agrobacterium* C9 QTLs. There was no apparent QTL for *PST* resistance in A12 x GD (Appendix 4) and further phenotyping was not continued.

5.3.6 The Locus resulting in low flg22 triggered ROS is likely to sit between the markers pN105E4NM and pO160E1

The flg22 C9 QTL, being highly significant and consistent between repeats was chosen for further study. The QTL interval between the markers pN180E1 and pW106E1 is 6.9 cM however. To try and narrow the likely range of the QTL further the genotypes of the A12 x GD offspring were screened for recombination events within the QTL. Only four lines four lines, AG2134, AG3070, AG3088 and AG5118, had recombination events within the significance interval (fig 5.8 A). The flg22 ROS phenotypes of these lines was compared to two lines with clear A12 and GD genotype at this locus, AG1002 and AGAG1012, which have high and low ROS respectively. The lines AG2134 and AG5118 both had a phenotype most closely related to A12 whereas AF3070 and AG3088 more closely resembled GD (fig 5.8 B). Because of the recombination events within the lines, it is highly likely that the loci of interest lies between the markers pN105E4NM (the QTL peak) and pO160E1.

5.3.7 Confirmation of the flg22 ROS C9 QTL through Substitution lines

In order to confirm the effect of GD locus at this position, A12 substitution lines incorporating genomic regions of GD (Ramsay, 1996), were screened for flg22 triggered ROS. Twelve substitution lines exist with GD insertions into an A12 background within C9 (fig 5.9 A). Only two of these, SL141 and SL142 have confirmed GD loci within the QTL of interest. Both of these lines had low flg22 triggered ROS compared to most of the lines with A12 genotypes at these loci (fig 5.9 B). Unfortunately the substitution lines do not have as clearly defined a differential in ROS production as A12 and GD. As such the substitution lines have only partially confirmed the phenotypic effects of the GD C9 locus. The substitution lines SL173 and SL178 for instance both have A12 genotype at the most significant marker (pN105E4NM) and relatively low ROS burst (fig 5.9 B). SL178, which may have a GD allele at pN105E4NM, also has a moderate ROS response. Furthermore, the low level of ROS at 100nm flg22 treatment seen in GD and lines such as AG1012, is not seen here. This might suggest that the C9 locus alone is not sufficient to recreate the extremely low level of ROS seen in AG1012 alone, and that other loci must be having an effect as well.



Multiple QTL Mapping of flg22 triggered ROS in A12 x GD

Because the C9 QTL is having a major effect on the phenotype, it's possible that it is affecting the LOD score of other loci across the genome. Multiple QTL mapping (MQM) allows identification of several markers as a cofactor, and then remaps the QTL taking into account the effect of these markers. As such it may identify other sources of variability in the genome that are masked by the C9 QTL.

The predicted mean of four phenotypic repeats of the flg22 triggered ROS was run in MAPQTLs multiple QTL mapping tool with the markers AC-CATE21 through LEW6G7E2 selected as co-factors. Interestingly, the minor QTL on C5 gains a higher LOD score, and other QTLs emerge on C4 and C6 (fig 5.10). The C5 QTL may share the same loci as the elf18 ROS C5 minor QTL, and the MQM QTL on C4 may be shared with the elf18 ROS and potentially the *B. cinerea* resistance QTL on C4 (fig 5.10, Appendix 4). The MQM mapping, and the substitution line phenotypes, do suggest that the C9 locus is interacting with other loci across the genome.

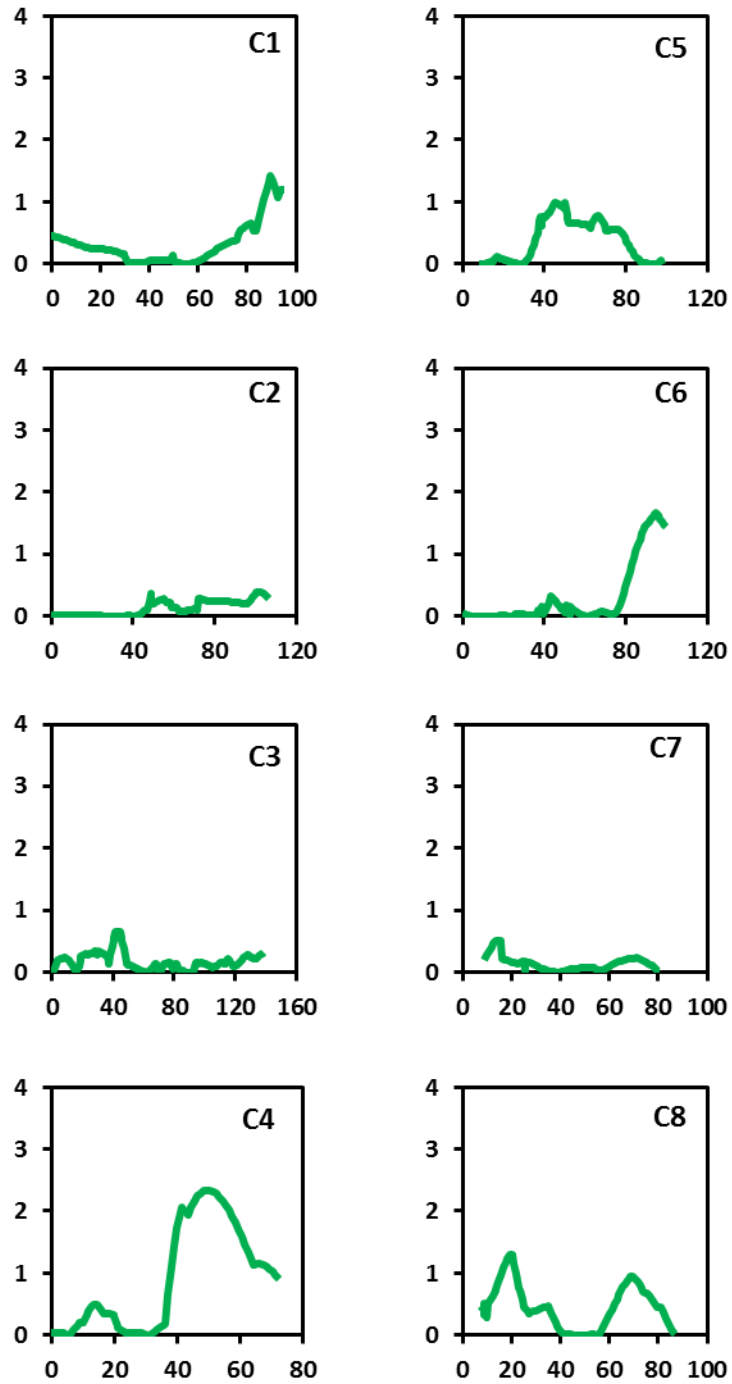


Figure 5.10 MQM mapping of the flg22 triggered ROS burst in A12xGD taking the C9 QTL as a Co-factor

The phenotype sampled was the predicted mean of four flg22 triggered ROS burst repeats. The markers AC-CATE21 through LEW6G7E2 were selected as co-Factors in MAPQTLs MQM mapping tool.

5.3.8 Illumina Sequencing of A12 and GD

In order to identify sequence and expression polymorphism between the two parents, and to serve as a source of SNP information for fine mapping, mRNA-seq of A12 and GD was needed. Sequencing of A12 had already been previously undertaken by Judith Irwin (JIC, Norwich) (personal communication), using Illumina GAIIx sequencing. The GD reference sequence was produced for this project. mRNA of 3 week old plants (the same conditions as the A12 RNA extraction), and was sequenced by Illumina TruSeq.

The Illumina reads were aligned against the version 4 pseudomolecule assembly, the same as that used in the association mapping. The mRNA seq coverage and depth was roughly comparable between the two runs with GD composed of 33,067,887 80 BP single end reads (of which 60% mapped to the reference), and A12 sequencing comprising of 29,120,665 76 BP single end reads (with 68% mapping to the pseudomolecules).

Between A12 and GD 43,473 SNPs were identified in the mRNA sequencing spread over 13,053 unigenes. On C9 alone, 6327 SNPs were identified within 1,815 genes (Appendix 5).

5.3.9 Identification of Non-synonymous SNPs in coding genes from A12 and GD

In order to predict codons of the A12 and GD mRNA reads, and therefore identify SNPs that result in non-synonymous (NS) AA changes, the predicted consensus sequence for each A12 and GD unigene was run in a custom script developed by Martin Trick (JIC, Norwich, UK). The script aligned consensus *B. napus* unigene sequence against the AA sequence of the closest *A. thaliana* homolog to identify the likely ORFs. This allowed the prediction of the AA sequence of the A12 and GD unigenes. Of the 6327 SNPs on C9, 3733 were predicted to encode synonymous amino acid changes, 1676 were predicted to be non-synonymous (Appendix 5). 918 SNPs were within unigenes that the script was not able to predict codons for, likely a result of either major changes in codon use or intron position between *B. napus*

and *A. thaliana*, or incomplete coverage of the unigene sequence by the illumina reads.

5.3.1 Transferring Markers from the Genetic Map to the Physical Map Based on the *B. napus* C genome Unigene Assembly

In order to identify all the genes within the QTL the markers used to build the Sebastian *et al* (2000) integrated genetic map of A12 x GD were blasted against the *B. napus* unigene assembly created by Harper *et al* (2012). As sequence was only available for the RFLP markers, the AFLP markers could not be blasted. This unfortunately included pN105E4NM, the most significantly associated marker. The QTL peak however is otherwise predominantly RFLP markers so defining the QTL within the unigene assembly should be possible.

Every RFLP marker on C9 for which sequence was available was BLASTed against the unigene assembly. Approximately two thirds of the markers had a clear hit in C9 (table 16). Unfortunately the colinearity between the genetic and the physical map breaks down towards the centre of the chromosome. The region delineated by the markers O119J1 and pN180E1 (a marker within the peak of the QTL) do not have any clear hits on C9 of the pseudomolecule assembly, with seemingly random BLAST hits to other chromosomes.

There are two major contributing factors to the discrepancy between the genetic and physical maps of C9 here. The first is errors in the assembly of the pseudo molecules. Many of the chromosomes were recently revealed to be chimeric, with large substitutions seen on some chromosomes. The second source of potential error here results from comparing a genetic map of *B. oleracea* to *B. napus*. Although by and large the chromosomal assembly between the species should be intact, as viable synthetic *B. napus* is producible from the progenitor species (Parkin, 1995), the extent of gene-by-gene rearrangement at a local level is currently unknown.

C9 Marker	Fig ROS LOD score	Marker Type	Sequence Data?	Pseudomolecules BLAST Location	Predicted Chromosome	Unigenes BLAST	Associated AT#
pN52E2	0.01	RFLP	Y	382620	C9	JCVI_28418	AT2G19610
pN87E3NP	0	RFLP	Y	35631998	C9	ES937270	n/a
pR116E3	0.03	RFLP	Y	26373	C9	JCVI_15549	AT4G00030
pO125E1NP	0.06	AFLP	N	-	-	-	-
AC-CTAE04	0.06	AFLP	N	-	-	-	-
pN101E2NM	0.91	RFLP	Y	3393549	C9	JCVI_14067	AT5G27920
pW167E2	0.91	RFLP	Y	3245595	C9	EE456025	AT5G27520
pW137J1	0.44	AFLP	N	-	-	-	-
pW114E2	0.96	AFLP	N	-	-	-	-
pO119J1	2.11	RFLP	Y	5242212	C2	JCVI_15157	AT5G62890
AC-CTAE16	2.67	AFLP	N	-	-	-	-
AC-CAGJ05	2.93	AFLP	N	-	-	-	-
pCFH8	3.38	AFLP	N	-	-	-	-
pO106E3	2.93	AFLP	N	-	-	-	-
AC-CATE21	3.38	AFLP	N	-	-	-	-
pN173E2	3.38	RFLP	Y	17462477	C1	JCVI_29159	AT1G57680
pO145E1	3.38	RFLP	Y	16811964	C5	JCVI_26417	AT1G10290
pW233J1	4.12	RFLP	Y	21352333	C9	JCVI_27944	AT5G43930
AC-CTCJ01	3.91	AFLP	N	-	-	-	-
pO127E1	3.91	AFLP	N	-	-	-	-
pN181E1	3.91	RFLP	Y	29211113	C9	JCVI_25203	AT4G11800
pO155E1	4.02	RFLP	Y	49226763	C3	EE420027	AT5G58410
AC-CAAE08	4.02	AFLP	N	-	-	-	-
AC-CTAJ08	4.02	AFLP	N	-	-	-	-
AC-CTAE02	4.02	AFLP	N	-	-	-	-
Pw240e1	4.02	RFLP	Y	3274410	C1	EE442102	AT4G32690
AA-CATE22	4.02	AFLP	N	-	-	-	-
AC-CACE04	4.02	AFLP	N	-	-	-	-
pR115E1	4.02	AFLP	N	-	-	-	-
Pw135e1	4.02	RFLP	Y	25359364	C7	-	-
AC-CACE16	4.02	AFLP	N	-	-	-	-
pR34E1	4.02	RFLP	Y	20354822	C9	JCVI_39809	AT5G51230
pO168J1	4.02	AFLP	N	-	-	-	-
pN180E1	5.14	RFLP	Y	18565492	C4	JCVI_28465	AT2G27040
AC-CAAE01	5.13	AFLP	N	-	-	-	-
pW212J1	5.13	RFLP	Y	54646385	C9	JCVI_24	AT5G19140
mBN83B1J1	5.61	MicrosαY	Y	55601328	C9	EV051882	n/a
pN105E4NM	5.94	Peak AFLP	N	-	-	-	-
pO160E1	5.18	RFLP	Y	56487800	C9	JCVI_2716	AT5G16660
pW106E1	5.18	RFLP	Y	50785644	C9	JCVI_7571	n/a
pW155E1	4.18	<-1.5 RFLP	Y	56747516	C9	EE392341	AT3G02540
pW195J1	4.18	RFLP	Y	56780174	C9	EE392255	AT3G02540
pO111E2	3.77	AFLP	N	-	-	-	-
pR64E1	3.6	RFLP	Y	58008395	C9	JCVI_13272	AT5G09220
LEW6G7E2	3.52	AFLP	N	-	-	-	-
pO7E1	2.56	RFLP	Y	59177515	C9	EV071580	AT5G11470
pO118J1	2.86	RFLP	Y	59225732	C9	JCVI_27106	AT5G11390
pN47E4NM	1.18	AFLP	N	-	-	-	-
pW200J1	0.34	RFLP	Y	61544289	C9	JCVI_29720	AT5G17780

Table 16 BLAST summary of C9 markers against the pseudomolecules.

Lines in green indicate sequence was available and BLASTed against the pseudomolecules. Pseudomolecule location, and predicted chromosome is listed, alongside the unigene the sequence is found in (if applicable) and the associated *Arabidopsis* gene (if applicable). Red boxes indicate a BLAST hit to a non-C9 unigene location. If any of the BLAST hits against homologous copies were present on C9, the box is coloured green. In non C9 hits, the location of the most significant BLAST hit between homologous copies is listed.

Despite the discrepancy between genetic and physical map on some aspects of C9, the pseudomolecule assembly is still a useful tool for defining the QTL. The majority of the flg22 ROS QTL is relatively collinear between the two maps, with the markers between pW212J1 and pW195J1 (which covers the region most likely linked to the loci of interest, (fig 5.8 B)) all BLASTing to C9. This covers a relatively tight QTL of approximately 18 mega base pair region under the peak of the QTL. However, using pW212J1, as the upper limit of the QTL does exclude many of the potential candidates within the QTL. The next possible marker defining the upper limit of the QTL is pW233J1, which has a higher significance than any of its surrounding markers (table 16). This might suggest its position in the genetic map is wrong. This marker does have a definite anchoring point on the pseudomolecules however, and as it is the closest marker that is inclusive of the entire peak this was used to define the upper limit of the QTL.

5.3.1 The Initial Candidate Gene list

An initial candidate list of non-synonymous SNPs was created. The markers pW155E1 and pW233J1 were taken to define QTL within the NS SNP list ordered by pseudomolecule position (Appendix 5). Within this QTL there were 795 predicted NS SNPs within 284 distinct unigenes in this region (Appendix 5). The likely errors in the pseudomolecule assembly mean we have limited confidence in the top half of this QTL.

Because of the syntenic relationship with *A. thaliana* we expect large collinear segments within a chromosome punctuated with islands of rearrangement and gene insertion when compared with the model species (Harper, 2012). We see this in the genes of the candidate list here, with a relatively well conserved syntenic region with *A. thaliana* chromosome 5 in the middle and bottom of the QTL, and a region of seemingly random *A. thaliana* genes towards the top (Appendix 5). Whether this represents a chromosomal region that has seen substantial rearrangement from *A. thaliana*, or just a result of errors in pseudomolecule assembly is unclear.

The full candidate list of unigenes between pW155E1 and pW233J1 can be seen in Appendix 5. From the initial candidate list of 284 unigenes with NS SNPs, there were many potentially interesting candidates. Some of these, selected because of a clear function in *A. thaliana*, a cell-membrane localisation or an association with defence, are summarised in table 17. There are many other potential candidates within this QTL however, so defining a narrow number of candidate genes cannot be achieved until after fine mapping.

As an immediate precursor and requirement for an oxidative burst, genes involved Ca^{2+} signalling are very strong candidates for regulators of ROS generation. Within the QTL there are multiple Ca^{2+} and calmodulin binding proteins with NS SNPs (table 17, Appendix 5). Some of the candidates are directly involved in hormone signalling, including *AOS*, essential in jasmonate signalling, and *XBAT32*, a regulator of BR biosynthesis. There are NS SNPs in three different oxidoreductases, three different ion-transporters and two major defence and developmental transcription factors *WRKY2* and *ATHB3* (table 17). Perhaps the most interesting candidate however is CYCLIC-NUCLEOTIDE GATED ION CHANNEL 4 (*CNGC4*) / DEFENCE NO DEATH 2 (*DND2*). This gene has been implicated in early signalling in response to the PAMP LPS in plants, and a number of defence and developmental phenotypes (Ali, 2007; Ma, 2011) .

It is important to note that the annotation of the genes is based on a relatively low stringency genome-wide BLAST between two different species. As such there are going to be errors in the annotation, particularly for large gene families like the WRKY transcription factors. Definite annotation of the genes would require direct sequencing in both A12 and GD and then BLASTing against *A. thaliana* sequence.

Chr	Unigene	AT#	Annotation	NS SNPs
C9	JCVI_18952	AT5G43970.1	TOM22-V	1
C9	ES940992	AT5G44090.1	calcium ion binding	1
C9	JCVI_38477	AT3G55410.1	oxidoreductase	3
C9	JCVI_1437	AT5G45350.1	rhodopsin-like receptor	1
C9	EV143470	AT5G45380.1	solute:sodium symporter	1
C9	JCVI_14385	AT5G45430.1	ATP binding protein serine/threonine kinase	1
C9	JCVI_16380	AT5G47760.1	ATPK5	2
C9	JCVI_20747	AT1G64720.1	CP5	1
C9	JCVI_16202	AT3G25860.1	LTA2 (PLASTID E2 SUBUNIT OF PYRUVATE DECARBOXYLASE)	2
C9	JCVI_186	AT3G25920.1	RPL15	4
C9	JCVI_17764	AT4G05390.1	oxidoreductase	6
C9	JCVI_6373	AT4G05190.1	ATK5	1
C9	JCVI_467	AT4G05180.1	calcium ion binding	1
C9	EV142997	AT4G05020.1	calcium ion binding	1
C9	JCVI_30440	AT4G04970.1	ATGSL1 (GLUCAN SYNTHASE LIKE-1)	2
C9	JCVI_25230	AT3G07160.1	ATGSL10 (GLUCAN SYNTHASE-LIKE 10)	1
C9	JCVI_34362	AT5G13000.1	ATGSL12 (GLUCAN SYNTHASE-LIKE 12)	1
C9	JCVI_38964	AT4G04955.1	ATALN	5
C9	JCVI_692	AT4G04910.1	NSF	3
C9	JCVI_12811	AT4G11410.1	oxidoreductase	3
C9	JCVI_17586	AT1G34000.1	OHP2 (ONE-HELIX PROTEIN 2)	4
C9	JCVI_3966	AT5G42650.1	AOS (ALLENE OXIDE SYNTHASE)	5
C9	JCVI_7183	AT1G32200.1	ATS1 (ACYLTRANSFERASE 1)	1
C9	JCVI_8355	AT5G53450.1	ORG1	1
C9	JCVI_4160	AT5G54160.1	ATOMT1 (O-METHYLTRANSFERASE 1)	1
C9	JCVI_20553	AT5G54250.1	ATCNGC4 (DEFENSE, NO DEATH 2)	4
C9	JCVI_10019	AT5G54650.1	Fh5 (FORMIN HOMOLOGY5)	2
C9	CD816074	AT5G55630.1	KCO1	1
C9	ES990089	AT5G56270.1	WRKY2	2
C9	EV157863	AT5G56290.1	PEX5	1
C9	EV165070	AT5G56360.1	calmodulin binding	5
C9	JCVI_14909	AT5G57030.1	LUT2 (LUTEIN DEFICIENT 2)	5
C9	JCVI_38595	AT5G57050.1	ABI2 (ABA INSENSITIVE 2)	1
C9	JCVI_31143	AT5G57580.1	calmodulin binding	3
C9	JCVI_13551	AT5G57740.1	XBAT32	1
C9	JCVI_34860	AT5G57800.1	WAX2	4
C9	EV046616	AT5G19130.1	GPI-anchor transamidase	3
C9	JCVI_41087	AT5G15150.1	ATHB-3 (ARABIDOPSIS THALIANA HOMEBOX 3)	2
C9	JCVI_8536	AT5G17630.1	antiporter/ glucose transporter	2
C9	JCVI_22771	AT5G17020.1	XPO1A	1
C9	ES980499	AT5G16830.1	SYP21	3

Table 17 Candidate genes in the C9 QTL.

Genes are taken from the *B. napus* pseudomolecule assembly version 4, and represent genes with predicted NS AA changes between pW155E1 and pW233J1. Candidates presented here have defined functions in *Arabidopsis* and are involved in defence, development, Ca²⁺ signalling or ion transport or cell membrane localised. The number of NS SNPs in the gene is listed in column 5.

5.3.2 PAMP-responsiveness of genes within the QTL in *A. thaliana* and *B. napus*

Many genes involved in PAMP perception and PAMP signalling are expressed or repressed upon PAMP treatment (Boller, 2009; Navarro, 2004; Zipfel, 2004). As such the expression of every gene within the QTL was examined in the PAMP induced transcriptome experiment in *B. napus* (Appendix 1, table 18). Further to this, the expression of these genes was compared within two separate microarray experiments from previously published *A. thaliana* work. Boudsouq et al (2010) published the flg22 induced transcriptome at 30 minutes and 1 hour post PAMP treatment. Added to this was the flg22 transcriptome from 1 and 2 hours post PAMP treatment, created at the Sainsbury Laboratory and given the PLEXDB identifier GSE17479. The transcriptional changes of all the genes within these three data sets can be seen in Appendix 5. The expression of some of the clear candidate genes can be seen in figure 5.11.

Of 3358 unigenes between the pW155E1 and pW233J1, 295 of them were greater than 4 fold up-regulated by flg22 in Temple, and 378 were greater than 4 fold down regulated at three hours post treatment (Appendix 5). Of the genes proposed to have a role in defence within the wider QTL, *CP5*, *LTA2* and *RPL15* are all down regulated by flg22 to a moderate extent across all time points (fig 5.11). The Ca²⁺ ion binding protein *AT4G05020* and FH5 are both induced by flg22. The *CNGC DND2* is very rapidly down-regulated by flg22 treatment, and is down regulated at all time points and across multiple experiments in both *B. napus* and *A. thaliana* (fig 5.11).

Unigene	AT#	Annotation	<i>B. napus</i>		<i>A. thaliana</i>			
			+60 min	+180 min	Boudsoug Et al (2010) +30 min	+60 min	PlexDB GSE17479 +60 min	+120 min
Fold Expression After flg22 Treatment								
JCVI_18952	AT5G43970.1	TOM22-V	-0.928	0.353	-0.072	-0.252	-0.698	-0.279
ES940992	AT5G44090.1	calcium ion binding	-0.101	0.534				
JCVI_38477	AT3G55410.1	oxidoreductase	1.269	1.777				
JCVI_1437	AT5G45350.1	rhodopsin-like receptor	0.710	-0.434	-0.010	0.112	0.084	-0.010
EV143470	AT5G45380.1	solute:sodium symporter	-0.469	-0.294	-0.033	0.038	-0.415	-0.351
JCVI_14385	AT5G45430.1	ATP binding serine/threonine kinase	-0.235	-0.192				
JCVI_16380	AT5G47760.1	ATPK5	-0.785	-0.823	-0.515	-0.282	-1.112	-1.364
JCVI_20747	AT1G64720.1	CP5	-2.141	-2.799	-0.136	-0.149	-0.614	-0.784
JCVI_16202	AT3G25860.1	LTA2	-1.162	-3.158	-0.231	-0.213	-0.344	-1.819
JCVI_186	AT3G25920.1	RPL15	-0.707	-3.913	0.056	-0.160	-0.458	-1.057
JCVI_17764	AT4G05390.1	oxidoreductase	-0.968	-0.098				
JCVI_6373	AT4G05190.1	ATK5	-0.393	-0.039		-0.004	0.232	-0.008
JCVI_467	AT4G05180.1	calcium ion binding	-0.614	-4.798	-0.029	-0.087	-0.010	-0.438
EV142997	AT4G05020.1	calcium ion binding	1.345	2.247	-0.113	0.492	1.350	1.233
JCVI_30440	AT4G04970.1	ATGSL1 (GLUCAN SYNTHASE LIKE-1)	-3.526	-0.526				
JCVI_25230	AT3G07160.1	ATGSL10 (GLUCAN SYNTHASE-LIKE 10)	0.940	0.736	-0.225	0.177	0.088	0.329
JCVI_34362	AT5G13000.1	ATGSL12 (GLUCAN SYNTHASE-LIKE 12)	-1.903	-2.990	-0.064	-0.116	-0.063	-1.000
JCVI_38964	AT4G04955.1	ATALN	-2.087	-0.647	-0.003	-0.488	-1.157	-1.071
JCVI_692	AT4G04910.1	NSF	1.498	1.927	-0.051	-0.063	-0.690	0.137
JCVI_12811	AT4G11410.1	oxidoreductase	-1.214	-2.294	0.109	-0.364	-0.443	-1.026
JCVI_17586	AT1G34000.1	OHP2 (ONE-HELIX PROTEIN 2)	-0.891	-3.589	0.169	-0.341	-0.294	-1.284
JCVI_3966	AT5G42650.1	AOS (ALLENE OXIDE SYNTHASE)	0.827	-2.195	-0.311	-0.427	0.364	-0.158
JCVI_7183	AT1G32200.1	ATS1 (ACYLTRANSFERASE 1)	n/a	n/a				
JCVI_8355	AT5G53450.1	ORG1	1.468	1.674	-0.122	-0.464	-0.696	-0.449
JCVI_4160	AT5G54160.1	ATOMT1 (O-METHYLTRANSFERASE 1)	0.729	0.184				
JCVI_20553	AT5G54250.1	ATCNGC4 (DEFENSE, NO DEATH 2)	-4.520	-4.599	-0.071	-2.199	-0.839	-2.580
JCVI_10019	AT5G54650.1	Fh5 (FORMIN HOMOLOGY5)	2.467	2.644	0.001	1.499	1.696	1.708
CD816074	AT5G55630.1	KCO1	n/a	n/a				
ES990089	AT5G56270.1	WRKY2	-1.091	-1.200	-0.033	-0.065	0.026	-0.406
EV157863	AT5G56290.1	PEX5	-1.979	-1.990				
EV165070	AT5G56360.1	calmodulin binding	-1.048	-0.074				
JCVI_14909	AT5G57030.1	LUT2 (LUTEIN DEFICIENT 2)	-0.162	2.487				
JCVI_38595	AT5G57050.1	ABI2 (ABA INSENSITIVE 2)	-0.990	-2.636	-0.326	-0.279	0.333	1.062
JCVI_31143	AT5G57580.1	calmodulin binding	0.914	1.128	-0.063	0.926	0.481	0.287
JCVI_13551	AT5G57740.1	XBAT32	1.577	2.210				
JCVI_34860	AT5G57800.1	WAX2	-5.385	-7.131				
EV046616	AT5G19130.1	GPI-anchor transamidase	0.458	0.531				
JCVI_41087	AT5G15150.1	ATHB-3 (A THALIANA HOMEBOX 3)	0.000	0.000	0.275	-0.472	0.654	0.332
JCVI_8536	AT5G17630.1	antiporter/ glucose transporter	-1.060	-0.691	0.009	0.089	0.105	0.169
JCVI_22771	AT5G17020.1	XPO1A	-0.557	-0.001	-0.172	0.026	0.379	0.501
ES980499	AT5G16830.1	SY2P1	0.575	-0.341	0.191	1.096	1.203	1.076

Figure 5.11 PAMP induced expression changes of candidate genes in the C9 QTL.

Expression is shown as fold induction compared to 0 hour, or water infiltrated controls. Colours indicate up regulation (orange-red) and down-regulation (green). Boxes indicate genes discussed in the text with consistent up or down regulation across multiple experiments and in both *B. napus* and *A. thaliana*.

5.3.3 Comparing Expression of all Genes between A12 and GD

Because mRNA seq was used to define the SNPs between A12 and GD, the expression of every gene within the QTL was also recorded. Any SNP between A12 and GD in an intron, promoter or epigenetic locus that has a significant effect on gene expression may be identified in this way.

Expression values for every unigene, expressed as reads per million to allow comparison between two different datasets, was aligned by unigene position and chromosome (Appendix 5). Within the expression dataset it became apparent there was usually stronger expression of most genes in the GD unigenes than the A12 ones. For example, more than 35,000 unigenes are more than 2 fold expressed in GD compared to A12, but only 4,198 are more than 2 fold expressed in A12 compared to GD (Appendix 8). This is a huge bias in the dataset, as given that the data was expressed as reads per million, the datasets should have been comparable. This is likely a result of comparing mRNA-seq from two different platforms. The GD mRNA seq was Illumina Hi-Seq2000 whereas the A12 expression set was GAIIX. Comparing expression statistics between mRNA-seq from different platforms is extremely problematic (Martin Trick, personal communication). Because of a longer read length and sequencing depth and coverage of the GD mRNA-seq, many problems arise in comparing it to A12. Accuracy of the alignment of reads to the pseudomolecules, sorting reads between homologous copies and the higher confidence in correct alignment due to greater sequencing depth and coverage means the GD sequence is of much higher quality. You can see the effect of this in the spreadsheet, where more genes have a “0” value for expression (meaning they were expressed less than 0.02 RPKM) in the A12 mRNA-seq than in GD (Appendix 5).

Because of the lack of consistency between the two datasets, a very high cut-off of was needed to identify genes with different expression patterns across C9. The full list of genes with more than ten-fold expression changes between A12 and GD can be found in Appendix 5. Amongst them there are no genes with clear roles in

defence amongst them, although with a such a high cut off point, a lack of sensible candidates is perhaps to be expected.

5.3.1 Obvious candidate genes for the flg22 triggered ROS burst did not have sequence or expression polymorphism in C9

There are many potential candidate genes that have been well characterised in defence that polymorphism within might immediately explain the low ROS phenotype. These include *RBOHD*, *FLS2*, *BAK1*, *BIK1* and *EIN2*. None of these genes are predicted to lie within the QTL, apart from *FLS2* which has close proximity to the marker pW233J1. The marker was the marker used to define the upper limit of the QTL, so it is not directly under the peak. No sequence polymorphism was observed in this line, and there was no difference in RPKM between A12 and GD (Appendix 5). We cannot rule out the possibility that an intronic SNP, or promoter polymorphism exists in the GD *FLS2* locus at present.

5.3.1 Adding KASPar Markers to A12 x GD

Using the SNP list of C9 between A12 and GD allowed the design of new KASPar markers. SNPs spread across C9, with a higher density of them within the middle of the QTL, were identified as potential new markers (fig 5.12). Although errors in the pseudomolecule assembly were suspected at this point, the additional markers that did map to C9 could potentially delineate the QTL further. Furthermore, markers that would not assemble into a viable map would provide further evidence of the errors in the C9 assembly, and indicate where the pseudomolecule is likely to be chimeric. 29 KASPar markers were originally designed (table 2), 26 of which worked in genotyping 56 of the A12xGD offspring (Appendix 5).

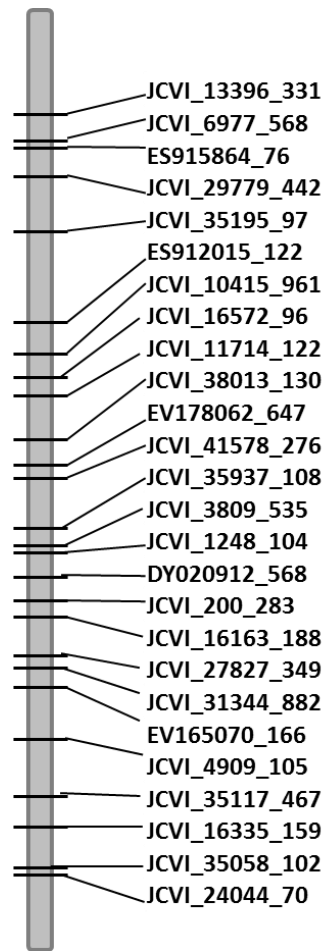


Figure 5.12 KASPar marker locations on the pseudomolecule assembly of C9

5.3.2 The New Map of C9

The new KASPar markers alongside the original Sebastian et al (2000) map were reassembled into a new integrated map in Joinmap 3.0. Of the 26 new SNP markers only 16 reassembled into the C9 linkage group (Appendix 5). The other 10 markers were ordered into different linkage groups across the genome. This was the second confirmation of errors in the pseudomolecule assembly. The predicted new map of C9 can be seen in table 18.

There is a high degree of colinearity between the original map markers and the newly produced of C9 (table 18, fig 2.1; 2.2; fig 5.8; fig 5.12). There are some minor changes in location, such as AC-STAE04 and pO125E1NP swapping position, but by and large there is a strong consensus of relative marker position. Only two markers have had significant rearrangement. The marker pW212J1 has been moved from within the original QTL position at 62.5 cM to 42cM. The marker pW233J1 is now located closer to the middle of our QTL, which is perhaps an improvement as its significance was very different from its neighbouring markers in its original position (fig 5.8, table 16).

Unfortunately, some of the markers added have not helped clarify the QTL due to a lack of recombination between them. The markers JCVI_16163_188 through EV165070_166 for example, are indistinguishable from each other genetically (table 18). In order to build a more reliable map, more offspring from the A12 X GD population will have to be genotyped. Although no seed was available at JIC, the wider A12xGD population seed held at the university of Warwick crop centre could help improve mapping resolution further. Furthermore more recombinants could be generated through producing more offspring of A12xGD, or backcrossing the A12 substitution lines into A12.

The markers identified as being within our QTL are largely intact and collinear in this new map. In addition to this, four new markers JCVI_29779_442, JCVI_40235_114, JCVI_13396_331 and JCVI_24044_70 have been added within the originally identified QTL. These new markers act to narrow the region we are

investigating and serve as an absolute reference within the pseudomolecule assembly.

Marker	cM	p
pN52E2	0	0.782
pN87E3NP	0.668	0.64
pR116E3	3.131	0.6995
AC-CTAE04	13.258	0.94
pO125E1NP	14.81	0.3759
pW137J1	21.811	0.1601
pW167E2	25.894	0.01438
pN101E2NM	26.878	0.02847
pW114E2	29.278	0.0548
AC-CTAE16	34.244	0.005743
pO119J1	36.806	0.005389
AC-CAGJ05	37.649	0.002931
pCFH8	39.226	0.01761
AC-CATE21	39.919	0.0007591
pN173E2	42.556	0.0001739
pW212J1	42.9	0.0000549
pO155E1	43.314	0.000215
pR115E1	43.324	0.000131
pW240E1	43.351	0.00008197
JCVI_16335_159	43.552	0.00004944
JCVI_35058_102	43.552	0.00004944
pN181E1	43.959	0.0003076
pR34E1	44.155	0.003233
pO127E1	44.415	0.0001027
AC-CACE04	44.793	0.001355
AC-CACE16	44.793	0.001355
AC-CTAJ08	44.793	0.001355
AC-CTAE02	44.793	0.001355
AA-CATE22	44.793	0.001355
AC-CAAE08	44.839	0.001321
JCVI_10415_961	44.842	0.0002262
JCVI_31344_882	44.851	0.0004166
JCVI_16163_188	44.867	0.00007428
JCVI_16572_96	44.867	0.00007428
JCVI_35195_97	44.867	0.00007428
EV165070_166	44.867	0.00007428
JCVI_27827_349	44.906	0.00008124
JCVI_4909_105	45.28	0.00004948
JCVI_35117_467	45.329	0.0002561
pN180E1	45.534	0.0001748
pO168J1	45.962	0.00002726
JCVI_29779_442	46.645	0.00007428
pN105E4NM	47.755	0.00001403
pW233J1	47.875	0.00009641
JCVI_40235_114	48.251	0.0000476
ES915864_76	48.251	0.0000476
JCVI_13396_331	48.487	0.0001781
pO145E1	49.204	0.00009174
pO106E3	49.987	0.0002349
JCVI_24044_70	52.67	0.000008619
pW106E1	53.651	0.00005305
pO160E1	53.891	0.00008954
pW155E1	56.039	0.00004049
pW195J1	56.299	0.00009905
pO111E2	59.884	0.03384
LEW6G7E2	61.631	0.0006279
pR64E1	61.876	0.001787
pO7E1	67.844	0.00106
pO118J1	68.012	0.0009219
pN47E4NM	71.187	0.006859
pW239E1	83.055	0.08678
pN3E1	84.47	0.1922
pW200J1	85.003	0.099

Table 18 New intergated map of C9 and single marker analysis for the flg22 -triggered oxidative burst

5.3.1 QTL Mapping using the New Integrated Map

The flg22 phenotypic data was remapped using the new integrated map of C9. Like before, a QTL was observed in the middle of C9 (fig 5.13). It might appear that the single peak has become two distinct peaks. This is difficult to be conclusive with as many of the markers between the peaks are AFLPs. These markers have many unknown genotyping values which may be biasing the data (Appendix 10). Nevertheless two RFLP markers with good genotyping coverage, pR34E1 and pO127E1, both have lower significance than the surrounding genes. This might be evidence for two distinct QTLs here, one at 42-43 cM, and one at 46-56cM. This is a very narrow interval however, and we do not have sufficient recombination within the population that has been genotyped at present to distinguish them.

5.3.2 Single Marker Analysis of flg22 ROS in the New Map of C9

As confidence in the new map was relatively low, single marker analysis was also chosen as a means of characterising the association between alleles and the flg22 ROS phenotyping scores. Like the QTL mapping we see two distinct peaks of significance, one in the marker pW240E1 and a larger one around the marker JCVI_24044_70 (table 18). The second QTL is the more significant of the two and contains many of the original significant markers.

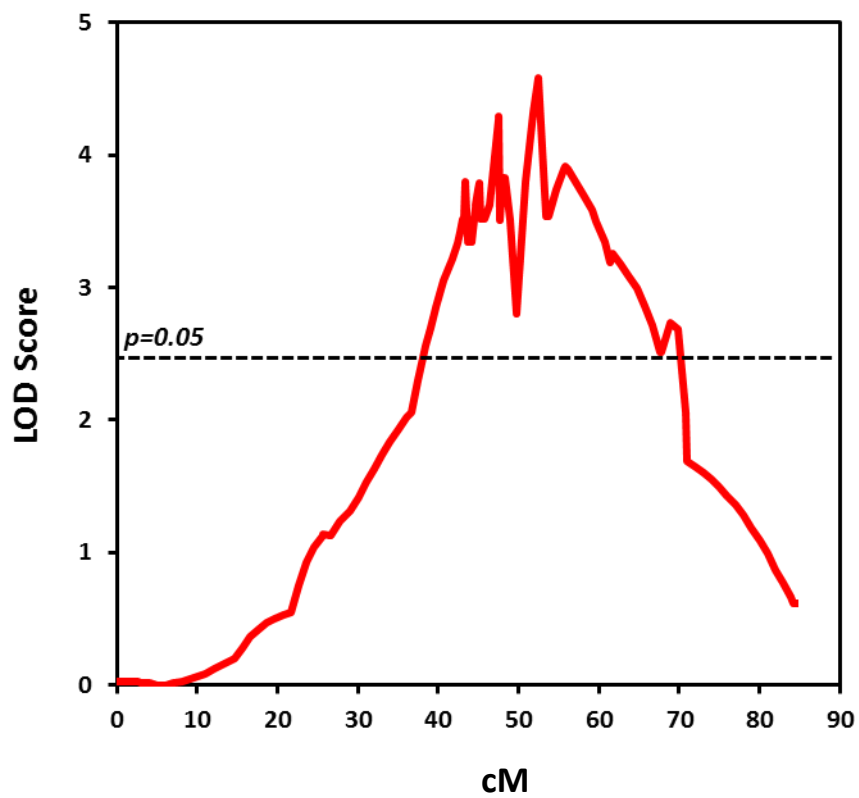


Figure 5.13 QTL on C9 of the flg22 triggered ROS burst using the new integrated map.

5.3.3 Establishing a new gene list

With additional markers added to the A12xGD cross it was hoped a narrower candidate list within the pseudomolecules could be generated. Aligning the genetic map of C9 with the pseudomolecules however was very difficult. Firstly, the middle of C9 in the pseudomolecules has no reference to the genetic map between JCVI_16572 and JCVI_16163 (fig 5.14). This was the same region that many of the RFLP markers BLASTED to seemingly random parts of the genome (fig 5.14). There appears to be an inversion of marker colinearity at the top of C9 between JCVI_40235 and JCVI_16572, although the order of the markers appears to be well maintained despite the inversion. The markers at the top and bottom of C9, and to a lesser extent the middle, appear to be co-linear between the genetic and physical map. A lack of recombination's between some of the new markers makes plotting there exact relative position difficult.

Errors might also exist within the genetic map. The map currently integrates AFLP, RFLP and SNP markers, which have been genotyped in different lines of the population, with the AFLP markers having particularly poor genotyping coverage. Only around 60 of the lines were available for flg22 ROS phenotyping and genotyping the SNP markers. The genetic map then could be improved substantially.

The original candidate list was generated between the markers pW233J1 and pW155E1. Within the pseudomolecules this represents a region between JCVI_27944 (21,352,333) and EE392341 (56,747,516), a distance of 35 mega base pairs. It is likely that the region between 31,204,288 and 43,306,831 is an error in pseudomolecule assembly.

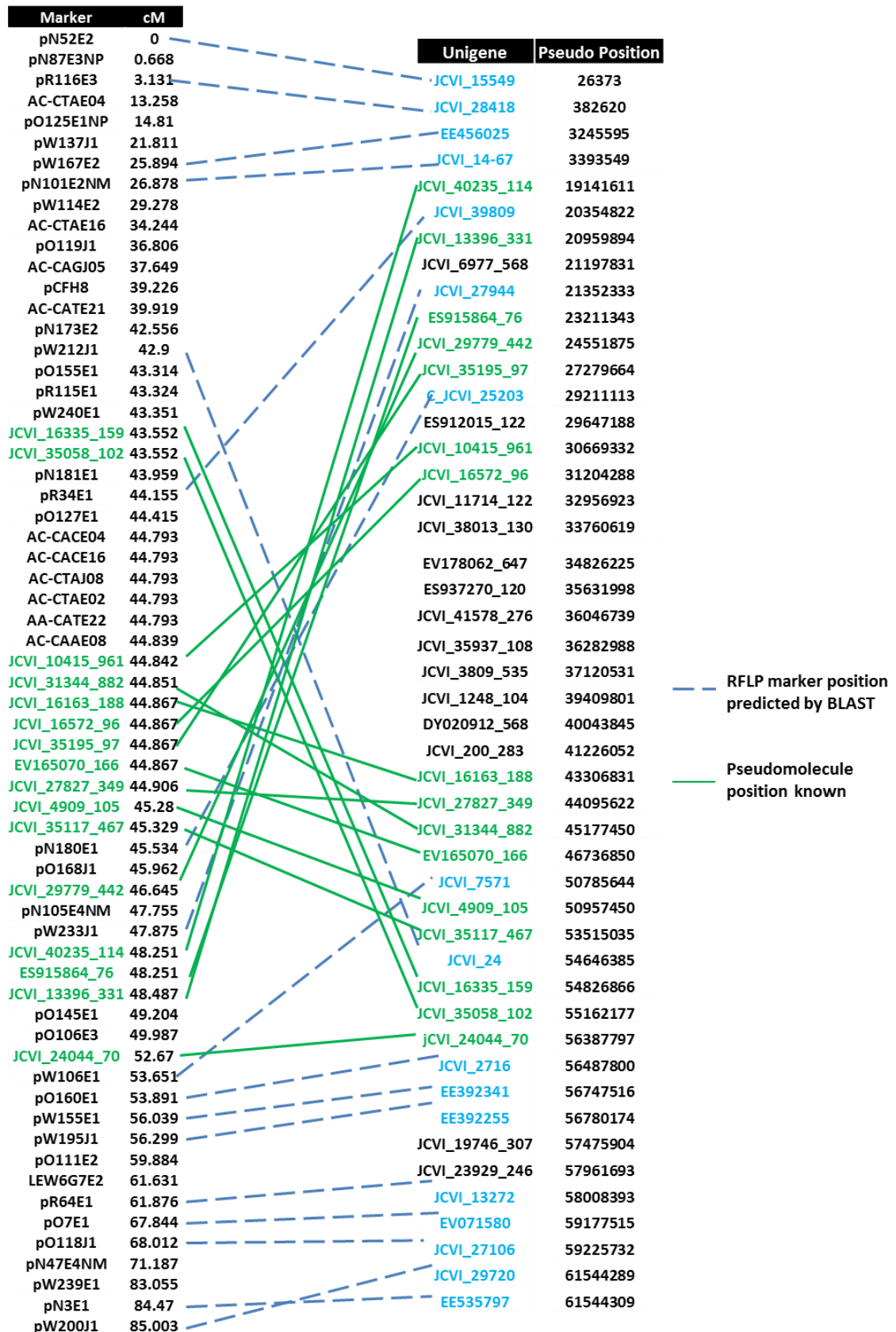


Figure 5.14 Position of the integrated genetic map markers in *Brassica oleracea* on the C9 pseudomolecule assembly of *B. napus*

Markers highlighted in green are KASPar markers which successfully integrated into the C9 *oleracea* map. Markers in blue are unigenes which are the likely genes that correspond to C9 map markers, after BLASTing marker sequence against the pseudomolecules.

5.3.4 DND2 is highly conserved between *A. thaliana* and *B. napus*, and GD has a number of potentially deleterious NS SNPS in the coding sequence

In the middle of the original candidate list is *DND2/CNGC4*. This is a strong candidate for a regulator of the flg22 triggered oxidative burst. Unigenes JCVI_20335 and JCVI_20553 overlap with Col-0 cDNA of *DND2*, with good coverage of the 3' and 5' ends of the gene (fig 5.15 A-B). There is a high conservation (>96%) of AA sequence between the *B. napus* unigene sequence, and the consensus A12 and GD reads (fig 5.15 A-B) for both unigenes. The alignment of both unigenes against full length *A. thaliana* can be seen in Appendix 13. There are a number of interesting NS SNPs across this gene. The most interesting is potentially at residue AtDND2 N89. The GD allele here substitutes asparagine for aspartic acid, a polar negative amino acid into a stretch of polar neutrals (fig 5.15, C).

The unigenes alone do not cover full length *DND2* cDNA sequence however, and as such a consensus full length sequence of A12 and GD was created using overlapping mRNA reads to bridge the gap (Appendix 13). No SNPs were predicted within this region.

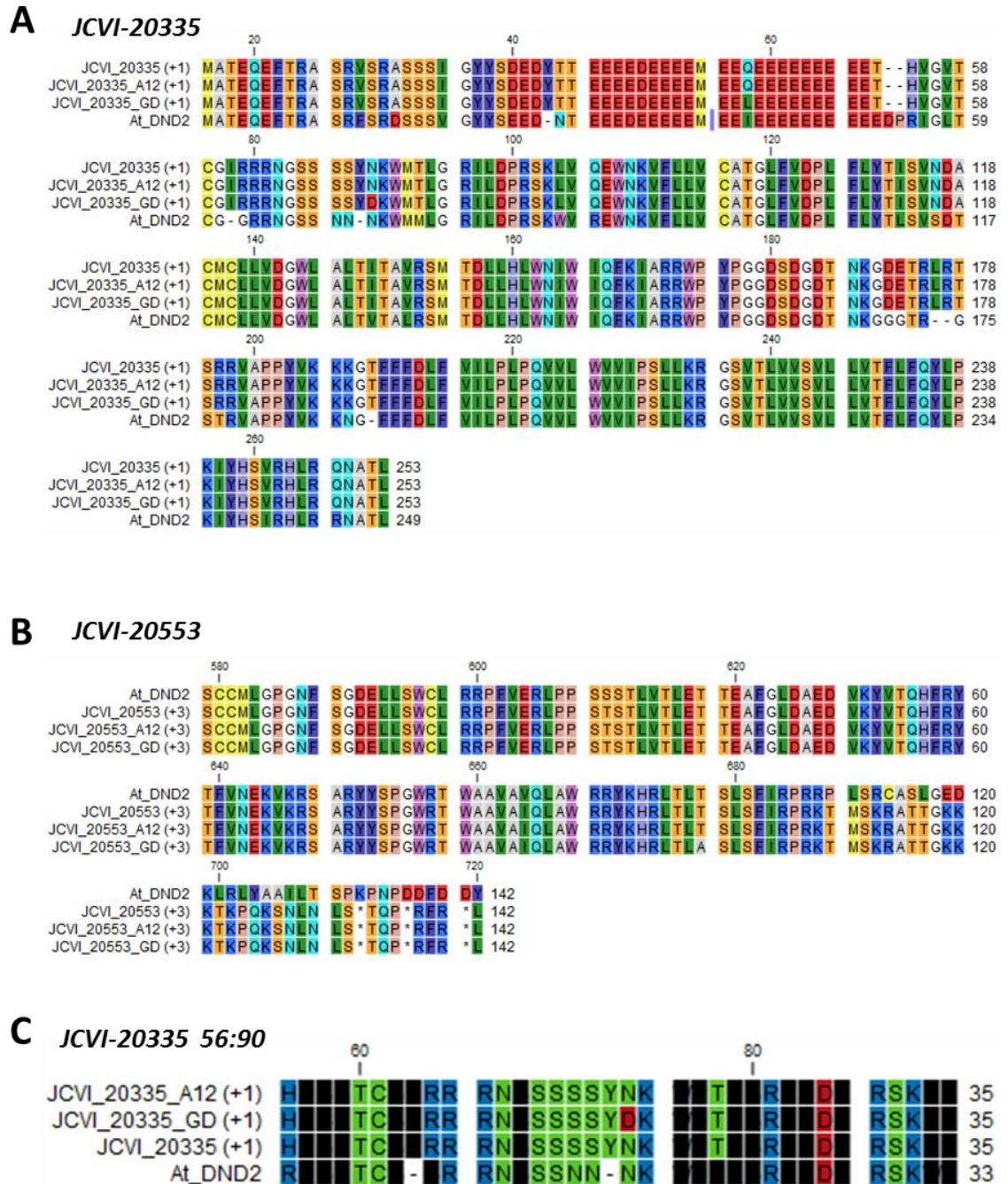


Figure 5.15 Alignment of *JCVI_20335* and *JCVI_20553* from the *B. napus* C genome consensus sequence, A12 and GD mRNA seq and *A. thaliana* DND2 cDNA.

A) Alignment in CLC genomics workbench version 7.3 of the unigene sequence of *JCVI_20335*. B) Alignment of *JCVI_20553*. C) Alignment of *JCVI_20335* showing charged and polar AA residues surrounding *At* DND2 N89.

5.4. Discussion

In this chapter variation in PAMP response and pathogen resistance within the A12xGD cross was explored. A significant QTL was identified on C9 regulating the flg22 oxidative burst. The QTL was significant, reproducible, and underpins the lack of flg22 ROS response found in the GD allele of this locus. The phenotype was confirmed in substitution lines, and perhaps unexpectedly, it is genetically separate from the previously identified *Agrobacterium tumefaciens* resistance QTL.

The initial plan to identify the genes underlying the QTL was to use mRNA seq to produce a candidate list and identify SNPs. This would be used to develop KASPar markers for fine mapping and defining a QTL within the pseudomolecule assembly. The phenotype of *A. thaliana* SALK insertion lines for each of the candidate genes within the QTL was planned as a means of narrowing down the candidates. Errors in pseudomolecule assembly and the relatively small population genotyped have limited the feasibility of this approach however.

mRNA seq of A12 and GD, aligned to the *B. napus* pseudomolecule assembly, was used as a means of generating a candidate list and the source of SNP data for fine mapping. This approach has a number of drawbacks. Firstly, as sequence information derived from mRNA seq is only covering exon sequence (and only then if the gene is expressed strongly enough to be identified) any intronic, promotor or epigenetic polymorphism is lost. Although expression of every gene in the QTL was measured, providing some indication of an intronic or regulatory allele effecting transcription, this approach does not cover all possible sources of underlying genetic polymorphism. Further to this, the unigenes do not exhaustively cover full length sequence of every gene in the QTL. As such a high number of SNPs within coding genes may be lost as a result of incomplete unigene coverage. This is a potential loss of a lot of genotypic variability that underpins the QTL.

Over the course of this project the *B. oleracea* C genome has not been released. The only reference available at present to align the reads from A12 and GD against

was a *B. napus* reference. Although assumed at the outset to be highly similar in chromosomal arrangement to *oleracea*, divergence between the two species may have contributed to the difficulty in moving from the genetic to physical maps. Errors within the pseudomolecule assembly also reduce the usefulness of this resource. Although chimeric regions in the pseudomolecules have been identified, a corrected version is not yet available.

Errors within the assembly have limited the fine mapping and the candidate list generation substantially. Nevertheless a candidate list, based around the markers that do have definite anchorage points in the unigene scaffold, has been produced. There are 285 genes with at least 1 non-synonymous AA change in the region delineated by the markers pW233J1 and pW155E1. The list contains many strong candidates for a novel regulator of the oxidative burst. The QTL at present represents too large a region for analysis of SALK lines for every candidate, and would require further mapping to delineate the QTL further.

The limited size of the available population would need to be improved to further map this QTL. Only 60 lines, from an initial population of 214, were available at the outset of the project, and these are the only lines that were genotyped with the KASPar markers. The lack of recombination's between them is limiting the resolution we can achieve with additional markers, particularly in the middle of C9. As such higher resolution might be achieved from phenotyping and genotyping the wider A12 x GD population, or by producing a new population through further backcrossing.

In this study, the QTL for *Agrobacterium tumefaciens* identified in 2004 has been transferred into the genetic map to produce a candidate list that included RESISTANCE TO AGROBACTERIUM TUMEFACIENS 4 (*RAT4*). This gene has previously been identified as a major determinant of *Agrobacterium* susceptibility in *A. thaliana* (Nam, 1999). It is a strong candidate to be the causative gene of this *B. oleracea* QTL. It was not within the scope of this project to prove this conclusively however.

At the outset of the work trying to characterise the low ROS and resistance of GD a loss of function in a positive regulator of PTI, or a gain of function in a negative one, was being searched for. In identifying potential candidates that can explain the GD low ROS and resistance phenotype, genes that fitted into a few categories were considered above any other. Any NS SNP within core constituents of early PTI signalling (such as *FLS2*, *BIK1* and *BAK1*) is a clear candidate, as any alteration in signalling throughput from the initial receptor complex could dramatically effect ROS production and downstream resistance. Much harder to define are any genes that indirectly effect the expression level of these core components. These include *WRKY* transcription factors for example, of which *WRKY2* is in the candidate list, but also more subtle changes in hormone signalling, such as the NS SNP in *AOS* and *XBAT32*. Variation in JA or BR that could perturb background *FLS2* expression indirectly for example. There is also the possibility that the machinery to produce H₂O₂ itself is impaired in GD, but the presence of a normal ROS burst at 1µM counteracts this somewhat (fig 5.1 B). Finally, the second branch of *NADPH* regulation in PTI comes from Ca²⁺ signalling, of which there many strong candidates in the gene list including Ca²⁺ ion binding proteins and the CNGC *DND2*.

As *DND2* was such a clear candidate after the initial candidate list was produced, genotyping and phenotyping of the SALK insertion line N319552 was carried out. This both served as a prototype for further analysis, and would allow functional testing of an obvious candidate gene. Preliminary analysis indicates that there is an flg22 ROS phenotype in the insertion line, with a gain of ROS observed (fig 5.16 A). This contradicts our observations between A12 and GD, with the GD allele resulting in lower ROS. The gain of ROS might be due its nature as a negative regulator of PTI, in which its possible GD has a gain of function mutation in a negative regulator to produce the low ROS observed (fig 5.1 A). However, the gain of ROS in the insertion could also be due to increased PAMP sensitivity through the pleiotropic effects *DND2* KOs have in regards to elevated SA, ET and JA mediated signalling previously reported (Ma, 2011; Chin, 2013).

There are a number of mysteries surrounding the defence no death phenotype. It is unknown if the effect of the *DND1/2* knockouts effect on resistance is a result of

being essential negative regulators of immunity, or if they are guarded by an unknown R gene. Furthermore, the absence of effector triggered HR but presence of spontaneous lesions in a background of elevated defence is not easily explained. It's possible that the two DNDs directly regulate HR, or that the induction of JA signalling in the KOs might suppress HR even with otherwise elevated defence signalling (Jurkowski, 2004).

A functional loss of DND2 in *B. oleracea* might not have the same pleiotropy observed in *A. thaliana*. As a polyploid we expect multiple copies of each *A. thaliana* gene, and there two different loci in the C genome which correspond to DND2 (Appendix 1). A deleterious mutation in one of them may decrease abundance of functional DND2 without triggering the elevated defence seen in *Arabdiopsis*. Any role CNGC2 has in regulating Ca²⁺ influx, or associated Na⁺ or K⁺ efflux, might then be more readily observable. It may also be the case that CNGC2/4 are not guarded in *B. oleracea*. Alternatively, the SNPs we have seen between A12 and GD may affect function of the gene in regards to PTI signalling without drastically altering the macrostructure of the protein or expression of the gene, as seen in SALK insertion lines or the premature stop codon in the commonly studied DND2-1 background (Jurkowski, 2004). If the GD allele of the gene is inhibiting its function as an ion channel without triggering the kind of defence responses seen in *A. thaliana*, it could be a valuable resource for functional studies of the DND genes.

Only a very preliminary study of CNGC2 function in A12 and GD has been carried out so far. It is philosophically an interesting candidate, but more work is required to confirm the effects of the A12 and GD snps. Expression of DND2 from A12 and GD in a DND2 KO background in *A. thaliana* is the logical next step. *B. rapa* or *B. napus* TILLING mutants in DND2 may help in confirm a phenotype in a brassica background, but might potentially suffer from the same pleiotropic effects seen in the DND2-1 line.

As new technologies are rapidly being adopted for high throughput genome analysis it is important not to neglect the wealth of QTL mapping resources that have previously been generated. In this chapter, mRNA sequencing was used within

a QTL mapping population to make the jump from QTLs to candidate genes within a wide genomic region. This has been largely successful despite errors in the assembly of the only viable reference scaffold at present. As many markers for partial resistance have been identified previously, it is important to then to bring these QTL into modern science through sequencing platforms such as Illumina Hi-Seq. The approach presented here could rapidly identify the genes behind a wide array of phenotypic traits in crop plants.

Chapter 6 : General Discussion

Understanding the molecular basis for what is alternately, and often indiscriminately, described as partial, quantitative, polygenic or horizontal resistance in the field is essential. This is particularly relevant to *Brassica* breeding, where the breakdown of strain-specific resistance genes, including *Rlm1* which was overcome within three years of deployment, have resulted in epidemics (Sprague, 2006). If the background level of resistance behind the R gene is limited, once an attacking pathogen has changed its effector repertoire, or modified any recognised protein, the commercial viability of the line is lost.

Although R-gene mediated resistance is highly effective at controlling disease in the short term, there is a need to supplement this with durable resistance effective against multiple pathogen strains which can still limit pathogen spread in the absence of a specific R gene. Brun et al (2009) suggest that quantitative resistance can even extend the duration of effective qualitative resistance, as demonstrated in the extension of *Rlm6* mediated resistance in *B. napus* by over two years. Durable quantitative resistance has been observed in field grown brassicas, with the variety 'Jet neuf' maintaining effective resistance for over twenty years before higher yielding varieties were introduced (Delourme, 2006; Fitt, 2006.).

PTI is a likely major determinant of quantitative resistance, but understanding PTI within crop species is only in its infancy. The expression of heterologous PRRs in crops has demonstrated great potential for disease control (Lacombe, 2010). Outside of a transgenic approach however, there is a need to identify natural variation in PTI, and to exploit this in breeding programs. The research presented within this thesis had the objective of developing the tools to investigate PTI within brassica species, to investigate natural variation in PAMP responses between diverse brassica lines and to investigate the role of PTI in susceptibility of the *B. oleracea* lines GD and AG1012.

6.1. Key questions addressed in this thesis

Several key questions were outlined at the start, and how these have been addressed are detailed below.

1. Can methods to study PTI in *A.thaliana* be used in *B. napus*?

To address this question a range of methods routinely seen in *A. thaliana* research, and some created here were tested in *B. napus*. The assays covered a very wide range of responses, including early molecular events like the ROS burst, MAPK phosphorylation, cell wall modifications including callose and lignin deposition, PAMP-induced gene expression changes and metabolome changes. The assays dissect the molecular immune response from early recognition events to PAMP-induced resistance. As such this objective has largely been met, and the assays presented here could have wide applicability amongst *B. napus* researchers in the near future.

There are still many assays that could be developed here. Of particular note are Ca²⁺ influx and ethylene biosynthesis. Ca²⁺ influx is an essential upstream component of PTI (Segonzac, 2011). Assaying PAMP responsive Ca²⁺ changes however requires the creation of reporter lines, commonly lines expressing aequorin. These were not available during the course of this project. As many genes involving Ca²⁺ homeostasis have been identified in chapter five within the *B. oleracea* QTL these might be a valuable resource in further characterising the QTL. Ethylene biosynthesis is a classic PAMP response assays seen in *A. thaliana* (Felix, 1999). No reliable method of recording ethylene was found during this project however.

The range of PAMPs and pathogens used here could be readily expanded in the future. Peptidoglycan and oligogalacturonides could be easily screened in *B. napus* as well as different preparations of chitin or chitosan. The two main pathogens used in this study, *P. syringae* and *B. cinerea* are only very minor problems in field production of *B. napus*. They have been selected here because of their utility as model organisms in the lab. In order for this work to have more widespread impact

within the breeding community it is necessary to demonstrate the role PTI or PAMP responses play in resistance to pathogens which are problematic in the field. One of the essential questions that could be addressed in the near future is the extent PTI plays in resistance to major *Brassica* pathogens like *L. maculans*. The pathogen presents many difficulties within a lab environment, having a long infection cycle with multiple different life cycle stages in multiple different tissues (Fitt, 2006). PAMP-induced resistance to major *Brassica* pathogens like *L. maculans* is an unknown that has not been addressed in this thesis and a clear target for future work.

The transfer of techniques from a model system into *B. napus* has been largely successful. Perhaps the biggest flaw in the pathology methods developed here is the use of model pathogens, in a crop system. Developing the tools to investigate PAMP-responses, and their role in resistance to key pathogens of *B. napus*, are the next essential steps.

2. What is the transcriptional response to PAMPs in *B. napus*?

In order to understand the transcriptional changes induced by PAMPs in *B. napus* two approaches were taken. The first was qRT-PCR of several early induced genes known to be up regulated at early time points in response to *S. sclerotiorum* infection (Zhao, 2008). BnMAPK3, BnMAPK4 and BnWRKY33 were all effectively up regulated by PAMPs at 1 and 3 hours post treatment. The level of induction was not huge however, and many marker genes for PAMP responsiveness in other systems are much more heavily induced by PAMPs including *FRK1*, *At2g17700* and *NHL10* in *A. thaliana* (Albrecht, 2012; Lozano-Duran, 2013).

The second approach to understand the PAMP-induced transcriptional response of *B. napus* was more extensive, using mRNA-seq to capture genome-wide expression changes throughout both the A and C *Brassica* genomes. This produced an extensive list of genes that were up or down regulated by PAMP treatment, with 25% of the genome seeing more than 4 fold up or down regulation. Some of these genes were very strongly expressed upon PAMP treatment, including *NRT2* and

WRKY28. Testing their responsiveness and reliability as marker genes for qPCR is an essential next step. The expression profiles of these putative marker genes need to be studied further under a wider range of time points and PAMP / pathogen treatments.

The mRNA seq data took the *B. napus* unigene models developed by Bancroft et al (2010) as the reference to assemble the reads too. At the time of writing this was the most complete assembly of *Brassicacae* we could have used. It does however have many disadvantages, including lack of coverage of the central regions of many large genes, resulting in alignments requiring a prediction pipeline based on assumed sequence. As such this might be a source of error when counting the reads aligning to each unigene. As Brassica genome sequencing becomes more advanced it would be better to align the mRNA-seq to the actual genome, a clear next step for future work.

We took the approach of annotating the mRNA-seq data using *A. thaliana* TAIR gene identifiers. In effect we annotated over 90% of the genes that we had sufficient coverage of to be included in the analysis. There are likely to be many instances of mis-annotation, a result of the low stringency genome to genome BLAST performed and problems arising from multiple homeologous copies of each gene within *B. napus*. Care must also be taken that a similar function is not assumed for homologous genes between the two species, as in some cases sequence identity alone could not predict functional homology (Liang, 2013). Nevertheless, the annotation of the *B. napus* unigenes did allow for further functional analysis of the gene expression changes we observed, including identifying the signalling pathways up and down regulated and the predicted localisation of PAMP-responsive genes. The transcriptional changes observed here very closely mirror the changes seen in *A. thaliana* and even rice (Akimoto-Tomiya et al. 2003; Navarro et al., 2004;), suggesting some degree of reliability in the data set as a whole.

The use of whole genome mRNA sequencing then has been an effective method to capture PAMP induced transcriptional changes in *B. napus*. Further to this the

analysis was extended to look at the expression pattern of homologous copies of the gene between the A and C genomes. How polyploidy organisms coordinate a complex transcriptional response is currently unclear. Here we have shown that most homologous pairs responded to a similar extent between the A and C genomes of *B. napus*, but that around 10% of them had no clear similarity of expression pattern. This is an interesting finding. It might potentially indicate that there is strong conservation of the promoter regions upstream of heterologous copies of a gene, and potentially that in response to an external stimuli like flg22 there is only very limited dominance of one genome over another, although neither of these possibilities are explored further here. PAMP-induced expression changes might be a great model system for investigating transcriptional regulation in *B. napus* because of the high selection pressures on PRRs (Monaghan, 2012) and the potential benefit of diversification of PAMP recognition domains between redundant homeologous copies. It would also be interesting to investigate the handful of genes that show opposing levels of expression between homologs, although many of these may be false positives as a result of extremely low basal expression.

It is important to recognise the technical limitations within the dataset presented here, including the use of pseudomolecules as a scaffold, the risk of mis-annotation and difficulties of sorting genes between homologous copies all likely to result in some degree of error. There are also limitations regarding the PAMPs and time points adopted. Samples were taken at one and three hours post PAMP treatment, in line with previous studies in *A. thaliana* (Navarro, 2004). This is a very limited snapshot of the transcriptional changes flg22 could induce. How *B. napus* responds to PAMPs over a longer time period is still unknown. As many pathogen interactions are continuous over a period of days or weeks, understanding how PAMPs can induce prolonged transcriptional reprogramming is one potential goal for the future.

Only the flg22 induced transcriptome has been recorded here, and then only at a single concentration, a saturating 1 μ M. This is potentially significantly higher than any feasible concentration of the elicitor within a natural infection. Furthermore, in

a natural infection multiple PAMPs are likely to be present, requiring the study of multiple PAMPs, or potentially PAMP combinations. It would be interesting to see a comparison of flg22 and pathogen-induced transcriptional changes within *B. napus*. The overlap or lack of, between pathogen and PAMP-induced genes might indicate the importance of PAMP perception in co-ordinating a transcriptional response to infection.

The expression dataset as it is presented here can also be used for further analyses. The observation that the PRRs *FLS2*, *EFR* and *CERK1* are all similarly up-regulated while *BRI1* is not (fig 3.16) might be used to identify other novel PRRs. Any LRR-RLK or LYS-M RLK showing a similar expression pattern to these PRRs could be identified and studied further.

The flg22 induced transcriptome presented here has gone a long way to addressing the question of what the transcriptional response to PAMPs is in *B. napus*. There are still some technical limitations in the methods used, and limitations on the number of PAMPs and time points adopted, but the dataset is likely to be valuable to many researchers in the immediate future. It acts as a strong reference for comparative studies, both between different treatments and between different species and it does represent the first genome wide assessment of PAMP responsive genes in *B. napus*.

3. Are PAMP responses polymorphic between genotypes of *B. napus*?

The variation in PAMP responsiveness between cultivars has been demonstrated in all three results chapters presented here. Significant variation between genotypes has been observed within three separate populations. The OREGIN diversity set used in chapter 3 consisted of field grown *B. napus*. Up to 20 fold differences were observed in ROS production in response to flg22, elf18 and CSC (fig 3.22). Interestingly the strength of the ROS response to one PAMP did not predicted responsiveness to any other PAMP, suggesting that responsiveness to different PAMPs may be genetically separate. Within two members of the OREGIN diversity set was also observed significant variation in callose deposition (fig 3.6).

The number of lines that were phenotyped were greatly expanded in chapter 4, in which the flg22 and elf18 triggered oxidative bursts were scored in 84 different *B. napus* accessions from diverse backgrounds representing seven different crop types (fig 4.1 and 4.5). Huge variation did exist between lines here, and this variation was consistently observed across multiple phenotyping repeats.

In chapter 5 the flg22 and elf18 triggered oxidative burst was scored in the A12xGD *B. oleracea* mapping population. Transgressive segregation was observed for these traits (fig 5.3), and even in this group of related lines significant variation existed. Having a high response to one PAMP did not necessarily co-segregate with a high response to the other in this population, again suggesting the regulation of the ROS burst to different PAMPs is genetically separate.

The observation that PAMP-responsiveness is polymorphic amongst different Brassica varieties is exciting for a number of reasons. First of all, variation of PAMP responses amongst different ecotypes has not been studied on this scale before, even in *Arabidopsis*. Secondly the variation observed in PAMP responses suggests traits like the oxidative burst could be used for population genetics studies including GWAS, and could be mapped using QTL mapping. It also raises the question of the connections between PAMP responsiveness and resistance, and whether one could predict the other.

Very clear phenotypic variability in the ROS responses of *B. napus* has been reported here. It might be possible to address this question further by looking at diversity in many different PAMP responses. For example, seedling growth inhibition was used on a diverse population of Brassicacea (Vetter, 2012), and marker gene induction has been scored in soybean (Valdez-lopez, 2012). Expanding the phenotyping of diverse accessions to include multiple PAMP response assays might be an avenue for future work.

4. Can PAMP responses predict disease resistance scores in a population of *B. napus*?

In the work presented here no evidence has been found that the oxidative burst in response to flg22 or elf18 can predict resistance to *P. syringae* or *B. cinerea*. When correlating the phenotypes of 86 lines of the association mapping panel, there was no correlation between either ROS burst and the two different pathogens (fig 4.14). Further to this, no correlation existed between ROS burst and pathogen resistance in the A12 x GD population.

This is perhaps to be expected to some extent. In terms of *Botrytis* resistance we expect no correlation, as the pathogen does not possess either flagellin or EFTU. Responses to any one PAMP are a massive simplification of any plant-pathogen interaction. Many more 'danger signals' are being perceived by the host, including numerous PAMPs, the pathogen is actively subverting defences (even in the absence of a TTSS we expect some degree of effector triggered susceptibility), the structural integrity of the tissues are changing, the plant is continuing growth and development and the environment around the plant pathogen interaction is constantly shifting. Real plant-pathogen interactions are significantly more complicated than can be summarised by the perception of a single PAMP.

It is also the case that the oxidative burst is an early signalling event and one small part of a much larger series of responses that constitute resistance. Variation is likely to exist at all levels of the PAMP and pathogen response. For example lines with a low oxidative burst may have significantly greater callose deposition, or stronger and faster defence gene induction, and could have better resistance than a line with high ROS, but deficiencies in other aspects of signalling. Predicting the overall phenotype of a complex trait from one very small component of it is going to be flawed.

It might also be that PAMP responsiveness as a whole is not a major determinant of resistance to these pathogens. Although several studies have highlighted the importance of PTI in resistance against pathogens in *A. thaliana*, most of these focus on a single genotype, col-0 and few strains of adapted and non-adapted *P.*

syringae (eg Zipfel, 2004). Outside of the model system, and outside of a controlled lab environment, the importance of PTI in resistance to more diverse pathogens is still largely unknown. Part of the zig-zag model would predict that in order to be pathogenic a pathogen must be able to suppress PTI (Segonzac, 2011). If this model is taken literally, it means all pathogens that can grow naturally on a plant already have the means to suppress PTI in the first place. This does raise the question of the usefulness of further enhancing PTI within a crop. The model should not be taken literally however, and in reality PTI represents a quantitative reduction in the growth of a pathogen as opposed to an 'on-off switch'.

The biggest shortfall in addressing the question of if PAMP response can predict pathogen resistance is how only a single PAMP response, the oxidative burst, has been looked at. Ideally, the association mapping panel could be phenotyped for a wide range of PAMP responses. Callose deposition, lignification, seedling growth inhibition and induced resistance are all relatively high-throughput and could be screened. After doing this the phenotypes of each successive PAMP response could be correlated to see if some responses group together and if some are more genetically distinct.

Within the data presented here no correlation was observed between ROS and resistance. This is only one small part of the question of whether PAMP responses can explain field resistance, and a substantial amount of work remains to be done before this question can be answered more thoroughly.

5. Can genes regulating PAMP-responses and disease resistance within *Brassica napus* populations be identified using a GWAS approach?

To assess this question, flg22 and elf18 triggered ROS, along with *P. syringae* and *B. cinerea* resistance were phenotyped in 84 lines of an association mapping panel. Even with a relatively small panel of lines many significant associations were identified in the population for both SNP and GEM markers. This was a successful proof of concept that highly polymorphic traits such as PAMP responses and resistance can be mapped effectively using GWAS in *B. napus*.

A lot of potential improvements could still be made regarding the population however. Successful GWAS require large population sizes, good SNP density and read depth and phenotypic variability. The phenotypic variability observed here has been very good, but both the number of lines and the quality of the sequence and expression that we have for them could be improved substantially. Population size is a major limiting factor here, as it reduces the power of the GWAS and forces a very high allelism threshold. This limits the number of genes that could be associated to the point that major components of PTI including EFR, BAK1 and RBOHD are not included as potential markers. The population itself will be expanded over the coming years, addressing this major issue. The second problem regards the quality of the mRNA data we have for the lines. The population was originally sequenced using 80bp reads which may be less effective than modern methods. Using longer reads, for example, limits the problem of ambiguous callings between homeologues due to a higher chance of a loci-specific SNP being present in any given read.

Despite the potential for improvement in the association mapping process itself, we have still found many meaningful and significant associations for each of the traits phenotyped here. As an initial proof of concept study, it is very promising. As such the question of whether PAMP responses and resistance can be used in a GWAS study in *B. napus* has been well addressed here, with the caveat that improvements could be made.

Much future work could spin out of this work. Within the SNP and GEM clusters identified it's essential that a full list of genes within the underlying genomic region be characterised. As the clustering occurred for GEM markers as well it's possible that there are islands of similarly transcribed genes, possibly part of a gene family, that are regulating PAMP responses. These regions would be of particular note to breeders that may get multiple beneficial SNPs / GEMs from introgressing a distinct region, as opposed to selecting for a small effect from individual SNPs. The dataset could be used in the future to identify the parents of potential mapping populations. Furthermore within the dataset are many SNPs within many important genes that could assist in future studies, and where the SNPs have already been

associated with a trait of interest this could help narrow down the selection of interesting alleles further.

The population can be used for surveying multiple defence traits in the future. Chitin triggered ROS could be correlated with *Botrytis cinerea* resistance, PAMP-induced lignification, seedling growth inhibition and resistance to *Sclerotinia sclerotiorum* or *L. maculans* are other phenotypes that could be added to the GWAS.

With an expanding population the statistical power available for these studies increases, as does the number of potential SNP markers. What is presented here is just the pilot study, and it has been a successful proof of concept. With an improving population the effectiveness and usefulness of GWAS studies in the population are only likely to improve in the future.

6. Is the susceptibility of the *B. oleracea* line AG1012 and its parent GD a result of an impairment in PTI?

The final part of the research here was to move closer to understanding the low resistance phenotype observed in *B. oleracea* variety GD, and its offspring AG1012 which is impaired in resistance to *Agrobacterium tumefaciens*. We set out to determine if the susceptibility was a result of impairment in PTI.

Unexpectedly the QTL for *Agrobacterium* resistance did not overlap with one for the oxidative burst. This suggests that the two traits are genetically separate. Although we cannot be conclusive that they are not caused by the same gene, as both QTLs are relatively wide, the peaks do not overlap.

The flg22 ROS QTL identified was on chromosome C9, was significant and is likely to represent a major determinant of the oxidative burst within this population. To identify the underlying polymorphism, QTL mapping and then fine mapping was progressed within the population to limited success. Using the *B. napus* pseudomolecule assembly as the reference for KASPar marker design was

ultimately flawed, with only 16 out of 28 markers actually assembled into C9 in the *B. oleracea* linkage map.

Using the new integrated map of C9 taking into account AFLP, RFLP and KASPar markers did allow some degree of fine mapping to occur which did improve the QTL identified (fig 5.13). It is essential however that more recombinants are identified with this region. At present no further resolution has been added between four of the markers because of a lack of recombination events (fig 5.11). This will require genotyping and phenotyping more lines from the original population, crossing A12 and GD to produce more lines or backcrossing from a substitution lines into A12 to try and break apart a GD C9 introgression further. These would be requirements to reduce the currently very large candidate list further.

Despite problems with the pseudomolecule reference in the middle of C9 and a lack of recombination events within the QTL limiting the fine mapping, a candidate list was generated for this QTL, of which there are many strong candidates. Further fine mapping of the QTL and analysis of the A12 and GD alleles of this gene are the immediate goals of any follow on work from this project.

6.2. Summary of key findings

1) Methods to study PAMP responses can be successfully used to measure PAMP responses in *B. napus*. A wide range of assays have been developed and the assays described here could have wide applicability in future *B. napus* research.

2) The transcriptional response to flg22 in *B. napus* is extensive, and mirrors closely the broad expression changes observed in *A. thaliana*. The transcriptional response is similar for homologous copies of the gene between the A and C genomes.

3) PAMP responses are highly polymorphic amongst populations of *B. napus* and *B. oleracea*. The oxidative burst is amenable to both QTL and association genetics studies.

4) The magnitude of the oxidative burst does not predict resistance to *B. cinerea* or *P. syringae* in *B. napus*.

5) Genome-wide association studies in *B. napus* can be used to identify the underlying genetic loci responsible for highly polymorphic PAMP responses and disease resistance. Associative transcriptomics can identify SNPs and GEMs giving rise to variation in resistance phenotypes in *B. napus*.

6) A major QTL for the flg22-triggered oxidative burst is present in the middle of C9 in the A12xGD *B. oleracea* mapping population.

The research presented in this thesis increases our knowledge of, and ability to characterise, PTI within brassica populations. The research demonstrates the potential of GWAS to identify defence linked genes and shows how mRNA-seq can be used to delineate and explore QTLs. These approaches are likely to be commonplace in the coming years, and the kinds of studies presented within this thesis might represent the future of brassica research and pre-breeding.

Bibliography

Adams-Phillips, L., Briggs, A.G., and Bent, A.F. Disruption of Poly(ADP-ribosyl)ation Mechanisms Alters Responses of *A. thaliana* to Biotic Stress. *Plant Physiology* 152, 267-280.

Aghnoum, R., Marcel, T.C., Johrde, A., Pecchioni, N., Schweizer, P., and Niks, R.E. (2010). Basal Host Resistance of Barley to Powdery Mildew: Connecting Quantitative Trait Loci and Candidate Genes. *Mol. Plant-Microbe Interact.* 23, 91-102.

Akimoto-Tomiyama, C., Sakata, K., Yazaki, J., Nakamura, K., Fujii, F., Shimbo, K., Yamamoto, K., Sasaki, T., Kishimoto, N., Kikuchi, S., et al. (2003). Rice gene expression in response to <i>N</i>-acetylchitooligosaccharide elicitor: comprehensive analysis by DNA microarray with randomly selected ESTs. *Plant Mol.Biol.* 52, 537-551.

Albert, M., Jehle, A.K., Mueller, K., Eisele, C., Lipschis, M., and Felix, G. (2010). *Arabidopsis thaliana* Pattern Recognition Receptors for Bacterial Elongation Factor Tu and Flagellin Can Be Combined to Form Functional Chimeric Receptors. *J. Biol. Chem.* 285, 19035-19042.

Albrecht, C., Boutrot, F., Segonzac, C., Schwessinger, B., Gimenez-Ibanez, S., Chinchilla, D., Rathjen, J.P., de Vries, S.C., and Zipfel, C. (2012). Brassinosteroids inhibit pathogen-associated molecular pattern-triggered immune signaling independent of the receptor kinase BAK1. *Proceedings of the National Academy of Sciences* 109, 303-308.

Ali, R., Ma, W., Lemtiri-Chlieh, F., Tsaltas, D., Leng, Q., von Bodman, S., and Berkowitz, G.A. (2007). Death Don't Have No Mercy and Neither Does Calcium: *Arabidopsis* CYCLIC NUCLEOTIDE GATED CHANNEL2 and Innate Immunity. *The Plant Cell Online* 19, 1081-1095.

Atwell, S., Huang, Y.S., Vilhjalmsson, B.J., Willems, G., Horton, M., Li, Y., Meng, D., Platt, A., Tarone, A.M., Hu, T.T., et al. (2010). Genome-wide association study of 107 phenotypes in *Arabidopsis thaliana* inbred lines. *Nature* 465, 627-631.

Aubertot, J.N., West, J.S., Bousset-Vaslin, L., Salam, M.U., Barbetti, M.J., Diggle, A.J., Fitt, B.D.L., Evans, N., Howlett, B.J., and Cooke, B.M. (2006). Improved resistance management for durable disease control: A case study of phoma stem canker of oilseed rape (*Brassica napus*)

Sustainable strategies for managing *Brassica napus* (oilseed rape) resistance to *Leptosphaeria maculans* (phoma stem canker). (Springer Netherlands), pp. 91-106.

Bancroft, I., Morgan, C., Fraser, F., Higgins, J., Wells, R., Clissold, L., Baker, D., Long, Y., Meng, J., and Wang, X. (2011). Dissecting the genome of the polyploid crop oilseed rape by transcriptome sequencing. *Nat Biotechnol* 29, 762 - 766.

Bancroft, I., Morgan, C., Fraser, F., Higgins, J., Wells, R., Clissold, L., Baker, D., Long, Y., Meng, J., Wang, X., et al. Dissecting the genome of the polyploid crop oilseed rape by transcriptome sequencing. *Nat Biotech* 29, 762-766.

Bohuon, E.J.R., Keith, D.J., Parkin, I.A.P., Sharpe, A.G., and Lydiate, D.J. (1996). . *Theor. Appl. Genet.* 93, 833-839.

Boller, T., and Felix, G. (2009). A Renaissance of Elicitors: Perception of Microbe-Associated Molecular Patterns and Danger Signals by Pattern-Recognition Receptors. *Annu. Rev. Plant Biol.* 60, 379-406.

Bolton, M.D., van Esse, H.P., Vossen, J.H., de Jonge, R., Stergiopoulos, I., Stulemeijer, I.J.E., van den Berg, G.C.M., Borrás-Hidalgo, O., Dekker, H.L., de Koster, C.G., et al. (2008). The novel *Cladosporium fulvum* lysin motif effector Ecp6 is a virulence factor with orthologues in other fungal species. *Mol. Microbiol.* 69, 119-136.

Boudsocq, M., Willmann, M.R., McCormack, M., Lee, H., Shan, L., He, P., Bush, J., Cheng, S.H., and Sheen, J. (2010). Differential innate immune signalling via Ca²⁺ sensor protein kinases. *Nature* 464, 418-422.

Boutrot, F., Segonzac, C., Chang, K.N., Qiao, H., Ecker, J.R., Zipfel, C., and Rathjen, J.P. (2010). Direct transcriptional control of the Arabidopsis immune receptor FLS2 by the ethylene-dependent transcription factors EIN3 and EIL1. *Proceedings of the National Academy of Sciences* 107, 14502-14507.

Bradbury, P.J., Zhang, Z., Kroon, D.E., Casstevens, T.M., Ramdoss, Y., and Buckler, E.S. (2007). TASSEL: software for association mapping of complex traits in diverse samples. *Bioinformatics* 23, 2633-2635.

Brun, H., Chevre, A.M., Fitt, B.D.L., Powers, S., Besnard, A.L., Ermel, M., Huteau, V., Marquer, B., Eber, F., Renard, M., et al (2009). Quantitative resistance increases the durability of qualitative resistance to *Leptosphaeria maculans* in *Brassica napus*. *New Phytol.* 185, 285-299.

Chapman, S.J., and Hill, A.V.S. (2012). Human genetic susceptibility to infectious disease. *Nat Rev Genet* 13, 175-188.

Chin, K., DeFalco, T.A., Moeder, W., and Yoshioka, K. (2013). The Arabidopsis Cyclic Nucleotide-Gated Ion Channels AtCNGC2 and AtCNGC4 Work in the Same Signaling Pathway to Regulate Pathogen Defense and Floral Transition. *Plant Physiology* 163, 611-624.

Chisholm, S.T., Coaker, G., Day, B., and Staskawicz, B.J. (2006). Host-microbe interactions: Shaping the evolution of the plant immune response. *Cell* 124, 803-814.

Clough, S., Fengler, K., Yu, I., Lippok, B., Smith, R., and Bent, A. (2000). The Arabidopsis *dnd1* "defense, no death" gene encodes a mutated cyclic nucleotide-gated ion channel. *Proc Natl Acad Sci USA* 97, 9323 - 9328.

Cockram, J., White, J., Zuluaga, D.L., Smith, D., Comadran, J., Macaulay, M., Luo, Z., Kearsley, M.J., Werner, P., Harrap, D., et al. (2010). Genome-wide association

mapping to candidate polymorphism resolution in the unsequenced barley genome. *Proceedings of the National Academy of Sciences* 107, 21611-21616.

de Jonge, R., Peter van Esse, H., Maruthachalam, K., Bolton, M.D., Santhanam, P., Saber, M.K., Zhang, Z., Usami, T., Lievens, B., Subbarao, K.V., et al. (2012). Tomato immune receptor Ve1 recognizes effector of multiple fungal pathogens uncovered by genome and RNA sequencing. *Proceedings of the National Academy of Sciences*.

Delourme, R., Chevre, A.M., Brun, H., Rouxel, T., Balesdent, M.H., Dias, J.S., Salisbury, P., Renard, M., and Rimmer, S.R. (2006). Major gene and polygenic resistance to *Leptosphaeria maculans* in oilseed rape (*Brassica napus*). *Eur. J. Plant Pathol.* 114, 41-52.

Denness, L., McKenna, J.F., Segonzac, C., Wormit, A., Madhou, P., Bennett, M., Mansfield, J., Zipfel, C., and Hamann, T. Cell Wall Damage-Induced Lignin Biosynthesis Is Regulated by a Reactive Oxygen Species- and Jasmonic Acid-Dependent Process in *Arabidopsis*. *Plant Physiology* 156, 1364-1374.

Dion, Y., Gugel, R.K., Rakow, G.F.W., Séguin-Swartz, G., and Landry, B.S. (1995). RFLP mapping of resistance to the blackleg disease [causal agent, *Leptosphaeria maculans* (Desm.) Ces. et de Not.] in canola (*Brassica napus* L.). *Theor. Appl. Genet.* 91, 1190-1194.

Dodds, P.N., and Rathjen, J.P. (2010). Plant immunity: towards an integrated view of plant-pathogen interactions. *Nat. Rev. Genet.* 11, 539-548.

Dubiella, U., Seybold, H., Durian, G., Komander, E., Lassig, R., Witte, C.P., Schulze, W.X., and Romeis, T. (2013). Calcium-dependent protein kinase/NADPH oxidase activation circuit is required for rapid defense signal propagation. *Proc Natl Acad Sci U S A* 110, 8744-8749.

Dunning, F.M., Sun, W., Jansen, K.L., Helft, L., and Bent, A.F. (2007). Identification and mutational analysis of *Arabidopsis* FLS2 leucine-rich repeat domain residues that contribute to flagellin perception. *Plant Cell* 19, 3297-3313.

Fabro, G., Steinbrenner, J., Coates, M., Ishaque, N., Baxter, L., Studholme, D.J., Körner, E., Allen, R.L., Piquerez, S.J.M., Rougon-Cardoso, A., et al. (2011). Multiple Candidate Effectors from the Oomycete Pathogen *Hyaloperonospora arabidopsidis* Suppress Host Plant Immunity. *PLoS Pathog* 7, e1002348.

Fan, J., Crooks, C., and Lamb, C. (2008). High-throughput quantitative luminescence assay of the growth in planta of *P. syringae* chromosomally tagged with *Photobacterium luminescens* luxCDABE. *The Plant Journal* 53, 393-399.

Faulkner, C., Petutschnig, E., Benitez-Alfonso, Y., Beck, M., Robatzek, S., Lipka, V., and Maule, A.J. (2013). LYM2-dependent chitin perception limits molecular flux via plasmodesmata. *Proceedings of the National Academy of Sciences*.

Felix, G., Duran, J.D., Volko, S., and Boller, T. (1999). Plants have a sensitive perception system for the most conserved domain of bacterial flagellin. *Plant J.* 18, 265-276.

Ferrari, S., Galletti, R., Denoux, C., De Lorenzo, G., Ausubel, F.M., and Dewdney, J. (2007). Resistance to *B. cinerea* Induced in Arabidopsis by Elicitors Is Independent of Salicylic Acid, Ethylene, or Jasmonate Signaling But Requires PHYTOALEXIN DEFICIENT3. *Plant Physiology* 144, 367-379.

Fitt, B.D.L., Brun, H., Barbetti, M.J., and Rimmer, S.R. (2006). World-wide importance of phoma stem canker (*Leptosphaeria maculans* and *L. biglobosa*) on oilseed rape (*Brassica napus*). *Eur. J. Plant Pathol.* 114, 3-15.

Fitt, B.D.L., Hu, B.C., Li, Z.Q., Liu, S.Y., Lange, R.M., Kharbanda, P.D., Butterworth, M.H., and White, R.P. (2008). Strategies to prevent spread of *Leptosphaeria maculans* (phoma stem canker) onto oilseed rape crops in China; costs and benefits. *Plant Pathol.* 57, 652-664.

Forsyth, A., Mansfield, J.W., Grabov, N., de Torres, M., Sinapidou, E., and Grant, M.R. (2010). Genetic Dissection of Basal Resistance to *Pseudomonas syringae* pv. *phaseolicola* in Accessions of Arabidopsis. *Mol. Plant-Microbe Interact.* 23, 1545-1552.

Fu, D.L., Uauy, C., Distelfeld, A., Blechl, A., Epstein, L., Chen, X.M., Sela, H.A., Fahima, T., and Dubcovsky, J. (2009). A Kinase-START Gene Confers Temperature-Dependent Resistance to Wheat Stripe Rust. *Science* 323, 1357-1360.

Garrigan, D., and Hammer, M.F. (2006). Reconstructing human origins in the genomic era. *Nat Rev Genet* 7, 669-680.

Genger, R.K., Jurkowski, G.I., McDowell, J.M., Lu, H., Jung, H.W., Greenberg, J.T., and Bent, A.F. (2008). Signaling Pathways That Regulate the Enhanced Disease Resistance of Arabidopsis "Defense, No Death" Mutants. *Mol. Plant-Microbe Interact.* 21, 1285-1296.

Gómez-Gómez, L., Felix, G., and Boller, T. (1999). A single locus determines sensitivity to bacterial flagellin in Arabidopsis thaliana. *The Plant Journal* 18, 277-284.

Hann, D.R., and Rathjen, J.P. (2007). Early events in the pathogenicity of *Pseudomonas syringae* on *Nicotiana benthamiana*. *The Plant Journal* 49, 607-618.

Harper, A.L., Trick, M., Higgins, J., Fraser, F., Clissold, L., Wells, R., Hattori, C., Werner, P., and Bancroft, I. (2012). Associative transcriptomics of traits in the polyploid crop species *Brassica napus*. *Nat Biotech* 30, 798-802.

Hasan, M., Seyis, F., Badani, A.G., Pons-Kühnemann, J., Friedt, W., Lühs, W., and Snowdon, R.J. (2006). Analysis of Genetic Diversity in the *Brassica napus* L. Gene Pool Using SSR Markers. *Genet Resour Crop Evol* 53, 793-802.

Higgins, J., Magusin, A., Trick, M., Fraser, F., and Bancroft, I. (2012). Use of mRNA-seq to discriminate contributions to the transcriptome from the constituent genomes of the polyploid crop species *Brassica napus*. *BMC Genomics* 13, 247.

Huang, Y.J., Pirie, E.J., Evans, N., Delourme, R., King, G.J., and Fitt, B.D.L. (2009). Quantitative resistance to symptomless growth of *Leptosphaeria maculans* (phoma stem canker) in *Brassica napus* (oilseed rape). *Plant Pathol.* 58, 314-323.

Hwang, I.S., and Hwang, B.K. (2011). The Pepper Mannose-Binding Lectin Gene CaMBL1 Is Required to Regulate Cell Death and Defense Responses to Microbial Pathogens. *Plant Physiology* 155, 447-463.

Iizasa, E., Mitsutomi, M., and Nagano, Y. Direct Binding of a Plant LysM Receptor-like Kinase, LysM RLK1/CERK1, to Chitin in Vitro. *J. Biol. Chem.* 285, 9.

Jeworutzki, E., Roelfsema, M.R.G., Anshütz, U., Krol, E., Elzenga, J.T.M., Felix, G., Boller, T., Hedrich, R., and Becker, D. (2010). Early signaling through the Arabidopsis pattern recognition receptors FLS2 and EFR involves Ca²⁺-associated opening of plasma membrane anion channels. *The Plant Journal* 62, 367-378.

Jones, J.D.G., and Dangl, J.L. (2006). The plant immune system. *Nature* 444, 323-329.

Jurkowski, G.I., Smith, R.K., Yu, I.C., Ham, J.H., Sharma, S.B., Klessig, D.F., Fengler, K.A., and Bent, A.F. (2004). Arabidopsis DND2, a Second Cyclic Nucleotide-Gated Ion Channel Gene for Which Mutation Causes the "Defense, No Death" Phenotype. *Mol. Plant-Microbe Interact.* 17, 511-520.

Kadota, Y., Sklenar, J., Derbyshire, P., Stransfeld, L., Asai, S., Ntoukakis, V., Jones, Jonathan D., Shirasu, K., Menke, F., Jones, A., et al. Direct Regulation of the NADPH Oxidase RBOHD by the PRR-Associated Kinase BIK1 during Plant Immunity. *Mol. Cell.*

Kaku, H., Nishizawa, Y., Ishii-Minami, N., Akimoto-Tomiyama, C., Dohmae, N., Takio, K., Minami, E., and Shibuya, N. (2006). Plant cells recognize chitin fragments for defense signaling through a plasma membrane receptor. *Proc. Natl. Acad. Sci. U. S. A.* 103, 11086-11091.

Kaur, S., Cogan, N.O., Ye, G., Baillie, R.C., Hand, M.L., Ling, A.E., McGearey, A.K., Kaur, J., Hopkins, C.J., Todorovic, M., et al. (2009). Genetic map construction and QTL mapping of resistance to blackleg (*Leptosphaeria maculans*) disease in Australian canola (*Brassica napus* L.) cultivars. *Theor Appl Genet* 120, 71-83.

King, S., Chapman, A., Garvey, L., Whalley, N., Bryant, R., MacFarland, A. M. C, Bowes-Hudson, S., Cooper, D., Cole, M., OConnor, F., (1992+), Thanks for everything, I love you all. I promise to spend more time with all of you in the future. *Journal of Amazing Friends*, 42-42.

Kishimoto, K., Kouzai, Y., Kaku, H., Shibuya, N., Minami, E., and Nishizawa, Y. (2010). Perception of the chitin oligosaccharides contributes to disease resistance to blast fungus *Magnaporthe oryzae* in rice. *The Plant Journal* 64, 343-354.

Klein, R.J., Zeiss, C., Chew, E.Y., Tsai, J.-Y., Sackler, R.S., Haynes, C., Henning, A.K., SanGiovanni, J.P., Sanchez, Dirty., Mane, S.M., Mayne, S.T., et al. (2005). Complement Factor H Polymorphism in Age-Related Macular Degeneration. *Science* 308, 385-389.

Koressaar T, Remm M (2007) Enhancements and modifications of primer design program Primer3 *Bioinformatics* 23(10):1289-91

Kuchitsu, K., Yazaki, Y., Sakano, K., and Shibuya, N. (1997). Transient Cytoplasmic pH Change and Ion Fluxes through the Plasma Membran in Suspension-Cultured Rice Cells Triggered by N-Acetylchitooligosaccharide Elicitor. *Plant and Cell Physiology* 38, AG1012-1018.

Kump, K.L., Bradbury, P.J., Wisser, R.J., Buckler, E.S., Belcher, A.R., Oropeza-Rosas, M.A., Zwonitzer, J.C., Kresovich, S., McMullen, M.D., Ware, D., et al. (2011). Genome-wide association study of quantitative resistance to southern leaf blight in the maize nested association mapping population. *Nat Genet* 43, 163-168.

Kunze, G., Zipfel, C., Robatzek, S., Niehaus, K., Boller, T., and Felix, G. (2004). The N terminus of bacterial elongation factor Tu elicits innate immunity in Arabidopsis plants. *Plant Cell* 16, 3496-3507.

Lacombe, S., Rougon-Cardoso, A., Sherwood, E., Peeters, N., Dahlbeck, D., van Esse, H.P., Smoker, M., Rallapalli, G., Thomma, B., Staskawicz, B., et al. (2010). Interfamily transfer of a plant pattern-recognition receptor confers broad-spectrum bacterial resistance. *Nat. Biotechnol.* 28, 365-U394.

- Lamb, C., and Dixon, R.A. (1997). The oxidative burst in plant disease resistance. *Annu. Rev. Plant Physiol. Plant Molec. Biol.* 48, 251-275.
- Lee, S., Sharma, Y., Lee, T.K., Chang, M., and Davis, K.R. (2001). Lignification induced by *Pseudomonads* harboring avirulent genes on *Arabidopsis*. *Mol. Cells* 12, 25-31.
- Levine, A., Tenhaken, R., Dixon, R., and Lamb, C. (1994). H₂O₂ from the oxidative burst orchestrates the plant hypersensitive disease resistance response. *Cell* 79, 583-593.
- Li, H., Peng, Z., Yang, X., Wang, W., Fu, J., Wang, J., Han, Y., Chai, Y., Guo, T., Yang, N., et al. (2013). Genome-wide association study dissects the genetic architecture of oil biosynthesis in maize kernels. *Nat Genet* 45, 43-50.
- Li, H., Ruan, J., and Durbin, R. (2008). Mapping short DNA sequencing reads and calling variants using mapping quality scores. *Genome Research* 18, 1851-1858.
- Liang, W., Yang, B., Yu, B.-J., Zhou, Z., Li, C., Jia, M., Sun, Y., Zhang, Y., Wu, F., Zhang, H., et al. (2013). Identification and analysis of MKK and MPK gene families in canola (*Brassica napus* L.). *BMC Genomics* 14, 392.
- Libault, M., Wan, J., Czechowski, T., Udvardi, M., and Stacey, G. (2007). Identification of 118 *Arabidopsis* Transcription Factor and 30 Ubiquitin-Ligase Genes Responding to Chitin, a Plant-Defense Elicitor. *Mol. Plant-Microbe Interact.* 20, 900-911.
- Liu, L., Li, Y., Li, S., Hu, N., He, Y., Pong, R., Lin, D., Lu, L., and Law, M. (2012). Comparison of Next-Generation Sequencing Systems. *Journal of Biomedicine and Biotechnology* 2012, 11.
- Lloyd, S.R., Schoonbeek, H.-j., Trick, M., Zipfel, C., and Ridout, C.J. (2013). Methods to Study PAMP-Triggered Immunity in Brassica Species. *Mol. Plant-Microbe Interact.* 27, 286-295.
- Lloyd, C., Lloyd, M., Lloyd, S. K., Lloyd, G. L., Lloyd, J., Lloyd-Mann, J. M., (1985+). Best family ever, love you lots, *Journal of Simons Life.* 16, 02-2014.

Lozano-Durán, R., Macho, A.P., Boutrot, F., Segonzac, C., Somssich, I.E., Zipfel, C., and Nürnberger, T. (2013). The transcriptional regulator BZR1 mediates trade-off between plant innate immunity and growth. *eLife* 2.

Lu, D., Lin, W., Gao, X., Wu, S., Cheng, C., Avila, J., Heese, A., Devarenne, T.P., He, P., and Shan, L. (2011). Direct ubiquitination of pattern recognition receptor FLS2 attenuates plant innate immunity. *Science* 332, 1439-1442.

Luna, E., Pastor, V., Robert, J.r.m., Flors, V., Mauch-Mani, B., and Ton, J. (2011). Callose Deposition: A Multifaceted Plant Defense Response. *Mol. Plant-Microbe Interact.* 24, 183-193.

Ma, W., and Berkowitz, G.A. (2007). The grateful dead: calcium and cell death in plant innate immunity. *Cell Microbiol.* 9, 2571-2585.

Medzhitov, R., and Janeway, C.A. (1997). Innate immunity: The virtues of a nonclonal system of recognition. *Cell* 91, 295-298.

Mei, J., Fu, Y., Qian, L., Xu, X., Li, J., and Qian, W. (2011). Effectively widening the gene pool of oilseed rape (*Brassica napus* L.) by using Chinese *B. rapa* in a 'virtual allopolyploid' approach. *Plant Breed.* 130, 333-337.

Mendes, B.M.J., Cardoso, S.C., Boscariol-Camargo, R.L., Cruz, R.B., Mourão Filho, F.A.A., and Bergamin Filho, A. (2010). Reduction in susceptibility to *Xanthomonas axonopodis* pv. *citri* in transgenic *Citrus sinensis* expressing the rice Xa21 gene. *Plant Pathol.* 59, 68-75.

Meuwly, P., Metraux, J.P. (1993). Ortho-Anisic Acid as Internal Standard for the Simultaneous Quantitation of Salicylic Acid and Its Putative Biosynthetic Precursors in Cucumber Leaves. *Analytical Biochemistry* 214, 500-505.

Mishina, T.E., and Zeier, J. (2007). Bacterial non-host resistance: interactions of *Arabidopsis* with non-adapted *Pseudomonas syringae* strains. *Physiologia Plantarum* 131, 448-461.

Mithen, R.F., and Magrath, R. (1992). Glucosinolates and Resistance to *Leptosphaeria maculans* in Wild and Cultivated Brassica Species. *Plant Breed.* 108, 60-68.

Miya, A., Albert, P., Shinya, T., Desaki, Y., Ichimura, K., Shirasu, K., Narusaka, Y., Kawakami, N., Kaku, H., and Shibuya, N. (2007). CERK1, a LysM receptor kinase, is essential for chitin elicitor signalling in *Arabidopsis*. *Proc. Natl. Acad. Sci. U. S. A.* 104, 19613-19618.

Mohr, P., and Cahill, D. (2007). Suppression by ABA of salicylic acid and lignin accumulation and the expression of multiple genes, in *Arabidopsis* infected with *Pseudomonas syringae*; pv. tomato *Functional & Integrative Genomics* 7, 181-191.

Monaghan, J., and Zipfel, C. (2012). Plant pattern recognition receptor complexes at the plasma membrane. *Curr. Opin. Plant Biol.* 15, 349-357.

Mysore, K.S., Nam, J., and Gelvin, S.B. (2000). An *Arabidopsis* histone H2A mutant is deficient in *Agrobacterium* T-DNA integration. *Proceedings of the National Academy of Sciences* 97, 948-953.

Nagaharu U.(1935) "Genome analysis in Brassica with special reference to the experimental formation of *B. napus* and peculiar mode of fertilization". *Japan. J. Bot* 7: 389-452

Nam, J., Mysore, K.S., Zheng, C., Knue, M.K., Matthyse, A.G., and Gelvin, S.B. (1999). Identification of T-DNA tagged *Arabidopsis* mutants that are resistant to transformation by *Agrobacterium*. *Mol Gen Genet* 261, 429-438.

Navarro, L., Dunoyer, P., Jay, F., Arnold, B., Dharmasiri, N., Estelle, M., Voinnet, O., and Jones, J.D.G. (2006). A Plant miRNA Contributes to Antibacterial Resistance by Repressing Auxin Signaling. *Science* 312, 436-439.

Navarro, L., Zipfel, C., Rowland, O., Keller, I., Robatzek, S., Boller, T., and Jones, J.D.G. (2004). The Transcriptional Innate Immune Response to flg22. Interplay and

Overlap with Avr Gene-Dependent Defense Responses and Bacterial Pathogenesis. *Plant Physiology* 135, 1113-1128.

Nguyen, H.P., Chakravarthy, S., Velasquez, A.C., McLane, H.L., Zeng, L., Nakayashiki, H., Park, D.-H., Collmer, A., and Martin, G.B. (2010). Methods to Study PAMP-Triggered Immunity Using Tomato and *Nicotiana benthamiana*. *Mol Plant Microbe Interact* 23, 991-999.

Nicaise, V., Roux, M., and Zipfel, C. (2009). Recent Advances in PAMP-Triggered Immunity against Bacteria: Pattern Recognition Receptors Watch over and Raise the Alarm. *Plant Physiology* 150, 1638-1647.

Ning, W., Chen, F., Mao, B., Li, Q., Liu, Z., Guo, Z., and He, Z. (2004). N-acetylchitooligosaccharides elicit rice defence responses including hypersensitive response-like cell death, oxidative burst and defence gene expression. *Physiological and Molecular Plant Pathology* 64, 263-271.

Nirmala, J., Drader, T., Chen, X., Steffenson, B., and Kleinhofs, A. (2010). Stem Rust Spores Elicit Rapid Rpg1 Phosphorylation. *Mol. Plant-Microbe Interact.* 23, 1635-1642.

Nirmala, J., Drader, T., Lawrence, P.K., Yin, C.T., Hulbert, S., Steber, C.M., Steffenson, B.J., Szabo, L.J., von Wettstein, D., and Kleinhofs, A. (2011). Concerted action of two avirulent spore effectors activates Reaction to *Puccinia graminis* 1 (Rpg1)-mediated cereal stem rust resistance. *Proc. Natl. Acad. Sci. U. S. A.* 108, 14676-14681.

Nishizawa, Y., Kawakami, A., Hibi, T., He, D.-Y., Shibuya, N., and Minami, E. (1999). Regulation of the chitinase gene expression in suspension-cultured rice cells by N-acetylchitooligosaccharides: differences in the signal transduction pathways leading to the activation of elicitor-responsive genes. *Plant Mol.Biol.* 39, 907-914.

O'Neill, C.M., and Bancroft, I. (2000). Comparative physical mapping of segments of the genome of *B. oleracea* var. *alboglabra* that are homoeologous to sequenced

regions of chromosomes 4 and 5 of *Arabidopsis thaliana*. *The Plant journal : for cell and molecular biology* 23, 233-243.

Parkin, I.A., Sharpe, A.G., Keith, D.J., and Lydiate, D.J. (1995). Identification of the A and C genomes of amphidiploid *Brassica napus* (oilseed rape). *Genome* 38, 1122-1131.

Perez-Perez, J.M., Candela, H., Robles, P., Lopez-Torrejon, G., del Pozo, J.C., and Micol, J.L. (2010). A role for AUXIN RESISTANT3 in the coordination of leaf growth. *Plant & cell physiology* 51, 1661-1673.

Petutschnig, E.K., Jones, A.M.E., Serazetdinova, L., Lipka, U., and Lipka, V. The Lysin Motif Receptor-like Kinase (LysM-RLK) CERK1 Is a Major Chitin-binding Protein in *Arabidopsis thaliana* and Subject to Chitin-induced Phosphorylation. *J. Biol. Chem.* 285, 28902-28911.

Pilet, M.L., Delourme, R., Foisset, N., and Renard, M. (1998). Identification of QTL involved in field resistance to light leaf spot (*Pyrenopeziza brassicae*) and blackleg resistance (*Leptosphaeria maculans*) in winter rapeseed (*Brassica napus* L.). *Theor. Appl. Genet.* 97, 398-406.

Pinosa, F., Buhot, N., Kwaaitaal, M., Fahlberg, P., Thordal-Christensen, H., Ellerström, M., and Andersson, M.X. (2013). *Arabidopsis* Phospholipase D δ Is Involved in Basal Defense and Nonhost Resistance to Powdery Mildew Fungi. *Plant Physiology* 163, 896-906.

Pomar, F., Merino, F., and Barceló, A.R. (2002). O-4-Linked coniferyl and sinapyl aldehydes in lignifying cell walls are the main targets of the Wiesner (phloroglucinol-HCl) reaction. *Protoplasma* 220, 0017-0028.

Proels, R.K., Oberhollenzer, K., Pathuri, I.P., Hensel, G.t., Kumlehn, J., and Hückelhoven, R. (2010). RBOHF2 of Barley Is Required for Normal Development of Penetration Resistance to the Parasitic Fungus *Blumeria graminis* f. sp. hordei. *Mol. Plant-Microbe Interact.* 23, 1143-1150.

Qi, Z., Verma, R., Gehring, C., Yamaguchi, Y., Zhao, Y., Ryan, C.A., and Berkowitz, G.A. (2010). Ca²⁺ signaling by plant *Arabidopsis thaliana* Pep peptides depends on AtPepR1, a receptor with guanylyl cyclase activity, and cGMP-activated Ca²⁺ channels. *Proceedings of the National Academy of Sciences* 107, 21193-21198.

Qiu, D., Xiao, J., Ding, X., Xiong, M., Cai, M., Cao, Y., Li, X., Xu, C., and Wang, S. (2007). OsWRKY13 mediates rice disease resistance by regulating defense-related genes in salicylate- and jasmonate-dependent signaling. *Mol Plant Microbe Interact* 20, 492 - 499.

Rietveld, C.A., Medland, S.E., Derringer, J., Yang, J., Esko, T., Martin, N.W., Westra, H.-J., Shakhbazov, K., Abdellaoui, A., Agrawal, A., et al. (2013). GWAS of 126,559 Individuals Identifies Genetic Variants Associated with Educational Attainment. *Science* 340, 1467-1471.

Robatzek, S., Bittel, P., Chinchilla, D., Köchner, P., Felix, G., Shiu, S.-H., and Boller, T. (2007). Molecular identification and characterization of the tomato flagellin receptor LeFLS2, an orthologue of *Arabidopsis* FLS2 exhibiting characteristically different perception specificities. *Plant Mol.Biol.* 64, 539-547.

Ron, M., and Avni, A. (2004). The receptor for the fungal elicitor ethylene-inducing xylanase is a member of a resistance-like gene family in tomato. *Plant Cell* 16, 1604-1615.

Roux, M., Schwessinger, B., Albrecht, C., Chinchilla, D., Jones, A., Holton, N., Malinovsky, F.G., Tor, M., de Vries, S., and Zipfel, C. (2011). The *Arabidopsis* leucine-rich repeat receptor-like kinases BAK1/SERK3 and BKK1/SERK4 are required for innate immunity to hemibiotrophic and biotrophic pathogens. *Plant Cell* 23, 2440-2455.

Schwessinger, B., and Ronald, P.C. (2012). Plant Innate Immunity: Perception of Conserved Microbial Signatures. *Annu. Rev. Plant Biol.* 63, 451-482.

Sebastian, R.L., Howell, E.C., King, G.J., Marshall, D.F., and Kearsey, M.J. (2000). An integrated AFLP and RFLP *B. oleracea* linkage map from two morphologically

distinct doubled-haploid mapping populations. *TAG Theoretical and Applied Genetics* 100, 75-81.

Segonzac, C., Feike, D., Gimenez-Ibanez, S., Hann, D.R., Zipfel, C., and Rathjen, J.P. (2011). Hierarchy and Roles of Pathogen-Associated Molecular Pattern-Induced Responses in *Nicotiana benthamiana*. *Plant Physiology* 156, 687-699.

Segonzac, C., and Zipfel, C. (2011). Activation of plant pattern-recognition receptors by bacteria. *Current Opinion in Microbiology* 14, 54-61.

Shiu, S.-H., and Bleecker, A.B. (2001). Plant Receptor-Like Kinase Gene Family: Diversity, Function, and Signaling. *Sci. STKE* 2001, re22-.

Sparrow, P.A.C., Townsend, T.M., Arthur, A.E., Dale, P.J., and Irwin, J.A. (2004). Genetic analysis of *Agrobacterium tumefaciens* susceptibility in *B. oleracea*. *Theor. Appl. Genet.* 108, 644-650.

Spoel, S.H., and Dong, X. (2008). Making Sense of Hormone Crosstalk during Plant Immune Responses. *Cell Host & Microbe* 3, 348-351.

Spoel, S.H., and Dong, X. (2012). How do plants achieve immunity? Defence without specialized immune cells. *Nat Rev Immunol* 12, 89-100.

Sprague, S.J., Balesdent, M.H., Brun, H., Hayden, H.L., Marcroft, S.J., Pinochet, X., Rouxel, T., and Howlett, B.J. (2006). Major gene resistance in *Brassica napus* (oilseed rape) is overcome by changes in virulence of populations of *Leptosphaeria maculans* in France and Australia. *Eur. J. Plant Pathol.* 114, 33-40.

Stearns, J.C., Woody, O.Z., McConkey, B.J., and Glick, B.R. (2012). Effects of Bacterial ACC Deaminase on *Brassica napus* Gene Expression. *Mol. Plant-Microbe Interact.* 25, 668-676.

Sun, W., Dunning, F.M., Pfund, C., Weingarten, R., and Bent, A.F. (2006). Within-Species Flagellin Polymorphism in *Xanthomonas campestris* pv *campestris* and Its Impact on Elicitation of *Arabidopsis* FLAGELLIN SENSING2-Dependent Defenses. *The Plant Cell Online* 18, 764-779.

Takai, R., Isogai, A., Takayama, S., and Che, F.-S. (2008). Analysis of Flagellin Perception Mediated by flg22 Receptor OsFLS2 in Rice. *Mol. Plant-Microbe Interact.* 21, 1635-1642.

Thimm, O., Bläsing, O., Gibon, Y., Nagel, A., Meyer, S., Krüger, P., Selbig, J., Müller, L.A., Rhee, S.Y., and Stitt, M. (2004). mapman: a user-driven tool to display genomics data sets onto diagrams of metabolic pathways and other biological processes. *The Plant Journal* 37, 914-939.

Thomma, B.P.H.J., Nürnberger, T., and Joosten, M.H.A.J. (2011). Of PAMPs and Effectors: The Blurred PTI-ETI Dichotomy. *The Plant Cell Online* 23, 4-15.

Tian, F., Bradbury, P.J., Brown, P.J., Hung, H., Sun, Q., Flint-Garcia, S., Rocheford, T.R., McMullen, M.D., Holland, J.B., and Buckler, E.S. (2011). Genome-wide association study of leaf architecture in the maize nested association mapping population. *Nat Genet* 43, 159-162.

Torres, M.A., Jones, J.D.G., and Dangl, J.L. (2006). Reactive oxygen species signaling in response to pathogens. *Plant Physiology* 141, 373-378.

Tomas, A., Braun, N., Muller, P., Khodus, T., Paponov, I.A., Palme, K., Ljung, K., Lee, J.Y., Benfey, P., Murray, J.A., et al. (2009). The AUXIN BINDING PROTEIN 1 is required for differential auxin responses mediating root growth. *PLoS One* 4, e6648.

Tronchet, M., BalaguÉ, C., Kroj, T., Jouanin, L., and Roby, D. (2010). Cinnamyl alcohol dehydrogenases-C and D, key enzymes in lignin biosynthesis, play an essential role in disease resistance in Arabidopsis. *Mol. Plant Pathol.* 11, 83-92.

Tsuda, K., Sato, M., Glazebrook, J., Cohen, J.D., and Katagiri, F. (2008). Interplay between MAMP-triggered and SA-mediated defense responses. *The Plant Journal* 53, 763-775.

Untergasser, A., Cutcutache, I., Koressaar, T., Ye, J., Faircloth, B.C., Remm, M., and Rozen, S.G. (2012). Primer3—new capabilities and interfaces. *Nucleic Acids Research* 40, e115.

Untergasser, A., Nijveen, H., Rao, X., Bisseling, T., Geurts, R., and Leunissen, J. (2007). Primer3Plus, an enhanced web interface to Primer3. *Nucleic Acids Res* 35, W71 - W74.

Valdezs-Lopez, O., Thibivilliers, S., Qiu, J., Xu, W.W., Nguyen, T.H.N., Libault, M., Le, B.H., Goldberg, R.B., Hill, C.B., Hartman, G.L., et al. (2011). Identification of Quantitative Trait Loci Controlling Gene Expression during the Innate Immunity Response of Soybean. *Plant Physiology* 157, 1975-1986.

Vanholme, R., Demedts, B., Morreel, K., Ralph, J., and Boerjan, W. (2010). Lignin Biosynthesis and Structure. *Plant Physiology* 153, 895-905.

Vetter, M.M., He, F., Kronholm, I., Hãwewer, H., Reymond, M., Bergelson, J., Robatzek, S., and de Meaux, J. Flagellin perception varies quantitatively in *Arabidopsis thaliana* and its relatives. *Molecular Biology and Evolution*.

Wan, J.R., Zhang, X.C., Neece, D., Ramonell, K.M., Clough, S., Kim, S.Y., Stacey, M.G., and Stacey, G. (2008). A LysM receptor-like kinase plays a critical role in chitin signaling and fungal resistance in *Arabidopsis*. *Plant Cell* 20, 471-481.

Wang, D., Pajerowska-Mukhtar, K., Culler, A.H., and Dong, X. (2007). Salicylic acid inhibits pathogen growth in plants through repression of the auxin signaling pathway. *Curr Biol* 17, 1784-1790.

Wang, X., Wang, H., Wang, J., Sun, R., Wu, J., Liu, S., Bai, Y., Mun, J.-H., Bancroft, I., Cheng, F., et al. (2011). The genome of the mesopolyploid crop species *Brassica rapa*. *Nat Genet* 43, 1035-1039.

Williams, B., Kabbage, M., Kim, H.-J., Britt, R., and Dickman, M.B. (2011). Tipping the Balance: *Sclerotinia sclerotiorum* Secreted Oxalic Acid Suppresses Host Defenses by Manipulating the Host Redox Environment. *PLoS Pathog* 7, e1002107.

Willmann, R., Lajunen, H.M., Erbs, G., Newman, M.-A., Kolb, D., Tsuda, K., Katagiri, F., Fliegmann, J., Bono, J.-J., Cullimore, J.V., et al. (2012). *Arabidopsis* lysin-motif proteins LYM1 LYM3 CERK1 mediate bacterial peptidoglycan sensing and immunity to bacterial infection. *Proceedings of the National Academy of Sciences*.

- Wu, J., Cai, G., Tu, J., Li, L., Liu, S., Luo, X., Zhou, L., Fan, C., and Zhou, Y. (2013). Identification of QTLs for Resistance to Sclerotinia Stem Rot and BnaC.IGMT5.aas a Candidate Gene of the Major Resistant QTL SRC6in Brassica napus. PLoS ONE 8, e67740.
- Yamada, A., Shibuya, N., Kodama, O., and Akatsuka, T. (1993). INDUCTION OF PHYTOALEXIN FORMATION IN SUSPENSION-CULTURED RICE CELLS BY N-ACETYL-CHITOOOLIGOSACCHARIDES. Biosci. Biotechnol. Biochem. 57, 405-409.
- Yang, B., Rahman, M.H., Liang, Y., Shah, S., and Kav, N.N.V. Characterization of Defense Signaling Pathways of Brassica napus and Brassica carinata in Response to Sclerotinia sclerotiorum Challenge. Plant Mol. Biol. Rep. 28, 253-263.
- Yang, Q., Fan, C., Guo, Z., Qin, J., Wu, J., Li, Q., Fu, T., and Zhou, Y. (2012). Identification of FAD2 and FAD3 genes in Brassica napus genome and development of allele-specific markers for high oleic and low linolenic acid contents. Theor. Appl. Genet. 125, 715-729.
- Yang, S., Yang, H., Grisafi, P., Sanchatjate, S., Fink, G.R., Sun, Q., and Hua, J. (2006). The BON/CPN gene family represses cell death and promotes cell growth in Arabidopsis. The Plant Journal 45, 166-179.
- Yin, H., Li, S., Zhao, X., Du, Y., and Ma, X. (2006). cDNA microarray analysis of gene expression in Brassica napus treated with oligochitosan elicitor. Plant Physiology and Biochemistry 44, 910-916.
- Yin, X., Yi, B., Chen, W., Zhang, W., Tu, J., Fernando, W.G.D., and Fu, T. (2010). Mapping of QTLs detected in a Brassica napus DH population for resistance to Sclerotinia sclerotiorum in multiple environments. Euphytica 173, 25-35.
- Yoshioka, K., Moeder, W., Kang, H., Kachroo, P., Masmoudi, K., Berkowitz, G., and Klessig, D. (2006). The chimeric Arabidopsis CYCLIC NUCLEOTIDE-GATED ION CHANNEL11/12 activates multiple pathogen resistance responses. Plant Cell 18, 747 - 763.

Zhao, J., Buchwaldt, L., Rimmer, S.R., Sharpe, A., McGregor, L., Bekkaoui, D., and Hegedus, D. (2009). Patterns of differential gene expression in *Brassica napus* cultivars infected with *Sclerotinia sclerotiorum*. *Mol. Plant Pathol.* 10, 635-649.

Zhao, K., Tung, C.-W., Eizenga, G.C., Wright, M.H., Ali, M.L., Price, A.H., Norton, G.J., Islam, M.R., Reynolds, A., Mezey, J., et al. (2011). Genome-wide association mapping reveals a rich genetic architecture of complex traits in *Oryza sativa*. *Nat Commun* 2, 467.

Zipfel, C., Kunze, G., Chinchilla, D., Caniard, A., Jones, J.D.G., Boller, T., and Felix, G. (2006). Perception of the bacterial PAMP EF-Tu by the receptor EFR restricts *Agrobacterium*-mediated transformation. *Cell* 125, 749-760.

Zipfel, C., Robatzek, S., Navarro, L., Oakeley, E.J., Jones, J.D.G., Felix, G., and Boller, T. (2004). Bacterial disease resistance in *Arabidopsis* through flagellin perception. *Nature* 428, 764-767.

Chapter 7 : Appendices

7.1. Appendix 1: flg22-Induced Transcriptomic Changes in *Brassica napus*

Excell Spreadsheet, located in CD on back cover.

Changes in gene expression after flg22 treatment at 1h and 3h following infiltration, determined by Illumina sequencing, and aligned to the A and C Genomes on the *Brassica napus* pseudo-reference genome. Data is listed as log2 of the fold expression between 1 or 3 hours (F1/F3) compared with 0 hours(F0). The A and C *Brassica* genomes are listed side by side and data is sorted by magnitude of log 2 expression change. Annotation is the Tair 10 description of the most closely related *Arabidopsis* gene.

Raw data was deposited in the EMBL short read archive under accession number ERA248806

7.2. Appendix 2: Association Mapping of SNP Markers in *Brassica napus*

Excell Spreadsheet, located in CD on back cover.

A Spreadsheet of all SNPs in *Brassica napus* unigenes used in the association mapping experiments and the significance of their association to the trait of interest. Each tab is a different trait, and include flg22 ROS, elf18 ROS, *Botrytis cinerea* resistance and *Pseudomonas syringae* DC3000 HrcC- resistance.

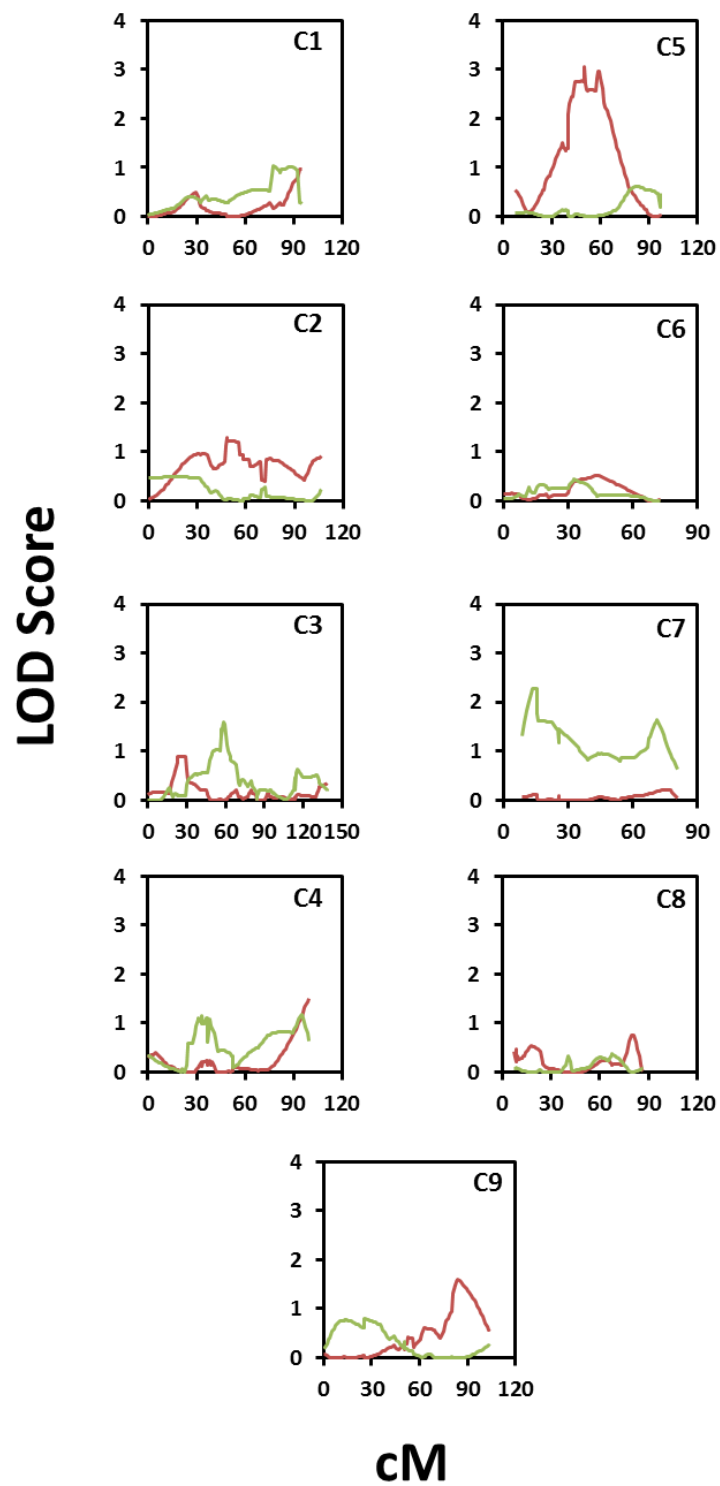
7.3. Appendix 3: Association Mapping of GEM Markers in *Brassica napus*

Excell Spreadsheet, located in CD on back cover.

A Spreadsheet of all GEMs in *Brassica napus* unigenes used in the association mapping experiments and the significance of their association to the trait of interest. Each tab is a different trait, and includes flg22 ROS, elf18 ROS, *Botrytis cinerea* resistance and *Pseudomonas syringae* DC3000 HrcC- resistance. Data is split into A and C genome gene lists. Annotation is the Tair 10 description of the most closely related *Arabidopsis* gene.

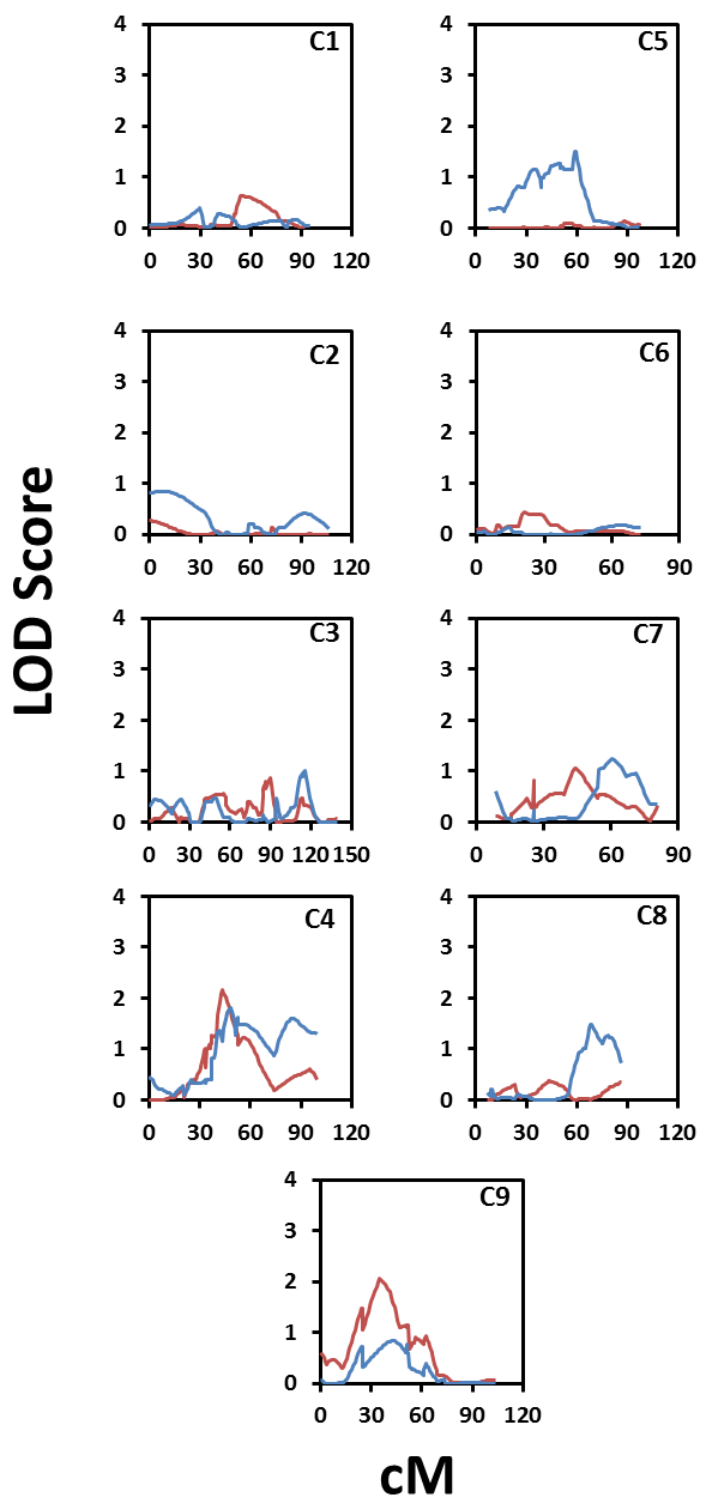
7.4. Appendix 4 : QTL Maps Of elf18 Triggered Oxidative Burst, *Botrytis cinerea* Resistance and *Pseudomonas syringae* Resistance in A12 x GD

Interval mapping of the elf12 triggered oxidative bursts, resistance to *B. cinerea* and Pst in A12xGD cross.

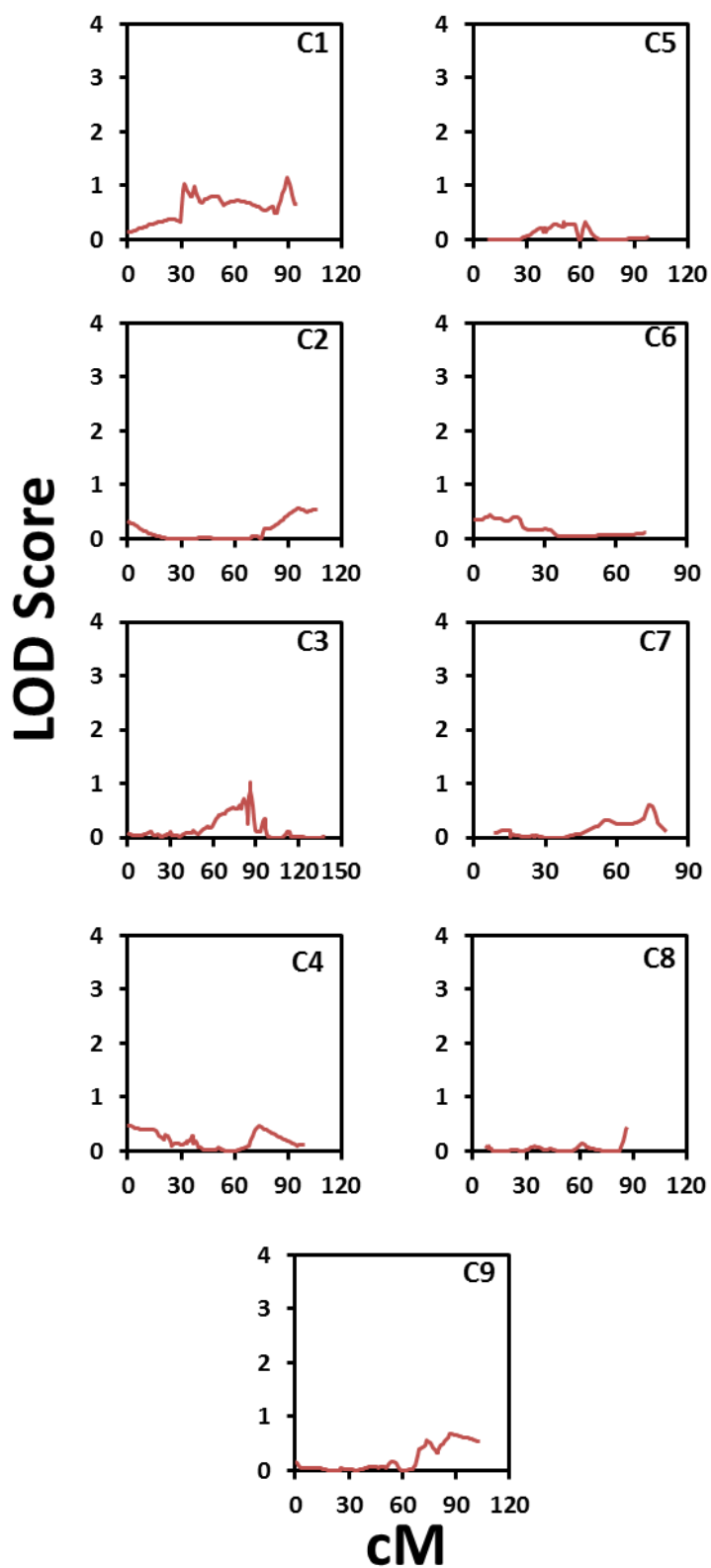


QTL profile of elf18 triggered ROS in A12 x GD

Interval mapping output from MAPQTL of two different experiments scoring the elf18 triggered ROS burst in *B. oleracea* A12xGD



QTL profile of *Botrytis cinerea* resistance in A12 x GD
 Interval mapping output from MAPQTL of two different experiments scoring *B. cinerea* resistance in *B. oleracea* A12xGD.



QTL profile of *Pseudomonas syringae* resistance in A12 x GD
Interval mapping output from MAPQTL of *P. syringae* resistance in *B. oleracea* A12xGD

7.5. Appendix 5: SNP List Between A12 and GD

Excell Spreadsheet, located in CD on back cover.

A list of SNPs between A12 and GD in the consensus sequence for each line based on alignment of Illumina reads against *B. napus* unigenes.

7.6. Appendix 6: Codon Use and Amino Acid Changes for SNPs between A12 and GD

Excell Spreadsheet, located in CD on back cover.

Predicted codon usage, and Synonymous / NS SNP calling for A12 and GD. Data is output from a custom script developed by Martin Trick that aligned unigene sequence against the *A. thaliana* cDNA sequence to predict ORFs. Not all unigenes had ORFs predicted for them, likely a result of incomplete sequence coverage by the mRNA reads or substantial differences in intron/exon use between *Arabidopsis* and *B. oleracea*.

7.7. Appendix 7: Predicted Synonymous, Non-synonymous and Unknown SNPs on C9

Excell Spreadsheet, located in CD on back cover.

7.8. Appendix 8: Basal Unigene Expression Level in A12 and GD

Excell Spreadsheet, located in CD on back cover.

Expression level, expressed as reads per million, of unigenes in A12 and GD.

7.9. Appendix 9: PAMP Induced Expression Changes of Unigenes Within the C9 QTL in *B. napus* and *A. thaliana*.

Excell Spreadsheet, located in CD on back cover.

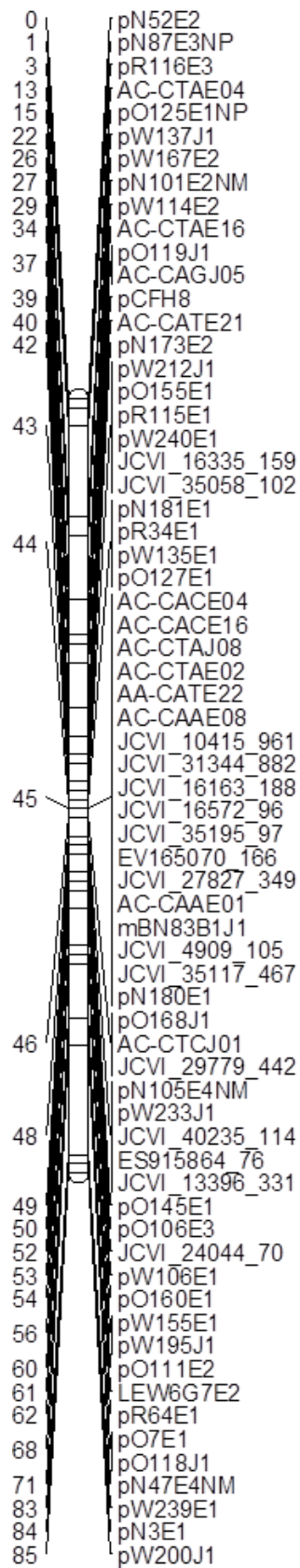
Data plots the fold expression between the listed time point and the 0 hour, or water treated controls. Raw data was taken from Boudsouq et al (2010) or the PLEXDB database GSE17479.

7.10. Appendix 10: Genotyping Matrix of AFLP, RFLP and KASPar Markers For the A12 x GD Mapping Population

Excell Spreadsheet, located in CD on back cover.

7.11. Appendix 11: New Integrated C9 Map

Map intergrating AFLP, RFLP and KASPar markers of *B. oleracea* C9. Constructed in joinmap v.3.0.



**Marker Map Intergrating AFLP, RFLP and SNP markers
in the A12xGD cross**

Generated in JoinMap v 3.0.

7.12. Appendix 12: Full Length DND2 from C9 consensus extraction for A12 and GD

PNG image, located in CD on back cover.

mRNA seq of A12 and GD was aligned to the C genome unigene reference assembly in Tassel. The consensus A12 and GD sequence for a region spanning both unigenes and 3' and 5' UTRs is presented.

7.13. Appendix 13: Alignment of JCVI_20335 and JCVI_20553 against full length AtDND2 cDNA

Alignment of JCVI_20335 and JCVI_20553 against full length AtDND2 CDNA in CLC workbench Version 13.

				20				40	
At_DND2	MATEQEFTRA	SRFSDSSS	GYSEED-NT	EEEEEEEEE	M	EEEEEEEEE			49
JCVI_20553 (+3)	-----	-----	-----	-----	-----	-----	-----	-----	49
JCVI_20553_A12 (+3)	-----	-----	-----	-----	-----	-----	-----	-----	49
JCVI_20553_GD (+3)	-----	-----	-----	-----	-----	-----	-----	-----	49
				60				80	
At_DND2	EEEDPRIGT	CG-GRRNGSS	NNNKWMMGR	LDPRS	KWYR	EWNKVFLLYC			98
JCVI_20553 (+3)	-----	-----	-----	-----	-----	-----	-----	-----	98
JCVI_20553_A12 (+3)	-----	-----	-----	-----	-----	-----	-----	-----	27
JCVI_20553_GD (+3)	-----	-----	-----	-----	-----	-----	-----	-----	27
				120				140	
At_DND2	ATGLFVDFLF	LYTLSVSDTC	MCLLV	DGWL	A	LTVTALRSMT	DLHLWN	WI	148
JCVI_20553 (+3)	-----	-----	-----	-----	-----	-----	-----	-----	148
JCVI_20553_A12 (+3)	-----	-----	-----	-----	-----	-----	-----	-----	33
JCVI_20553_GD (+3)	-----	-----	-----	-----	-----	-----	-----	-----	33
				180				200	
At_DND2	QFKIARRWPY	PGGSDSDGTN	KGGGTR--GS	TRVAPPY	VKK	NG-FFFFL	LFY		195
JCVI_20553 (+3)	-----	-----	-----	-----	-----	-----	-----	-----	195
JCVI_20553_A12 (+3)	-----	-----	-----	-----	-----	-----	-----	-----	63
JCVI_20553_GD (+3)	-----	-----	-----	-----	-----	-----	-----	-----	63
				220				240	
At_DND2	LLPLPQVYVW	VVIPSLLKRG	SVTLVSVLL	VTELFQYLPK	IYHSIRHLRR				245
JCVI_20553 (+3)	-----	-----	-----	-----	-----	-----	-----	-----	245
JCVI_20553_A12 (+3)	-----	-----	-----	-----	-----	-----	-----	-----	75
JCVI_20553_GD (+3)	-----	-----	-----	-----	-----	-----	-----	-----	75
				280				300	
At_DND2	NATLSGYIFG	TVWGTALNM	IAYEVA	AAHAA	GACWYLLG	VQ	RS	AKCLKEQC	295
JCVI_20553 (+3)	-----	-----	-----	-----	-----	-----	-----	-----	295
JCVI_20553_A12 (+3)	-----	-----	-----	-----	-----	-----	-----	-----	75
JCVI_20553_GD (+3)	-----	-----	-----	-----	-----	-----	-----	-----	75
				320				340	
At_DND2	ENTIGCDLRM	LSCKEPIYYG	TTVMVLDRAR	LAWAQNHQAR	SVCLDINTNY				345
JCVI_20553 (+3)	-----	-----	-----	-----	-----	-----	-----	-----	345
JCVI_20553_A12 (+3)	-----	-----	-----	-----	-----	-----	-----	-----	75
JCVI_20553_GD (+3)	-----	-----	-----	-----	-----	-----	-----	-----	75
				380				400	
At_DND2	TYGAYQWTIO	LVSSSRLEK	ILFPIFWGLM	TLSTFGNLES	TTEWSEVVFN				395
JCVI_20553 (+3)	-----	-----	-----	-----	-----	-----	-----	-----	395
JCVI_20553_A12 (+3)	-----	-----	-----	-----	-----	-----	-----	-----	75
JCVI_20553_GD (+3)	-----	-----	-----	-----	-----	-----	-----	-----	75
				420				440	
At_DND2	IIVLTSGLLL	VTMLIGNIKY	FLHATTSKKQ	AMHLKMRNIE	VWVKRRHLP				445
JCVI_20553 (+3)	-----	-----	-----	-----	-----	-----	-----	-----	445
JCVI_20553_A12 (+3)	-----	-----	-----	-----	-----	-----	-----	-----	75
JCVI_20553_GD (+3)	-----	-----	-----	-----	-----	-----	-----	-----	75
				480				500	
At_DND2	GFRQRVRYE	RQRWAAMRG	DECEMVQNP	ELRRD	KYH	LCLDLVRQHM			495
JCVI_20553 (+3)	-----	-----	-----	-----	-----	-----	-----	-----	495
JCVI_20553_A12 (+3)	-----	-----	-----	-----	-----	-----	-----	-----	75
JCVI_20553_GD (+3)	-----	-----	-----	-----	-----	-----	-----	-----	75
				520				540	
At_DND2	DDLVLN	ICD	RVKSLIFTKG	ETIQKEGD	AV	QRMLEFVVRGH	LQSSQLLRD	G	545
JCVI_20553 (+3)	-----	-----	-----	-----	-----	-----	-----	-----	545
JCVI_20553_A12 (+3)	-----	-----	-----	-----	-----	-----	-----	-----	75
JCVI_20553_GD (+3)	-----	-----	-----	-----	-----	-----	-----	-----	75
				580				600	
At_DND2	VKSCCM	LP	GF	NFSGDELLSW	CLRRPFVERL	PPSSSTLTVL	ETTEAFGLDA		595
JCVI_20553 (+3)	-----	-----	-----	-----	-----	-----	-----	-----	595
JCVI_20553_A12 (+3)	-----	-----	-----	-----	-----	-----	-----	-----	123
JCVI_20553_GD (+3)	-----	-----	-----	-----	-----	-----	-----	-----	123
				620				640	
At_DND2	EDVKYVTQHF	RYTFVNEKVK	RSARYYSPGW	RTWAAVAIQ	AWRRYKHR	LT			645
JCVI_20553 (+3)	-----	-----	-----	-----	-----	-----	-----	-----	645
JCVI_20553_A12 (+3)	-----	-----	-----	-----	-----	-----	-----	-----	173
JCVI_20553_GD (+3)	-----	-----	-----	-----	-----	-----	-----	-----	173
				680				700	
At_DND2	LTSLSF	IRPR	RPLSRCAS	G	EDKLRLYAAI	LTSPKPNPDD	FDDY	-----	689
JCVI_20553 (+3)	-----	-----	-----	-----	-----	-----	-----	-----	689
JCVI_20553_A12 (+3)	-----	-----	-----	-----	-----	-----	-----	-----	223
JCVI_20553_GD (+3)	-----	-----	-----	-----	-----	-----	-----	-----	223
				720					
At_DND2	-----	-----	-----	-----	-----	-----	-----	-----	689
JCVI_20553 (+3)	-----	-----	-----	-----	-----	-----	-----	-----	242
JCVI_20553_A12 (+3)	-----	-----	-----	-----	-----	-----	-----	-----	242
JCVI_20553_GD (+3)	-----	-----	-----	-----	-----	-----	-----	-----	242

7.14. First author publications of candidate

7.14.1 “Methods to Study PTI in Brassica napus”